On near-free-surface dynamics of thin polymer films

by

Dongping Qi

A thesis
presented to the University of Waterloo
in fulfillment of the
thesis requirement for the degree of
Doctor of Philosophy
in
Physics

Waterloo, Ontario, Canada, 2009

AUTHOR'S DECLARATION

I hereby declare that I am the sole author of this thesis. This is a true copy of the thesis, including any required final revisions, as accepted by my examiners.

I understand that my thesis may be made electronically available to the public.

Abstract

In the past 15 years, studies show that the dynamical properties of ultra-thin (especially less than 100nm thick) polymer films deviate from those of the bulk counterpart materials. These studies are interesting in terms of both fundamental and practical significance. Despite some controversial issues, there is growing evidence, including experimental, computer simulation and theoretical studies, indicating that the interfacial properties play a key role for observed dynamical anomalies. However, how and how much the interfacial properties affect the average dynamics, which usually are measured by most experiments, of the whole nanometer scale systems are still elusive. In addition, due to limited availability of conventional techniques the measurement of the interfacial region (with probing resolution of a few nanometers) of thin polymer films is very rare. In the present studies of four projects we developed several novel techniques to investigate near-free-surface dynamics of thin polymer films.

In the first project, we studied the dynamical properties of the first 2-3 nm region of glassy isotactic poly (methyl methacrylate) (*i*-PMMA) films by means of the nano surface hole relaxation technique. We found that for the measured surface relaxation times there is a strong substrate property dependence, which can propagate into i-PMMA films for a distance of more than 100nm. The chain confinement mechanism is excluded for the observed substrate dependence of near-free-surface dynamics. An unexpected molecular weight (M_w) dependence of the near surface relaxation time is found for thick i-PMMA films, which, together with the finding that the free surface could be assigned a local surface glass transition temperature of ~40K below bulk T_g, indicates a viscous liquid regime while the rest of the underneath bulk part is in the glassy state.

In the second project, the nano gold sphere embedding technique was used to study the near-free-surface dynamics of polystyrene (PS) films within wide temperature and time windows. Three sections of measurements are conducted in this project. In the first section, we studied

the M_w dependence of the near-free-surface dynamics of PS films and found that at temperatures above bulk T_g there exists a M_w dependence which can be explained using the Rouse dynamics for melt polymers. However, at a temperature of ~16K below bulk T_g no M_w dependence is discernable, which is in contrast to that for i-PMMA films where even at a temperature of ~36K below bulk T_g a M_w dependence of the near free surface dynamics is still observed. In the second section of this work, we studied the nano gold sphere embedding behavior within a wide temperature and time window, and for the first time the depth dependence of the near-free-surface dynamics with the nanometer scale resolution was observed. By an embedding-model-free data analysis the results show that when the measurement temperature is above a temperature of ~378K for polystyrene films the whole film average dynamics are homogeneous; when the temperature is below this temperature the average dynamics for the PS films are heterogeneous; when the measurement temperature is below ~287K no gold sphere embedding is observed and the PS films are in the complete practical glassy state— the whole film average dynamics are homogeneous again. In particular, it is found that for the first ~5.5nm surface region the dynamics are enhanced compared with those in the bulk material region and the liquid surface size decreases with decreasing temperatures; there exists an ~3.3nm sub-surface layer region where some elastic properties in this region are found; in regions beyond the first ~8.8nm of glassy PS films the dynamics are similar with those of bulk materials. Both the liquid surface size and the heterogeneous dynamics in the near free surface region are in contrast to some other studies. The third section of this work focused on the viscoelastic or elastic properties of near free surface region of glassy polystyrene films. It is shown that for the first ~5.5nm free surface layer the gold sphere embedding in not reversible. However, for the ~3.3nm sub-surface layer region the gold sphere embedding is reversible, for which there is no strong evidence to differentiate two possible mechanisms: is this phenomenon due to any built-in stress during gold sphere embedding or any potential intrinsic structural properties in this region?

In the third project we built a low level noise measurement system to study the thermal polarization noise in thin polymer films. The polymer films are sandwiched between two ultra-flat electrodes and pure thermal polarization noise can be collected and amplified by the noise measurement system. The noise power spectral density (PSD) of thin polymer films is found to fluctuate around a certain average level. For thinner films, both the fluctuation and the integration (energy) of the power spectral density are found to be larger than those of the relatively thicker films, which we think is due to the increase of the number of the mobile cooperative rearranging regions(CRR's) in thinner films. There is no dependence of the dominant PSD peak position on polymer film thickness is observed, which is in agreement with findings in some other dielectric spectroscopy studies. For the first time we observe that in the integrated power spectral density there are some relatively big jumps or fluctuations at some times of the successive measurements, which may indicate some energy exchange between different microscopic domains in glassy polymer systems.

In the fourth section of this study we developed a novel nano rheology AFM technique to study the near-free-surface dynamics of thin polymer films. Being different from common AFM techniques working with the dynamic torsional AFM tip mode, the technique in this study measures the transient retardation response of the polymer film surfaces to the step-like applied tip torsional force within the time domain. Enhanced near-free-surface dynamics, with weak temperature dependence, are observed for PVAc films. Similar surface dynamical features are also observed in thin PS films (in the second project).

Acknowledgements

My PhD research and studies would not have been possible without valuable assistances and supports from many individuals who deserve to be recognized.

It was a great opportunity for me to work with Professor James A. Forrest, an insightful and knowledgeable expert in the field of studying polymers on the nanometer scale. I am grateful to Professor James A. Forrest for providing guidance and supports in the past few years. I would also like to thank members of my research advisory committee: Professor Stefan Idziak, Professor Qing-Bin Lu and Professor Pu Chen, for their helpful advices at my committee meetings and for their reviewing my thesis and providing me with insightful questions at my oral defense. I appreciate kind helps from my external examiner Professor Ophelia K. C. Tsui (Boston University), who is a recognized expert in the field of dynamics of nano-confined polymers. Professor Qing-Bin Lu and Professor John Dutcher (University of Guelph) were very helpful with my PhD qualifying exam. I appreciate all administrative helps from Ms. Judy McDonnell and Ms. Linda Stadig as well.

I would like to express my acknowledgments to many nice fellow students or friends, who gave me some important technical supports and created friendly learning environments in the past few years. These people are: James Chan, James Benson, Zahra Fakhraai, Jonathan Teichroeb, Gianfranco Mazzanti, Sara Guthrie, Vadoud H. Niri, Maria Khomenko, Valentina Ngai, Patrick McVeigh, Jane Robinson, Ryan Speller, Kanwarjeet Kaur, Mark Ilton, Chad Daley, Victor Wollesen, James Sharp, Sina Valadkhan. Of significance as well, I would like to thank Lixin Zhan, Zhenwen Wang, Anming Hu, Yidun Wan, Shuchao Meng, Yongsong Liu, Jianzhen Liang, Ronghu Wu, Xiangqun Yuan, Liping Yu, Henghua Deng, Runqing Jiang, Weihong Huang.

Finally, I would like to acknowledge the endless love and support from my mother, my brothers and sister. I wish my father could have lived to enjoy the achievements I have made. My special thanks are extended to my wife Wenli and my daughter Wanfang.

Dedication

This thesis is dedicated to my wife Wenli and my daughter Wanfang.

Contents

List of Figures

Chapter 1

Introduction A— Polymeric chain molecules

1.1 Polymeric chain molecules— the chemical perspective

1.1.1 What are polymeric chain molecules?

Polymers or macromolecules are almost everywhere in our daily life, such as various fibers our clothes are made of, many foods we eat regularly, and numerous materials we use for housing or traveling equipments. People use polymers based on the knowledge of their properties, which results from the tremendous fundamental scientific and application engineering research contributions made by scientists worldwide over a long period of time. "Chemists started polymerizing synthetic macromolecules in the middle of the nineteenth century, but they did not believe that they were creating very large molecules." The concept of "macromolecule", being initially ridiculed, was first proposed by Staudinger in 1920. Its gradual acceptance during the 1920s allowed for substantial progress in this field [1, 2].

Nowadays, people know that polymers are actually macromolecules, which are long chains of *covalently bonded* chemical repeat units—unreacted units are called monomers, which are small *covalently bonded* atomic groups. Some common polymers include polystyrene(PS), poly(methylmethacrylate)(PMMA), poly(vinylacetate)(PVAc), poly(butyl methacrylate)(PBMA).

Fig. 1.1 depicts chemical structures of the aforementioned polymers. Fig. 1.2 shows the three-dimensional representation of a small section of PMMA molecule.

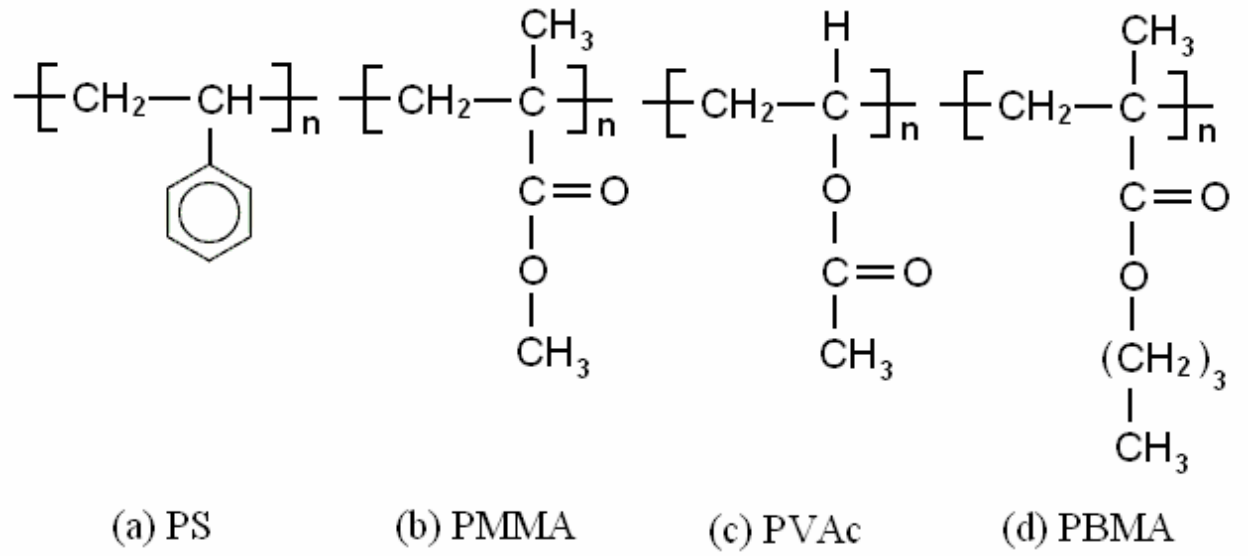

Fig. 1.1 Chemical structures of some common polymers.

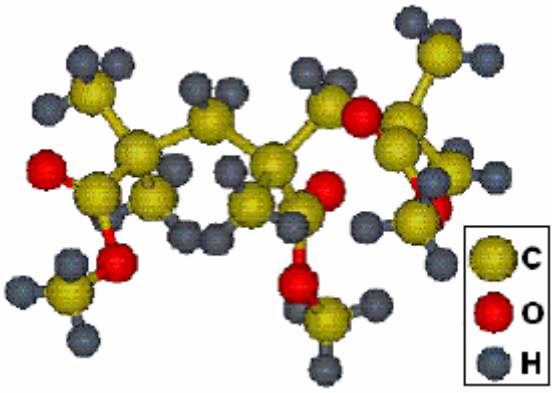

Fig. 1.2 Three-dimensional representation of a small section of PMMA molecule. (Graph from [3])

The number of chemical repeat units of a polymer molecule is called *degree of polymerization* N. The molar mass of a polymer molecule is therefore equal to the degree of polymerization N times the molar mass M_0 of its chemical repeat unit. Because there is usually a distribution of synthetic polymer chains with different molecular weights as a result of the process of polymerization, people use two variables to characterize the size/weight of a polymer: *number average molecular weight* M_n and *weight average molecular weight* M_w [4], which are defined as

$$M_n = \int p(m) m dm \,. \tag{1.1}$$

$$M_w = \frac{\int p(m) m^2 dm}{\int p(m) m dm} = \frac{\int p(m) m^2 dm}{M_n} \,. \tag{1.2}$$

In the above equations, $p(m)$ is the distribution function of polymer chains with molecular weight m. Another useful parameter describing the width of the molecular weight distribution of a polymer is the *polydispersity index*

$$r_{PDI} = \frac{M_w}{M_n} \,. \tag{1.3}$$

r_{PDI} is unity if all polymer chains have a uniform molecular length, but for most synthesized polymers $r_{PDI} > 1$.

1.1.2 Architecture/microstructure of polymeric chain molecules

From Fig. 1.1 we see that most polymers have some *side groups* attaching to the macromolecule backbone, which usually constitutes carbon atoms. In some polymers, there are also some short chains attaching to the main chain backbone. Based on different chemical *architectures*, polymers can be classified as:

Linear polymer— without side chains, but there might be side groups;
Branched polymer— with side chains attaching to the main chain backbone;
Network polymer— polymer chains interconnected with each other by chemical or physical crosslinks.

Fig.1.3 shows some schematic architecture of different polymers. It is noteworthy that polymer architecture and polymer conformation are two different concepts (refer to the section of "1.2 Polymeric chain molecules—the physical perspective").

Linear Branched Network

Fig. 1.3 Schematic architectures of different polymers.

On the microscopic level, polymers have a rich distribution of *microstructures*. Some polymers have the same molecular formula but different microstructures. People call this kind of polymer *isomeric polymer*. Usually, isomeric polymers are categorized as:

Structural isomeric polymer —In chemical repeat units atoms are arranged in different ways, for example,

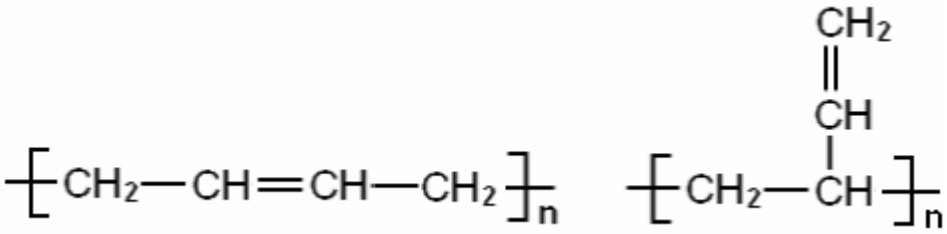

(a) cis or trans polybutadiene (b) vinyl polybutadiene

Fig. 1.4 Schematic diagram of structural isomers of polybutadiene.

Sequence isomeric polymer —In chemical repeat units the adjacencies of some functional groups is different, for example:

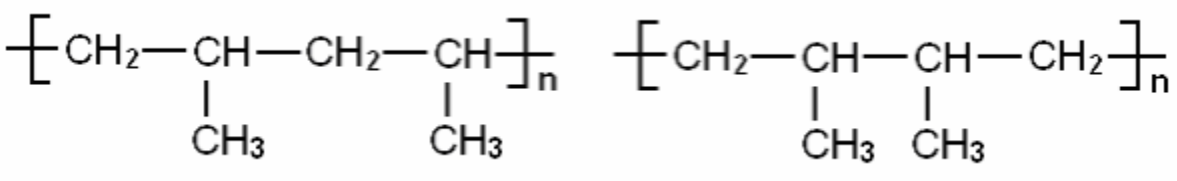

(a) Head-to-tail polypropylene (b) Head-to-head polypropylene

Fig. 1.5 Schematic diagram of two sequence isomers of polypropylene.

Stereoisomers/tacticity isomeric polymer — Side groups attach to the mainchain backbone in different arrangements:

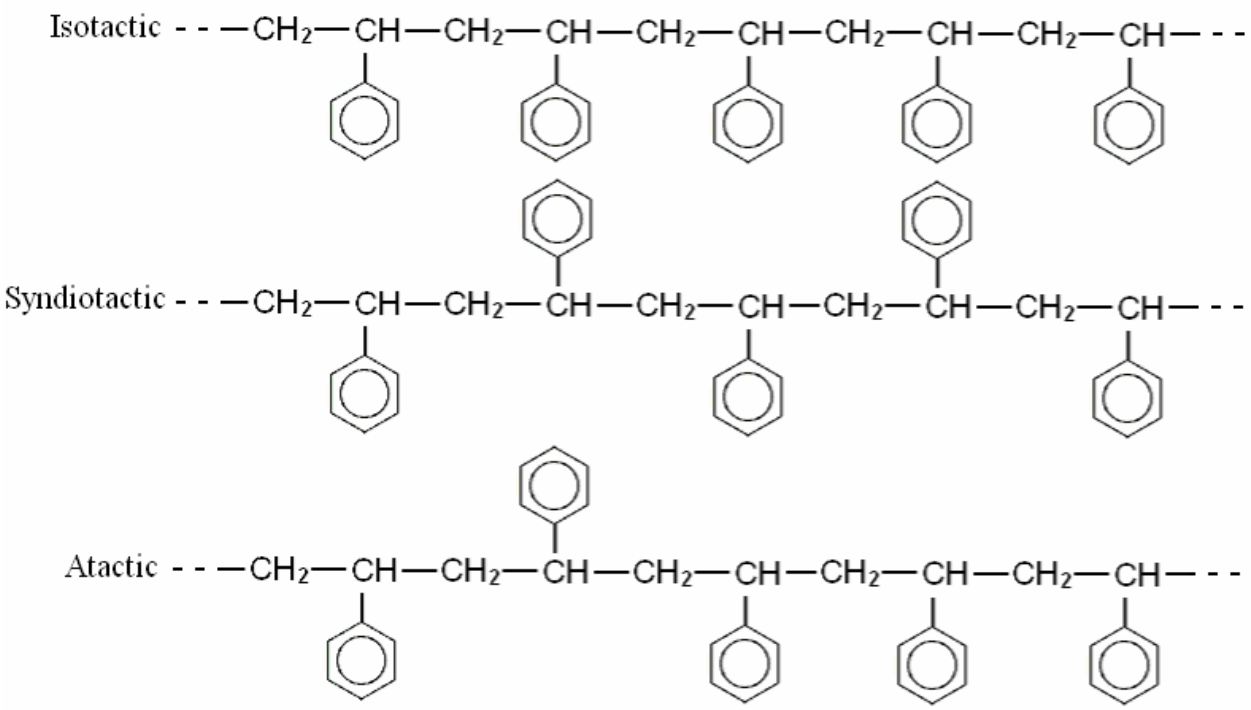

Fig. 1.6 Schematic representation of three isomers of polystyrene.

The architecture and microstructure of a polymer is fixed after the process of polymerization. To change the architecture and microstructure of a polymer it is necessary to break and reform covalent bonds in the macromolecule. In many dynamics studies of polymer systems, there is no chemical reaction involved and only physical treatments are introduced to the materials studied, such as changing of temperature, volume, pressure, or exposing to electric fields.

1.2 Polymeric chain molecules— the physical perspective

1.2.1 Characterizing polymer molecules

On the level of a single polymer molecule, the relative spatial locations of atoms or atomic groups of the long chain repeat units determine the *conformation* states of the macromolecules. The concept of long chain conformation is different from the concept of polymer chain microstructure or architecture. One can change the conformation states of polymer chains by physical treatments such as thermal or mechanical methods, but the microstructure or architecture of the macromolecules does not change during such treatments.

To understand conformation states of macromolecules having different energies, as an example, let us consider the different states of three adjacent C-C bonds in a polyethylene chain. Fig. 1.7 shows three conformation states with different energies: the green arrow shows the C-C bond with the *torsion angle* $\varphi = 0^o$, which, together with the two red C-C covalent bonds, corresponds to the *trans* state with the minimum potential energy due to the largest separation of hydrogen atoms; the two dash pink arrows indicate two *Gauche* states($\varphi = \pm 120^o$) with the local minimum energy. For a polymer molecule, there are a large number of combinations of Trans and Gauche states along the long chain. Therefore, there are many conformation states for a macromolecule with different energies.

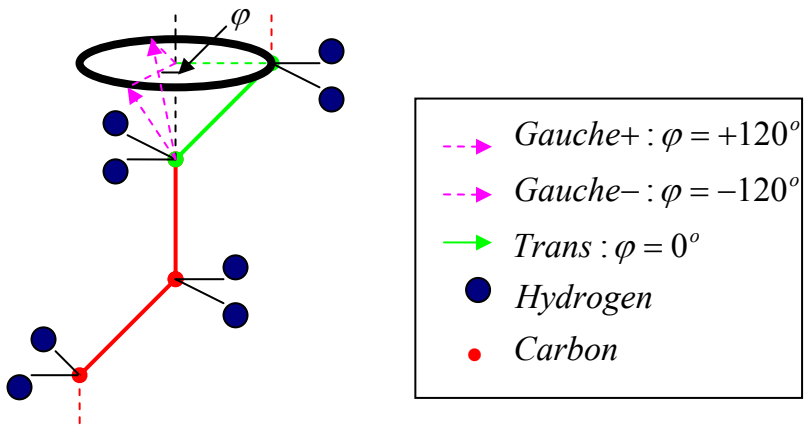

Fig.1.7 Three conformation states of three adjacent C-C bonds in a polyethylene chain (for illustrating convenience the symbols for atoms are not to scale).

As mentioned before, there are a large number of main chain bonds in a polymer molecule, which can adopt many conformation states by changing the torsion angle between adjacent mainchain bonds. To characterize the properties of polymer molecules, many chain models have been proposed. The simplest one is the *freely jointed chain model*[5], which captures the major features of polymer molecules in most cases. In this model, the polymer molecule is taken as a long chain of successively jointed vectors denoting mainchain bonds, and the angle (not torsion angle) between two neighboring vectors can be any value between $0-2\pi$. The *end-to-end vector* is the sum of all the bond vectors:

$$\vec{R}_n = \sum_{i=1}^{n} \vec{r}_i \ . \tag{1.4}$$

The *mean-square end-to-end distance* of a macromolecule is

$$\left\langle R^2 \right\rangle = \left\langle \vec{R}_n \bullet \vec{R}_n \right\rangle = \sum_{i=1}^{n}\sum_{j=1}^{n} \left\langle \vec{r}_i \bullet \vec{r}_j \right\rangle = l^2 \sum_{i=1}^{n}\sum_{j=1}^{n} \left\langle \cos\theta_{ij} \right\rangle . \tag{1.5}$$

In Eq. (1.5), $\langle\ \rangle$ denotes the ensemble average, l is the length of the bond vectors, and θ is the angle between two neighboring bond vectors. For a freely jointed chain, there is no correlation between

different bond vectors, $\left\langle \cos\theta_{ij} \right\rangle = 0$ for $i \neq j$. Therefore, the mean-square end-to-end distance of a freely jointed chain is

$$\left\langle R^2 \right\rangle = nl^2 . \tag{1.6}$$

In addition to mean-square end-to-end distance $\left\langle R^2 \right\rangle$, another variable people often used to characterize the size of a polymer chain is the *radius of gyration* R_g, which has a relation with the mean-square end-to-end distance $\left\langle R^2 \right\rangle$ as

$$\left\langle R_g{}^2 \right\rangle = \frac{\left\langle R^2 \right\rangle}{6} . \tag{1.7}$$

In cases in which the mainchain bond interactions cannot be ignored, one can use Flory's *characteristic ratio* C_n to describe the specific properties of the polymer molecules

$$\left\langle R^2 \right\rangle = l^2 \sum_{i=1}^{n} \sum_{j=1}^{n} \left\langle \cos\theta_{ij} \right\rangle = l^2 \sum_{i=1}^{n} C'_i = nl^2 C_n , \tag{1.8}$$

where $C_n = \frac{1}{n} \sum_{i=1}^{n} \sum_{j=1}^{n} \left\langle \cos\theta_{ij} \right\rangle$ is the Flory's characteristic ratio. For different polymer chain models, C_n are different [1, 4], for example the value of C_n is 9.5 for polystyrene(PS), 9.0 for poly(methyl methacrylate)(PMMA), and 4.6 for polyisoprene(PI).

In practice, there are some correlations between mainchain bonds in polymer chains and $\left\langle \cos\theta_{ij} \right\rangle \neq 0$ for $i \neq j$. However, if one considers some length scales, on which the mainchain bonds are adequately separated, the corresponding interactions between monomers is weak, and accordingly the polymer chains can then be treated as ideal freely jointed chains and Eq. (1.6) and Eq. (1.7) can still be used to estimate the size of the molecules. In this case, the original mainchain bond length l

and number of mainchain bonds n in Eq. (1.6) need to be substituted with b (*Kuhn length*) and N (number of Kuhn monomers) respectively.

1.2.2 Microscopic dynamics properties of polymers

Free energy of a polymer chain

As already mentioned, a long polymer chain can adopt a large number of microscopic conformation states. Therefore, the long chain *conformational entropy* ($S = k_B \ln \Omega$, with k_B being the Boltzmann constant and Ω the number of *long chain conformation states*) is very large. If a polymer long chain is deformed, whether compressed or elongated, its conformational entropy will be changed and accordingly its free energy will be changed as well. Many physical properties of polymer chains can be derived from their free energy [1], which is a function of chain end-to-end vector $\vec{R}$ and temperature T

$$F(N,\vec{R},T) = \frac{3}{2} k_B T \frac{\vec{R}^2}{Nb^2} + F(N,0,T) , \tag{1.9}$$

where $F(N,0,T)$ is the free energy of the polymer chain with both chain ends being together. By Eq.(1.9), real polymer chains are treated as effective Kuhn chains. As an example, we can calculate the force needed to elongate a polymer chain by distance R , as

$$\vec{f} = \frac{\partial F(N,\vec{R},T)}{\partial \vec{R}} = \frac{3k_B T}{Nb^2} \vec{R} . \tag{1.10}$$

Eq. (1.10) has a significant consequence: at a constant temperature a polymer chain can be regarded as an effective entropic spring with a "spring constant" of $3k_B T/(Nb^2)$.

Rouse model

Rouse model is a theoretical model describing the microscopic dynamics properties of polymers in the melt state. In this model, a polymer molecule is represented as a chain of N massless beads connected by $N-1$ small springs based on the "spring" like properties of Eq. (1.10).

In the polymer melt state, the total friction coefficient of a Rouse chain is $\varsigma_R (= N\varsigma_0)$, where ς_0 is the friction coefficient of one Rouse bead. According to the Einstein relation, the diffusion coefficient of the Rouse chain is

$$D_R = \frac{k_B T}{\varsigma_R}. \tag{1.11}$$

The characteristic time for a Rouse chain to diffuse a distance of the order of its own size is called the *Rouse time*

$$\tau_R \approx \frac{R^2}{D_R} = \frac{\varsigma_0 N R^2}{kT} = \frac{\varsigma_0 b^2}{k_B T} N^2 = \tau_0 N^2, \tag{1.12a}$$

where $\tau_0 = \varsigma_0 b^2 / k_B T$. Eq. (1.12a) is the relaxation time for the 1st Rouse mode with all chain segments move in the same direction. For the other Rouse mode, e. g., the pth mode, the corresponding relaxation time is

$$\tau_P \approx \tau_0 (\frac{N}{P})^2. \tag{1.12b}$$

At time $t \le \tau_R$, there are N/P unrelaxed sections or modes in a polymer chain, each of which contributes energy of $k_B T$ to the stress modulus. The total unrelaxed modulus at $t \le \tau_R$ is

$$G(t) \approx \frac{k_B T}{b^3 (N/P)} = \frac{k_B T}{b^3 N} P \approx \frac{k_B T}{b^3} (\frac{t}{\tau_0})^{-1/2}. \tag{1.12c}$$

In the following section of Maxwell model for viscoelastic materials, it will be shown that beyond the longest molecular relaxation time, the stress modulus decays exponentially. Therefore, for long time stress relaxation measurements, the Rouse model predicts

$$G(t) \approx \frac{k_B T}{b^3}(\frac{t}{\tau_0})^{-1/2} \exp(-\frac{t}{\tau_R}). \tag{1.12d}$$

In the Rouse model for unentangled polymer chain melts, the viscosity η is proportional to the degree of polymerization N

$$\eta = \int_0^\infty G(t)dt = \frac{\varsigma_0}{36b} N \approx G(\tau)\tau, \tag{1.13}$$

where $G(t)$ is the stress relaxation modulus at time t. From Eq. (1.13) we notice that for polymers in the melt state, the viscosity is proportional to the size or degree of polymerization N of polymer molecules.

de Gennes Reptation model

In network polymers or long linear polymers, the motion of a specific chain is affected by the crosslinks or the topological constraints formed by the other surrounding chains— due to the chain connectivity the chain molecules can not pass through each other. This is called *entanglement effect*. In the aforementioned Rouse model, the linear polymer chain considered is short and there is no entanglement effect involved. To study the dynamics of entangled polymers, de Gennes developed the reptation model[1, 6]. In this model, for a specific long linear polymer chain, the entanglement constraints are treated as a *confining tube*, which is shown in Fig. 1.8.

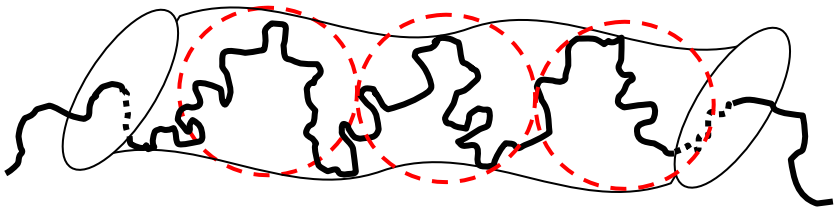

Fig. 1.8 Schematic diagram of Reptation model of an entangled polymer chain.

In Fig. 1.8, the red dash circles represent thermal blobs of size l_b. The thermal blob is defined as a subunit volume or length scale within which the polymer chain section (the *entanglement strand*) of N_e Kuhn monomers do not feel entanglement constraints and the Rouse model can be applied. The average contour length of the primitive path of the confining tube is $\langle L \rangle$ $(\approx l_b N / N_e)$. The characteristic reptation time for the specific polymer chain to move out the confining tube is

$$\tau_{rep} \approx \frac{\langle L \rangle^2}{(kT / N\varsigma_0)} = \frac{\varsigma_0 b^2}{kT} N_e^2 (\frac{N}{N_e})^3 = \tau_e (\frac{N}{N_e})^3, \tag{1.14}$$

where τ_e is the Rouse relaxation time of the entanglement strand within the thermal blob. The viscosity of entangled polymer melt is

$$\eta = \int_0^\infty G(t)dt \approx G(\tau_e)\tau_{rep} \approx G(\tau_e)\tau_e (\frac{N}{N_e})^3. \tag{1.15}$$

We note from Eq. (1.15) that the viscosity of entangled polymer melt is proportional to N^3 for polymers with the same entanglement density.

1.2.3 Viscoelastic properties of polymers

It is well known that if one applies a stress to deform a perfect elastic material within a suitable range, the work done on it is stored as the energy of deformation, which will be completely released when the applied stress is removed. This mechanism can be well described by Hooke's law of elasticity

$$\sigma = c\varepsilon, \tag{1.16}$$

where σ denotes the stress, ε denotes the strain and c denotes modulus, which could be tensile or shear modulus, conventionally represented by E and G respectively.

On the other hand, if one applies a stress to a perfect viscous liquid, the work done on it is dissipated as heat due to frictions between molecules and there is no tendency for the liquid to recover its original state. This mechanism can be well described by Newton's law of viscosity

$$\sigma = \eta \frac{d\varepsilon}{dt}, \tag{1.17}$$

where η is the viscosity of the liquid.

For polymers, however, within an intermediate range of temperatures or frequencies (e.g., in a dynamic measurement, where an oscillating field is applied to the sample), an effect or response of a complex combination of elastic and viscous properties is usually observed. That is to say, polymers behave neither like perfect elastic nor viscous materials but rather somewhere in between. This phenomenon is called *viscoelasticity*[7]. If the applied strain or rate of strain to the polymers is very small, the resulting stress will be *linearly* dependent on ε and $\dot{\varepsilon}$. This behavior is called *linear viscoelasticity*. From the previous section, we already see that long chain polymer molecules have very complex structures and there are a large number of conformation states they can adopt. For polymers to change from states to states, for example by thermal or mechanical treatments, there are many kinds of motions involved such as rotational and translational motions. Different molecular motions and complex structures of polymers are the origin of the phenomena of linear viscoelasticity.

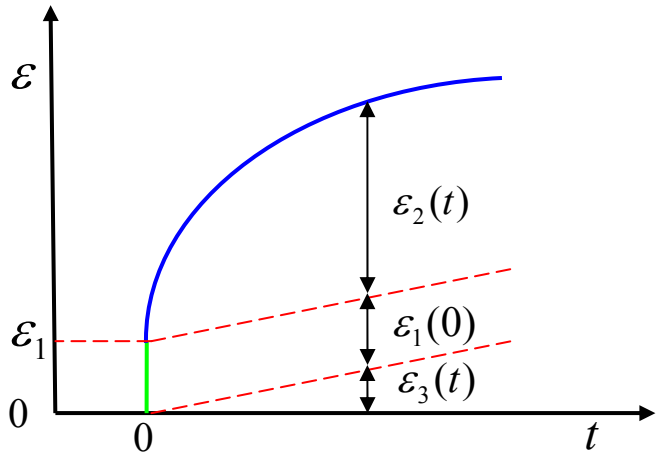

Fig. 1.9 Schematic representation of viscoelasticity phenomenon.

Fig. 1.9 shows the schematic representation of viscoelasticity phenomenon. If one applies a small stress at time 0, then a viscoelastic polymer will have an instantaneous elastic response strain ε_1, shown as the vertical green line; in the process of elastic response, some energy is stored in the material. With time elapses, the response strain ε_2 of this material develops gradually, shown as the upper blue curve; in this process, called *retarded elasticity*, there is also some energy stored, which is recoverable. The third mechanism involved is related to the viscous flow behavior, shown as ε_3, in which a small amount of energy is dissipated as heat; for crosslinked polymers(often called viscelastic solid) the amount of dissipated energy due to viscous flow is very small and can be neglected, but for uncrosslinked polymers(often called viscoelastic liquid) there is a amount of flow-dissipated energy. If the applied stress is removed at a specific moment, then the previous stored energy in the elastic and retarded elastic processes will be released and the viscoelastic material recover its original shape partially—the flow process induced deformation is irreversible.

The viscoelastic properties can usually be exhibited by the well-known Maxwell and Kelvin(or Voigt) models[2], in both of which the combination of *elastic springs* and *viscous dashpots* is considered. In the Maxwell model, a spring and a dashpot are in series; while in the Kelvin model, the two components are in parallel. The schematic representations for the two models are shown in Fig. 1.10.

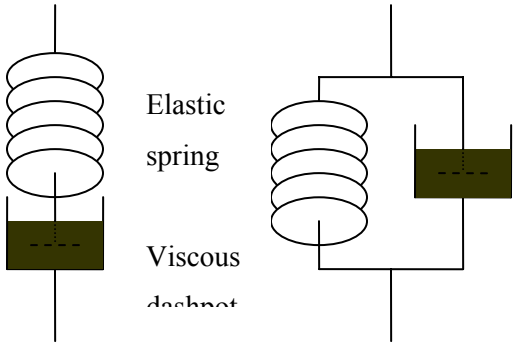

(a) Maxwell model (b) Kelvin model

Fig. 1.10 Schematic representations for the two models for viscoelastic materials.

Using the relation of Eq. (1.16) and Eq. (1.17), the Maxwell model predicts

$$\sigma = \sigma_0 \exp(-\frac{ct}{\eta}) = \sigma_0 \exp(-\frac{t}{\tau}), \tag{1.18}$$

where $\tau = \eta / c$ is the characteristic relaxation time. Similarly, the Kelvin model predicts

$$\varepsilon = \frac{\sigma_0}{c}\left[1 - \exp(-\frac{t}{\tau})\right]. \tag{1.19}$$

From Eq. (1.18) and Eq. (1.19), we see that for viscoelastic materials the response σ and ε develop with time following an exponential law. Also, we should note from these two models that viscoelastic does not mean simple addition of pure elastic and viscous effects, but rather a complex retarded procedure is involved.

1.2.4 Superposition principles for viscoelastic polymers

Boltzmann superposition principle

This principle states that the linear viscoelastic response of a polymer system is dependent on the history of the applied loads, which have their own independent contributions to the final response, and all the specific contributions are additive

$$\varepsilon(t) = \int_{-\infty}^{t} J(t-t')d\sigma(t') \quad or \quad \sigma(t) = \int_{-\infty}^{t} G(t-t')d\varepsilon(t'). \tag{1.20}$$

In the above equation, the response strain ε or stress σ is a function of compliance J or modulus G. Consider a simple two-step stress loading creep measurement. Fig. 1.11 is the schematic representation strain response: at time t_1 a stress σ_1 is applied to a polymer sample, which results in a strain shown as the black and dash curve; at time t_2 another stress σ_2 is applied, which has a strain contribution shown as the upper solid curve (pink); the resultant strain response[8] is

$$\varepsilon(t) = J(t-t_1)\sigma_1 + J(t-t_2)\sigma_2. \tag{1.21}$$

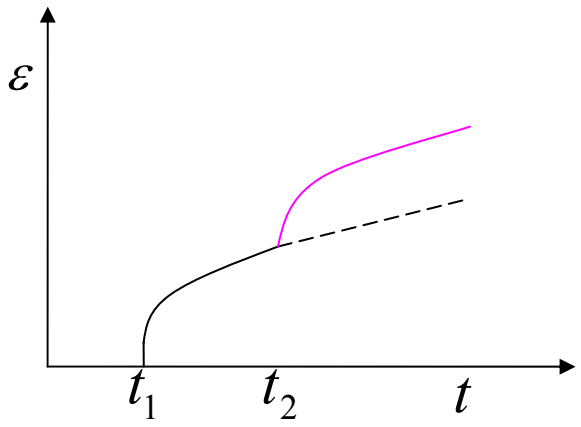

Fig. 1.11 Schematic strain response of a sample polymer.

Time temperature superposition principle

We have seen that the aforementioned Boltzmann superposition principle describes viscoelastic properties of polymers in the time domain [9]. From dynamics theories such as the Rouse model and de Gennes repetition model, we see that some dynamics properties such as relaxation times and viscosities, are a function of temperature as well. We can imagine that if we increase the temperature from a reference temperature for a viscoelastic polymer, the motions involved in the viscoelastic response of the polymer can be speed up. Therefore, suppose in a creep experiment, a strain response as a result of a long waiting time from the application of a constant stress at a relatively low temperature can be reached after a relatively short period of time in another creep experiment at a relatively higher temperature using the same stress. That is, for viscoelastic responses of polymers *time* and *temperature* are equivalent: long times or low frequencies (in dynamic measurements) correspond to high temperatures. This is often called *time temperature superposition principle.* We should note that this principle can be valid if only one major relaxation process is probed and within the experimental frequency or time range the shape of the sample response is not changed. One example of time temperature superposition principle is the famous Williams-Landel-Ferry (WLF) equation, which is valid for a wide variety of polymers,

$$\log a_T = \log \frac{\tau(T)}{\tau(T_{ref})} = \frac{-C_1(T - T_{ref})}{C_2 + (T - T_{ref})}, \tag{1.22}$$

where if the reference temperature T_{ref} is chosen as the glass transition temperature T_g, then $C_1 = 17.44K$ and $C_2 = 51.6K$ are suitable for most polymers; $\log a_T$ is the so called *shift factor*, which can be used to construct a composite master curve[10] from some measurements within a relatively short time range at some specific temperatures.

Chapter 2

Introduction B— Glass transition and glass transition in polymers

2.1 Present general picture of the glass transition phenomena

Almost all materials on earth can undergo *glass transition* if we cool them fast enough from the liquid state. That is, materials will change from the liquid or rubbery state (in case of polymer) with low viscosity, e.g., on the order of 10^{-3} Pa·s for normal liquid, to the glassy state (with much higher viscosity, e.g., of the order of 10^{13} Pa·s) without major structural change— *glasses are actual amorphous solid with liquid-like structures*. The reason that a fast cooling rate is necessary to form a glass is that under fast cooling conditions the kinetic energy of the molecules reduces dramatically and the molecules move so slowly and do not have enough time to fully relax to reach the equilibrium state within the experimental time scale. In addition, different fast cooling rates result in different glassy states, which are not equilibrium thermal dynamics states but with a trend evolving toward the final equilibrium states. During the glass transition there is no pronounced structural change and accordingly there is no large change in molecular potential energy and no latent heat involved, but there are dramatic changes in molecular motions. Therefore, the glass transition is a type of kinetic arrest phenomena [11, 12] other than thermal dynamic phase transition. The glass transition

phenomenon is related more to dramatic particle or molecular kinetic energy variation than to potential energy change.

There are a variety of methods to define a glass transition temperature such as by dielectric [13], mechanical[14] and thermodynamic or calorimetric [15] measurements. Conventionally, the glass transition temperature is the temperature where the viscosity of glass forming materials reaches 10^{13} Pa·s or the temperature where the molecular relaxation of the sample materials is approximately 100 seconds. Fig. 2.1 schematically shows an example of glass transition temperature definition in thermodynamic measurements of the specific volume as a function of temperature, in which the glass transition temperatures are defined as the intersection of the extrapolation lines from both the melt and glass states. The green curve qualitatively represents a measurement with a lower cooling rate compared with the upper blue curve. We see that a higher cooling rate usually results in a higher glass transition temperature. Although the experimentally measured glass transition temperatures are cooling rate dependent, the variation of their values is around 3 to 5 Kelvin when the cooling rates change by an order of magnitude [16]. Therefore, the glass transition temperature is an important property parameter for glass forming materials. In Fig. 2.1, T_m is the melting temperature and T_k is the Kauzmann temperature[17] at which the supercooled liquid is supposed to have the same specific volume or entropy as that of the well ordered crystal.

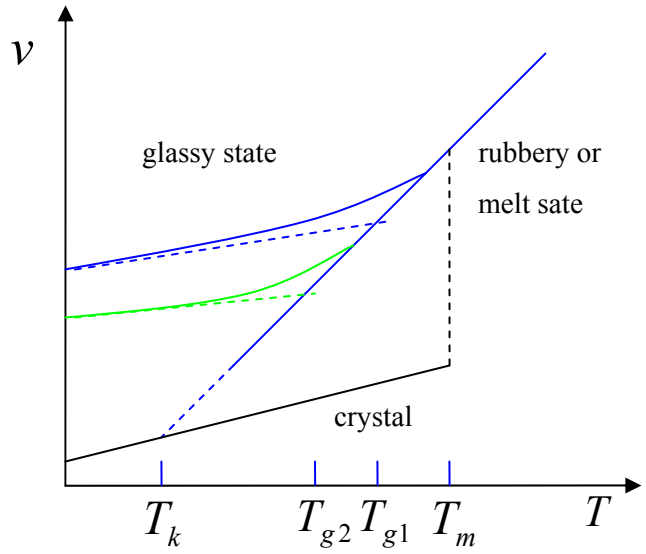

Fig. 2.1 Schematic illustration of glass transition definition(based on Ref.[16] &Ref. [18]).

The nature of glass transition is still an open question despite long-time considerable experimental and theoretical research efforts—"the deepest problem in condensed matter physics"[18, 19, 20, 21, 22, 23]. Generally speaking, a current picture or view of glass transition can be schematically summarized in Fig. 2.2, in which the vertical axis is the molecular relaxation time on the logarithmic scale and horizontal axis the inverse temperature. For a glass forming system, at high temperatures molecules (or chain segments for polymer material) have fast motions and accordingly can freely sample system configurations within relatively short times; the whole system is in the equilibrium and *dynamically homogeneous state* without long range orders. In the case of thin polymer film systems, studies [24, 25] show that at or higher than a temperature of ~8K above bulk glass transition temperature the local surface region and the bulk material region have the same molecular dynamics. When the system temperature decreases with a fast cooling rate, the molecular mobility decrease with increasing molecular relaxation times; when the temperature is low enough, the molecules move so slow that they do not have enough time to samples most system configurations to reach the equilibrium state—in most cases, for some specific molecules their neighboring counterparts tend to form *cages* surrounding them and these molecules can only rattle within such cages. In one glass transition theory—the mode coupling theory (which will be described in more detail later), the phenomena of kinetic arrest occurs at the critical temperature T_c. Because the mode coupling theory is based on molecular diffusion motion mechanism, it can only be applicable within a temperature range higher than the critical temperature T_c. The problem is that the experimentally observed glass transition temperature T_g is lower than T_c by ~20 percent. Up to now, there no successful theory addressing dynamical features below the temperature of $1.2\,T_g$, especially between T_c and T_g. For glass forming systems at temperatures lower than T_c, most part of the glass systems are kinetically frozen but with some mobile clusters sporadically separated in the whole system and within the mobile clusters particles can only relax through *cooperative motion*. The concept of cooperative motion, which is a significant concept in glass studies, was first proposed by Adam and Gibbs in their seminal paper [26], in which they postulated that in a supercooled glass forming liquid there are many local mobile regions within which particles relax *independently and simultaneously* and there is no correlation between different mobile clusters. Basing on this important cooperative motion concept, people have improved a lot in understanding the glass transition by studying the distribution, characteristic length, dimension and correlation of clusters(mostly by computer simulations) of

cooperative relaxing molecules [27, 28, 29, 30, 31, 32]. Compared with homogeneous dynamics in glass forming systems at temperature higher than T_c, the dynamics of glass forming systems at temperatures around and below T_g are *heterogeneous*. On the one hand, different regions of the system studied have different degree of dynamics—some regions have high molecular mobilities but other regions with slow molecular mobilities. In Fig. 2.2, the different dynamics of different sub-regions are shown using different colors and the shape and dimensions of different mobile region are different as well. Some studies show that with decreasing temperatures, the characterestic size of the mobile regions increases [28, 33, 34, 35, 36, 37]. In the present studies for thin polymer systems [see chapter 5 and chapter 7], when the experimental temperatures are close or below the bulk material glass transition temperature T_g, the temperature dependence of relaxations in the near free surface region is different from that of the bulk materials. On the other hand, the location of mobile regions is time evolved—any particles have chances to relax within a wide enough experimental observation window [25, 38].

In Fig. 2.2, we should also note that the molecular alpha relaxation times have a strong temperature dependence: with decreasing temperatures the value of alpha relaxation times increase dramatically, which is closely related to the dramatically reduction in molecular motions. Such phenomena can usually be described by Vogel-Fulcher-Tammann (VFT) equation [39, 40]

$$\tau_\alpha(T) = \tau_\infty \exp(\frac{B}{T - T_V}). \tag{2.1}$$

In the VFT equation, $\tau_\infty (\sim 10^{-12}\,\mathrm{s})$ is the high temperature relaxation time and T_V is the *Vogel temperature*, at which the alpha relaxation time diverges. One should note that the VFT equation does not hold in some temperature ranges [40, 41]. For example, for Glycerol when the temperature is higher than 413K, the Arrhenius behavior is observed which corresponds to $T_V = 0K$ [39]; for Polystyrene when the temperature is below ~350K, VFT equation is not valid[42,43].

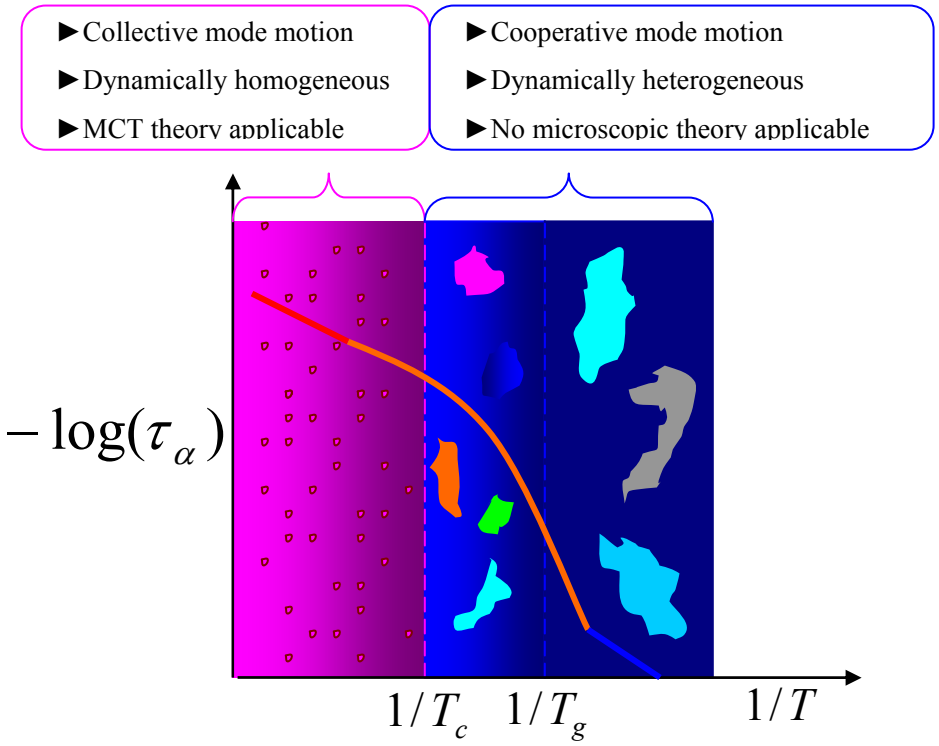

Fig. 2.2 Current picture or view of the glass transition; the bold red curve, orange curve and blue curve schematically depict high T Arrhenius, around T_g VFT and low T Arrhenius behavior respectively; the irregular sub-regions show CRR's with different mobilities.

In the foregoing section, the phenomenon of glass transition and the corresponding current picture are briefly outlined. As has been pointed out, the glass transition is not thermodynamic phase transition and there are no fixed or definite T_g values for glass forming materials. It is well known that for bulk materials the measured glass transition temperatures depend on the way and the history the materials is cooled or heated. In the following section of "2.3 Glass transition, dynamics and structure studies of polymers on nanometer scales", we will see that the glass transition occurs within a pronounced transition range which is broadened when the polymer films are thin enough.

2.2 Glass transition theories

2.2.1 Free volume theory

The free volume theory for molecular relaxations in liquids can be traced back to the early twentieth century and is based on contributions from many researchers, for example, Eyring, Doolittle, Williams, Landel, and Ferry[44]. However, the central concept in the theoretical frame, the *free volume*, has no rigorous physical definition. Generally, the free volume can be treated as the volume accessible to mobile molecules. Since in different liquid systems molecular compressibilities and packing (accordingly potential fields) may be different, the free volumes may be system dependent. In other words, the concept of free volume is actually an average physical quantity treatment which may be coupled to many physical quantities, for example, system temperature, pressure, inter- and intra-molecular interactions, material density, and so on. According to Doolittle[45],

$$v_f(T) = v(T) - v_o, \tag{2.2}$$

where $v_f(T)$ is the free volume per unit mass and $v(T)$ is the specific volume, both being a function of temperature T. The quantity v_o is the molecular occupied volume with a constant value at the absolute temperature zero degree. When applying to glass forming systems, especially approach or beyond the glass transition from the liquid side, the concept of the free volume is problematic. Since in the frame of the free volume theory the free volume is a statistical average quantity determined from equilibrium states, it smears out the effects of dynamical relaxation time distributions or dynamics heterogeneity. In addition, in the free volume approach, the molecular mobility is determined by or depends on the available free volume, which may be also questionable. A spacious free volume does not necessarily induce enhanced molecular mobility; molecules with sufficiently rapid motions can produce more free volume. When a liquid is cooled down, the molecular mobility decreases, which may be followed with reduced free volume. Therefore, the free volume can serve as a measure of the molecular mobility. Some study shows that the glass transition is not due to the lack of free volume [46]. It is possible that the glass transition can happen at a constant sample volume [47]. There is experimental evidence showing that there is no direct correlation between the free volume and the fast dynamics of compressed polymers [48]. In [49] by molecular dynamics computer

simulations, it is also shown that the dynamics of glass forming materials can be slowed down without changing the free volume.

The free volume theory for the description of the viscosity or relaxation time of small molecule liquids or polymers at temperatures above the glass transition temperatures are based on two unsubstantiated assumptions and accordingly it is a phenomenological theory. This first assumption was proposed by Doolittle [50], which relates the viscosity of the liquids to the free volume in the form

$$\eta = a\exp(\frac{b}{f(T)}), \tag{2.3}$$

where a and b are constants and $f(T) = v_f / v$ is the fractional free volume. The other assumption states that the fractional free volume increase linearly with temperatures above T_g according to

$$f(T) = f(T_g) + \alpha(T - T_g), \tag{2.4}$$

where α is the thermal expansion coefficient of the free volume. By introducing the above two assumptions to the well known Williams-Landel-Ferry equation, a useful relation can be reached, which describes the temperature dependence of relaxation times or viscosity and is almost always applicable to most polymers,

$$\begin{aligned}\log a_T &= \log\frac{\tau(T)}{\tau(T_g)} \approx \log\frac{\eta(T)}{\eta(T_g)} = \frac{b}{(1/\log(e))}(\frac{1}{f(T)} - \frac{1}{f(T_g)}) \\ &= \frac{-(b/2.303 f(T_g))(T - T_g)}{f(T_g)/\alpha + (T - T_g)} = \frac{-c_1(T - T_g)}{c_2 + (T - T_g)}\end{aligned} \tag{2.5}$$

where c_1 and c_2 are almost constant for most polymers with values of 17.44K and 51.6K respectively and $f(T_g) = 0.025$. Since c_1 and c_2 have almost fixed mean values, the above equation is often called the "universal relation" for polymers.

There might be some points one should pay more attention when considering the free volume theories. Firstly, as has been mentioned, the reduction in free volume with temperature may rather be the result than the cause for reduced molecular mobility. Secondly, for a system where thermodynamics or thermal energy involved the three quantities of pressure P, volume V and temperature T are usually convoluted. Therefore, in equation (2.2) the free fractional volume may be a function of both pressure P and temperature T. Thirdly, although there is no substantial base for the free volume theory especially for the two foundational assumptions in equation (2.3) and (2.4), the success of this theory in relating the relaxation times or viscosity of liquids to temperature is rather appreciable and a prudent investigation of the physical picture behind these two assumptions may help improving our understanding of the nature of the well known unresolved puzzle of the glass transition. Last but not the least, the free volume theory is applicable to the liquid state where the free volume is treated as a thermodynamics average quantity and no heterogeneous dynamics, which is more pronounced when a glass forming system approaches the glass transition zone from the liquid side, are considered.

2.2.2 Adam-Gibbs molecular-kinetic theory

In 1965, Adam and Gibbs [26] developed a molecular kinetic theory focusing on describing the temperature dependence of time relaxation behavior of glass forming liquids or polymers in terms of the variation of the configurational entropy of the *cooperatively rearranging region(CRR)*. Although it did not give any interpretation of the mechanism of the glass forming process, e.g., how the CRR's are distributed or what is the explicit temperature dependence of the size of CRR's, this theory does predict the relaxation behavior of glass forming materials which coincides with the empirical WLF equation. What is more important is that it introduced and applied a very important concept of cooperatively rearranging region, which is still heavily cited and tested by many researchers today [27, 28, 29, 30, 35, 36, 37, 51]. For super-cooled glass forming liquids, the individual molecule(/polymer chain segment) has very slow mobility and can not maintain molecular motion individually, but it can somehow move or wiggle depending on cooperative rearranging motions of the neighboring molecules.

Within the Adam-Gibbs molecular kinetic theory frame, the glass forming material systems are assumed to be "an isothermal-isobaric ensemble of small systems of the size of the cooperatively rearranging region." One should note that such cooperatively rearranging regions are independent of each other and independent of the environments as well. That is to say, the CRR's are freely self-relaxing domains without or with weak interactions with each other or with any boundary interfaces. This picture about glass forming systems is different with the present concept of spatially and temporarily evolving heterogeneous dynamics. In addition, this theory treats the glass forming systems in the equilibrium states and after adequate thermal fluctuations one CRR can rearrange from one configuration into other configurations. Being different from the free volume theory, in which the physical relaxation quantities (e.g. the system relaxation time or viscosity) are described in terms of the temperature variation of free volumes, the Adam-Gibbs molecular kinetic theory calculated the temperature variation of the configurational entropy of the glass forming systems. If the average number of molecules or polymer chain segments in one CRR is z and the chemical potential or molecular/segmental potential energy barrier is μ, then the Gibbs free energy is $G(=z\mu)$ and the probability of cooperatively rearranging configuration transition is

$$W(T) = A\exp(\frac{-z\Delta\mu}{k_B T}), \tag{2.6}$$

where k_B is Boltzmaan constant. To get the average configuration transition probability, all values of $W(T)$ corresponding to different CRR's of different z should be summed over:

$$\overline{W(T)} = \sum_{z=z^*}^{\infty} A\exp(\frac{-z\Delta\mu}{k_B T}) = B\exp(\frac{-z^*\Delta\mu}{k_B T}), \tag{2.7}$$

where z^* is the lower limit of the size of CRR's that can have nonzero configuration transition probabilities and B is a constant.

If a macroscopic glass forming system has N CRR's and the configurational entropy of one CRR is s_c, then the total configurational entropy should be

$$S_c = Ns_c = N\left[k_B \ln(W_c^{1/N})\right], \tag{2.8}$$

where W_c is the total number of cooperatively rearranging configurations of the macroscopic system. If the macroscopic system has one mole of molecules or segments, then

$$S_c = \frac{N_A}{z} s_c = \frac{N_A}{z}\left[k_B \ln(W_c^{z/N_A})\right], \tag{2.9}$$

where N_A is Avogadro's number. To describe the macroscopic configurational entropy S_c in terms of the lower limit CRR size z^*, we get the flowing relation

$$S_c = \frac{N_A}{z^*} s_c^*. \tag{2.10}$$

Combining Eq. (2.7) and (2.10), we get

$$\overline{W(T)} = B\exp(\frac{-\Delta\mu N_A s_c^*}{k_B T S_c}) = B\exp(-\frac{C}{TS_c}). \tag{2.11}$$

The system relaxation time is related to the configurational transition probability according to

$$\tau(T) \propto \frac{1}{\overline{W(T)}} \approx \exp(\frac{C}{TS_c}), \tag{2.12}$$

where the configurational entropy S_c is a function of temperature as well. The WLF equation can now be obtained

$$\log(\frac{\tau(T)}{\tau(T_r)}) = \frac{C}{T}\left[\frac{1}{S_c(T)} - \frac{1}{S_c(T_r)}\right], \tag{2.13}$$

where T_r is the reference temperature.

Considering $S_c^b - S_c^a = \int_{T_a}^{T_b} \frac{\Delta C_P}{T} dT$ and the configurational entropy at the second order phase transition $S_c(T_2) = 0$, equ (2.13) can be transferred to the following general WLF form

$$\log a_T = \log(\frac{\tau(T)}{\tau(T_r)}) = \frac{-c_1(T - T_r)}{c_2 + T - T_r}, \tag{2.14}$$

where

$$c_1 = 2.303 \frac{C}{\Delta C_P T_r \ln(T_r / T_2)}$$

and

$$c_2 = \frac{T_r \ln(T_r / T_2)}{\ln(T_r / T_2) + \left[1 + T_r /(T - T_r)\right] \ln(T / T_r)}.$$

By comparing the theoretical prediction of equ (2.14) with experimental data of ~20 different glass forming liquids, the above Adam-Gibbs molecular kinetic theory reaches the following relation between the conventional glass transition temperature T_g and the ideal second order phase transition temperature $T_2 : T_g - T_2 = 55°C \pm 10.9\%$. Therefore, for most glass forming materials the second order phase transition temperature is about $55°C$ below the glass transition temperature. Although, the concept of the second order phase transition is still under debate, the estimation of a temperature ($\sim 55°C$ below T_g) at or below which the configurational entropy vanish is in agreement with other theoretical prediction that the relaxation time of glass forming systems diverge around such a temperature.

2.2.3 Mode coupling theory

The mode coupling theory [52, 53, 54, 55] is based on the stochastic differential equation (Langevin) initially developed for Brownian motion of particles in simple liquids or colloidal suspensions. It is the only theory that microscopically explains some aspects of the singular glass transition phenomena in terms of both the liquid structure and molecular motions.

The density in a liquid can be expressed as

$$\rho(\vec{r},t) = \sum_i \delta(\vec{r} - \vec{r}_i(t)), \tag{2.15}$$

In the Fourier reciprocal space domain, the liquid density is

$$\rho_k(t) = \sum_i \int e^{i\vec{k}\bullet\vec{r}} \delta(\vec{r} - \vec{r}_i(t)) = \sum_i e^{i\vec{k}\bullet\vec{r}(t)}, \tag{2.16}$$

The density-density correlation function, which is usually termed as intermediate scattering factor in scattering measurements, is

$$F(k,t) = \sum_{ij} e^{i\vec{k}\bullet\vec{r}_i(0)} e^{i\vec{k}\bullet\vec{r}_j(t)}, \tag{2.17}$$

The generalized Langevin equation is

$$\frac{dF(t)}{dt} = i\Omega_0 F(t) - \int_0^t M(t')F(t-t')dt' + R(t), \tag{2.18}$$

where Ω_0 is a constant related to some variables such as temperature and molecular mass, $M(t)$ is the memory kernel (because it is related to the past density-density correlation function), and $R(t)$ is the random force. To solve the above Langevin equation, Götze treated the memory kernel as a function of density-density correlation function $F(t)$

$$M(t) = c_1 F(t) + c_2 (F(t))^2. \tag{2.19}$$

Treating the memory kernel as a nonlinear function of density-density correlation is the major point of the so-called mode coupling theory. In the memory kernel of equ (2.19), the two coupling

parameters c_1 and c_2 are the kinetic mode coupling parameters, which may be functions of temperature or pressure. Many nonlinear mechanisms such as particle caging and cage-breaking and feedback or backflow can be modeled by such kinetic mode coupling parameters.

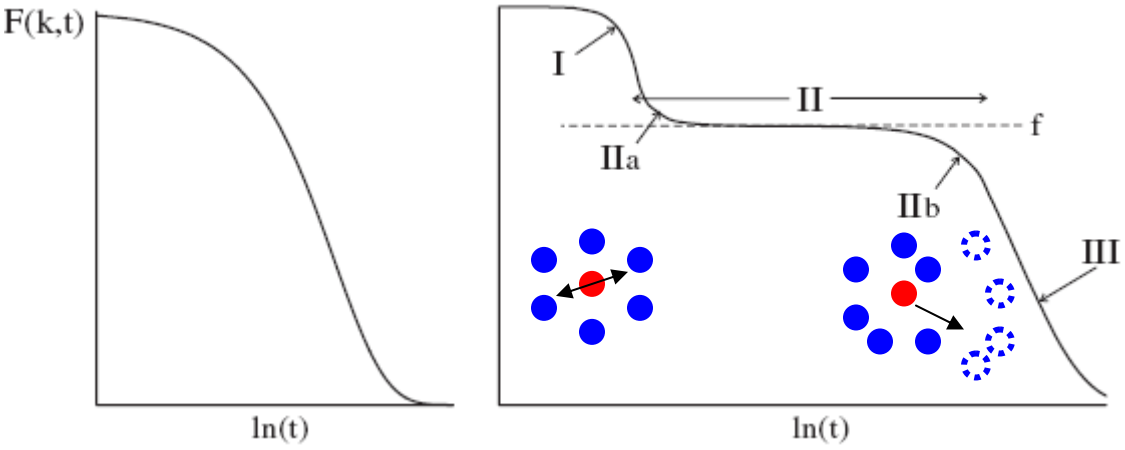

Fig. 2.3. Schematic diagram of the MCT prediction of the density-density correlation function $F(k,t)$ for liquids at high temperature (left) and low temperature (right). (Modified Graph based on [54])

Fig. 2.3 schematically shows the mode coupling theory predictions for liquids at different temperatures. For liquids at temperatures higher than the melting temperatures (normal liquids), the density-density correlation function $F(k,t)$ decays following a single exponential function, shown as the left graph. For super-cooled liquids at lower temperatures(right graph), the $F(k,t)$ shows a two-step decay characterization. At short time scales (regime I), the fast $F(k,t)$ decay reflects molecular collision events related to local dynamics, which is often called cage rattling— the red probe molecule in the center rattles in the transient cage formed by the neighboring blue molecules. The molecular rattling process with the caging constraints is the β relaxation. At long time scales (regime III), $F(k,t)$ decays following a stretched exponential function

$$F(k,t) \approx e^{-(t/\tau)^{\beta}}, \tag{2.20}$$

where $0 < \beta < 1$, and τ is the characteristic relaxation time. The corresponding microscopic molecular process at this long time scale is related to cage-door opening and probe molecule escaping or diffusing dynamics, which is the α relaxation process. One should note that after escaping from the old cage, the probe molecule run into a new transient cage formed partially by its new neighboring molecules (shown as dash circles). At intermediate time scales (regime II), the probe molecule experiences the transition from the β to α relaxation process. If the density-density correlation function $F(k,t)$ vanishes at finite time scales, the liquids at the corresponding temperatures are in the ergodic super-cooled states— here the ergodic means that in finite time window the sample liquid can adapt all possible configurations(the time average is equal to the ensemble average). Otherwise, if $F(k,t)$ maintains a plateau even after infinite times, the liquids are in the non-ergodic glassy state. The highest temperature at which the liquid systems transit from the ergodic super-cooled states to non-ergodic glassy states is the MCT *critical temperature* T_c, which is the mode coupling theory predicted glass transition temperature. The relaxation time $\tau(T)$ relates to T_c according to

$$\tau(T) \sim (T - T_c)^{-\gamma}. \tag{2.21}$$

The major success of the mode coupling theory is that it microscopically explain multiple-stepped pattern of the β to α process and the corresponding transition zone. However, there is also a well-known failure for MCT— the predicted critical temperature is about 1.2 times of the experimentally observed glass transition temperature T_g for most glass forming systems, which means that the MCT kinetic arrest happens while the glass forming systems are still in the ergodic super-cooled liquid state. This is natural actually since MCT is based on or studies the molecular diffusion mechanism and the theoretical predicted kinetic arrest should be referred to the arrest of diffusion processes which should occur at temperatures above T_g. That is to say, the model coupling theory is only suitable to super-cooled liquids at temperatures above $\sim 1.2T_g$. In addition, MCT treats glass forming systems in the ergodic liquid states and provides no information about the temporal-spatial dynamical heterogeneity(such as the variations in the size of some mobile CRR clusters), which is pronounced especially around T_g. Moreover, in ref. [54], we note that the glass forming systems transit from the

ergodic liquid states to non-ergodic solid states at a critical temperature T_c and Reichman and Charbonneau say that "However, no information of an ordered state was used or imposed. Thus, the solid could only be a disordered one, i.e. *a glass*." This means that in the mode coupling theory there is no solid or explicit theoretical evidence showing that the solid is a real amorphous glass or not.

2.2.4 Edwards tube theory

As mentioned before, in long linear polymer melt polymer chain molecules expose topological constraints on each other. This is usually called the chain entanglement effect because polymer chains can not pass through each other. To address the glass transition phenomena in entangled polymer melt, Edwards developed a tube model, in which any specific polymeric chain molecule is confined in a tube, which is formed by the topological constraints of the surrounding molecules. In addition, to reduce considerable analytical difficulties, the curved tube is further simplified and the polymeric chain molecule in the tube is represented as a rigid rod in the Edwards glass transition theory. Fig. 2.4 shows the schematic representations of polymeric chain molecules in the Edwards tube model: in graph (a), the curved entanglement tube is treated as a rod tube; in graph(b), the polymeric chain molecules are represented as rigid rods, which have "much reduced rotational freedom" and can only have translational diffusion motions within the tube; the motions of the rigid rod molecules can be blocked or allowed by the surrounding other rigid rod molecules (see graph (c) in Fig. 2.4).

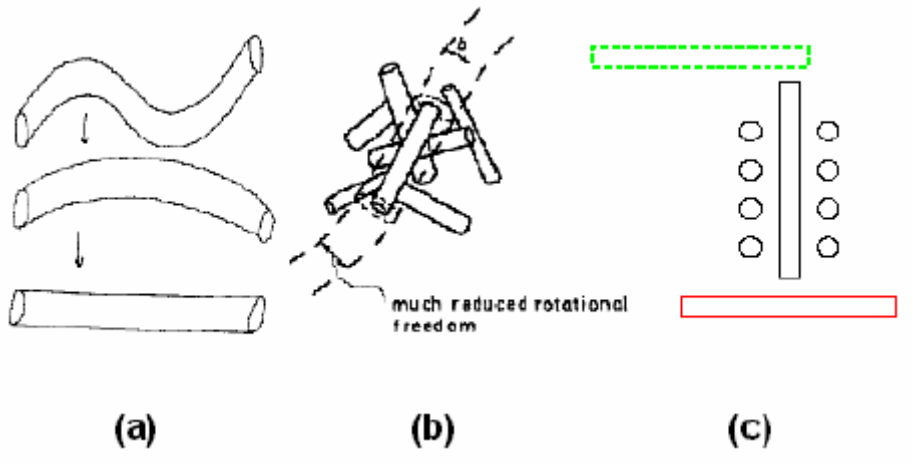

Fig. 2.4 Schematic representations of polymeric chain molecules in the Edwards tube model.((a) and (b) from[68] and [69] respectively)

The theoretical analysis of the Edwards tube model can be found in [69], which is briefly outlined here. Suppose the length of the rigid rod molecules is L, the free translational diffusion constant (without blockages from other molecules) is D_0, and the time for the test rod molecule to diffuse a distance of a is t_a. Then we have

$$D_0 \propto \frac{a^2}{t_a}. \tag{2.22}$$

If we assume a is the average distance between blocking barriers of rod molecules and each of which remains on for an average time τ, then the diffusion constant with blocking barriers considered is

$$D \propto \frac{a^2}{t_a + g\tau(L/a)} = \frac{a^2/t_a}{1 + g\tau(L/at_a)} = \frac{D_0}{1 + g\tau(L/at_a)}, \tag{2.23}$$

where g is a constant. Since the barrier rod molecules are also affected by other molecules, we have

$$D \propto \frac{L^2}{\tau}. \tag{2.24}$$

From the combination of Eq. 2.22, 2.23, and 2.24, we get

$$D \propto \frac{D_0}{(1 + g\frac{L^3 D_0}{a^3 D})} \approx D_0(1 - gL^3/a^3) \approx D_0[1 - C(cdL^2)^{3/2}], \tag{2.25}$$

where C is a constant, c is the molecular concentration, and d is the diameter of the rod molecules. Therefore, we see that the rod molecule diffusion constant decreases with increasing molecular concentration, and when $c \sim 1/L^2 d$ the rod molecule diffusion motion ceases. As in colloidal glass forming systems [28], the molecular concentration has the same effect as temperature— increasing concentration corresponds to decreasing temperature. In [69], it is shown that both d and D_0 depend

on temperature. Based on Eq. 2.25, some typical features of polymeric glass forming systems, such as the VFT behavior and T_g of polymer blends(Fox-Flory relation), can be reconstructed. The major point of the Edwards tube theory is that the molecular motions around the glass transition is cooperative, which can be completely ceased at high enough concentration or low enough temperature.

2.3 Glass transition, dynamics and structure studies of polymers on nanometer scales

As already mentioned in the previous sections, our understanding of the glass transition is still very limited and the nature of such phenomenon remains a challenge in the field of condensed matter physics. One wise way to resolve such puzzle is to conduct studies methodologically. On the one hand, the studies of some specific aspects first may help improving our understandings about the glass transition. One promising method may be the studies the dynamics of glass forming materials. Some outstanding unresolved issues about the glass transition are: (1) Is there or/and what is the explicit form of the characteristic length scale of the dynamics related to glass transition? (2) Is the glass transition related non-exponential decay behavior of some relaxation functions the collective contribution of many local regions with exponential decay dynamics or the local dynamics themselves are non-exponential[30,56]? (3) Are the glass transition related dynamics of the same mechanism in different glass forming materials? On the other hand, we need to study some model systems using different probe techniques and extract some universal features (if any) of the elusive glass transition by comparing different study results. Also, such model systems or materials should be easily accessible and experimentally manageable, for example in terms of experiment conditions such as time, pressure and temperature. It has been shown through many research efforts that polymers are one suitable model candidate for such studies.

As for the availability of polymers, nowadays chemists can produce polymers by some routine polymerization methods and there are a variety of different polymers available to researchers. In addition, due to the high viscosity of polymers, one can make polymer glasses using experimentally manageable means, for example, by moderate cooling rates ~1-20K/min or fast solvent evaporation

methods. As for the properties of polymers, there are some different length scales and different motions in polymer materials, which may contribute differently to the glass transition. Furthermore, people can make polymer glasses in a variety of dimensions from several micrometers to a few nanometers using some conventional methods, such as polymer solution dipping technique and the spincoating technique. The studies of polymers on the mesoscopic scale, where the finite size effects and/or chain confinement effects may dominate, can make it possible to investigate the local dynamics and some characteristic correlation length scales involved in the glass transition. All these advantages make polymers a suitable model system for studying the glass transition phenomena.

The first study of the glass transition of thin polymer films is conducted by Beaucage, Composto and Stein [57] in 1993. In their original study, the authors observed the glass transition temperature for Polystyrene films ~300nm on Silicon wafers using a novel technique—ellipsometry, by which the refractive index and thickness of the polystyrene films can be measured as a function of temperatures and specific cooling or heating procedures. In addition, the authors predicted that there might be some film thickness dependence for the glass transition temperatures and such glass transition shifts might be observed for the other polymer films such as poly (methyl methacrylate) (PMMA). The subsequent researches proved all the observations and predictions of this seminal work. In 1994, Keddie, Jones and Cory [58] conducted an extensive study of the glass transition of Silicon-supported thin Polystyrene films and observed a strong film thickness dependence of the glass transition temperature T_g — the measured T_g decreases with decreasing film thickness in the range of a few tens of nanometers. A T_g shift of $-25K$ was observed for Polystyrene films as thin as 10nm. The authors proposed an empirical relation for the estimation of T_g as a function of film thickness h

$$T_g(h) = T_g(\infty)\left[1-(A/h)^{\delta}\right], \tag{2.26}$$

in which $T_g(\infty)$ is the glass transition temperature of bulk Polystyrene films ($h \to \infty$) and the constant A (=3.2nm) is related to the length scale of the near free surface region with enhanced molecular mobility due to the relaxation of constraints to molecular motions. In addition, the constant A has no molecular weight dependence. This is the first suggestion that a near free surface mobile region might play a role for the on-average enhanced dynamics in ultra-thin polymer films and

accordingly for the observation of the T_g reduction. Since then many research investigations have been performed to study the glass transition and dynamics of thin polymer films and both positive and negative glass transition temperature shifts have been observed [59, 60, 61, 62, 63, 64, 65, 66]. Many mechanisms or models have been proposed for such observations. Among them, the most accepted explanation for such glass transition temperature shifts observed for ultra-thin polymer films is that both the vacuum(/air)-polymer interface and the substrate-polymer interface dominantly contribute to the average dynamics of the whole polymer systems. In the following, some typical outstanding studies of thin polymer film T_g measurements will be classified according to specific emphasis on effects of different interfaces in an arrangement as: (1) T_g measurements for substrate supported thin polymer films with weak substrate-polymer interactions; (2) T_g measurements for free standing polymer films emphasizing the vacuum(/air)-polymer interface effects; (3) measurements separately addressing effects of both interfaces.

2.3.1 T_g measurements for substrate supported thin polymer films

Forrest, Jones and Dalnoki-Veress[67, 73] have extensively reviewed the glass transition temperature measurements for Silicon supported thin Polystyrene films. Fig. 2.5 shows a compilation of measured T_g values for PS films by seven independent studies, for which the studied Polystyrene films span a molecular weight range of 63k[74]-2900k[58]—a factor of 46 difference. Several different probing techniques measuring quantities such as changes in the film thickness or density(/free volume) are used for these T_g measurements. From this figure we can see some major observations of the measured T_g's: (1) All measurements, except the one of the top three triangle data points, observe a film thickness dependence of the glass transition temperature T_g (negative T_g shifts) of Polystyrene films especially thinner than ~40nm. (2) Since the Polystyrene studied span a wide molecular weight range of a factor of 46 difference, the chain confinement effects can be ruled out for the enhanced molecular mobility in ultra-thin Polystyrene films which is indirectly evidenced by the reduced glass transition temperature values—as low as ~40K below the bulk T_g. (3) Given that different substrates are used in the studies in Fig. 2.5, all data included, except the top three triangle data points, indicate

a weak or none substrate dependence of the measured T_g values. (4) As for the top three triangle data points [75] standing out in contrast with all the other data, in Ref. [67, 73] Forrest *et al.* gave detailed controversy resolving explanations: one is related to the specific probing technique sensitivity to the substrate (Hydrogen-terminated Silicon substrate in Ref. [75]) and the other involves the variation of glass transition contrast with different film thicknesses (for details, the reader can refer to Ref. [67, 73]).

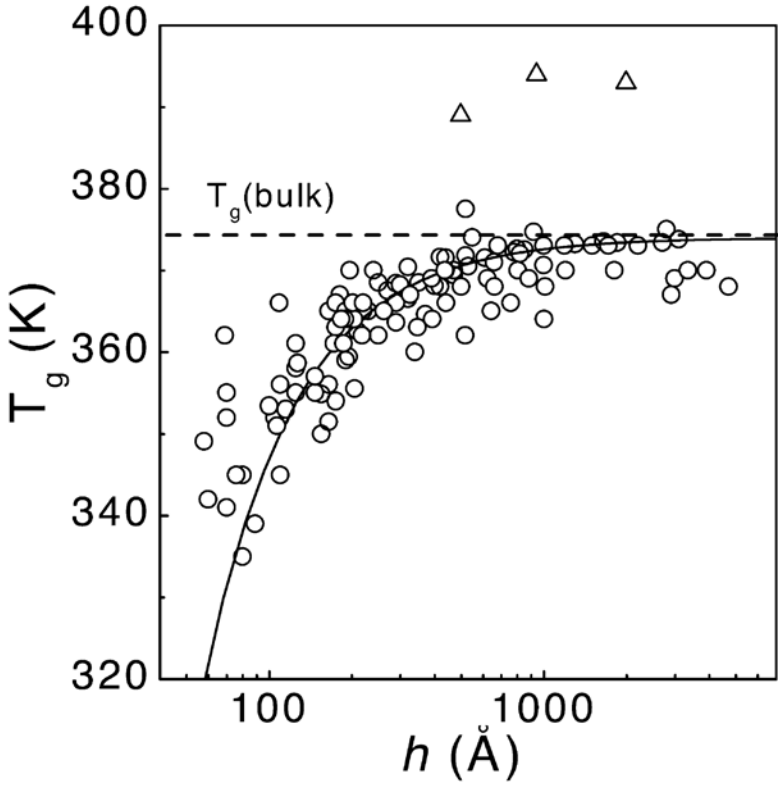

Fig. 2.5. Compilation of measured T_g values as a function of film thickness h for supported PS films by seven independent studies (Graph from [67]).

In summary, from the above studies we see that when polymer films are thinner than a few tens of nanometers, reduced glass transition temperature can be measured. It is possible that as the film thickness decreases the more contribution weight the free surface region may have to the overall dynamical properties of the whole film. In the case of systems with a vacuum(/air)-polymer interface and a substrate-polymer interface of weak interactions, the average dynamics are enhanced compared with those of the bulk counterpart and the glass transition temperature reductions can be

experimentally observed. To further make clear such anomalous phenomena—dynamical deviation from the bulk materials, further studies of specific interfacial effects have been made (see below).

2.3.2 T_g measurements for free standing polymer films

Compared with substrate supported polymer films, the geometry of freely standing films is symmetric along the normal of the film surfaces. On the one hand, the complex situations of combinations or competitions of more than one non-identical interfacial effect can be circumvented—*how two interfacial effects collectively contribute to the average dynamical properties remains elusive in this area*. On the other hand, the effects of the near free surface regions with enhanced molecular mobility can be enlarged in this symmetric geometry. Up to now, the most studied freely standing polymer films are again made of Polystyrene [76,77,78,79,80,81] because it is relatively easy to make freely standing films by floating spincoated films off Silicon or glass slide substrates in distilled water.

A very detailed review of studies of freely standing Polystyrene films has been made by Forrest *et al*. in Ref. [67] as well. Here I just briefly outline the major observations in such studies. Fig. 2.6 shows the combination of all measured glass transition temperatures of freely standing Polystyrene films with a wide molecular weight ranges. We note that in the low molecular weight range of 120k-378k, the T_g shift behavior is very similar to that of the substrate supported polymer films illustrated in Fig. 2.5. Actually, the T_g shift behaviors for both cases (low M_w freely standing films and substrate supported films with weak substrate-polymer interactions) can be well described by a layer dynamics model (see next section). Apart from the T_g shift similarity, there are some points one should be noticed. On the one hand, a much larger T_g reduction (~70K) was observed in the freely standing films. On the other hand, the threshold film thickness, where T_g deviates from the bulk glass transition temperature, is about 70nm, while that of substrate supported films is about 40nm. It is interesting to note that a T_g-deviated substrate-supported film with film thickness h can be approximately mapped to a $2h$ thick free standing film with the similar measured T_g. These features reflect the fact that the near free surface region effects are enlarged due to the symmetric geometry in the case of free standing films.

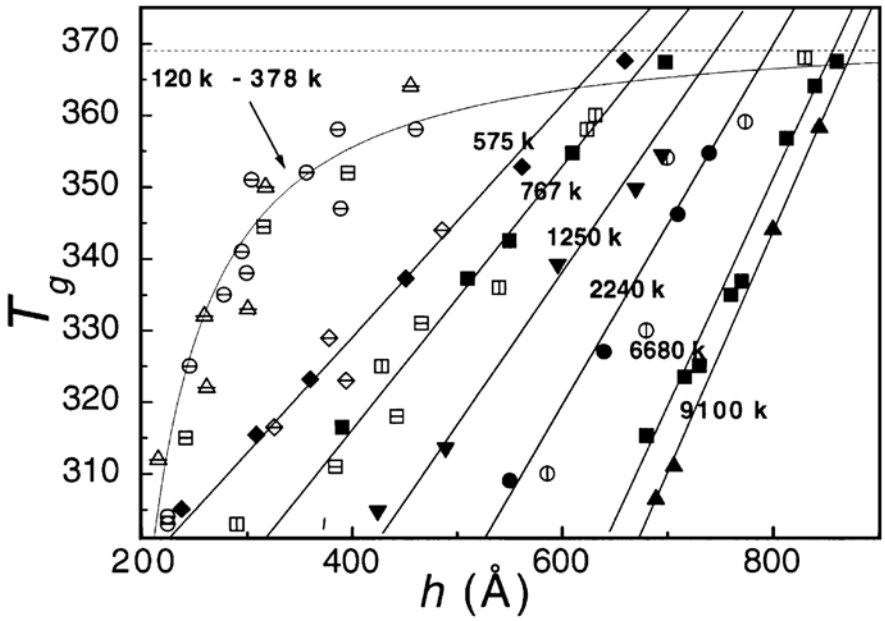

Fig. 2.6 Measured T_g values as a function of film thickness h for freely standing polymer films with different molecular weights shown as black numbers. (Graph from [67]; data from [76, 77, 78])

In stark contrast to the T_g shift behavior of the freely standing films of low molecular weights, that of high molecular weights (575k-9100k) warrant more observations. Firstly, a linear film thickness dependence of the measured T_g's is observed in this high M_w regime. The larger the molecular weight is, the stronger is the film thickness dependence of measured T_g. Secondly, the transition from the measured bulk T_g's to the reduced T_g's is very sharp compared with the smooth transition behavior of the cases of the freely standing films of low molecular weights and substrate supported films, where there almost no molecular weight dependence for measured glass transitions. Forrest *et al*. suggested this sharp transition to a linear film thickness dependence as a sudden switch from the bulk relaxation mode to a chain confinement dominated thin film mode. Thirdly, the threshold film thickness where the bulk T_g's change to linear dependent reduced thin film T_g's is related to the polymer molecular weight or size but not in an obvious fashion.

2.3.3 Measurements separately addressing effects of both vacuum(/air)-and substrate-polymer interfaces

Studies emphasizing effects of the vacuum(/air)-polymer interfaces

From numerous studies of the anomalous phenomena of polymer thin film glass transition temperature T_g shift or deviation from bulk, some researchers proposed that it is the free surface (with enhanced molecular mobility) that dominantly contributes to the T_g deviation feature in thin polymer films. Therefore, a variety of research efforts are made to test this mechanism [82, 83, 84, 85, 86, 87, 88].

Since it is supposed that it is the free surface layer of enhanced higher molecular mobility that contributes dominantly to the experimentally observed glass transition temperature reduction in thin polymer films, measuring the on-average thin polymer film T_g as a function of dynamically modified free surface effect may evidence such propositions. In Ref. [86], Tsui and coworkers measured the glass transition temperature of thin films Polystyrene terminated with low energy groups on both chain ends. Experimental evidences in Fig. 2.7 show that the near free surface regions of such PS films are substantially enriched with the lower energy chain end groups and accordingly the surface molecular mobility is substantially enhanced. Compared with other films of Polystyrene terminated with other groups, the measured whole film glass transition temperatures of the former case are almost twice lowered or reduced compared with those of the latter case. Although the effects of surface segregated chain ends may be not the sole cause for the T_g reduction, the comparison between films of Polystyrene of different modified end groups may be sufficient to show the free surface effects—remember the bulk T_g's for both cases in Ref. [86] are very similar and the chain confinement effect can be negligible in data analysis/interpretations. Other studies [59, 60] of blends of two miscible polymers also show that the interfacial effects dominantly contribute to the glass transition temperature behavior of thin polymer films.

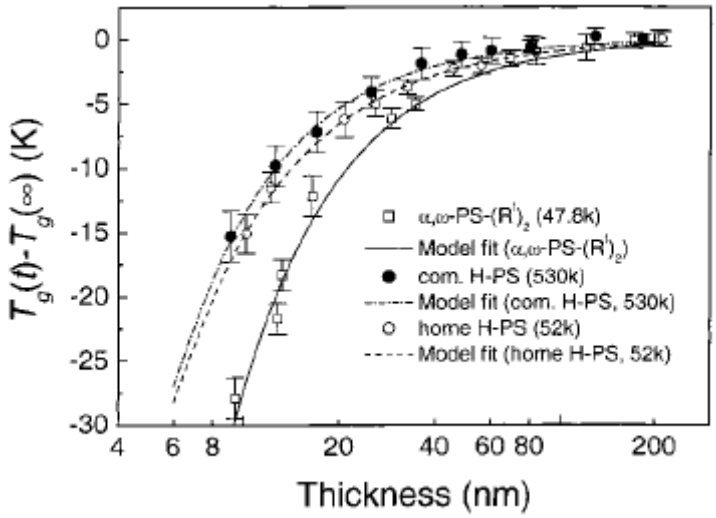

Fig. 2.7 Comparison of measured glass transition temperature T_g between PS films with different molecular weights and chain end groups. (Graph from [86])

Compared with the above method of modifying the molecular motions of the near free surfaced regions, another strategy may be to remove the effect of free surface *completely* and then measure the film thickness dependence of glass transition temperatures of thin polymer films. However, to really eliminate the free surface effects in thin polymer films is not an easy task. In Ref. [89], the authors covered the free surface of thin poly (vinyl acetate) (PVAc) films by evaporating an Aluminum layer on top of the film free surfaces, but T_g reductions are still observed. One possible explanation about these studies is that the thermal evaporated metal coating layer may not have good contacts with the samples and the free surface layer is not removed completely. Similar observation was found in ref. [77, 88], where the free surface covering layer is aluminum or oxidized silicon. A carefully designed experiment was recently conducted by Forrest and Sharp [88]. In this study, the authors made thin films of Polystyrene without the free surface effects in this way: Firstly, a sets of Polystyrene films of thickness of $h/2$ are spin-cast onto Silicon substrates from Toluene solutions; Secondly, another sets of Polystyrene films of thickness of $h/2$ are spin-cast onto single crystal sodium chloride (NaCl) optical windows which are coated with a thermally evaporated Aluminum layer (5 nm in thickness; Oxidized Aluminum layer intact) before using. The second sets of Polystyrene films (supported on Oxidized Aluminum layer) are then placed on top of the first sets of Polystyrene films (supported on Silicon substrates with native Oxidized Silicon layer) in *face-to-face contacts*; Thirdly, the top NaCl

window substrate is dissolved using deionized water thoroughly and then the resulting films of thickness h are annealed under vacuum at 403 K (34K above the bulk T_g) for 8 hours. By these treatments, the metal layer evaporation procedure can be avoided.

The measured T_g values of the specifically prepared Polystyrene films in Ref. [88] are shown in Fig. 2.8. In this figure, the thickness of the as-produced 2(h/2) Polystyrene films ranges from 7nm to 270nm; the hollow diamond symbols represent T_g values for films truly without free surfaces, which exhibit, on average, the bulk behavior even when the films are thinner than 10 nanometers; results of the same films with restored free surfaces, shown as filled circles, show T_g reductions again as the results of most studies of thin substrate supported polymer films with free surfaces. It is remarkable that the free surface effects can be reintroduced by immersing the Al coated PS films in NaOH solutions for 5 minutes and then rinsed with deionized water. This is similar with treatments in [90 ,91], where some free surface regions are first covered with nano gold spheres and then restored by dissolving the gold spheres using mercury.

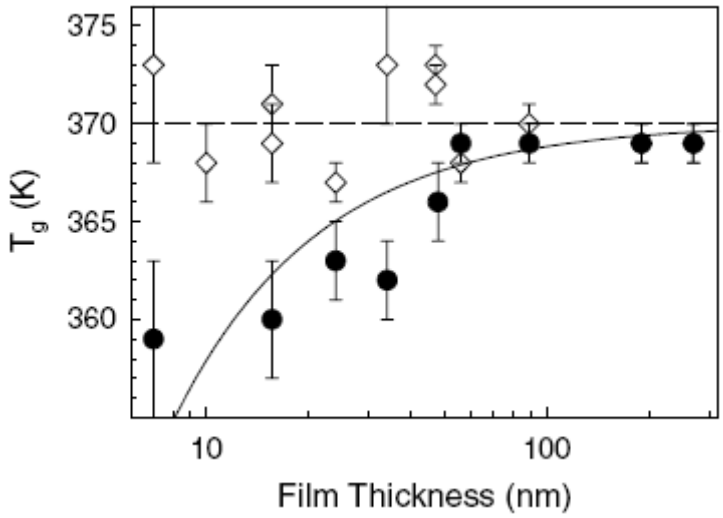

Fig. 2.8 Glass transition temperatures for the 2(h/2) films: before (hollow diamond) and after (filled circles) restore of the free surface. The solid line describes the thickness dependence of the T_g of thin substrate supported Polystyrene films obtained for uncapped Polystyrene films (Graph from [88]).

The compelling results of Ref. [59, 60, 86, 88] show that the free surface effects are crucial for observing T_g compressions in thin polymer films. Due to the release of steric constraints or the truncation of the 3-dimentional potential fields the molecular motions are enhanced in the near free surface region, but the quantitative characterizing of how and how far this free surface effects can penetrate into the whole thin polymer films has yet to be studied so far.

Although there is a large body of studies in the literature showing glass transition temperature deviations in thin (/confined) polymer systems due to the interfacial effects, there are also some studies showing that there is no difference between the near free surface region and the bulk part in thin polymer films [93, 94]. As for such controversies, one should be noticed that the enhanced dynamics in some interfacial regions in nanometer confined systems are one necessary condition but not the sufficient condition for the observed T_g deviations. One prudent question may be to ask if the studied near free surface effects in some cases make a substantial contribution to a broadened dynamics distribution which usually follows with glass transition temperature deviations in thin polymer films. For example, in Ref. [86] the T_g reductions are attributed to the sufficiently plasticized near free surface regions. In glass transition temperature studies based on Atomic Force Microscopy (AFM) involving solid contacts between AFM tips and polymers, e.g. Ref. [94], such factors should be considered when interpreting any experimental findings: measurement applied loads and probing frequencies, size of both vertical and horizontal probe areas, geometry shapes of the AFM tips, etc. Another factor should be considered in data interpretations is any potential material-specific dependences in different studies. For example, if the strong substrate/polymer interactions overwhelm the free surface effects no or limited enhanced dynamics could be expected in the average whole system dynamics or even in the near free surface regions.

Studies emphasizing effects of the substrate-polymer interfaces

The first study of glass transition temperature of Polystyrene thin films[58], in which the vacuum (/air)-polymer interfacial effects are supposed to be the cause of the T_g deviations from the bulk materials, motivates more research interests in investigating the role played by interfaces in determining the overall dynamics of thin polymer films. In this section, I briefly review some studies emphasizing the effects of the substrate-polymer interfaces on the experimentally measured glass transition temperatures [59, 63, 96, 97, 98, 99, 100, 101]. From these studies people found that when

the interaction between polymers and substrates are very strong the positive T_g shifts in thin polymer films can be observed, in contrast with the negative T_g shifts mostly measured in polystyrene films which has weak substrate dependence. In polymer systems, e.g. poly (methyl methacrylate) (PMMA) [63, 96, 99, 102] and tetramethylbisphenol-A polycarbonate (TMPC) [59], the positive T_g shifts mean that the substrate-polymer effects overwhelm the vacuum (/air)-polymer effects and the overall dynamics are slower than those in the bulk materials.

In Ref. [96], Nealey and co-workers studied the glass transition temperatures of thin polystyrene (PS) and poly(methyl methacrylate) (PMMA) films as a function of substrate-polymer interaction energies. The substrates used are silicon wafers coated with thermally stable self-assembled (SA) films (2.6nm in thickness) of octadecyltrichlorosilane (OTS). Fig. 2.9 shows the compiled results of T_g deviations from the bulk value for PS and PMMA films of three thicknesses as a function of polymer-substrate interaction energies, in which the dashed line is a linear regression of the data for both 22 nm PS films and 20 nm PMMA films.

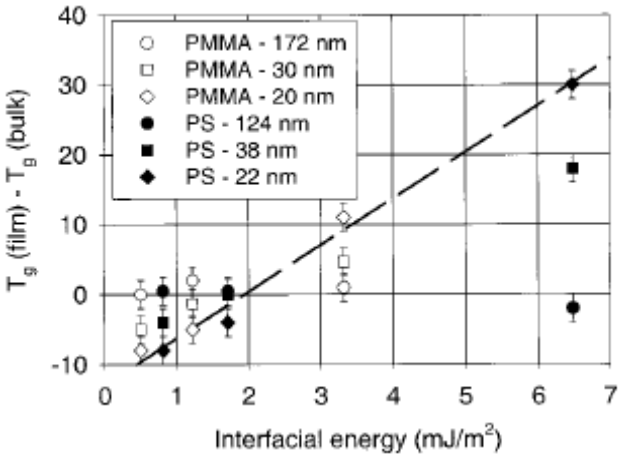

Fig. 2.9 Compiled results of T_g deviations from the bulk value for PS and PMMA films of three thicknesses as a function of polymer-substrate interaction energies (Graph from [96]).

In Fig. 2.9 such features can be seen: (1) For both PS and PMMA films, the measured T_g deviations are almost a linear function of polymer-substrate interaction energies for a constant film thickness. (2) The T_g deviations can be negative or positive depending on the strength of the polymer-substrate

interaction energy. (3) The T_g deviations are a function of film thickness. For thinner films, the T_g deviations are larger. (4) The crossing of the bulk T_g line and the T_g deviation line means that for films ~20nm thick a bulk glass transition temperature can be observed, which means that the measured T_g's are a combining results of both substrate-polymer and vacuum (/air)-polymer interface effects.

In [97], Tsui and co-workers studied the glass transition temperature of thin PS films by modifying the substrate interactions. Therein, the substrate used is ~3nm thick P(S-*r*-MMA) brushes anchored on silicon wafers and the homopolyer/copolymer interactions are modified by changing the styrene fraction. When the styrene fraction of the copolymer brushes is larger than 0.75, the measured T_g seems have a linear dependence on the homopolyer/copolymer interaction, which is similar with that in [96]. Tsui and co-workers noticed that the sole substrate interaction energy may be not sufficient to describe the observed T_g deviations and instead proposed a model incorporating the potential chain segment density variations in the interfacial regions. According to this model, a small variation in chain segment density in the interfacial regions can result in a T_g shift of ~20K. The effect of narrow interfacial regions of two immiscible polymers on the thin polymer film dynamics is also observed in [70], in which the cooperative rearranging motions of two unlike chain segments are considered.

2.3.4 Models addressing T_g anomalies in thin polymer films

In the past 15 years of dynamics studies of thin polymer films, one major observation is that the measured glass transition temperatures deviate from those of the bulk counterpart polymers, which means indirectly that the dynamics in polymers confined on the nanometer scale are different from those of the conventional bulk materials. People find that the sign of T_g deviation can be negative for thin polymer film systems with weak polymer-substrate interactions [59, 60, 61, 62], or positive for systems with strong polymer-substrate interactions [63, 64,65, 66]. Some theoretical models have been proposed to interpret such observations. Here I just outline three general example models which are not system or polymer specific. One can refer to Ref.[67, 101, 103, 104]for some models developed for some specific systems.

Layer model

Although finite size or confinement effects may work in systems on the nanometer scale, one pronounced difference between nanometer scale and bulk systems is that the area-to-volume ratios are very different in both cases. In addition, the potential fields at the interfaces are not symmetric or truncated compared with those in the interior of the system studied. Therefore, it is reasonable to consider the interfacial effects first, which may play a key role for the T_g deviation phenomena observed in polymer systems on the nanometer scale. A layer model was developed by Forrest and Mattsson [80], in which the authors incorporate the idea of cooperative dynamics to describe the length scale of the interfaces with molecular mobility different from that of the system bulk part, and such interface affects the neighboring materials through molecular cooperative motions. In addition, the dynamics of the nanometer scale polymer systems are *heterogeneous on average*, which means that the interface may have different dynamics compared with the rest of the system, but the whole system might have one average, for example, glass transition temperature.

For a polymer thin film system with a vaccum(/air)-polymer or substrate-polymer interface, the picture of the layer model is as follows: to describe the dynamics of the vaccum(/air)-polymer interface, a glass transition temperature $T_g^{surface}$ is assigned to this region which is lower than the bulk T_g^{bulk}; the length or thickness of this interface follows

$$\xi(T) = r_0 + \alpha(T_{ons} - T)^{\gamma}, \tag{2.27}$$

where r_0 is the average distance between monomer units, T_{ons} is the onset temperature for cooperative motion, α and γ are two model dependent constants. Using this model, the average glass transition temperature $\overline{T_g}$ of polymer films with the thickness h can be estimated as:

$$\overline{T_g} = \begin{cases} T_g^{bulk} + \dfrac{2\xi(\overline{T_g})(T_g^{surface} - T_g^{bulk})}{h} \\ T_g^{bulk} + \dfrac{\xi(\overline{T_g})(T_g^{surface} - T_g^{bulk})}{h} \\ T_g^{bulk} + \dfrac{\xi(\overline{T_g})(T_g^{surface} - T_g^{bulk})}{h} + \dfrac{\lambda(T_g^{substrate} - T_g^{bulk})}{h} \end{cases} . \quad (2.28)$$

In the above equation, the top formula is for the case of freely standing films, the middle formula is for the case substrate-supported films with negligible substrate-polymer interactions, and the bottom formula is for the case of substrate-supported films with non-negligible substrate-polymer interactions, in which λ and $T_g^{substrate}$ are length scale and glass transition temperature of the polymer-substrate interface respectively. Fig. 2.10 shows the application of the dynamics layer model to the measured glass transition temperatures of freely standing Polystyrene ($M_n \leq 347k$) films as a function of film thickness. From Fig. 2.10, we see that the glass transition temperature estimations by the layer model match the experimental data well. In addition, from Ref. [80], the model fitted parameters are physical reasonable. The layer model can also be applied to the case substrate supported polymer films— the model predicted glass transition temperatures varies depending on the nature and strength of the polymer-substrate interactions. These behaviors are experimentally observed in ref. [74, 100, 105, 106, 107].

The major success of the dynamics layer model is that it incorporates the dynamically different interface layer with a *temperature dependence length scale*—for the case of Polystyrene this model predicts the length scale of cooperative motions below bulk glass transition temperature, and it can quantitatively estimate the average glass transition temperature values of thin polymer films. For nanometer scale polymer systems with the vaccum(/air)-polymer interface, the dynamics of the near free surface region(with enhance molecular mobility due to the release of steric constraints) play a key role in determining the experimentally measurable on-average dynamical properties, for example, the glass transition temperature. This model did not specify the physical origin of the temperature dependence of the interface length scale, which beyond the scope of the layer model and more theoretical considerations are warranted. In addition, this model is applicable only in a molecular regime $M_w \leq 378k$ for Polystyrene.

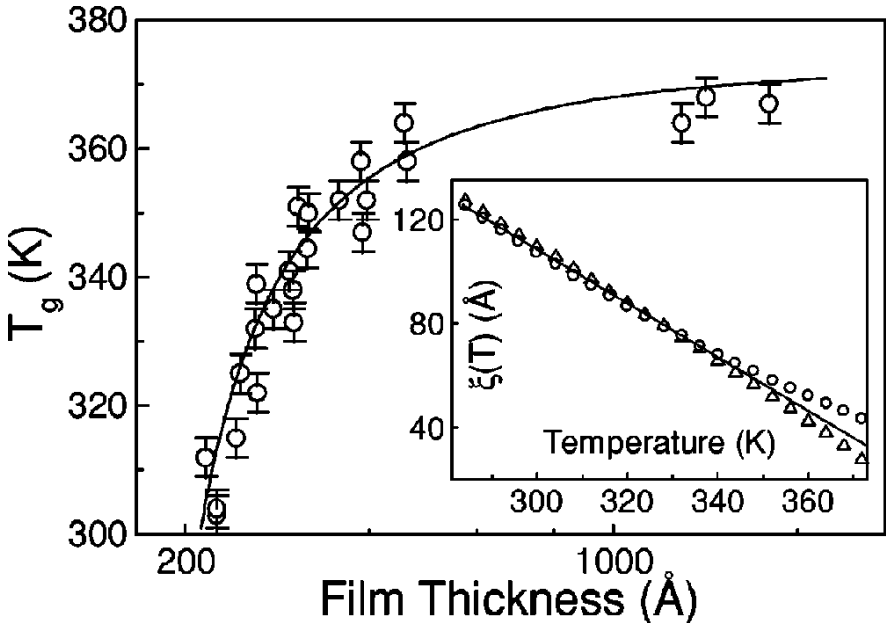

Fig. 2.10 Application of the dynamics layer model to the measured glass transition temperatures of freely standing Polystyrene ($M_n \leq 347k$) films. (Graph from [80])

Percolation model

In the percolation model [109, 110], a glass forming system changes from the melt state to the glassy state when domains of slow dynamics percolate through out the whole system and the average high viscosity and dramatic enhanced relaxation times are determined by the dominant dynamics of slow subunits. The distribution of domains of fast, intermediate and slow dynamics is the results of thermally induced density fluctuations. Fig. 2.11 illustrates the picture of a glassy system, in which the slow domains (grey) percolate through out the whole system. What is interesting is that if the dash-line-exhibited region is treated as a separate independent system at the same temperature of the whole system in Fig. 2.11, then the dynamics or viscosity of such small system may be lower compared with those of the bigger system, which means that the glass transition temperature might be reduced. Long and co-workers[109,110] predicted the glass transition temperature reduction phenomena for freely standing polymer films and supported films with weak substrate-polymer interaction based on such mechanism that to form glassy ultra-thin polymer films a quasi-2D slow domain aggregation in the direction parallel to the film is necessary at a lower temperature. In the

case of polymer films with strong substrate interactions, the pathway of percolated slow domains connects both vacuum(/air)-polymer and substrate-polymer interfaces and the experimentally measured glass transition temperature will be increased as a consequence of strong adsorption of slow domains on the substrate.

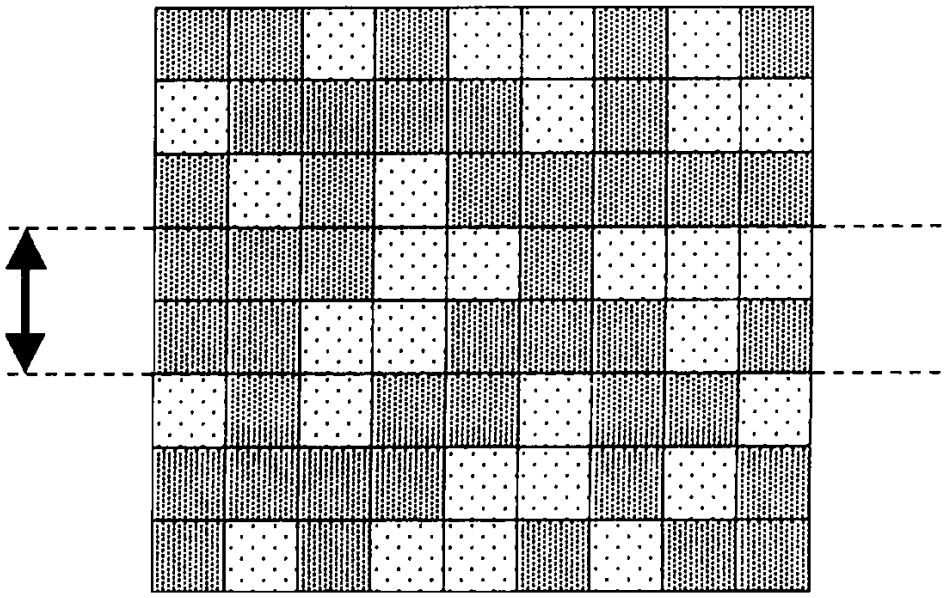

Fig. 2.11 Schematic illustration of a glassy slow-domain-percolated system. (Graph from [109])

One should note that the percolation model is based on thermally induced density fluctuations and is actually a kind of thermodynamic interpretation of the glass transition phenomena. In cases of thin polymer films, the density profile for the vaccum(/air)-polymer interface is very narrow, and the vaccum(/air)-polymer interface effect is ignored in the percolation model. Another point to which we should pay attention is that in this model the dynamical domains are treated as three dimensional no matter the system studies is in bulk or thin film cases. This might be problematic since some studies have shown that the dynamical domains in supercooled liquid may be one or two dimensional [111, 112]. In these cases, the interfacial effects can play a key role in determining dynamical properties of glass forming materials on the nanometer scale.

de Gennes model

In ref [113], de Gennes proposed a “kink” sliding (along polymer chains) mechanism to explain the reduced glass transition temperature in thin polymer films, which also explains the linear dependence

on film thickness of the experimentally measured T_g's in free standing polymer films. In this mechanism, the chain motions are mapped as kink's sliding along the chain molecules. The jump or moving rate of the kink at specific chain sequence depends on the available free volume. Assuming the chain sequence related free volumes follows the Gaussian distribution

$$p(w) \to (consant)\exp(-\frac{w^2}{2w_0^2}), \tag{2.29}$$

where w is the chain sequence free volume, and w_0 is the average free volume, which is much smaller than the chain sequence volume a^3 because the motions along the chain "are easier than the standard bulk motions". From this assumption, one should note that *the kink sliding motions along the chain molecule are different from the chain sequence 3-D diffusion motions.* Based on Eq. (2.29), the average relaxation time for the kink sliding dynamics is obtained as

$$\tau = (const)\tau_0 \exp(\frac{N}{4}\frac{(w_0)^2}{v(T)^2}), \tag{2.30}$$

where $\tau_0 \sim 10^{-11}s$ is the high temperature microscopic relaxation time and N is the degree of polymerization. In Eq. (2.30) the free volume v at temperature T is

$$v(T) = C(T - T_0), \tag{2.31}$$

C is a constant related to thermal expansion coefficient of the polymer and T_0 is the temperature where the free volume is 0. There might be a slight issue in Eq. (2.30) and (2.31)— the kink jump/moving required free volume is related to *kink sliding motion free volume* w_i, but the *3-D standard free volume* $v(T)$ is used to estimate the average kink sliding characteristic time. However, the basic proposal for this kink sliding mechanism is important. When being applied to bulk polymer materials, the effect of the kink sliding motions/mechanism is weak because the two chain ends are buried in bulk materials and the free volume required for chain ends to move is of the order of chain sequence volume a^3 which is much larger than the kink sliding volume w_0. However, when being

applied to the case of thin polymer films, the kink sliding mechanism could play a key role in determining the whole film dynamics. Fig. 2.12 is a schematic representation of a polymer chain with two contacting sites (red crosses) with the thin film free surface (dash line). The chain section between the two surface contacting sites forms a loop, in which the kink sliding motions dominate since the two surface contacting sites have fast motions in the potential liquid like near free surface region. de Gennes estimated the typical loop length(in monomer units) as

$$g \cong h^2 / a^2, \tag{2.32}$$

where h is the film thickness and a is the monomer size. Based on Eq. (2.30, 2.31, 2.32), a linear dependence of T_g on h can be obtained. For free standing polymer films, when the film thickness is small enough that the middle plane in the film can be connected by such kink sliding loops from both free surfaces, the average glass transition temperature can be much lower than the bulk T_g.

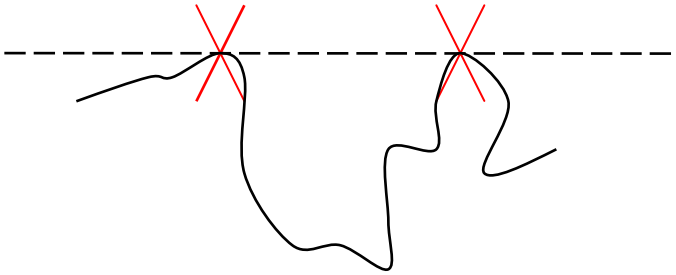

Fig. 2.12 Schematic representation of a polymer chain with two surface contacting sites, which form a typical loop.

In summary, the kink sliding mechanism can explain how the free surface molecular motions can affect the whole polymer film dynamics— actually by the *cooperative* kink sliding mechanism. Another conclusion one can draw from this mechanism is that the radius of gyration of polymer chain molecules is the upper limit of a length scale through which the free surface effect can propagate into the thin polymer film. The weak point of this mechanism is that it is based on the free volume assumption.

2.3.5 T_g distribution studies of thin polymer films

In the layer model for interpreting the glass transition behavior of ultra-thin polymer films or nanometer confined glass forming systems, an on-average heterogeneous dynamics distribution is assumed, that is, the molecular dynamics in the interfacial regions are different from those in the bulk part regions, which usually results in glass transition temperature deviations in nanometer confined glass forming systems. However, what the dynamics gradient look like in such systems—abrupt or smooth transition in dynamics is unclear. In Ref. [103], de Gennes predicted that "future experiments should aim not at the determination of a single T_g, but at a distribution of T_g's." In 2003, Ellison and Torkelson conducted, for the first time, the experiment of investigating the glass transition temperature distributions in thin polystyrene films [66].

The fluorescence technique is employed for thin polystyrene film T_g distribution studies [66], in which a dye doped or labeled (by covalent attachments) thin polystyrene film (~14 nm thick) is used as a trace layer. The fluorescence of the dye (pyrene) itself is not sensitive to the glass transition. The fluorescence reaches the detector is the competition results between the fluorescence radiated from the excited state of the dye of pyrene and the non-radiative decay depending on the vibration and other modes of the surrounding environments—a denser environment will induce less non-radiative decay. During the glass transition, both the material density and the molecular motions will be affected and accordingly the intensity of fluorescence will reflect such transition.

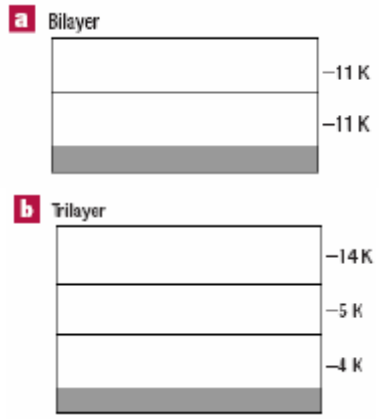

Fig. 2.13 Glass transition deviation ($T_g(trace) - T_g(bulk)$) for a pyrene-labelled PS layer (12 nm) inserted at specific locations in unlabelled PS films (Graph from [66]).

Fig. 2.13 shows some results of T_g distributions in multiple-layered polystyrene films. The grey area shows the glass slide substrates. The molecular weight of the polystyrene studied is ~400k and the thickness of the specific layers is 12nm. From graph (b) we can see that there is a transition in the glass transition temperatures from the very top layer to the bottom layer *across a length scale of ~36 nanometers*. As expected the top near free surface layer or region has the highest molecular dynamics since the T_g reduction is the largest. From graph (a) we see that when the confinement dimension is less than a critical length scale, ~25nm in this case study, the interface effects dominate the whole system. In both cases in graph (a) and (b), only one average glass transition temperature is measured if one dope or label the whole film using trace dyes, as is observed in most glass transition temperature studies for ultra-thin polymer films.

Although the studies of Ref. [66] exhibit new features of the picture of the glass transition in nanometer confined glass forming materials, there are some points to which the authors did not pay much attention. Firstly, in order to determine the glass transition temperatures at well-defined locations within thin polymer films, the authors made some measurement controls such as "By heating the layered films for short time periods above T_g, the layers fuse, producing a continuous film with label only at particular depths within the film." and "The labeled and unlabelled PS chains are of sufficiently high molecular weight to ensure that the labeled PS diffuses, at most, several nanometers during measurement." We note that such controls have double-fold effects. While a good definition of the T_g trace location is achieved, a unwanted measurement of dynamics is also possible. We note that a very dilute solution is used to make ultrathin polymer films using the spincoating technique. In the as-produced films the polymer molecules are strongly confined—the radius of gyration of the polystyrene used in this study is ~17nm, which is very close to the size of the dye-labeled trace layers ~12nm, and the entanglement density is very low. When contacting with some medium, the highly confined chain molecules in the dye-labeled trace layer tend to relax or diffuse into the neighboring medium to relieve the confinement effect. Since the molecules in the dye-labeled trace layer have no much chance to fuse with the adjacent polymer molecules due to the specific control for good definitions of trace location, the actual measured glass transition temperatures of the dye-labeled trace layers must have some contribution from such strong tendency of relaxation of the highly confined polymer molecules and such effects are similar with some kind of built-in stresses or strains. In Ref. [88], to let the two contacted near free surface regions to reach an equilibrium state,

the two $h/2$ samples are annealed under vacuum at 403 K for 8 hours and the measured glass transition temperatures for the $2(h/2)$ films (ranging from 30-7nm thick) are bulk like. This annealing procedure is very different from that in Ref. [66] where the multilayer samples are only annealed at 403K for 10 minutes. Remember, the buried dye-labeled trace layer has two interfaces with the neighboring polymer molecules and the tendency of the highly confined polymer molecules to diffuse into the neighboring medium can not be ignored. Therefore, the measured dynamics are higher than what is expected and T_g reductions can be observed in much deep location of polymer films. Secondly, according to the studies of the effects of near free surface region on glass transition temperatures of thin polymer films[77, 88, 89], it is not an easy task to remove the effects of near free surface regions in thin polymer films. In Ref. [66], many thin layers (~14nm) of polystyrene films are layered up to make the multilayer samples. We can imagine that the free surface effects might be incorporated to such multilayer samples as well since specific controls are made to achieve good definitions of locations of the dye-labeled trace layers (see Fig. 2.14, in which the red lines highlight the potential buried "free surface regions"). Thirdly, in graph (a) of Fig. 2.13 we see that the T_g's for the two trace layer locations are identical. However, such narrow T_g distribution in polystyrene films thinner than 25nm is in stark contrast to most studies where the glass transition is much broadened due to the high dynamics heterogeneity. In addition, if the results of graph (a) are real, there are no bulk properties in the 25nm thick polystyrene films at all, which is not the case in most studies.

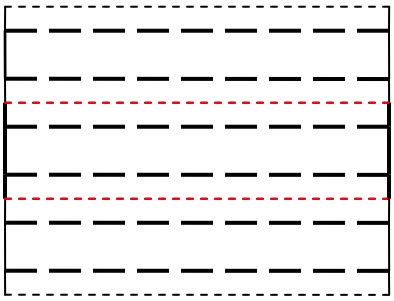

Fig. 2.14 Schematic diagram of a multilayer system considering the buried "free surface" effects shown as red thin dash lines.

In summary, the fluorescence technique is suitable for measuring glass transition temperatures of dye-labeled thin polymer films since the detected signal is very sensitive to the density variations of the

glass forming materials. The results of the measured glass transition temperatures (shown in Fig. 1, 2, 3 of Ref. [66]) of single dye-labeled thin polymer films (in some cases sitting on un-labeled polymer films) are reasonable and in agreements with results of other studies. But when being used to measure the glass transition temperatures of *buried dye-labeled thin polymer layers* in multilayer systems, this technique should be properly controlled and the corresponding measured results should be interpreted with much caution, especially considering the potential buried *"free surface regions"*.

2.3.6 Local dynamics studies of polymers on nanometer scales

In the foregoing sections we have seen that the glass transition temperature deviations from bulk materials for nanometer confined polymer films are observed by extensive studies. Since the interfacial effects may play a key role for such observations, a variety of studies focusing on investigating the effects of both the vacuum (/air)-polymer and substrate-polymer interfaces on the glass transition temperatures of thin polymer films have been conducted. Usually, if the substrate-polymer interactions are very weak and the effects of the vacuum (/air)-polymer interface dominate, negative glass transition temperature shifts in thin polymer films can be expected; on the other hand, if the substrate-polymer interactions are strong enough to overwhelm the vacuum (/air)-polymer interface effects, positive glass transition temperature shifts can be observed. In order to study the length scale over which the interfacial effects can influence the dynamics of thin polymer films, the glass transition temperature distributions in thin polymer films have been measured and a length scale ~ several tens of nanometers for such effects is observed. However, the glass transition temperature is an indirect measure of the dynamics in nanometer confined glass forming materials. In addition, many mechanisms, for example, different motions, are coupled to the glass transition temperatures in different glass forms, and even in the same glass forming materials there are might be different mechanisms contributing to some dynamical or mechanical quantities at different temperature windows. Therefore, definite dynamics studies, and for the first step at specific locations are always necessary to improve our understanding of the glass transition mechanism in nanometer confined glass forming materials. Since the near free surface effects might have dynamics different from those in the bulk materials and may, as observed in lots of studies, be the cause for the glass transition temperature deviations in thin polymer films, to specifically study the dynamics in this region is rewarding for unfolding the puzzle of the glass transition phenomena.

Some studies [90, 91, 114, 115,116,117, 118, 119] have been made focusing on dynamics of specific locations in nanometer confined polymer systems. There is much evidence that the molecular mobilities are enhanced compared with those in bulk materials at the same temperatures studies. In addition, some unexpected features are observed in the near free surface regions of thin polymer films as well.

In Ref. [90], a novel technique is used to study the dynamical properties in the near free surface regions (~2-4nm) of thin polystyrene films. The nanometer scale hemispherical surface holes are produced by partially embedding gold spheres (~20nm in size) into polystyrene film surfaces at a temperature about 5 Kelvin above the bulk glass transition temperature and then using mercury to dissolve the embedded gold spheres at the room temperature. The time and temperature dependent relaxation of the as-produced surface holes is probed by measuring the evolution of the surface holes using Atomic Force Microscopy. From the data of surface hole relaxations at a specific temperature the characteristic surface hole lifetime can be extracted by an exponential function fitting. Fig. 2.15 shows the measured surface relaxation times as a function of inverse temperature. We can see that the dynamics (evidenced as the characteristic times) of the near free surface regions of the thin polystyrene films are remarkably different from those of the local vibration related β mode (shown as the long dashed line) and chain segment related α mode(shown as the solid black curve) in bulk polystyrene systems. The dynamical behavior shown by the solid black curve is from Ref. [120], in which the rotational motions of chromophores doped in bulk polystyrene systems are studied. We see that below the bulk glass transition temperature the α mode (suggested by the authors) has the energy activated Arrhenius temperature dependence. Although this suggested α mode for bulk glass forming materials below bulk T_g is questionable (usually rotational mode and translational mode decouple to glass translational related quantities below and above T_g), the observed Arrhenius temperature dependence means that the probed motion is more localized and less related to the cooperative mode. Now, let us see the features of the surface dynamics in Fig. 2.15. In a relative high temperature window including the five hollow triangle data points from left, the temperature dependence is close to the Arrhenius activation behavior, but the dynamics are faster than those in bulk materials shown by the solid black straight line. Clearly, compared with the well known VFT behavior, the temperature dependence is weak in the near free surface regions of thin polymer films. In a lower temperature window including the right three triangle data points, the temperature dependence is even

weaker and almost indiscernible. Aside from the unusual weak temperature dependence of the surface relaxation of the near free surface regions of thin polystyrene films, it is also noteworthy that surface relaxation is observed at temperatures where the bulk material would be in the glass state below bulk T_g, which means the surface dynamics are enhanced compared with the bulk counterpart otherwise surface relaxation would not be measured at the measurement manageable timescale. However, even with fast molecular motions in the near free surface regions the surface relaxation observed is still slower than the bulk β mode.

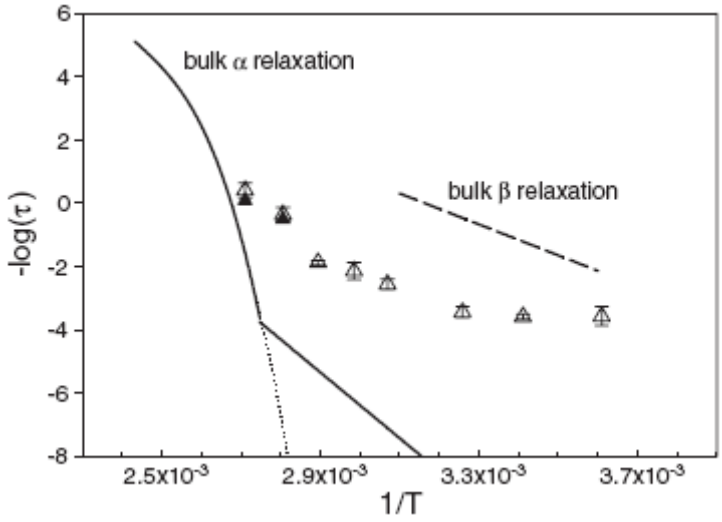

Fig. 2.15 Surface relaxation times along with plots of α and β (local vibrational) mode relaxation as a function of inverse temperature for polystyrene films. (Graph from [90])

In [119], Papaléo *et al.* studied the relaxation of nanometer-scaled surface structures on the surface of PMMA films. The surface structures are ~4nm in height and ~110nm in length, which are produced using ion implantation technique. When ions with high energy impact the PMMA film surfaces, craters can be produced and due to the high energy gradients in the surrounding area some nanometer scaled protrusions (or tails) of PMMA molecules are produced as well. By studying the relaxation of such surface protrusions/tails at different temperatures, the dynamical properties of the PMMA film surfaces can be investigated. Fig. 2.16 shows the temperature dependence of the characteristic relaxation times for the volume, length, and height of the nano protrusions on PMMA film surfaces. From this graph, three dynamical features can be seen: (1) Compared with the bulk PMMA dynamics, those for the free surface region are enhanced; (2) The measurement results for the higher experiment temperature range have the similar temperature dependence of the bulk VFT curve, but the latter has

to be shift by ~30K to match the measurement data, by which Papaléo *et al.* assign a local surface T_g much lower than bulk T_g ; (3) The data for lower experiment temperatures shows an Arrhenius-like temperature dependence, which is similar with that of the nano surface hole relaxation studies for PS films[90].

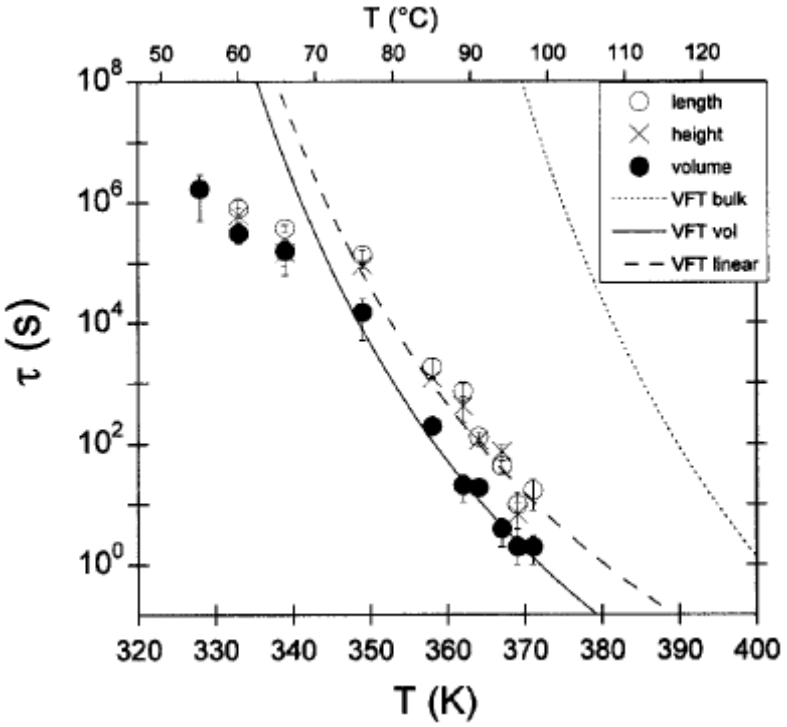

Fig. 2.16 Temperature dependence of the characteristic relaxation times for the volume, length, and height of the nano protrusions on PMMA film surfaces. (Graph from [119])

The relaxation of artificially produced surface nano-deformations [91] or asperities [115] have also been experimentally studied, all of which observed enhanced molecular mobilities in the near free surface regions of polymer films at temperatures well below the bulk glass transition temperatures. In Ref. [118, 114] computer simulation techniques are used to investigate the dynamical properties of the near free surface regions of thin polymer films and similar observations are evidenced—there is a liquid like surface layer covering the bulk part in the glassy state. Considering that the size of the liquid like surface layer in thin polymer films is less than 10nm [121,122, 123] and enhanced molecular mobilities are observed in such nanometer scale regions, one may refer to more studies

about polymer molecule mobility studies[116, 117], in which the extreme spatial confinements are applied to polymer molecules and dramatic enhanced molecular mobilities are observed.

In summary, the studies of the polymer molecule dynamics in local nanometer confined regions are relatively new. Generally speaking, much fast molecular dynamics are observed in the near free surface regions of thin polymer films or in extreme spatial confinements of polymers. In addition, new features are also found, for example, the much weak temperature dependence [90, 122] and chain size dependence [91] of molecular dynamics in the near free surface regions of thin polymer films. More theoretical considerations for such dynamical features in nanometer scale confined polymer systems are warranted.

2.3.7 Computer simulation studies of confined glass forming systems

Computer simulation studies (sometimes called computer simulation experiments) can provide a connection between experimental and theoretical investigations. On the one hand, the advanced computer technologies make it possible for researchers to conduct enormous calculations to mimic real world experiments or to test theoretical predictions. On the other hand, some computer simulation work can provide valuable guidance or directions for both experimental and theoretical researches. By and larger, there are two major approaches to do computing simulations: molecular dynamics method and Monte Carlo method. The former one is based on the classical Newton's equation of motion and the time domain numerical integrations are performed for particles or monomers (in the case of polymers) of the system. In Monte Carlo simulations, the ensemble average of the statistical system is calculated. Both approaches have been extensively used by researchers. In this section, only some computer simulation works of confined glass forming systems are briefly described, mainly focusing on dynamical features related to the glass transition phenomena.

In the previous sections, we have seen that in some theories of the glass transition phenomena, such physical quantities as the free volume, characteristic length scale of CRR's and the distribution of local molecular relaxation times, are studied trying to explaining the dramatic slow down of dynamics of glass forming systems. Unfortunately, most of them can only be indirectly measured and in most cases only averaged variables are obtained in real world measurements. However, almost all local properties can be measured or calculated directly in computer simulation studies [29, 31, 124, 125,

126, 127]. However, there are limitations for computer simulation studies as well, two of which are: (1) some controlling variables in computer simulations are too ideal to be realized, such as interface- or particle- particle interactions; (2) inaccessible low temperatures (especially below T_g's) in simulations due to the dramatic slowing down molecular motions and accordingly the prohibited long calculation times. Nevertheless, the results of some computer simulation studies are still very helpful in improving our understanding of the glass transition phenomena. Considering the scope of this introduction section, only several interesting findings about super-cooled glass forming liquids are reviewed here.

The first is the nature of the mobile clusters and their effects in super-cooled glass forming liquids. In the seminal work by Adam and Gibbs [26], the concept of cooperative rearranging dynamics was proposed and in such CRR's the molecules relax independently and simultaneously. There is no information about the CRR's dimension mentioned in that work. It is possible that the CRR's could be one, two, or three dimensional. In [29, 127], it is observed, by computer simulations, that the mobile cooperatively rearranging molecules can form one dimensional string-like clusters. Fig. 2.17 depicts one of such clusters, in which the dark spheres show the particles at the initial time and the light spheres are for the same set of particles at a later time. In [29], it is observed that the dynamics of the super-cooled liquid are heterogeneous in that particles with similar mobility are spatially correlated and the mobile clusters evolve with time— every particle has the chance to move by cooperative rearranging motions with other particles. This picture is different from that of Adam and Gibbs [26], where the molecules relax independently and simultaneously with their own time constant. Another interesting finding in [29] is that for super-cooled liquids, there almost no tendency for the system to undergo bulk phase separation between mobile and immobile clusters because the former is highly ramified and extended.

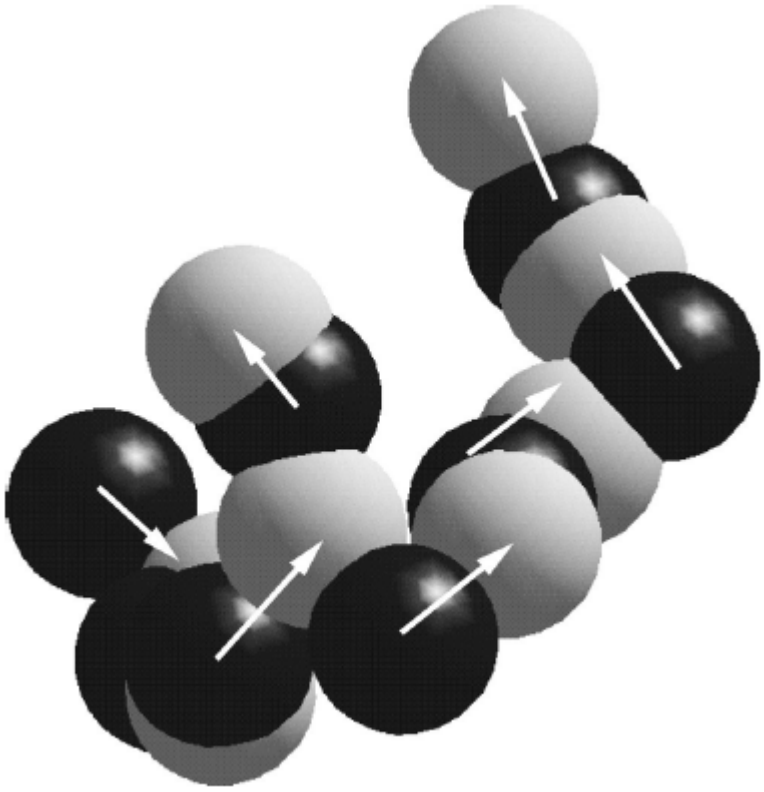

Fig. 2.17 Representation of string-like mobile cluster in a glass forming liquid.(Graph from[29])

The second important findings from some computer simulation works are about the distribution of the local relaxation time or dynamics in confined glass forming systems. As mentioned in the previous section, as of today there is no available measurement techniques to obtain such information as the distribution of the local relaxation time or dynamics in confined glass systems. Therefore such studies using the computer simulations are welcome and valuable to researchers. In [49], the relaxation dynamics of a super-cooled liquid confined between two rough walls are studied. The glass forming liquid is a mixture of A (80% in number concentration) and B (20% in number concentration) particles that interact via a Lennard-Jones (LJ) potential. In this system, all results are given in reduced LJ units, e.g., Boltzmann's constant $k_B = 1$ and the unit of temperature is 1; the mode coupling theory critical temperature is $T_c = 0.435$(please note this temperature is higher than experimentally measured T_g); due to the prohibited calculation time, the lowest temperature studied is T=0.5; the system confining rough walls are obtained by freezing the configurations of the same liquid at a fixed temperature— the as obtained walls have the identical structure of wall-sandwiched

liquid in the bulk state. To obtain the dynamical properties of the glass forming super-cooled liquid, the basic quantity is the intermediate scattering function $F_S(q,z,t)$:

$$F_S(q,z,t) = \frac{1}{N_\alpha}\sum_{j=1}^{N_\alpha}\left\langle \exp\left[i\vec{q}\bullet(\vec{r}_j(t)-\vec{r}_j(0))\right]\delta(z_j(0)-z)\right\rangle, \tag{2.33}$$

where z is the distance from the confining wall, t is time and $\vec{q}$ is the wave vector. In Fig. 2.18, the intermediate scattering function $F_S^P(\vec{q},z,t)$ for different location (slices) are shown as thin curves. For most of the $F_S^P(\vec{q},z,t)$ curves, the features are in agreement with the prediction of the mode coupling theory: the first decay corresponds to the fast particle motions within the cage formed by the surrounding particles of any test particle; the plateau at the intermediate times corresponds to the temporarily cage trapping test particles, which is related to the β relaxation; the second decay at long times corresponds to the cage-opening and escape of the test particles, which is related to the α relaxation. It is also possible to assign different mode coupling theory critical temperatures to different locations/slices[128]. In this study the α relaxation times are defined as the time when the $F_S^P(\vec{q},z,t)$ decreases to $1/e$, as shown in Fig. 2.18, for different location/slices of the rough wall confined liquid. We note that for locations near to the rough wall, the α relaxation decays are stretched and the dynamics therein are slowed down due to the interface/wall effects; at the central parts of the liquid, the dynamics are very close to the bulk values. The authors also note that the stretched exponential index β decreases when the specifc location approaches to the rough wall. Therefore, we can say that for this system studied, the dynamics are heterogeneous in terms of both points: different system locations have different dynamics or α relaxation times; the time-temperature superposition principle is not valid in that the β values are location specific. Another important feature one should note in Fig. 2.18 is that the *whole system averaged* $F_S^P(\vec{q},z,t)$ (shown as the bold solid curve) has a *three-step decay feature,* which is in contrast to the two-step decay for the specific location $F_S^P(\vec{q},z,t)$. The long time tail in the whole system averaged $F_S^P(\vec{q},z,t)$ mainly results from the local dynamics of the locations near the rough wall where the dynamics are dramatically slowed down. In real world experiments, most measured variables are the averaged dynamics and sometimes it is hard to explain the results properly. In [129], Scheidler, Kob and Binder

point out the popular interpretation of different relaxation peaks in some dielectric spectroscopy measurements could be questionable, where some potential smooth gradient/distribution of local dynamics are usually overlooked.

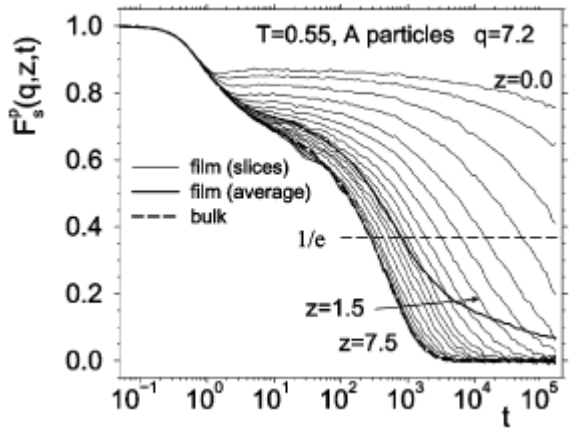

Fig. 2.18 Intermediate scattering function (for A particles) taking angular average over wave vectors parallel to the walls; the bold dashed curve is for the bulk system; the thin curves are for different location in terms of the distance of z from the walls; the bold solid curve is for the average $F_S^P(\vec{q},z,t)$ over the whole confined system (the distance between the two walls are 15.0). (Graph from [49])

Fig. 2.19 shows the α relaxation times for glass forming liquids confined between two rough and smooth walls as a function of temperature and particle distance z from the walls. We note that the rough and smooth wall interfaces have opposite effects on the particle dynamics: the particle motions are slowed down by the rough wall and accelerated by the smooth wall. At the center of the liquid system, the bulk dynamics are reconstructured. The smooth transition of the α relaxation times from the enhanced or slowed-down dynamics to the bulk dynamics can be fitted using the exponential function (shown as the dashed curve in Fig. 2.19). In addition, we note that the interfacial effect penetration depth increases with decreasing temperatures. By some empirical fitting functions, the authors find that this characteristic interfacial effect penetration depth scales with an exponential function of the temperature, $\xi \propto \exp(E/T)$. The temperature dependence of the cooperative rearranging motion related characteristic length scale is in agreement with the results of some experimental studies [27, 32, 80].

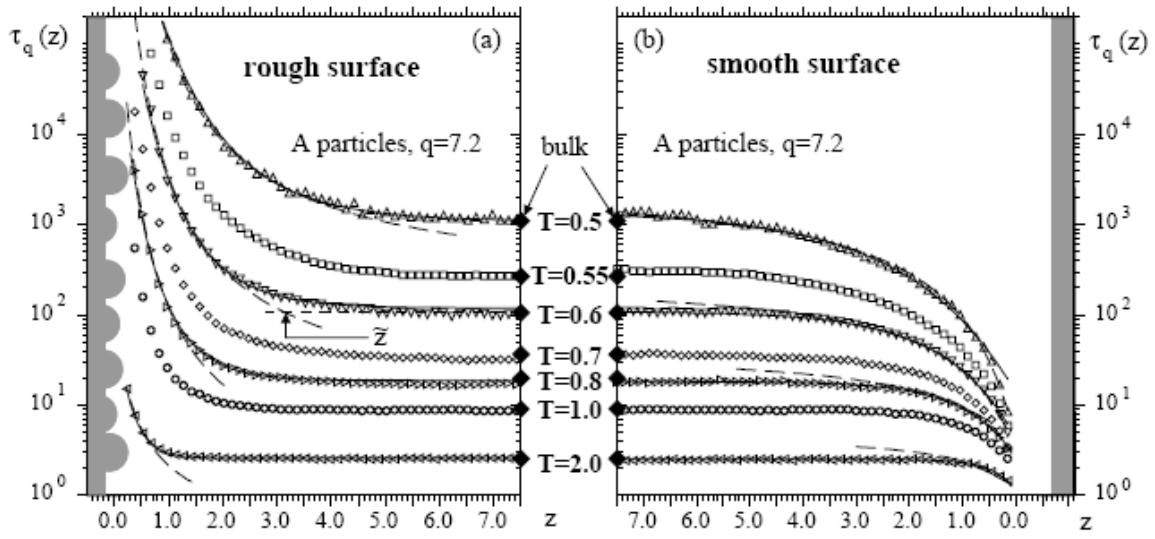

Fig. 2.19 α relaxation times for glass forming liquids confined between two rough and smooth walls as a function of temperature and particle distance z from the walls; the filled diamonds correspond to bulk relaxation times at different temperatures. (Graph from [129])

In the above studies, both the interfacial effects of rough and smooth confining walls are studied. There are some interesting findings about these two different confining interfaces. In the case of the rough confining wall, Scheidler, Kob and Binder [129] noticed that some basin-hopping mechanism can be observed in the local region near the rough walls. It is pointed out that the rough wall can form some potential energy landscape, which has some local energy minima (basins). When one test particle jumps from one minimum basin to another minimum basin, the neighboring particle can usually jump into the voided basin minimum. By doing this, the motions of the particles near the rough walls are correlated together, and the basin-hopping dynamics are energy activated. Such rough wall potential energy landscape can have a long range effects by the cooperative rearranging motions of the particles. Refer to findings in [25, 90], we observe a weak temperature dependence of the near free surface dynamics in glassy thin polymer films, which has the signature of energy activated mechanism as well. It is interesting that if we treat the free surface underneath bulk glassy regions as a "rough wall", which may form potential energy landscape as well, and the energy activated dynamics in the near free surface regions of glassy polymer films can be explained. In the case of the smooth confining walls in [129], Scheidler, Kob and Binder mentioned that close to the smooth wall strong layering effects occur. To avoid such strong layering effects, an external modification potential

has to be added to the system and any configurations deviating from a constant density profile are energetically disfavored. Due to this modification, the results of the system confined between two smooth walls may not be directly compared with real experiment results. If we treat the air/vacuum – polymer interface as the "smooth wall", in real world measurements some potential layering effects might exist [25].

In the above section, some computer simulation studies for confined simple glass forming liquids are described, especially focusing on the dynamical properties on the microscopic level. There are also many computer simulation studies for confined polymeric glass forming systems. Some of them focus on chain conformation variations near planar plates [130, 131, 132]. Some focus on the glass transition temperature or dynamics heterogeneity of polymer films [128, 133, 134, 135, 136]. It is interesting to note that many experimental observations of the glass transient temperature deviations in confined thin polymer films can be found in computer simulated polymer systems as well. In [128], the free standing polymer films are simulated with a bead-spring model, in which the interactions between non-bonded monomers are described using the Lennard-Jones(LJ) potential and those for bonded monomers along the polymer chains are described using a harmonic potential

$$U_{bond}(r) = \frac{k}{2}(r - r_0)^2, \tag{2.34}$$

where k is the entropic spring constant for polymer molecules. The monomer mean square displacement (MSD) are used to extract the dynamical properties from the simulation calculations

$$g_1(t) = \left\langle [\vec{r}(t) - \vec{r}(0)]^2 \right\rangle. \tag{2.35}$$

Fig. 2.20 shows some results of mean square displacements and relaxation times for free standing films and bulk system. In this graph, h is the thickness of the free standing films; the relaxation time τ_1 is defined as time where $g_1(t = \tau_1) = 1$; T_C and γ_1 are parameters of the mode coupling theory prediction of $\tau_1(h,T) \propto (T - T_C(h))^{-\gamma_1(h)}$. From the mean square displacement data, we see: (1) Every MSD data set has three regimes, e.g., the short time ballistic regime, the sub-diffusive regime (related to chain connectivity), and translational diffusion regime. (2) The free standing films have

lower relaxation times. By fitting the relaxation time $\tau_1(h,T)$ to temperature T, the critical temperature $T_C(h)$ can be obtained for free standing films with different thicknesses. The $T_C(h)$ scaled relaxation times are shown in the upper graph of Fig. 2.20, from which we see that at high temperatures a master curve is consistent with the mode coupling theory prediction.

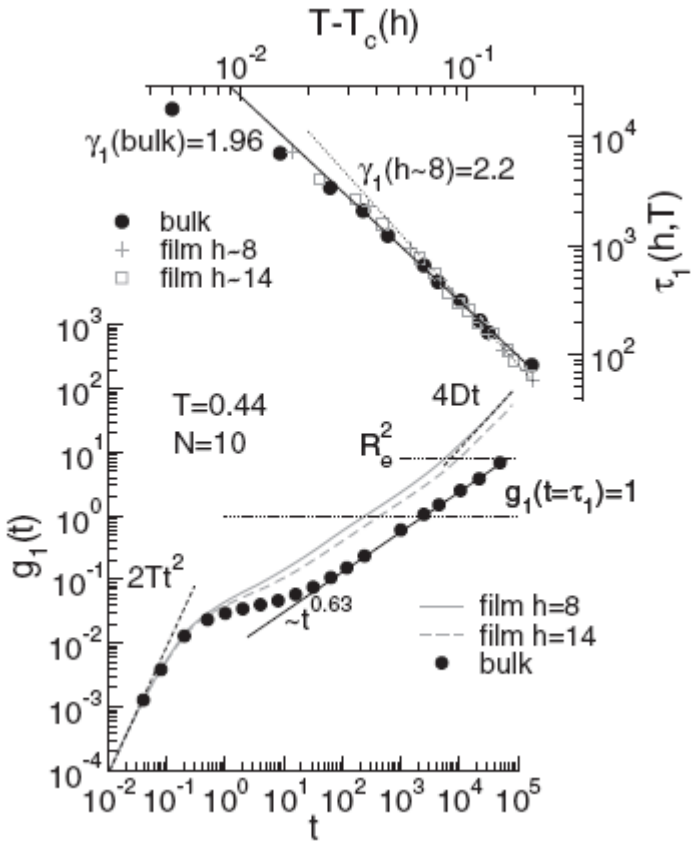

Fig. 2.20 Mean square displacements and relaxation times for free standing films and bulk system. (Graph from [128])

In [123, 137] a glass transition temperature scaling relationship is proposed

$$T_g(h) = \frac{T_g}{1 + h_0 / h}, \tag{2.36}$$

where T_g and $T_g(h)$ are the glass transition temperatures for bulk and thin film polymer systems; h is the film thickness and h_0 is a material constant. Based on Eq. (2.36), Peter *et al* [128] proposed a scaling technique— $T_g(h)$ (or $T_C(h)$) scaled by T_g (or T_C) and h by h_0, by which many results of simulation and experimental studies collapse together(shown in Fig. 2.21). From the right side of Eq. 2.36, we note that the only parameter that can include interfacial effects is the material constant h_0. If we pay more attention to the results of different systems in Fig. 2.21, we have to consider more seriously the potential different interfacial interactions in them. The system for "T_C (confined)" is for "melt confined between two smooth repulsive walls"; from the results of [129], we note that the molecular dynamics near such smooth repulsive walls are enhanced. The system for "T_C (supported)" is for melt supported on a smooth weakly attractive substrate on one side and has a polymer-vacuum interface at the opposite side, which is very similar with situations for the experimental data of "T_g (PS, high Mw)" and "T_g (PS, low Mw)". The system for "T_g (MC: PP)" is Monte Carlo simulations of free-standing polypropylene (PP) films. Therefore, all these systems can be treated as effective "free standing films". Accordingly the values of h_0 varies weakly from system to system, which may be why the proposed scaling approach work so well for these systems. A real challenge for this scaling technique could be to apply it to both free standing polymer films and systems with strong sample-substrate interactions, such as those systems being confined between two "rough walls"[49].

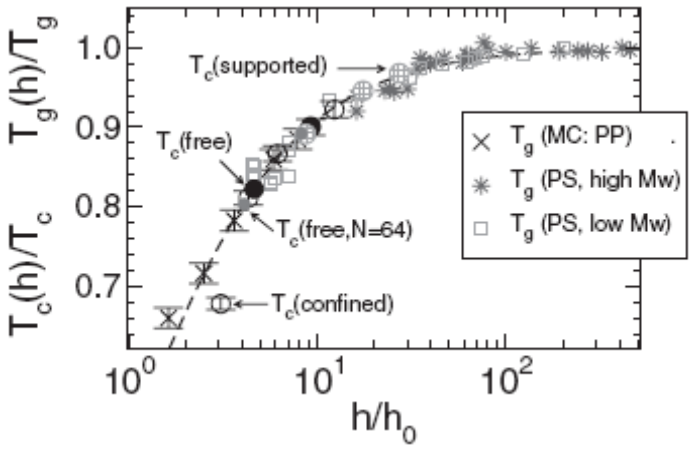

Fig. 2.21 Scaling plot of $T_g(h)$ and $T_C(h)$ for different studies.(Graph from[128]).

In [128], the mode coupling theory critical temperature $T_C(h)$ for free standing films is compared with the glass transition temperature $T_g(h)$ using a scaling approach, and it is shown that the former for free standing films is reduced compared with bulk T_g. In [114], the computer simulation studies of free standing polymer films are carried out, in which the surface and bulk T_g are obtained directly from the temperature dependence of the chain segment MSD's at different locations. It is found that the glass transition temperatures of the surface regions are in good agreement with the experimental results, which shows that the surface T_g are reduced compared with that of the bulk materials.

In summary, computer simulation studies of glass forming systems can, on the one hand, test theoretical predictions and, on the other hand, observe new aspects of physical problems, especially from the microscopic perspective, for example many aspects of the mode coupling theory predictions are proved, but unexpected features such as the dimensions and time evolving properties of mobile clusters are observed as well, which is more important for further experimental investigations and more theoretical considerations. In the case of polymeric glass forming systems, especially for free standing polymer films, many experimental observed dynamical features, such as enhanced dynamics and reduced T_g in the near free surface region can be observed in computer simulation studies.

Chapter 3

Experimental techniques

3.1 Thin polymer film preparation

3.1.1 Preparation of substrate supported films

In the present projects, most polymer samples are planar substrate supported thin films of thickness of the order of several tens of nanometers. To make high quality planar polymer samples on such small length scale, it is crucial to choose suitable ultra-flat substrates and use a suitable technique to make sure the polymer film surface is ultra-flat as well.

We use three kinds of substrates in our measurements. The first one is single side polished silicon wafers, which are purchased from Silicon Quest Int'l and have a crystal orientation of <100>. The polished front-side, ~0.1nm in roughness (Silicon Quest Int'l; $R_a \approx 0.25nm$ by our measurements), is used as the substrate surface. Before being used, the big silicon wafers(3" in diameter) are cut into many $1 \times 1cm^2$ square pieces, which is important to make polymer films of uniform thickness— for big substrates it is hard to make polymer films of the same thickness. During silicon wafer cutting, we put the front-side face down on top of lens cleaning papers(Kodak) and use a diamond knife to scratch the back-side with the help of a ruler along the crystal orientation direction and then the gentle

bending along the scratch while the wafer is still face-down is sufficient to set silicon wafers apart. The advantage of such gentle bending technique is that there are very few solid silicon dusts contaminating the front-side of the silicon wafer pieces. Otherwise, once the solid silicon dusts, which are produced during the cutting procedure, contaminate silicon wafers, it is very hard to get rid of them. Another point about silicon wafer cutting is that we tried other wafers of a crystal orientation of <111> and found that the <100> wafers are the easiest ones that can be cut into neat small square pieces. The second kind of flat planar substrate used is $22 \times 22 mm^2$ microscope cover glasses and $3'' \times 1'' \times 1mm$ Premium microscope glass slides both obtained from Fisher Scientific with a surface roughness <3nm[138]. The third kind of substrate used is ultra-flat aluminum layer(1.2nm in roughness and ~100nm in thickness; determined by AFM) coated onto the aforementioned silicon wafers and glass slides, which will be described in more detail in the section of "3.6 Preparing ultra-flat metal substrate by thermal metal evaporation".

There are many methods of making thin polymer films, such as the spin-coating technique, dip- and flow-coating [139]. To make ultra-flat and ultra-thin polymer films, we choose the spin-coating technique [140, 141]. The major process of the spin-coating technique is that the high speed horizontal rotation of the substrate spreads the polymer solutions on top to form a uniform film, which depends on the balance of the centrifuge force and the polymer solution viscous force and polymer solution-substrate adhesive force. The thickness of polymer films made by the spin-coating technique is a function of spin-coating speed, solution concentration/viscosity and polymer molecular weights[140, 141, 142, 143]. Quantitatively, the polymer film thickness h follows the formula

$$h = k\eta_0{}^{\beta}\Omega^{\alpha}, \tag{3.1}$$

where k and β are material specific constants, η_0 is the initial polymer solution viscosity, Ω is the spin-coating angular velocity and α is a constant around -0.5 for most polymers. The following is how we make thin polymer films using the spin-coating technique.

First, polymer solutions of weight percentage concentration of 0.4%-5.0% are made. All utilities, such as 10 ml glass bottles, pipettes and tweezers are cleaned using the solvent before making polymer solutions. To get uniformly dissolved transparent solutions, sometimes it is necessary to heat

the polymer-solvent mixture up to ~ 313K for some time. Usually, after being kept at room temperature for ~3 days, the as-produced solutions are then used to make polymer films. Before depositing polymers, all substrates are properly cleaned by careful treatments (see the section of "3.6 Preparing ultra-flat metal substrate by thermal metal evaporation"). When doing spin-coating, first, two drops of polymer solution are put at the center of the cleaned substrate sitting on the static spin-coating disc— to make uniform polymer films it is important to avoid bubbles when depositing polymer solutions; then we start spin-coating with a preset rotation speed and let the spin-coating disc rotate for 10 seconds until the color of the polymer film is stable. The qualities of the polymer films depend on many factors. Specifically, the following factors are considered when we make polymer films using the spin-coating technique:

● *Solvent choice*: In our measurements, all polymers are dissolved in toluene; We also tried acetone and found that it can dissolve polystyrene and i-PMMA quickly but the films made from such solutions are not uniform with some small holes in the film surfaces; the difference between toluene and acetone is that the former solvent evaporates slowly while the later evaporates quickly, which is the cause whether the as-produced polymer films are uniform or not [140, 142, 143].

● *Air circulation in the spin-coating chamber*: During spin-coating the evaporation of solvent can change the viscosity of the polymer solution and accordingly has an effect on the final film thickness. Therefore, it is important to avoid large fluctuations in the air circulation in the spin-coating chamber.

● *Polymer solution concentration*: In our studies, the polymer solutions have a weight percentage concentration of 0.4%-5.0%— if the concentration is too low it is very easy for polymers get dewetting and non-uniform films can be produced; on the other hand, if the solution concentration is too high, some corrugations can be formed on the surfaces of non-uniform polymer films, especially when making thick(>200nm) films.

● S*pin-coating speed*: Usually, we use a spin-coating speed within a range of 1000-5000 RPM. For the same polymer solution, a higher spin-coating speed results in thinner polymer films.

● *Molecular weight* M_w *of polymers*: For the same concentration, solutions of polymers with higher M_w have higher viscosity. Consequently, the thickness of polymer films made by the spin-coating technique depends on M_w as well.

After spin-coating, the polymer films are usually kept at room temperature for ~4 hours to let the solvent in the polymer films evaporate slowly. The films are then annealed at a temperature ~20K above bulk T_g for more than 16 hours in a home-built oven to remove residual solvent and stress introduced by spin-coating procedure. Another point of such high temperature annealing treatment is to relax polymer chain molecules in the films to reach an equilibrium state— one should note that at a temperature ~20K above bulk T_g the chain segment characteristic relaxation time is ~0.001s and accordingly the chain segments can "freely" wiggle around to reach an local equilibrium state. During the sample annealing in the oven a purge of dry Nitrogen gas is used to avoid any potential thermal chemical reaction between the sample and ambient atmosphere. After annealing, the samples are cooled down to room temperature with a cooling rate of 0.5K/min in the oven. After all these treatments, the polymer films are kept in clean plastic containers for use in the future. In some studies people do high temperature polymer sample annealing in vacuum to avoid potential chemical attack from the ambient. However, in most cases there are often some oil molecules in the vacuum chamber which come from the low-pressure pump-down system and the small oil molecules may either react with the polymer sample at high temperatures or contaminate the polymer sample by acting as plasticizers. If oil-free vacuum system is used, it is not a big concern.

We use two techniques to generally characterize thin polymer films. Both the film surface roughness and thickness can be determined by the Atomic Force Microscopy (AFM). Using the non-contact mode AFM, we found that the surface roughness of the polymer films we made is ~0.5nm determined in a scanning area of $80 \times 80 \mu m^2$. To determine the film thickness, we use a new sharp medical injection needle to scratch the polymer sample and then from an $80 \times 80 \mu m^2$ AFM scanning image of the scratch area the film thickness can be obtained. We use the Ellipsometry to determine the glass transition temperature T_g and film thickness of thin polymer films. More details about the Ellipsometry measurement can be found in the section of "3.9 Thin polymer film characterization using Ellipsometer".

3.1.2 Preparation of free standing films

Compared with the substrate supported thin polymer films, free standing polymer films have some novel properties such as pronounced T_g reductions[67, 73, 74, 75, 76, 77, 78, 144], which may result from the unique symmetric geometry along the surface normal direction in terms of some potential dynamics gradient distribution. In addition, the free standing films can be a model system to test some theoretical models addressing the outstanding T_g anomalies [80, 109, 110, 103] in thin polymer films.

Forrest and co-workers [77, 78], for the first time, developed the novel water transfer technique to produce free standing polymer films. In their pioneering work, the well annealed polystyrene films on glass slides or fresh cleaved mica are cut into many pieces of size $\sim 1\times 1 cm^2$ and then floated onto the surface of distilled water, which are then transferred to sample holders of 3mm-diameter holes. Recently, Torkelson and co-workers [145] conducted T_g measurements of free standing films (on 1mm diameter hole) using the same water transfer technique. In reference [146], McKenna and co-worker modified the water transfer technique a little bit: they float off as-produced polymer films (after drying and cutting) onto water and transfer them onto free standing film holders; the high temperature annealing treatments are then carried out for such free standing films. We tried the similar procedure and found that it is very easy for unannealed polymer films to be floated off the glass substrate. In addition, We found another much easier method to make free standing polymer films. A $10\times 10 mm^2$ square patch of double-side tape with a 2mm-diameter hole in the center is first attached to well annealed polymer films; then after cutting and immerging the tape-covered polymer film into distilled water it can be gently picked up using a tweezer — the film at the center of the tape serves as the designed free standing film. Considering some specific factors such as potential effects of tape glue molecules on properties of the polymer sample, the original water transfer technique [77, 78] is used for all measurements. We need to study the near free surface region dynamical properties of free standing polystyrene films by means of the nano gold sphere embedding technique. After the gold spheres are cast onto the surface of PS films, any high temperature treatment should be avoided when making free standing films. Therefore, it is necessary to float well annealed PS films (with nano gold spheres) onto water surface to make free standing films. In addition, by the same water transfer technique, the present results can be compared directly with those in literature [77, 78].

In one project, the nano gold sphere embedding behavior in the near free surface region of free standing films is studied by AFM scanning. A big challenge for such polymer samples is to avoid PS film vibrations during AFM scanning. We tried different free standing film holders of different size and found that if the film holder hole size is too big, e.g. ~2mm in diameter, the free standing film can not be properly scanned by AFM due to sample vibrations and if the sample holder hole size is smaller than $25\mu m$, it is very hard to locate the AFM tip to the area of the free standing film. Therefore, we choose the Transmission Electron Microscopy(TEM) grids (PELCO 3HGT 75 mesh; center-marked; material-Titanium) of square mesh size $284 \times 284 \mu m^2$ (bar width: $55\mu m$)as the free standing film holder, which are glued onto an aluminum sheet with a hole of a diameter of 2mm. The glue used is "5 minutes epoxy glue" (LEPAGE), which is water resistant. The following is the specific procedure of preparing free standing films sitting on TEM grids.

First, the polystyrene films, which are spin-coated on glass sides, are annealed at 393K for more than 16 hours in the home-built oven with a purge of dry nitrogen gas. After cooling down to room temperature, the PS films are cut into small $5 \times 10 mm^2$ pieces using sharp one-side blade. Then, the PS film on the glass side is immerged into warm distilled water (~313K) carefully with an obliquity $\sim 45^o$. When the water approaches the front scratch of the designed small PS piece, usually we use a new sharp medical injection needle to tear the corner section of the PS piece a little bit and then the water surface tension can drive to float the PS film off the glass slide. Because the PS film on glass slide is transparent and it is hard to see the scratch on the film by eyes, a table light is needed when making free standing films. After being floated onto water surface, the small piece of polymer film can be picked onto the TEM grid from underneath in distilled water. The as-produced free standing films sitting on TEM grids are kept at room temperature for at least one day in a purge of dry nitrogen gas to get rid of the residual water. It is noteworthy that any heating treatment should be avoided before starting measurements. On the one hand, unwanted nano gold sphere embedding can be introduced if heating treatments are used. On the other hand, any high temperature heating can enhance the evaporation rate of water, which, we found, can introduce many small wrinkles to the free standing films. One may ask if there is water left in the free standing film, which may act as plasticizer for the polymer films. Considering that the major point of this project is to test de Gennes model(see chapter 2) for free standing films, the effect of potential water residues is negligible.

We use AFM to characterize the surface of free standing films by applying carefully chosen scanning parameters such as AFM cantilever set-point, scanning range and rate, and AFM internal feedback controlling parameters of Proportional(P)& Integral (I). The thickness of the free standing films is determined by floating the same PS films onto silicon wafers and then measured with AFM and ellipsometry.

Fig. 3.1 shows four AFM images of free standing films. We can see wrinkles in every image. The sample corresponding to the upper-right AFM image was put on a sample holder with a 2mm hole in the center; the samples for the other image were put on TEM grids with square mesh size of $284 \times 284 \mu m^2$. The relatively big deep wrinkles in the upper-right image may be due to the large size of sample holder used. Also shown in the upper-right image are some gold spheres, which are spin-coated onto substrate supported PS films first and, then such films with gold spheres on are floated onto water surface and transferred to the sample holders to form free standing films.

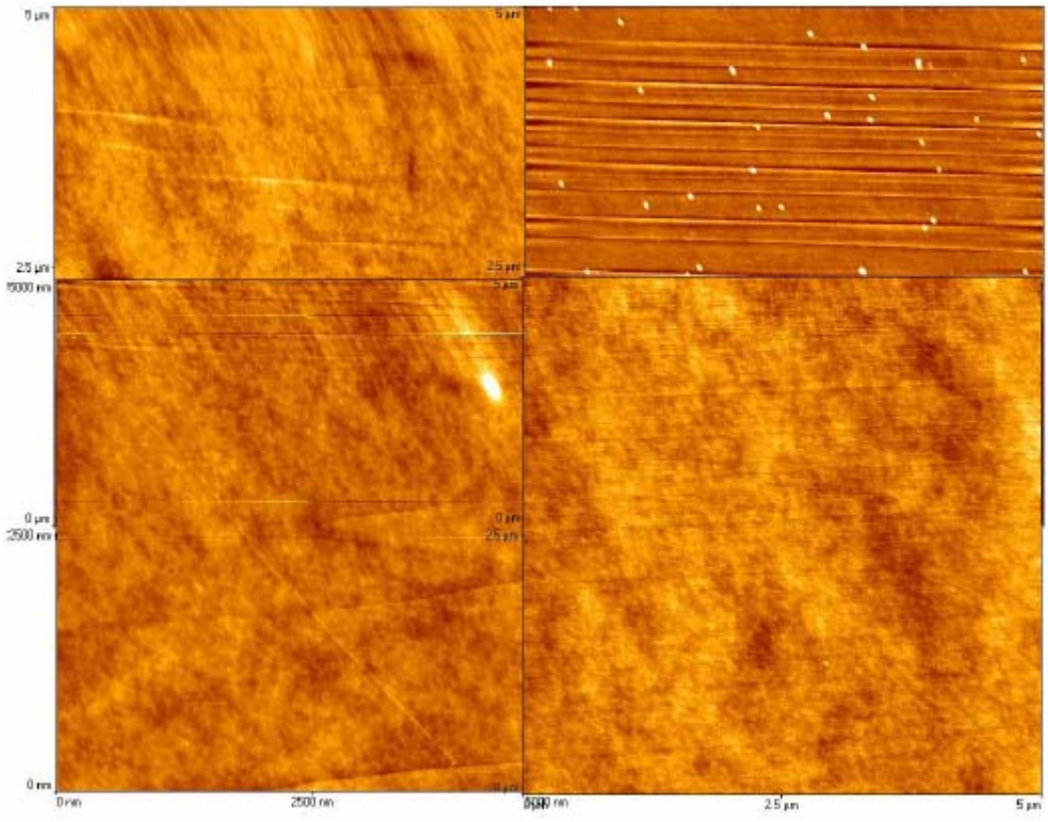

Fig. 3.1 Four AFM images of free standing films: wrinkles can be seen in every image; in the upper-right image also shown are some gold spheres.

3.2 Thermal treatments of polymer films

There are many ways to change molecular motions such as by changing the pressure or temperature of the samples [147, 148]. In some systems [149, 150], the molecular motion controlling parameter is the volume faction of materials studied. In the present projects, we study dynamical properties of thin polymer films by changing the temperature of the samples. In addition, since the present projects focus on dynamics in the *near free surface region* of substrate supported polymer films and free standing films, it is crucial to have a good control of the real temperature of the polymer regions investigated. In this section, all thermal treatments in the measurements are described separately.

High temperature long time annealing treatment of polymer film

As already mentioned, for glass forming materials the glassy state is not an equilibrium state and the system in the glassy state always has a tendency to evolve to the potential final equilibrium state through structural relaxations. Except for specifically designed aging studies, it is important to get the systems studied into the equilibrium state before real measurements. Conventionally, this is achieved by high temperature long time annealing treatments. Compared with some thermal treatments, for example, in [66], all thin polymer films in our measurements are thermally treated in the following way.

Firstly, after being cast onto substrates, the polymer films are kept at room temperature for ~ 4 hours to let the solvents evaporate slowly. This actually has similar effect of "solvent annealing" [151], by which the polymer chains can relaxation with the presence of solvent molecules and a uniform film can be formed. Otherwise, if the freshly spin-coated polymer films(especially for ultra-thin films) are put in the high temperature oven, some small holes can be formed in the polymer films due to rapid evaporation of the solvent and polymer dewetting from the substrate. Secondly, after the first-step treatment, the polymer films are put in a home-built oven at a temperature of ~20K above bulk polymer T_g to do annealing for more than 16 hours. At this high temperature, the polymers are in the rubbery state and chain molecules can relax completely with fast enough mobilities to reach the equilibrium state. In addition, any residual solvent or stress resulting from the spin-coating procedure can be removed by the high temperature annealing treatment. To avoid some potential thermal chemical reaction between the polymer sample and the ambient, the high temperature annealing

treatment is carried out with a purge of dry nitrogen gas in the oven. Thirdly, after the second-step annealing treatment, the heating system of the oven is switched off to naturally cool down the polymer samples to room temperature in about 4 hours (with an average cooling rate of ~0.4K/min) and then the samples are taken out for measurements. If the freshly annealed polymer samples are quenched from a temperature of ~20K above bulk polymer T_g to room temperature, the aging effect or large structural relaxation can not be negligible, which should be differentiated from the polymer chain relaxation propertied interested.

Temperature control for the near free surface region of thin polymer films

General temperature control

Since we study the thermal dynamical properties of the near free surface region in thin polymer films, it is important to make sure that the real temperature in this region is what we set. To confirm this, we performed some measurements of the quasi-surface temperature of silicon substrate supported 100nm thick i-PMMA films sitting on a Linkam heating stage(Linkam Scientific Instrument Ltd, UK; temperature controlling precision: $0.1^{\circ}C$) with a series of setting temperatures. The measurements are carried out at a room temperature of $14^{o}C$ and the near free surface temperature of the i-PMMA film is monitored using a thermocouple gently touching the sample surface. Fig. 3.2 shows the measurement results. We see that for the measured results there is a systematic deviation from the heating stage set temperatures within a temperature window of $25-60^{o}C$.

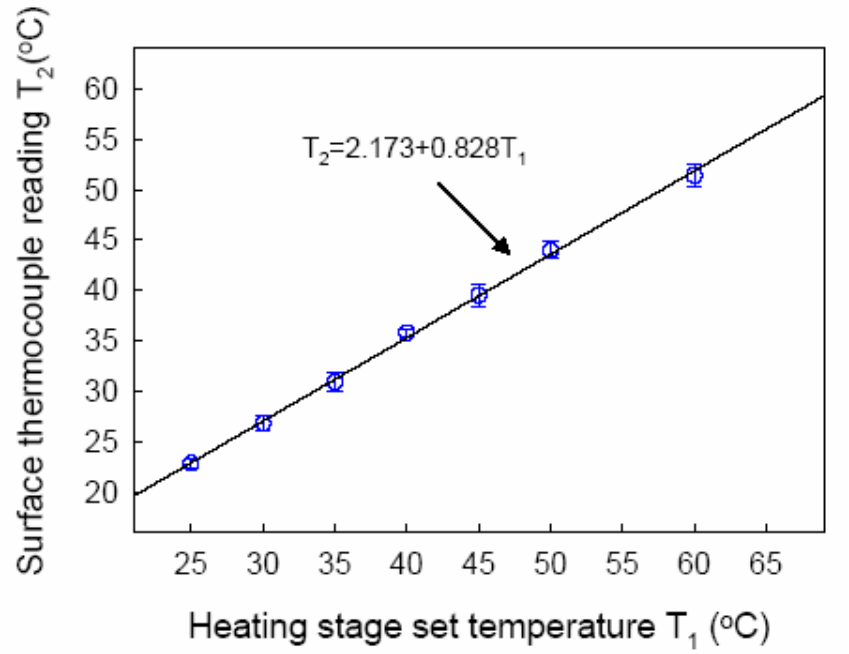

Fig. 3.2 Results of polymer surface temperature measurements: blue circle symbols show data measured using a thermocouple on a thin polymer film surface.

Considering the above mentioned temperature deviation together the fact that the operation temperature of our AFM is $5-40^{o}C$, our experiments involving high temperature treatments such as the nano gold sphere embedding measurements are conducted using the home built oven. For experiments involving low temperature treatments such as the studies of i-PMMA nano surface hole relaxation are carried out within a small box where the temperature is controlled using ice. In both cases, a thermocouple is used to monitor the experiment temperature.

Temperature control for free standing film studies

From the foregoing section, we see that even for substrate supported polymer films, which are heated from the substrate side, there is a temperature deviation from the hot stage setting temperature in the near free surface regions of the samples. The best way to solve this problem is to reduce the temperature difference between the desired hot stage and the ambient, and the most straightforward strategy is to use an isothermal oven. In our studies of near free surface dynamical properties of free standing films, the potential temperature deviation is even severe since the heat can only be transferred to the sample through thermal radiation from the heat source other than the common physical thermal conduction. To address this specific issue, we design the thermal treatment system

for free standing film studies in the following way. Fig. 3.3 schematically depicts our experimental setup.

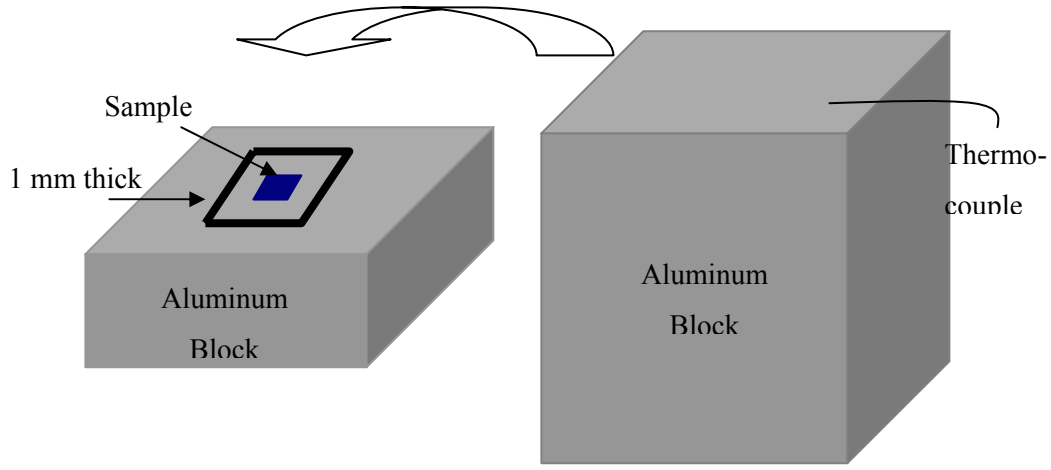

Fig. 3.3 Schematic setup for free standing film temperature control.

As shown in Fig. 3.3, we use two aluminum blocks ($2\times 8\times 10cm^3$ and $5\times 10\times 10cm^3$ in size) as the heat sources which are put in the home-built oven for a long time to reach the desired temperature. The reason that we choose aluminum blocks as the heat source is that aluminum has a high specific heat capacity (see Table 3.1) and the temperature fluctuation is less than $0.2K$ when we open the oven to put in or take out the samples. We use a thermocouple, which is glued to the aluminum block surface using high temperature high thermal conductivity epoxy adhesive(Omegabond "200" Resin and Catalyst; Omega Engineering, Inc), to monitor the temperature of one surface of the big aluminum block, which is put on top of the smaller aluminum block. In between of the two blocks are the free standing films with the surface containing nano gold spheres. Between the two aluminum blocks are 1mm thick glass slide spacers closely surrounding the polymer samples. Since the distance between the two heating sources and free surfaces of the free standing film is ~1mm and the thermal fluctuation of the heat reservoir (Al blocks) is negligible, the real temperature at the free surface of the free standing film is almost identical to the desired temperature. Considering that the sample surrounding spacers are close and the air flow in the 1mm gap of the two aluminum blocks is blocked, the two-Al-block system can be taken as an isothermal oven. That is, the temperature controlling

system for the free standing films is actually a combination of two ovens — the two-Al-block assembly oven in the big home-built oven.

Table 3.1 specific heat capacity of some common metals.

Metal	Al	Fe	Cu	Pb
C_p (kJ/kgK)	0.91	0.46	0.39	0.13

Ultra-low temperature control

In the study of nano surface hole relaxation in polystyrene films [90], Fakhraai and Forrest observed a very weak temperature dependence of chain segmental dynamics in the near free surface region, where the lowest measurement temperature is 277K. It is surprising that even at a temperature ~94K below bulk T_g the nano surface holes in the near free surface region of 100nm thick polystyrene films can still relax, which indicate enhanced chain segmental motions in this region, and the temperature dependence of polymer surface dynamics is very weak compared with that of bulk materials at the same temperature. To further check this weak temperature dependence, we conducted measurements of nano surface hole relaxation in polystyrene films at a ultra-low temperature of 243K(~130K below bulk T_g). Considering that this measurement might run for a long time (actually ~398 days), we use a refrigerated circulator to achieve this low temperature. Fig. 3.4 depicts the setup of the ultra-low temperature control. The circulator used is a VWR Refrigerated Circulator with a cold plate (TCP-2, Thermoelectrics Unlimited Inc). The circulating fluid in the reservoir is a ~20% ethylene glycol based water solution. We use a 5mm high plastic circular box, on which is attached a thick thermo insulating foam, to cover the sample stage of the cold plate. A thermocouple is used to monitor the temperature of the sample. The cold plate and the sample are in a purge of dry nitrogen gas. Before taking out the sample for AFM imaging, we shut down the refrigerated circulator for 25 minutes to let the sample on the cold plate to warm up to the room temperature of 287K to avoid moisture condensation from the ambient— we also use a dehumidifier in the small AFM room to reduce moisture in the air. According to [90], the characteristic nano surface hole life time (at 287K) $\tau >> 25$ minutes and any surface hole leveling can be negligible. Another point needed to be stressed is that we use silicone sealant to seal the outer cold plate covering and found that some sealant molecules evaporated to the air can be easily condensed onto surfaces of the cold plate and the polymer sample which are at a temperature of 243K. Therefore, after applying the silicon sealant, we

wait for more than 4 days to let the sealant completely cure and dry, and then set up the ultra-low temperature control measurement. After turn on this temperature control system, it takes about 7 minutes for the sample on the cold plate to reach the desired temperature of 243K. To maintain good performance of the long-time- running system, about every month we need to clean out some ice on the wall of the reservoir of the VWR Refrigerated Circulator and fill in more ethylene glycol based water solution.

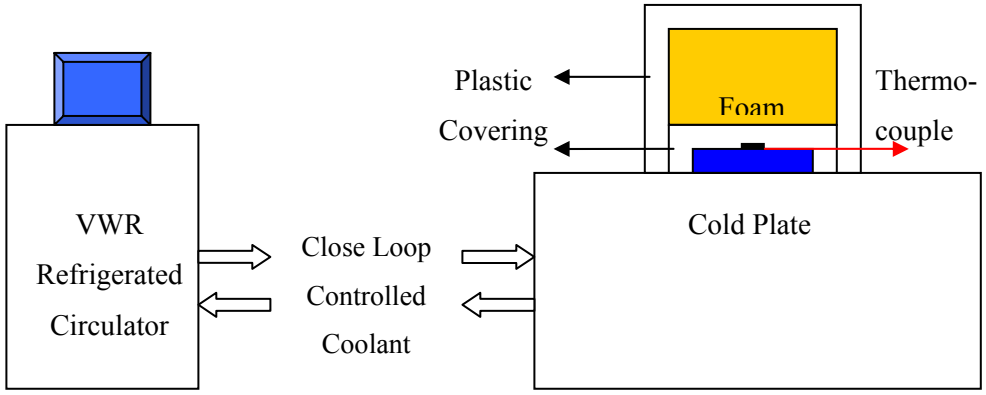

Fig. 3.4 Schematic setup for ultra-low temperature control.

3.3 Preparation of nanometer scale colloidal gold spheres

Nano gold sphere colloidal are heavily used in the present projects. By referring to different references [152, 153, 154, 155, 156, 157, 158] and practising by myself, the following information is obtained about preparing nano gold spheres.

Materials:

(1) Deionized water; (2) Citric Acid Trisodium Salt, Dihydrate- $C_6H_5O_7Na_3 \cdot 2H_2O$ (99%; SIGMA-ALDRICH CO.); (3) Gold chloride hydrate- $HAuCl_4 \cdot xH_2O$ (99.999%; SIGMA-ALDRICH Inc.).

Procedure:

1. Make a gold salt solution of 0.01699g $HAuCl_4 \cdot xH_2O$ in 50 ml deionized water;

2. Heat the above solution in a flask for about 30 minutes until boiling;
   (During heating a magnetic stir bar is used for stirring.)

3. Make a citric acid solution of 0.05g $C_6H_5O_7Na_3 \cdot 2H_2O$ in 5g of deionized water;

4. When the gold salt solution boils, rapidly add the above citric acid solution into the boiling gold salt solution and speed up stirring for about 10 minutes until the color of the mixture is stable(grape wine red— the colloidal strongly absorbs green light[158]).

5. Divide the above gold colloidal into 3 small glass bottles and let them cool down to room temperature and seal them for future use.

In the above procedure, the volume ratio of the gold salt solution to the citric acid solution is 10:1, which results in a gold colloidal with the average nano gold sphere size of $18.7 \pm 1.2nm$ (determined by AFM; more than 200 spheres sampled).

Major factors considered for the gold colloidal:

● All glass wares are cleaned using concentrated detergent and rinsed thoroughly using deionized water.

● Use glass pipettes to handle gold salts when making solution— $HAuCl_4 \cdot xH_2O$ can erode metal utensils.

● After rapidly adding in citric acid solution, vigorous stirring is necessary to keep reduced gold atoms from aggregation during the reduction process; afterwards, the adsorbed citrate anion layer prevents gold spheres from aggregating by electrostatic repulsion forces. .

● If well sealed in glass bottles, the as-produced gold colloidal can have a shelf life of ~ 1 month.

● The average size of the colloidal gold spheres mainly depends on the ratio of the gold salt solution to the citric acid solution: the smaller the ratio is, the smaller is the size of the nano gold spheres in the colloidal. However, the specific procedure preparing nano gold spheres of a certain size may vary from case to case depending on specific lab conditions.

3.4 Producing nano surface holes in surface region of polymer films

In reference [90], Fakhraai and Forrest studied the near free surface region dynamics of glassy polystyrene films using the nano surface hole relaxation technique. In this project we extend this technique to the studies of isotactic poly(methyl methacrylate) (i-PMMA) films, focusing on the dependence of the near free surface dynamics of i-PMMA films on polymer/substrate interactions and polymer chain sizes. In addition, the nano surface relaxation behavior of polystyrene (PS) films in the much deep glass state (~130K below bulk T_g) is investigated as well. To carry out such projects, nano surface holes (~3nm deep) in the near free surface region of thin polymer films have to be produced first. In this section the procedure of preparing such nano surface holes is described.

Materials

i-PMMA and PS are purchased from Polymer Source, Inc.:

i-PMMA: $M_w = 212.4k$, $r_{PDI} = 1.21$, ISO > 98%;

$M_w = 436k$, $r_{PDI} = 1.4$, ISO>98%;

$M_w = 889k$, $r_{PDI} = 1.15$, ISO>95%.

PS: $M_w = 641.0k$, $r_{PDI} = 1.11$.

Mercury: EM SCIENCE, MERCIK KGaA, Darmstadt, Germany;

Johnson Matthey LTD, Canada.

Gold spheres: ~20 nm in diameter; prepared using the citric acid reduction technique.

Nano surface holes preparing in i-PMMA and PS films

Thin polymer films of different thicknesses are produced by spin-coating polymer solutions in toluene with different solution concentrations and spin-coating speeds onto substrates. Details about preparing substrate supported polymer films and different substrates are described else where.

We use nano gold spheres of size ~20nm in diameter to make nano surface holes on well annealed i-PMMA films. The method of making nano gold spheres is described in the forgoing section. Given that the affinity between gold spheres and i-PMMA is stronger than that between gold spheres and polystyrene[159, 160], it is relatively easy to cast gold spheres on the surface of i-PMMA films by spin-coating with the sphere covering density ~ 10 spheres per μm^2. The average centrifuge force acting on ~20nm gold spheres is $\sim 1\times 10^{-18} N$, which is much smaller than the force $\sim 6.9\times 10^{-10} N$ acting on the gold sphere due to the polymer surface tension. We checked from the AFM images of i-PMMA films covered gold spheres and no surface damage is found. After casting gold spheres on the sample surfaces, we then embed the gold spheres into the i-PMMA film surfaces for about 3 nm at a temperature of 4K above the bulk T_g within a dry nitrogen gas in the home-built oven. The gold sphere embedded samples are then cooled down at room temperature for 30 minutes. By comparing the average apparent gold sphere height before and after embedding, we can make sure that the gold spheres embedding depth is ~3nm. After this, we dissolve the already embedded gold spheres on i-PMMA film surfaces using mercury at a temperature of 275–276 K for 2 hours in a fume hood. Considering that i-PMMA has a relatively low bulk T_g ~323K and chain segment mobilities may be fast at room temperature, if the gold spheres are dissolved using mercury at or above room temperature the nano surface holes will be relaxed substantially or completely. Therefore, the procedure of gold sphere dissolving using mercury is carried out at low temperature of 275–276 K, which is achieved in this way: The gold sphere covered i-PMMA film sample is put on a steel sheet (~1mm thick) and a thermal insulating box is used to cover the sample and the steel sheet; this sample-steel-sheet ensemble is put on a dewar, in which is filled liquid nitrogen; the cold nitrogen gas evaporated from the liquid nitrogen can cool down the temperature of the sample-steel-sheet ensemble to ~275-276K which can last for about three hours and is monitored with a thermocouple; a drop of mercury is gently put on the surface of the i-PMMA sample to dissolve the gold spheres; two hours later the drop of mercury is slid off the i-PMMA sample; open the dewar a little bit to let the temperature of the steel sheet increase to ~283K in about 5 minutes and the i-PMMA film sample is

taken out for AFM scanning to track the nano surface hole relaxation at desired temperatures. The mercury dissolving process is carried out in a fume hood. We use the very sharp AFM tips for imaging (NANOSENSORS: Type—PPP-NCH; typical tip curvature radius ~7nm) and the measured size of the as-produced surface holes is ~3nm depth and ~20nm in width. In addition, to avoid polymer surface damaging during AFM imaging we use the non-contact mode to track the relaxation of nanometer surface holes. Usually after being used for scanning several samples, the AFM tip gets dull (not sharp enough). Therefore, we change the AFM tip regularly, e.g. after scanning for three samples, to properly track the leveling of the nano surface holes on polymer film surfaces.

To study the near free surface region dynamics of polystyrene films at deep glassy states, we also make nano surface holes in thin polystyrene films using the similar mercury dissolving technique. Given that the gold sphere affinity to polystyrene is not as strong as i-PMMA, when we cast gold spheres onto the surface of polystyrene films a small amount of ethanol is used in this way: one drop of ethanol is put into 10 drops of gold colloidal and spin-coat such mixture onto polystyrene film surfaces using a spin-coating speed of ~800 RPM. In addition, in the case of polystyrene films we perform mercury dissolving at room temperature since the bulk T_g of PS is relatively high (373K) and any relaxation of the nano surface holes in the two-hour mercury dissolving period can be negligible— we checked through AFM images and found that both the gold sphere embedding depths before and after gold sphere are almost the same value of ~ 3nm. Fig. 3.5 shows some results of nano surface holes in i-PMMA and PS films. The surface hole depth is defined as the distance from the average local surface height to the bottom of the surface hole, shown in (c) —a line scan of one nano surface hole. Also, we note that the appearance of the surface holes, especially the rim surrounding the surface hole, seems different on the same length scale for i-PMMA and PS films. The mechanism of the formation of the rim structures during gold sphere embedding in these two different polymers is unknown.

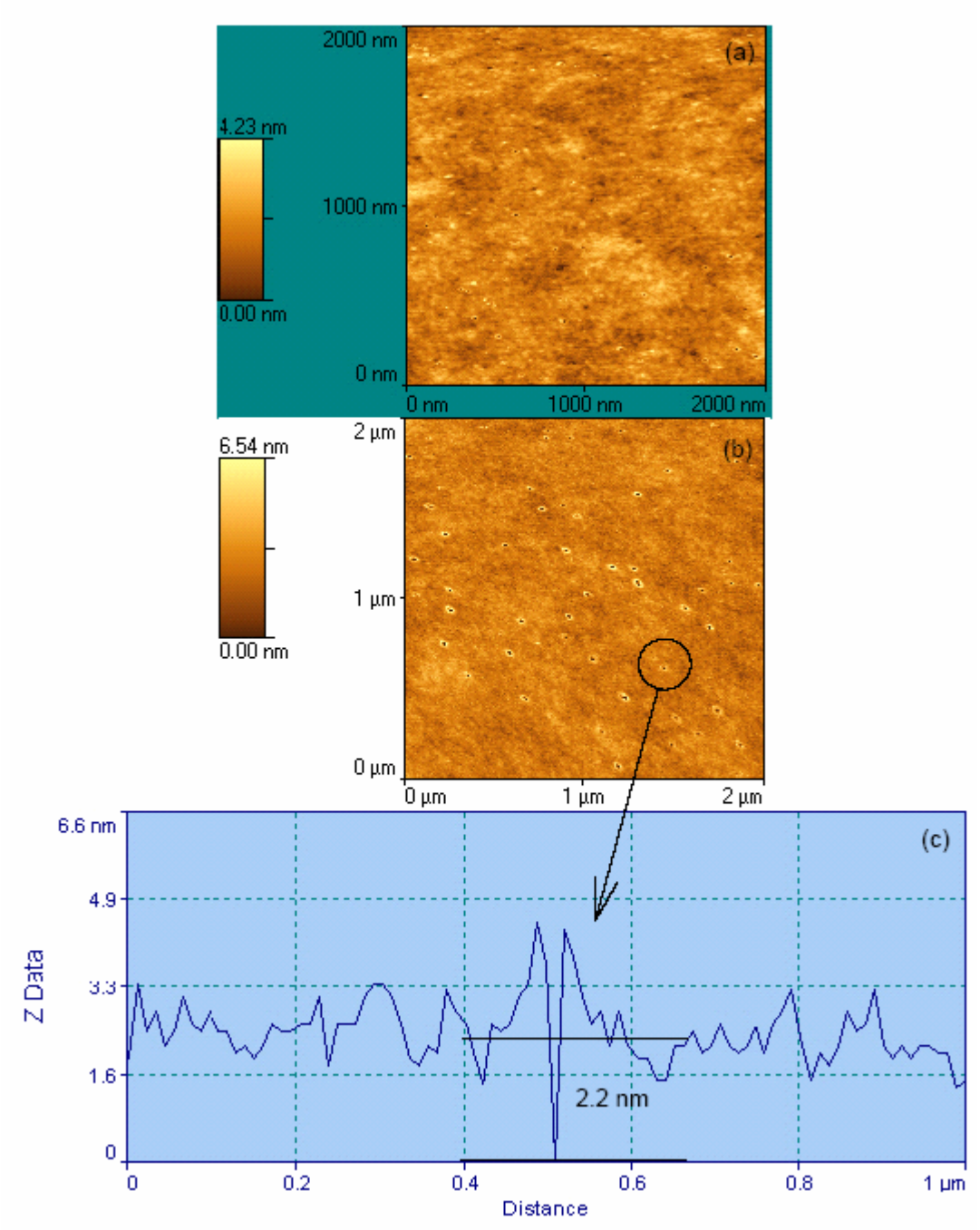

Fig. 3.5 Nano surface holes in i-PMMA (a) and PS(b) films; (c) showing the definition of the nano hole depth.

3.5 Nano gold sphere embedding technique studying surface properties of thin polymer films

In our nano gold sphere embedding measurements (see chapter 5), the gold spheres used are homemade using the citric acid reduction technique described in aforementioned section. The gold spheres are of an average size of 18.8nm, which are spin-coated onto the surface of PS films from gold colloidal solutions. No apparent polymer film surface damage is observed after gold sphere spin-coating from AFM images of the samples. The gold sphere covering density on the polymer film surface is ~10 spheres per micrometer square. It has been checked that the polymer sample's exposure to ionic solutions during gold colloidal spin-coating has no or negligible plasticization effects on samples [162]. Many films covered with gold spheres are put in the home-built oven to do gold sphere embedding at preset temperatures with a purge of dry nitrogen gas to avoid some potential chemical attack to the samples. After some time, one sample is taken out of the oven to do AFM imaging. In the oven, the polymer films are put on a big block of aluminum and the temperature is monitored by a thermocouple, by which we make sure that the temperature fluctuation, especially when we take out samples from the oven, is within $\pm 0.2K$.

The non-contact mode is used for AFM imaging to avoid big probing force that might affect the heights of embedded gold spheres. The same imaging parameters are used for all imaging processes to ensure no differences resulting from imaging for all AFM images. The height of each embedded gold sphere is defined as the difference from the top of the sphere to the average height of the local polymer sample surface region ($1\times 1\mu m^2$) where the sphere locates (without considering the other gold spheres). Some of the gold sphere height data is obtained by a computer program written by M. Ilton. Because the interaction between the AFM tip and the sample materials (Au or PS) is different, the "height" of Au and PS sample surface features might not be comparable directly, but the relative change of the gold sphere heights as a function of embedding time and temperature are comparable. In addition, we know that the lateral dimension of surface features in AFM imaging is the convolution of the AFM tip and the real sample surface features, but in the vertical dimension such effects are not a big concern. In particular, the measured nano gold sphere height by AFM is not sensitive to the tip-sample convolution effects. Therefore, from this relative change of the average gold sphere apparent

heights as a result of embedding at different temperatures and times we can get dynamical properties of the near free surface region of the polymer films. We should stress that there is no plasticizing effects involved in nano sphere embedding due to the contacting of gold sphere on polystyrene. In Ref. [88, 163], it is shown that there are strong interactions between gold and PS, and the chain motions in the gold neighboring regions are slowed down compared with those in the bulk part. Therefore, the gold sphere embedding is due to the enhanced dynamics in the near free surface regions of thin polymer films.

3.6 Preparing ultra-flat metal substrate by thermal metal evaporation

One of the present projects is studying the polarization noise of thin polymer films, which are sandwiched between two capacitor electrodes. First we tried using two hand-polished round steel plates as the capacitor electrodes. Considering the relative big roughness of the surface of the steel plates (~100 nm), especially for ultra-thin polymer film studies, we built capacitors constituting two silicon plates coated with aluminum layers. Some small pieces of Silicon wafers ($14\times14mm^2$) are cut from single side polished silicon wafers (3" in diameter; ~0.4mm in thickness; Crystal orientation: <100>; Silicon Quest international) and then cleaned using ultrasonic bath in Toluene and Acetone for 20minutes separately. The silicon wafers are further cleaned by UV Ozone treatment [164, 165, 166] (with silicon wafers being ~3mm away for the UV source) for 20minutes before being put in the bell jar of the evaporator. To do the aluminum evaporation, the as-cleaned silicon wafers are put on top of a chimney inside the bell jar of our home-built evaporator. Seven Aluminum pellets (99.99% purity), which are already cleaned using Methanol, are put in one spring-like Tungsten basket boat underneath the chimney. After the bell jar is closed, the evaporator is then pumped down for ~ 24 hours to get a bell jar pressure of $\sim 2\times10^{-6}$ Torr. During the process of pumping down pressure, cold trap (using liquid Nitrogen bath) is applied to reduce the water moisture and oil contents inside the bell jar. It needs to be stressed that any dust, organic contaminations, or water moisture on the silicon wafers would result in metal crystallization during the evaporation process, which is the major problem preventing one to get ultra-flat evaporated metal surface. That is why great attention should be paid to cleaning the silicon wafers thoroughly and applying cold trap to reduce water moisture and oil contents inside the evaporator bell jar. When the bell jar pressure is below 2×10^{-6} Torr, the following steps were performed to do Aluminum evaporation:

● Turn off the Ion Gauge measuring bell jar pressure to avoid ion contaminations during evaporating;
● Close the shutter underneath the chimney;
● Turn on the VARIAC and increase the setting to 30 Volts for 30 seconds to dry off water on the evaporation boat and Aluminum pellets;
● Increase the VARIAC setting to 60 Volts for 15 seconds to let the Aluminum pellets melt and wet the evaporation boat;
● Turn off the VARIAC for 5 minutes to get water molecules or Aluminum gas atoms settled down, which are produced during Aluminum wetting;
● Turn on the VARIAC and increase the setting to 80 Volts, 10 seconds later open the shutter for 20 seconds to expose the silicon wafers to aluminum atomic gas, and then close the shutter;
● Turn off the evaporator according to the corresponding operation instructions;
● One hour later, gently fill in the evaporator bell jar with dry nitrogen gas;
● Half an hour later, open the evaporator bell jar and take out the silicon wafers and put them in a clean box for future use.

Note:
● When handling something inside the bell jar, gloves should always be worn to avoid organic oil contaminating the stuff inside;
● The key points of making ultra-flat thermal evaporation metal layer/coating include: clean enough substrate; clean and high purity metal source and spring-like Tungsten basket boat; low enough pressure inside the bell jar of the evaporator; low enough temperature of the substrate to be coated with metal layer; low contents of O_2, H_2O and pumping oil[167];
● The spring-like Tungsten basket boat is used so that the maximum deposition rate and minimum radiant heating to the silicon substrate can be achieved.

To make a silicon wafer based capacitor electrode, the cleaned silicon pieces(resistance $>10^6\,\Omega$) are coated with evaporated Aluminum layer on the front side, back side and one edge side (see Fig. 3.6). The surface resistance of the ~100 nm Al coating layer is less than $10\,\Omega$ and the surface roughness is ~1.2nm determined by Atomic Force Microscopy.

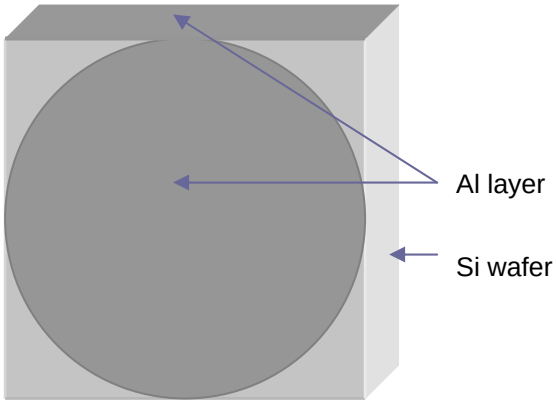

Fig. 3.6 Schematic graph of silicon wafer based capacitor electrode.

AFM images of some Al coating layer on silicon wafers are as follows. Please not the effects of applying some specific treatments during aluminum evaporating, such as water dry off the aluminum pellets and the spring-like Tungsten basket boat, pre-evaporation aluminum wetting, and cold trap used to trap H_2O and pumping oil in the bell jar.

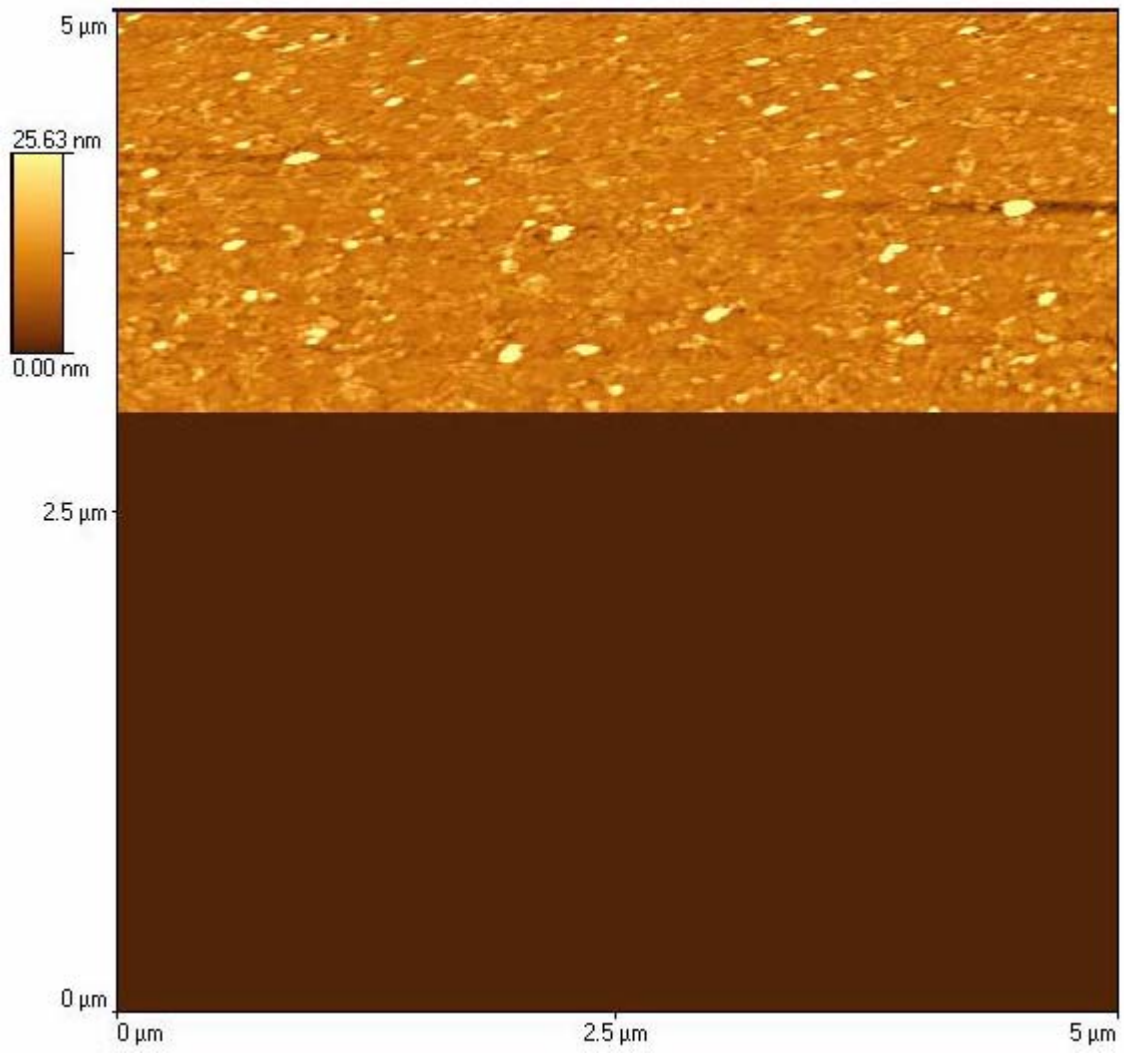

Fig. 3.7 AFM image of thermal evaporated Al coating on Silicon wafer; surface roughness: 3.62nm; no H_2O dry-off, Al wetting treatment, or cold trap used during evaporating.

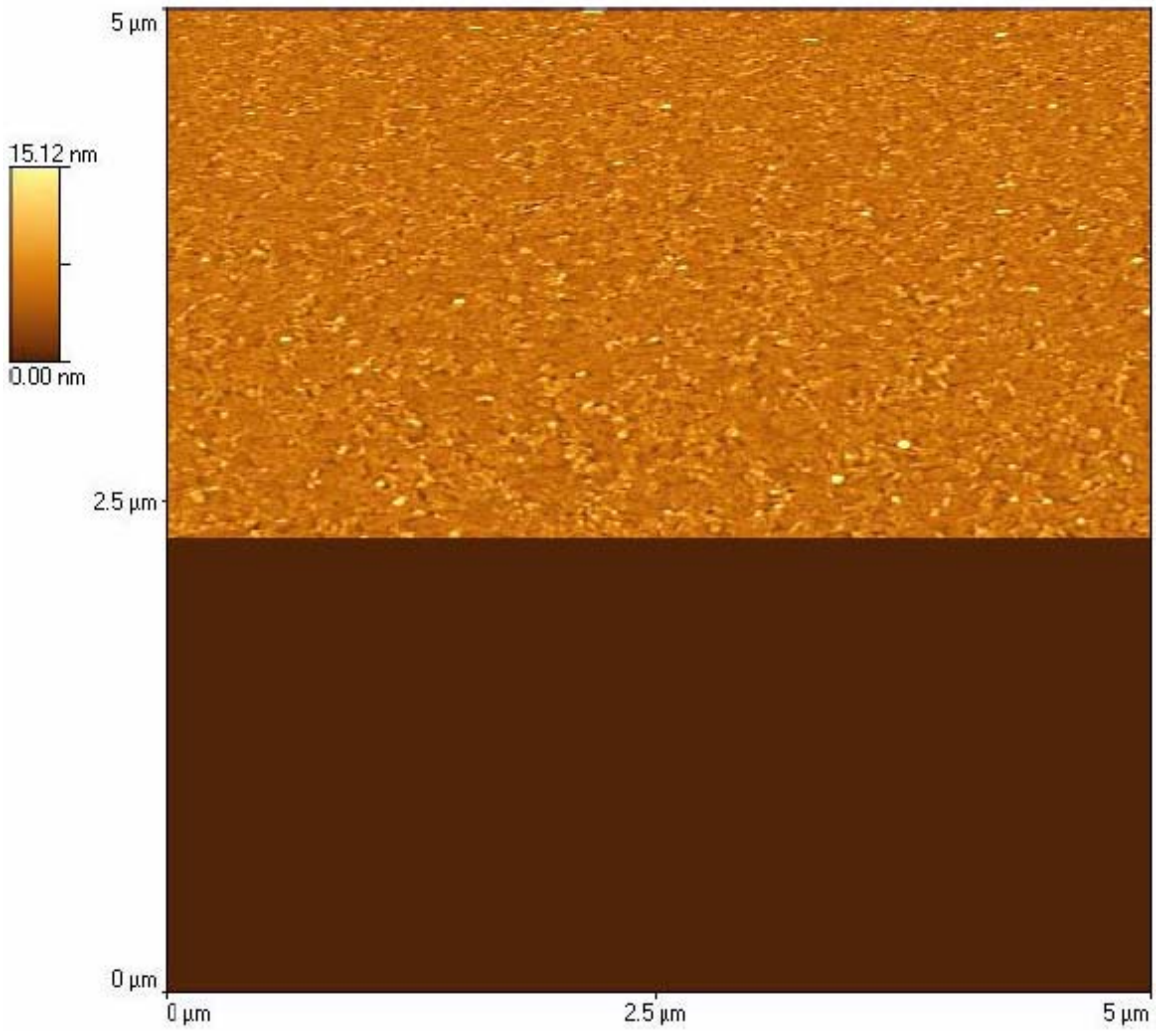

Fig. 3.8 AFM image of thermal evaporated Al coating on Silicon wafer; surface roughness: 1.12nm; H_2O dry-off, Al wetting treatment, and cold trap used during evaporating.

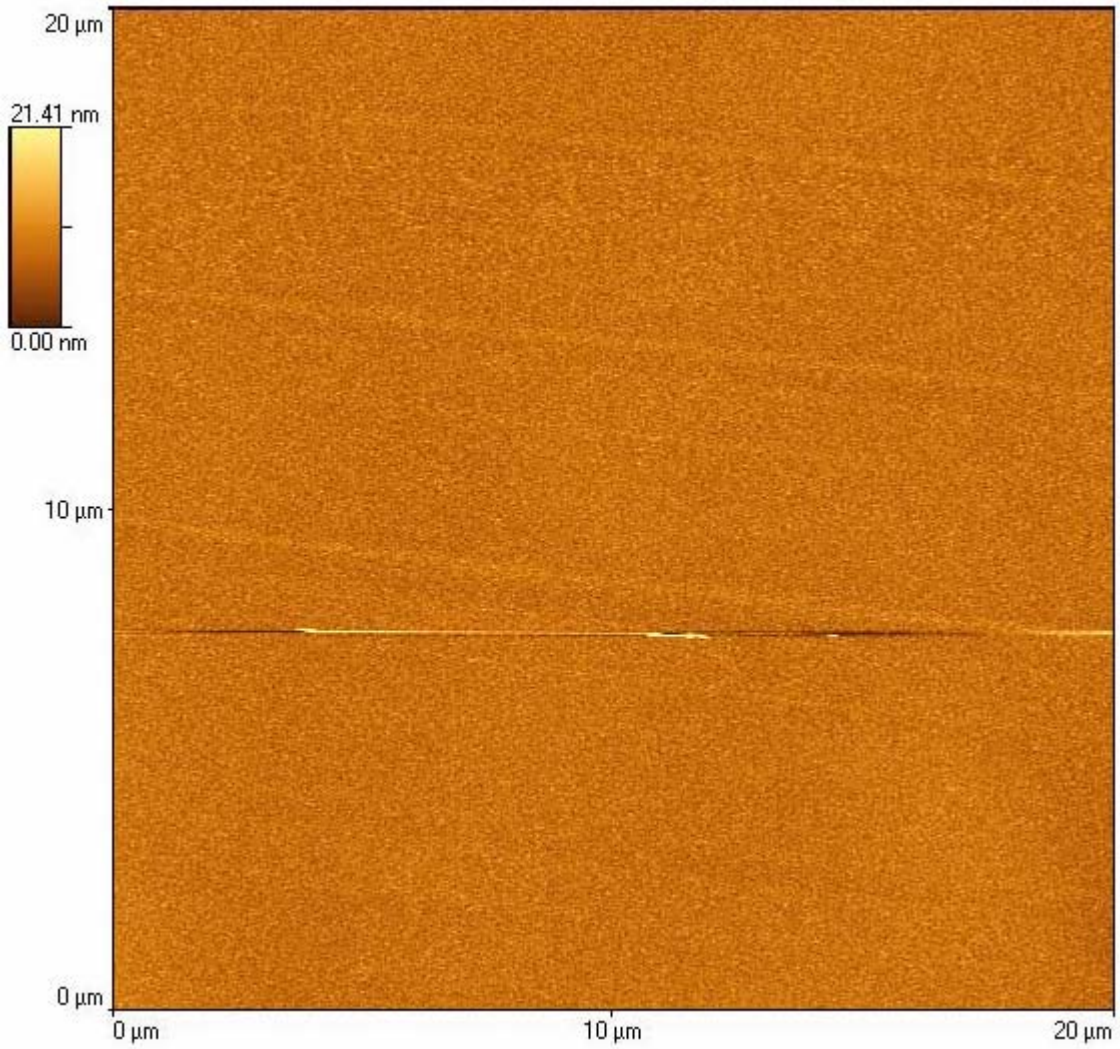

Fig. 3.9 AFM image of thermal evaporated Al coating on Silicon wafer; surface roughness: 1.44nm; H_2O dry-off, Al wetting treatment, and cold trap used during evaporating.

3.7 Building thin polymer film polarization noise measuring system

We built a low level noise measurement system to measure the intrinsic polarization noise in thin polymer films, which reflects the thermal dynamics of polymeric chain molecules. Fig. 3.10 is the corresponding setup block diagram.

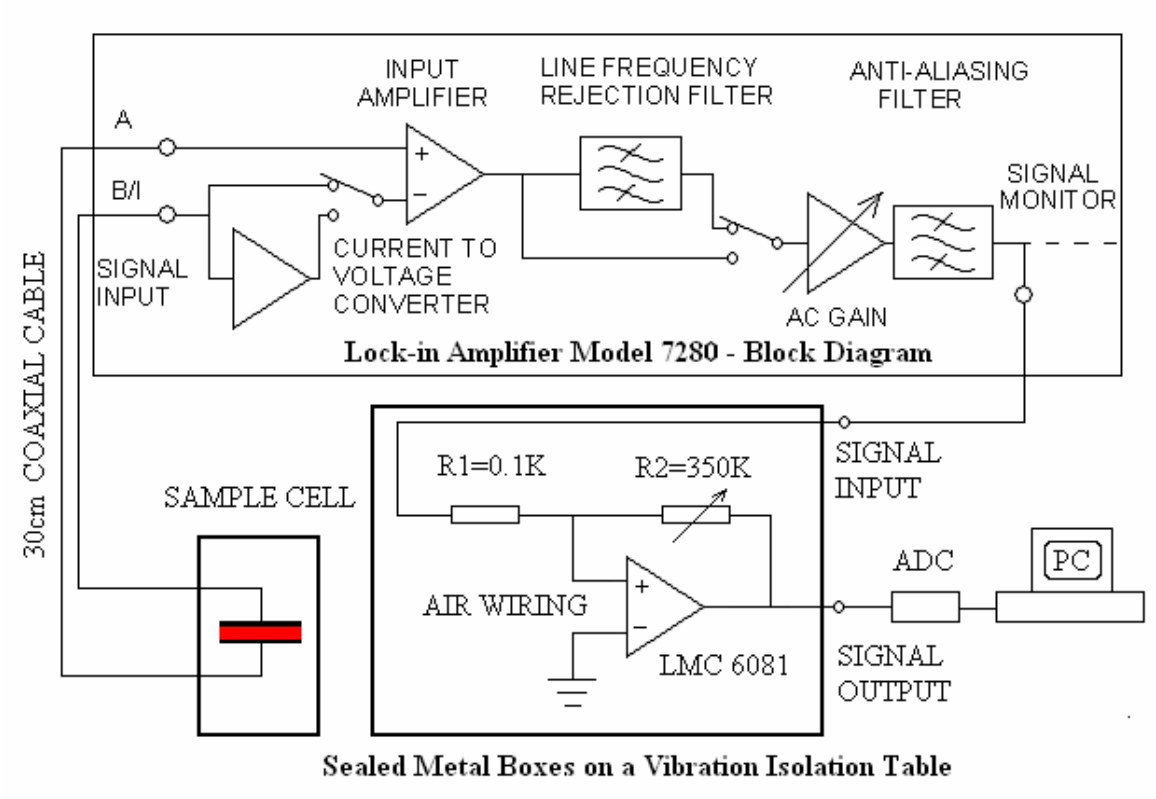

Fig. 3.10 Schematic block diagram of the polarization noise measurement system.

We use three kinds of parallel plate capacitors to collect the polarization noise (see the following for details of the capacitors used). Since we do low level noise measurements, any ambient electromagnetic field or mechanical vibration, which will produce big enough deleterious interference signals, should be avoided. Therefore, the capacitor with the thin polymer film is electrically sealed in a small metal box (shown as the sample cell in Fig. 3.10) sitting on a vibration isolation unit during measurements. Two short coaxial cables ("BELDEN 8263 RG-59B/U 70903"; 30 cm in length), which is necessary to reduce signal/voltage drops, are used to connect the sample cell and the input connectors "A" and "B/I" of our Lock-in amplifier (Model 7280, PerkinElmer). By means of electrically sealed metal box and coaxial cables the ambient electromagnetic fields are shielded out. The polymer film polarization noise is primarily amplified by the Lock-in amplifier and then introduced, through the "signal monitor" connector, to our home-built amplifying unit to be further amplified. In this noise measurement system, we take the advantage of the ulta-high sensitivity to low level noise of the Lock-in amplifier by using the output of the signal monitor (see below for the specifics of the Lock-in amplifier). Because the gain of the Lock-in amplifier itself is not high

enough, a home built second-stage amplifying unit, which is electrically sealed in a metal box and sits on the same vibration isolation unit as well, is applied in our system. The high gain of the system is mainly achieved by the second amplifying unit of the precision low offset voltage high gain operational amplifier. If this high gain operational amplifier is used as the first stage amplifying unit, the non-interesting thermal noise can be amplified as well. The output signal from the second-stage amplifying unit is digitalized by the analog-to-digital converter (ADC) unit, collected and analyzed using our spectra analysis program written in Labview.

The following describes the components of our polarization noise measurement system.

Capacitors:

Steel-plate capacitor

Two stainless steel disks (3 mm in thickness and 20 mm in diameter) are used as the capacitor electrode plates. They are firstly polished using four different aluminum oxide slurries with particle size ranging from 1 to 0.05 μm and then carefully cleaned by rinsing in isopropanol and deionized water. After drying, one such steel plate is coated by a thin polymer film using the solution spin-coating technique. The other steel plate was put on top of the first plate with the polymer film in between. Four pieces of $2 \times 2 mm^2$ spacers (polytetrafluoroethylene (PTFE)-goodfellow; 10 μm in thickness) are used in between the two capacitor plates. A Teflon tube (20 mm in diameter) was used to hold the capacitor plates. We tried two different ways to connect the capacitor to the signal measuring circuit: Capacitor geometry 1— two pointer needles with two small springs at the end are used as connecting wires (see Fig. 3.11); Capacitor geometry 2: two Teflon plugs were used to hold the capacitor plates and two gold wires (5 μm in diameter; SIGMUND COHN CORP) were connected to the capacitor plates through central holes in the plugs. We found that the case of Capacitor geometry 2 works well in terms of measurement reproducibility.

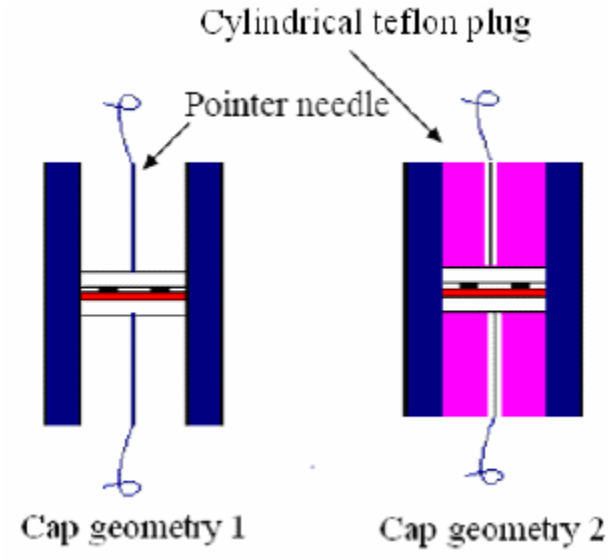

Fig. 3.11 Scechmatic setup for steel plate capacitors: red region showing polymer films; outer blue region showing the 20mm Teflon tube.

Silicon wafer based capacitor

We use two square silicon wafers, which are coated with aluminum layer on the front side, back side and one edge (as described in "3.6 Preparing ultra-flat metal substrate by thermal metal evaporation"), to form a noise measurement capacitor. Such capacitor is put in the Teflon tube with two cylindrical Teflon plugs to hold the two electrodes as shown in Fig. 3.11. The major point of this silicon based capacitor is that the electrodes are ultra-flat (surface roughness ~1.2nm) and ultra-thin polymer films can be studied.

Microscopic glass slide based capacitor

In addition to the silicon-based capacitors, we also built microscopic glass slide based capacitors. Some glass slides (Premium clean; Fisherfinest; 3"×1"×1mm) are cleaned using the same method for cleaning silicon wafers and then put in the evaporator bell jar to do aluminum coating(the same aluminum evaporation procedure as Al coating on silicon wafers). The diameter of the Al layer disc is 10 mm and the surface roughness is ~4nm (determined by AFM). The Al coated glass slides are schematically shown in Fig. 3.12, in which the leg of the Al layer was used for electric wiring. Two such glass slides are put face to face to form a capacitor with the spin-coated polymer film in between. To study dynamics of thin polymer films with one free surface, we used 10 μm thick

polytetrafluoroethylene (PTFE) or 1 μm silicon spheres as spacers to space the two glass slides. For studies of polymer films without free surfaces, we evaporate one aluminum layer on top of the polymer film which is spin-cast onto one aluminum coated glass slide.

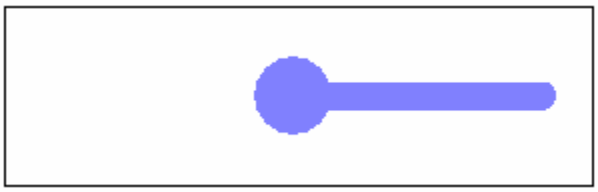

Fig. 3.12 Schematic graph of glass slide based capacitor electrode; blue area showing the Al coating.

First-stage signal amplifying unit

To measure low level noise, an amplifying unit with the lowest possible voltage noise and highest possible input impedance is necessary [168]. In this project, we use the PerkinElmer Model 7280 Lock-in amplifier to primarily amplify the polarization noise in the polymer films. The voltage noise of Model 7280 Lock-in amplifier is $5nV/\sqrt{Hz}$ and the input impedance is $100M\Omega$ [169]. The sample cell was connected to the Model 7280 Lock-in amplifier by the voltage differential input mode (A-B) though two short coaxial cables. By doing this, the ambient electromagnetic noise could be screened from the sample cell. The setting of the Lock-in amplifier during measurements is: Input coupling: Float, Slow; Input mode: Voltage; Input connector: A-B; Input limit: 32mV; AC gain: 34dB.

Home built second-stage signal amplifying unit

We choose LMC6081, which is a precision low offset voltage operational amplifier, for the second-stage voltage amplifying unit, shown as the bottom big bold square box in Fig. 3.10. Its major features include: high voltage gain (130 dB); low offset voltage (150μV); ultra low input bias current (10 fA). To avoid PC board surface leakage current, the input pin of LMC 6081 is soldered directly to the input resistor using the air wiring method. We tried some different power supplies ($\pm$9V) for the op amp and found that only the battery power supply ($\pm$7V) has the lowest noise because higher supply voltage usually results in higher power dissipation and bias current to the op amp[169]. In addition, by using the battery supply the whole second-stage amplifying circuit can be integrated and electrically sealed in a small metal box. During measurements, this unit sits on a

vibration isolation unit to avoid noise induced from mechanical vibrations. The voltage gain of this unit is set as 3500.

Noise data collecting and power spectrum analysis unit

The amplified polarization noise of the polymer samples through the primary- and second stage amplifying units is collected by the DAQ card (PCI 6035E) though a BNC 2120 connector (National Instruments). We wrote a Labview program to do data collection and analysis. The number of data points to get one power density spectrum is set as 16384 and the data sampling rate is 1000/s. We used the average of 200 successive power density spectra for the molecular dynamics analysis. This 200 spectra averaging treatment can reduce random or white noise from bias current from the electronic components of the measurement system.

3.8 Operation principle of Atomic Force Microscopy (AFM)

General AFM background

Atomic Force Microscopy (AFM), being invented only ~30 years ago, is widely used in a variety number of commercial and research fields due to its powerful merits such as high spatial resolution (lateral: on the order of nanometers; vertical: on the order of fractions one nanometers), true 3-D imaging, ease of operation (in ambient air without vacuum requirements), applicability to various samples, etc.. As a member of the big family of scanning probe microscopy, AFM is based on a raster-scan fashion, during which the sharp AFM tip moves and probes the sample surface point by point— more strictly speaking several or tens of atoms on the very end of the sharp AFM tip interact with individual or several atoms at the sample surfaces [170, 171, 172]. Here, "probe" has different physical meanings in the two conventional AFM operation modes: in the contact mode, the AFM tip "physically touch" the sample and a repulsive force between the tip and sample surface is probed; in the non-contact mode, the attractive force between the tip and sample surface is measured. The tip-sample interaction force can be capillary force, Van de Waals force, electrostatic force, magnetic force, chemical bonging force, etc..

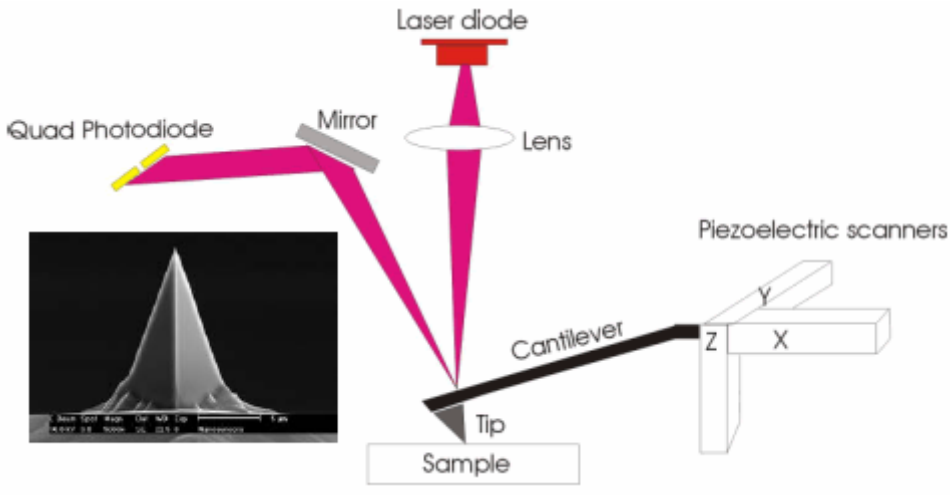

Fig. 3.13 Schematic representation of the AFM operation principle. (Graph from [173]; inset of one AFM tip image from[174])

To measure the tip-sample interaction force, a specially designed optical-electronic integral operation system is applied, shown in Fig. 3.13. The AFM system change the position of the sharp tip, which is integrated with a tiny cantilever(several tens of micrometers in size), by applying voltages to the piezoelectric scanners during scanning— the high resolution of AFM comes from the combination of the tip sharpness and the accurate control of piezoelectric materials. The tip-sample interaction force cause deflection of the cantilever, which is amplified and measured by the optical deflection detecting system (as small as ~0.1nm can be measured): the laser light is focused on the end of the cantilever and reflected to the quadrant photodiode detector through a mirror. During scanning, a feedback loop is used to control or detect the tip-sample interaction and accordingly the 3-D sample surface features. The error signal, which is the difference between the setpoint determining the cantilever deflection and the actual detected signal from the quadrant photodiode detector, is used as the feedback to control the position of the AFM tip by applying corresponding voltage to the piezoelectric scanners to maintain either constant tip height or constant tip-sample interaction force. To obtain high quality AFM image or accurate sample surface features, optimum parameters are usually required, such as suitable values of setpoint, scanning rate, scanning resolution, and feedback controlling parameters of P(proportional), I(integral), D(derivative) related to error signal and surface features.

Generally, three AFM operation modes are widely used. In the contact operation mode, the tip-sample interaction force is repulsive (typically ~0.01-100nN) and the cantilever deflection is used as the feedback signal for the AFM scanner to maintain a constant cantilever deflection— constant force mode. When imaging atomically flat surfaces, the constant height mode is usually used, in which the cantilever deflections is small and can be transformed to surface features directly [175]. At every scanning point/position, the AFM tip is at the static state and is very sensitive to noise and scanner drift. Usually a cantilever with low spring constant is used in the contact mode, which, in addition, can reduce the chance of sample surface damaging since the tip is in "physical contact" with the sample surface. One major advantage of the contact mode is that it can be used to do some artificial material manipulation or nanolithography.

Another widely used AFM operation mode is the non-contact mode. In this mode, the oscillating driving signal is applied to one piezoelectric element at the AFM tip holder to let the cantilever oscillate at or around its resonance frequency. The cantilever oscillation amplitude, phase and resonance frequency can be modified by the tip-sample interaction forces. By maintaining constant cantilever oscillation amplitude or frequency through the AFM feedback loop, or monitoring the variation of cantilever oscillation amplitude or frequency [176, 177], the sample surface features can be obtained. To avoid jump-to-contact of the AFM tip during oscillation, the cantilever with high spring constant(10-130N/m for PPP-NCH tips) is usually used in the non-contact mode. In addition, the cantilever oscillating at a high frequency, generally 50k to 500k Hz is not sensitive to noise and drift. This scanning stability makes it possible to get true atomic resolution for AFM imaging.

Compared with the non-contact AFM operation mode, the tapping mode is similar with the non-contact mode in that the AFM tip is also oscillated with the cantilever resonance frequency during scanning, but the cantilever oscillation amplitude is much larger, typically between 100 and 200nm, than that of non-contact mode(<10nm). In the tapping mode, the cantilever has sufficient oscillation amplitude to overcome the tip-sample adhesion forces, and accordingly the potential sample damage due to tip-sample sticking can be avoided. This is where this name of "tapping mode" comes from. The AFM tapping mode operation is gentle enough even to image single polymer chain molecule without changing its conformation state [178]. This mode is widely used for scanning very soft polymer or biophysical samples.

The major disadvantages of AFM include: The scanning range is very limited($\sim 100 \times 100 \mu m^2$) and to obtain reliable statistical sample characteristics is very hard; AFM is not a good imaging candidate to do real time measurements since it is relatively slow to obtain high quality AFM images.

AFM applications in the present projects

AFM is used in many aspects of the present projects, such as characterizing thermal evaporated metal coatings and polymer films— surface roughness and film thickness determining, and measuring the size of nano gold spheres. In addition to such general applications, we also developed some specific projects in which AFM is very much involved.

In one project, we use the torsional information of the AFM cantilever working in the contact mode to study dynamic properties of the near free surface region of thin polymer films. Once the AFM tip is engaged to (/in the feedback with) the polymer film surfaces, we downwardly move the tip to the sample surface by several nanometers to etch it to the sample free surface region and then laterally move the rear end of the AFM cantilever with a suitable moving rate to avoid tip-sample slippage. Because the very end of the AFM tip is physically fixed to the sample surface the cantilever/tip will be twisted and the built-in torque of the cantilever will reduce as the results of the polymer sample surface relaxation. This sample surface relaxation behavior at a certain temperature can be obtained by monitoring the left-minus-right signal of the quadrant photodiode detector of the AFM. More details and primary results can be found in chapter 7.

In another project, we use the AFM to track the relaxation of nano surface holes in the near free surface region of polymer films. Because the nano surface holes are only ~3 nm deep and ~ 20 nm wide, very sharp AFM tips are used(NANOSENSORS: Type—PPP-NCH; typical tip curvature radius ~7nm). To avoid sample surface damage, the non-contact AFM mode is used in tracking the nano surface hole leveling process. To make sure that all results for different polymer samples at different annealing temperatures are comparable, the same AFM scanning conditions are used:

AFM room temperature(~287K): The AFM operation temperature range is 278K-313K, but we found that at ~287K the AFM scanner piezo drift is minimized and negligible. In addition, by scanning the piezo for ~20 minutes with the system not in feedback before real measurements, the piezo drift can be minimized.

AFM tips(typical tip curvature radius ~7nm): Although very sharp AFM tips are used for nano surface hole scanning, we also change tips from time to time since after several scanning's the tips can get dull.

AFM scanning(on a benchtop vibration isolation unit): Although our lab is on the third floor of our building, the mechanical ambient vibrations can be shielded when doing AFM scanning by using a vibration isolation unit(HALCYONICS, MOD-1).

Scanning range($5\times5\mu m^2$) and *scanning rate*($4\mu m/s$): In this scanning range with this scanning rate, we can obtain more than 100 nano surface holes in ~15minute.

Scanning resolution(500): We also tried the scanning resolution of 1000 and found no appreciable nano hole depth difference within the measurement error range.

Feedback controlling parameters(P-0.24, I-0.05, D-0): Except ~3nm deep nano holes in the flat polymer sample surfaces there is no big surface features, accordingly the relatively high P value and low I value are sufficient to get reproducible results.

Z piezo gain(low) and *data channel*(Z piezo forward and backward): To reduce noise and piezo drift we use the low piezo gain; to make sure that the AFM tip reach bottoms of most nano surface holes and no potential AFM tip tilt effects involved during scanning, we use both forward and backward scanning data to do data analysis.

In the project of studying nano gold sphere embedding behavior in thin substrate supported polystyrene films; the similar AFM scanning technique is used.

We also planned to do nano gold sphere embedding measurement on free standing PS films. Although nano surface hole relaxation studies of free standing films may be feasible, it is very hard to be conducted. The nano surface holes have to be produced before the procedure of transferring polymer films onto sample holds to obtain free standing films. The water transferring procedure may ruin or deform the nano surface holes due to some potential transfer-built-in stresses. In comparison, such issues can be avoided in the nano sphere embedding studies of free standing films. During the water transferring procedure to obtain free standing polymer films (with nano spheres on top) at room

temperature, the nano sphere embedding at such low temperature can be negligible. Therefore, nano gold sphere embedding is a practical technique to study surface properties of free standing polymer films.

In the project of studying nano gold sphere embedding behavior in thin free standing polystyrene films, the samples are put on TEM grids with square mesh of size $284 \times 284 \mu m^2$ (bar width: $55 \mu m$). To avoid free standing film vibration during AFM scanning, carefully chosen scanning parameters should be applied.

3.9 Thin polymer film characterization using Ellipsometer

Principle of the ellipsometer

Ellipsometry is an optical technique to characterize thin film properties such as film thickness, index of refraction and film growth. In the present projects, we use ellipsometry to measure thickness and the glass transition temperature of thin polymer films. In the following the principle of ellipsometry is briefly described.

By probing the change of the polarization state of light reflected off or transmitted through film samples, the ellipsometer can accurately measure film thicknesses ranging from several angstroms to several micrometers. Fig. 3.14 depicts the major point of how an ellipsometer works. If the linearly polarized light with two components p and s in phase is shone onto the film sample with an incidence angle θ_i, then the sample reflection will introduce amplitude variation and phase shift to the p and s components of the reflected light. Since the p electric field oscillates in the plane of incidence and the s electric field oscillates perpendicularly to the plane of incidence, from mathematics we know that two vectors oscillating perpendicularly with each other with a non-zero phase difference will produce a resultant vector oscillating elliptically. As shown in Fig. 3.14, the reflected beam is an elliptically polarized light with the resultant electric field vector $\vec{E}_r$. For a typical self-nulling ellipsometer, the system will automatically adjust the polarization state of the incident light to a specific situation

where the p and s components have some amplitude and phase differences which can be cancelled out by the sample reflection and accordingly the reflected light is just linearly polarized. This is actually the application of the reversibility principle in optics. Conventionally, an ellipsometer uses a combination of a polarizer and a quarter wave plate to adjust the polarization state of the incidence light, and the linearly polarized light can be detected using another polarizer called analyzer. When the direction of the oscillating electric field of the reflected light is perpendicular with the transmission axis of the analyzer, there will be no light reaching the optical detector, which is called a null condition.

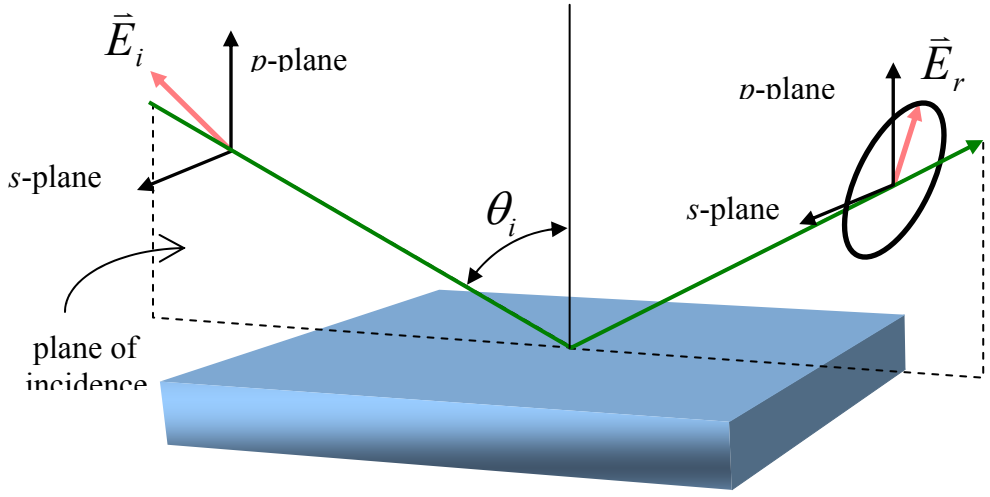

Fig. 3.14 Schematic geometry of the reflection ellipsometry.(Graph from [179])

According to optics, the Fresnel reflection coefficients[180] are

$$r_p = \frac{\tilde{n}_2 \cos(\theta_1) - \tilde{n}_1 \cos(\theta_2)}{\tilde{n}_2 \cos(\theta_1) + \tilde{n}_1 \cos(\theta_2)},$$
$$r_s = \frac{\tilde{n}_1 \cos(\theta_1) - \tilde{n}_2 \cos(\theta_2)}{\tilde{n}_1 \cos(\theta_1) + \tilde{n}_2 \cos(\theta_2)}. \quad (3.2)$$

In Eq. (3.2), r_p and r_s are reflection coefficients of p and s component respectively, subscripts 1 and 2 represent medium 1 and 2, and $\tilde{n} = n + ik$ is the complex index of refraction of corresponding

mediums(n related to the velocity and k related to the attenuation of light waves in the medium). Similarly, the transmission coefficients [180] are

$$t_p = \frac{2\tilde{n}_1 \cos(\theta_1)}{\tilde{n}_2 \cos(\theta_1) + \tilde{n}_1 \cos(\theta_2)}, \qquad t_s = \frac{2\tilde{n}_1 \cos(\theta_1)}{\tilde{n}_1 \cos(\theta_1) + \tilde{n}_2 \cos(\theta_2)}. \tag{3.3}$$

In ellipsometry, the two measured variables Ψ and Δ relate to the total sample reflection coefficients R_p and R_s according to

$$\frac{R_p}{R_s} = \tan(\Psi)\exp(i\Delta). \tag{3.4}$$

In Eq. (3.4), the total sample reflection coefficients R_p and R_s include sample properties such as thickness and index of refraction of individual materials. In the conventional self-nulling ellipsometer, the directly measured varibles are angles of the polarizer(P) and analyser(A) with fixed angle of quarter-wave-plate (Q), which are related to Ψ and Δ according to

$$\left.\begin{aligned} P_1 &= \Delta/2 - \pi/4, A_1 = \Psi; \\ P_3 &= \Delta/2 + \pi/4, A_3 = -\Psi; \end{aligned}\right\}(Q = -\pi/4); \qquad \left.\begin{aligned} P_2 &= -\Delta/2 - \pi/4, A_2 = \Psi; \\ P_4 &= -\Delta/2 + \pi/4, A_4 = -\Psi; \end{aligned}\right\}(Q = +\pi/4). \tag{3.5}$$

From Eq. (3.4), we see that the ellipsometry actually measures the ratio of reflection of the p and s components. Therefore, it is insensitive to the absolute values of the light beam intensity and accordingly insensitive to light intensity fluctuations. This makes the ellipsometry a robust and accurate technique. When extracting sample property parameters from the measured variables Δ and Ψ (or P and A), usually an optical model consisting layered mediums needs to be built with adjusting variables of individual layer thickness or index of refraction. Then an iterative computing procedure gives the optimum results that match the experimentally measured results.

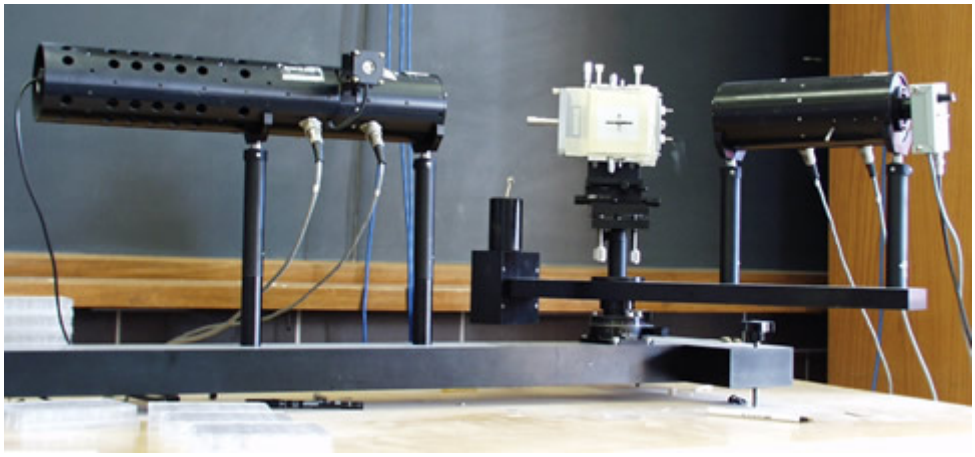

Fig. 3.15 Image of the self nulling ellipsometer.(image from [181])

Applications of the ellipsometer in the present projects

The polymer film thickness is determined both by AFM and the ellipsometry in present projects. In our lab we use the Exacta 2000 self-nulling ellipsometer(Waterloo Digitlal Electronics; P or A angle precision: 0.0006 degrees; null state detecting time: <0.3s[182]) to characterize polymer films. Fig. 3.15 is the image of the ellipsometer used. The experimental conditions are: light wavelength $\lambda = 632.8nm$; angle of incidence $\theta_i = 60^o$; ambient index of refraction $n = 1$. To determine the thickness of one polymer sample, we use the Linkam stage to hold the sample and put them on the sample stage of the ellipsometer. After careful laser light alignment and polarizer and analyzer home-position checking, the ellipsometer can automatically find the null state corresponding to the sample in less than 0.3 seconds. To reduce the systematic error as much as possible, we use the average of P and A angle values in two different zones to find the sample thickness by an ellipsometer optical model. The index of refraction for the silicon substrate is a complex variable $n_s = 3.875 + 0.02i$ [183]. From the model calculation we can obtain the thickness and index of refraction of the polystyrene films.

In present project, we also use the ellipsometer to measure the glass transition temperature T_g of thin polymer films. Compared with the film thickness determination using the ellipsometer, the T_g measurement is a dynamic process, in which the sample undergoes temperature ramps and its properties change with time consequently. Because the ellipsometer can detect transient null states with a sampling rate of more than 3 points per

second, the measurement error can be reduced by measuring a large number of data points. We use a Linkam temperature controlling stage to do sample temperature ramps. The laser light is shone onto the sample surface in the small sample cell through the slot in the covering lid with an incident angle of $60.0 \pm 0.1^{\circ}$. After the laser is well aligned through the polarizer and analyzer arms, the polymer sample is first heated from room temperature to a temperature ~30K above bulk sample material T_g with a heating rate of $5K/\min$ and kept at this temperature for 15 minutes to let the sample reach an equilibrium state; then the sample is cooled down to a temperature ~ 30K below bulk sample material T_g with a cooling rate of $5K/\min$; another heating cycle as the first one is repeated again; Then the sample is cooled down with a cooling rate of $1K/\min$ and during this cooling procedure the ellipsometer self-nulling data are collected with a sampling rate of one data point every 5 seconds. During the heating and cooling cycles the sample cell is filled with dry nitrogen gas to avoid moisture or potential oxidization attack from the ambient. Every sample is measured more than one time and the results are reproducible with such pre-measurement temperature ramps. Normally [121], the glass transition temperature T_g is determined as the intersection point of two linear fitting lines, which are fitted respectively to the glassy (low temperature) and melt (high temperature) regions of the polarizer or analyzer angle versus temperature data. To reduce error due to the linear fitting, the glassy and melt data regions for linear data fitting are at least $20^{\circ}C$ wide each. Some typical measured T_g results can be found in chapter 4 and chapter 5. For ultra-thin polymer films, the glass transition is broadened. In this case, the derivative technique[47, 121] of dP/dT or dA/dT is usually used to obtain the glass transition temperature T_g.

Chapter 4

Near-free-surface dynamics of glassy isotactic poly (methyl methacrylate) and polystyrene films using the nano-scale surface hole relaxation technique

4.1 Studies of near-free-surface dynamics of glassy isotactic poly (methyl methacrylate) films

4.1.1 Introduction

The studies of dynamical properties of thin polymer films have been almost fifteen years since the pioneering work in reference [57, 58], in which the ellipsometry technique is used to study properties of ultra-thin polystyrene films and an unexpected glass transition temperature T_g reduction, compared with the bulk material T_g, was observed. Since then, many experimental techniques and theoretical approaches have been applied or proposed to study the unique properties of polymers on the nanometer scale [59, 60, 61, 62, 63, 64, 65, 66, 185, 186, 187]. The present picture is that the

dynamics of polymers on the nanometer scale are in a stark contrast to those of bulk polymers as indirectly evidenced by the experimentally measured T_g deviation (both negative and positive in specific cases). Although there is a large body of experimental evidences showing that the interfacial effects play a key role for the observed dynamics deviations[66, 88,90,119,188,189,190,191,193], there are also some measurements arguing against this interpretation [93, 94]. The unique nature of long chain structures of polymer molecules may make the nanometer scale sample situations even more complex. For example, polymer molecules can be of size of several tens of nanometers and chain confinement effects may contribute to the observed properties different from those of the bulk materials. Another important aspect about polymer molecules is that dynamical properties on different length scale are different and special attention should be paid when comparing observations of measurements using different probe techniques. Besides research interests in terms of specific polymer properties and technical considerations, the other perspective that makes studies of polymer on the nanometer scale remain active is the possibility of helping improving the understanding of the notorious nature of the glass transition. One promising strategy may be to study the finite size effect related to some glass transition characteristic length scale, e.g. size of cooperative rearranging region, since polymers can be easily made into amorphous glassy states with varying sample geometries and sizes. When the size of the polymer samples approaches the glass transition related characteristic length scale (on the nanometer scale), dynamical deviation may be observed.

Many research effects have been conducted by measuring the T_g of two model polymers—polystyrene (PS) and poly (methyl methacrylate)(PMMA) on the nanometer scale. For thin PS films, studies show that when the film thickness is less than ~60nm the measured T_g values decrease with decreasing film thickness and there is no or very weak substrate dependence [67]. For thin PMMA films, however, a strong substrate dependence of T_g is observed and both positive and negative T_g shifts can be observed depending on the nature of PMMA/substrate interactions. A generally accepted explanation for the observed T_g deviations is that the vaccum/polymer or substrate/polymer interfacial properties play a key role for such dynamics anomalies. Specifically, some studies [59, 60 86, 88] observed that in the near free surface regions of thin polymer films the molecular dynamics are enhanced compared with the underneath bulk regions due to the release of steric constraints, which is the major negative contribution parts to the average measured T_g. In cases where there are

strong attractive substrate-polymer interactions which can inhibit molecular motions in the neighboring regions, the substrate/polymer interfacial effects may overwhelm the vaccum/polymer effects and accordingly the enhanced T_g may be observed [59, 63, 96, 97, 98, 99, 100, 101, 102]. However, how and to what extent the interfacial effects can propagate in thin polymers is still elusive. To study how far the interfacial properties can affect the dynamics of thin polymer films, one direct way may be to study the T_g distribution within polymer films [103, 194]. Due to lack of suitable techniques, only one study [66] has been conducted as of today. In this study, Torkelson and coworkers used the fluorescence technique to investigate the T_g distribution by measuring T_g of dye-labeled PS layers (~14nm) located in different regions in thin PS films. The authors observed a length scale of ~36nm over which the vacuum/polymer interfacial properties can affect the polymer dynamics. In addition, when the film thickness is less than ~25nm it seems the polymer dynamics are homogeneous, which is in contrast with other studies showing strong dynamics heterogeneity for polymer films of similar thicknesses. To study interfacial effects, especially when polymer films are thinner than ~14nm, the spatial resolution of such fluorescence technique is not high enough. Moreover, considering the dye-labeled polymer trace layer may be not sufficiently annealed during the measurements [88], it is very likely that the measured dynamics have some substantial contribution from potentially buried free surface effects.

In this chapter, we describe our studies of interfacial dynamics of thin polymer films using a novel technique. By measuring the nanometer scale surface hole(~3nm deep) relaxation as a function of film thickness, the polymer surface dynamics can be measured directly and the length scale over which the substrate/polymer interfacial properties affect polymer surface dynamics can be investigated. We study isotactic poly (methyl methacrylate) (i-PMMA) films because it is a well studied model polymer and the measured T_g values have a strong substrate dependence depending on the nature of substrates used. The novel nano hole relaxation technique is originally developed for studying surface dynamics of PS films [90]. In the present study, it is shown to be suitable to i-PMMA studies as well. We measure the near free surface dynamics of thin i-PMMA films on two different substrates and can determine the range across which the substrate/polymer properties propagate. Such studies of near free surface dynamics dependence on substrate or on film thickness has application significance. For example, if the polymer near free surface region is used as some information storing medium the lifetime of the physically stored information may vary depending on

the substrates of the polymer films. In addition, we study the dependence of pure near free surface dynamics (without the substrate influence) on polymer molecular weight (M_w) and found an unexpected near linear M_w dependence.

4.1.2 Experimental section

In the chemical repeat units of poly(methyl methacrylate) (PMMA) molecules there are polar side groups($-COOCH_3$) which can form hydrogen bonds with $-HO-$ polar groups of other materials. According to the arrangement of the side groups in chemical architectures, PMMA molecules can be classified as isotactic, syndiotactic and atactic isomers. Due to the deficiency in molecular packing, isotactic PMMA has the lowest glass transition temperature $\sim 323K$. Considering the fact in the deep glassy state the surface molecular motions may be very slow and the corresponding measurement may be very time consuming, in this study we choose i-PMMA as the model polymer system. Three kinds of i-PMMA are purchased from Polymer Source, Inc.: $M_w = 212.4k$, $r_{PDI} = 1.21$, ISO > 98%; $M_w = 436k$, $r_{PDI} = 1.4$, ISO>98%; $M_w = 889k$, $r_{PDI} = 1.15$, ISO>95%; where M_w is the weight average molecular weight, r_{PDI} is the polydispersity index showing the polymer molecular weight distribution—the lower value of r_{PDI} the more uniform the polymer molecular weight distribution is, and ISO means the isotactic contents. The as-received i-PMMA are dissolved in toluene to make solutions. Thin *i*-PMMA films were prepared using the spin-coating technique with spin-coating speed around 3000 RPM. To make uniform i-PMMA films, some factors should be considered (see chapter 3). To make polymer films of different thicknesses, different solution concentrations ranging from 0.5 wt% to 3.99 wt% are used. The thickness of polymer films made by the spin-coating technique is a function of spin-coating speed, solution concentration and polymer molecular weights. In order to change the polymer/substrate properties, we make i-PMMA films on two kinds of substrates. One substrate is single side polished silicon wafers with <100> crystal orientation purchased from Silicon Quest International and the native oxide layer are left intact, referred to SiO_2 / Si. The other substrate is the same silicon wafers but with a thermally evaporated aluminum layer coated on the polished side. Such aluminum layer is ~100nm in thickness and ~1.2nm in surface roughness, both determined using Atomic Force Microscopy, referred to

Al_2O_3 / Al after at least one day of exposure to air after evaporation. High purity (99.99%) Aluminum slugs are used as evaporation metal sources. The vaccum pressure is ~ 2×10^{-6} Torr before evaporating (for details of aluminum layer evaporation, refer to the technique chapter 3). After spin-coating i-PMMA solutions onto substrates, the as produced films are kept in air for about 4 hours to let the solvent evaporate gently and then annealed in dry nitrogen gas for more than 16 hours at an annealing temperature of 336 K (~13 K above bulk T_g) in a home-built oven. After such sufficient annealing treatment, the residual stress resulting from the spin-coating process can be released and the solvent contents can be removed. In reference [90], the method to make nanometer semispherical-cap holes on PS film surfaces is described. In the present study, we developed this technique further to make nanometer surface holes on i-PMMA films. The nanometer gold spheres used are made using the standard citric reduction method. By changing the ratio of gold salt solution to citric acid solution, we can make nanometer gold colloidal solutions with sphere size ranging from ~15nm to 30nm (detailed receipt can be found in the technique chapter). In this work, we used nano gold spheres of size ~20nm in diameter to make nano surface holes on i-PMMA films. Because of the affinity between gold spheres and i-PMMA[159, 160], it is relatively easy to cast gold spheres on the surface of well annealed i-PMMA films by spin-coating with a sphere covering density ~ 10 spheres per μm^2. We checked from the AFM images of i-PMMA films covered gold spheres and no surface damage is found. We do gold sphere embedding into the i-PMMA film surfaces for about 3 nm at a temperature of 4K above the bulk T_g within a dry nitrogen gas in the home-built oven for 10 minutes. The gold sphere embedded samples are then cooled down at room temperature for 30 minutes. After this, we dissolve the already embedded gold spheres on the i-PMMA film surfaces using mercury at a temperature of 275–276 K for 2 hours in a fume hood. After the gold sphere dissolving treatment, the i-PMMA films are left with semispherical-cap holes ~ 3nm deep on the surfaces, which are then imaged using a ThermoMicroscopes Explorer atomic force microscopy (AFM, Veeco) at the preset surface hole relaxation probing temperatures. The same sample is scanned by AFM after a number of annealing times until surface holes vanish. We use very sharp AFM tips for imaging (NANOSENSORS: Type—PPP-NCH; typical tip curvature radius ~7nm). In addition, to avoid polymer surface damaging during AFM imaging we use the non-contact mode to track the relaxation of nanometer surface holes. One needs to note the fact that because the T_g of i-PMMA is about 323K, if the gold sphere dissolving process is carried out at room temperature the surface holes may

relax to some extent due to relatively high surface molecular mobility. In contrast, as in the work of reference [90], the gold sphere dissolving can be done at room temperature considering that the PS films are in the deep glassy state at ambient temperature—the PS bulk T_g is 373K. Therefore, in this study we chose the temperature of 275-276K for gold sphere dissolving. We checked through AFM images and found that both the gold sphere embedding depth before gold sphere dissolving and the surface hole depth are almost the same value of ~ 3nm. The potential surface hole relaxation during gold sphere dissolving is negligible.

4.1.3 T_g measurements for three i-PMMA's

We measured the bulk T_g for three i-PMMA films on silicon wafers with thickness of ~200nm, using an Exacta 2000 self-nulling ellipsometer (Waterloo Digitlal Electronics). The laser light with a wavelength of ~633nm is shined onto the i-PMMA sample mounted on a Linkam temperature controlling stage (Linkam Scientific Instrument Ltd, UK) with an incident angle of $60.0 \pm 0.1^\circ$. After the polarizer and analyzer arms are aligned well, the ellipsometer can automatically track to reach the null state under which the phase and amplitude difference of the two optical components of laser light from the polarizer arm can be cancelled out by those differences introduced by sample reflection and the laser light passing through the analyzer arm is linearly polarized which can be detected by the analyzer. To measure the T_g of the sample, several temperature ramps are necessary. The sample is first heated from room temperature to $85^\circ C$ with a heating rate of $5^\circ C/\min$ and kept at this temperature for 15 minutes to let the sample reach an equilibrium state; then the sample is cooled down to $20^\circ C$ with a cooling rate of $5^\circ C/\min$; The first heating cycle is repeated again; Then the sample is cooled down to $20^\circ C$ with a cooling rate of $1^\circ C/\min$ and during this cooling procedure the ellipsometer self-nulling data are collected with a sampling rate of one data point every 5 seconds. Every i-PMMA sample is measured twice and the results are reproducible. Fig. 4.1 shows a typical ellipsometry measurement result for one i-PMMA sample with $M_w = 889k$. From the polarizer angle versus temperature data, the glass transition temperature T_g is determined as the intersection point of two linear fitting lines, which are fitted to the glassy(low temperature) and melt (high temperature) region experimental data points respectively. To reduce error due to the linear

fitting, the glassy and melt data regions are $20^{\circ}C$ wide each. The measured T_g results for three i-PMMA's are shown in Fig. 4.4.

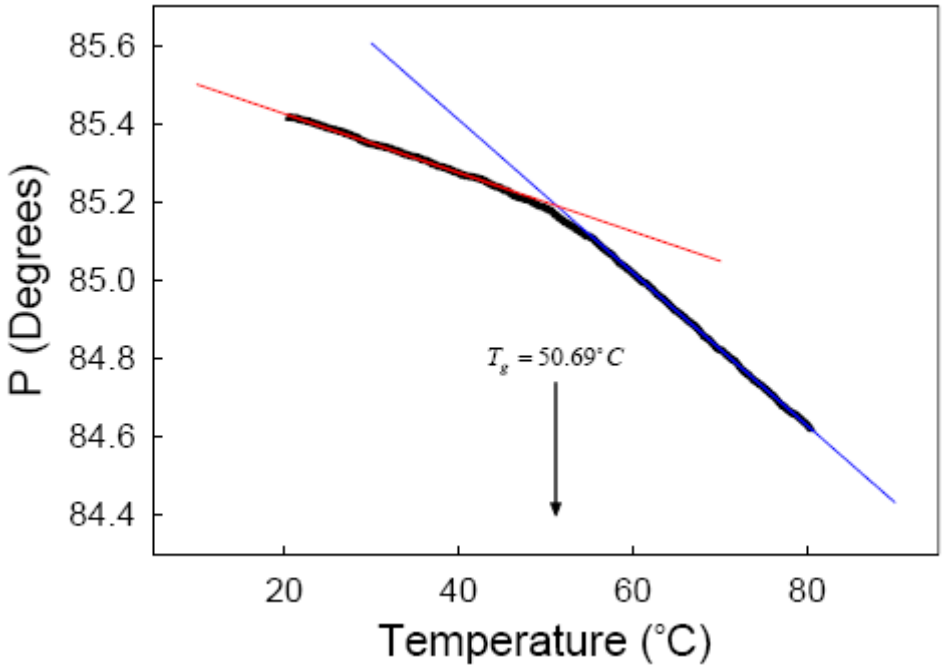

Fig. 4.1 Typical ellipsometry measurement result for 180nm thick i-PMMA sample with $M_w = 889k$.

4.1.4 Surface hole relaxation as a function of temperature

Fig. 4.2 shows the result of nanometer surface hole relaxation at 287K for 60nm thick 212.4k i-PMMA on the silicon substrate. The inset (left) shows one section of a typical AFM image of nanometer surface holes. The surface holes have surrounding rims, which may be formed as the result of i-PMMA wetting on gold spheres. These rims can help distinguishing artificially produced nanoscale surface holes from the natural polymer surface roughness. In addition, the rims have a lifetime that is significantly larger than that of the holes since they have larger radius of curvature, which means that these rims still show up even after the nanometer surface holes are annealed out. Therefore, according to the rims we can know for sure that a hole is(was) present even if the actual hole depth is too small to be measured. This is important as the average depth of holes is used to

determine the nano hole lifetime, and the inability to count holes with immeasurably small depth would skew the hole depth distribution to large values. As shown in the inset (right), which is the line scan of one surface hole using the commercial AFM data analysis software, the lateral dimension of the surface holes is ~ 20nm and the depth of one surface hole is defined as the distance from the average local surface height to the bottom of the hole. In the main panel, every data point represents the average hole depth of more than 100 surface holes at specific surface hole annealing times. To obtain the nanometer surface hole lifetime at a specific temperature, we use a single exponential function ($\exp(-(t/\tau))$) to fit the experimental data, where τ is the fitted surface hole lifetime. The solid curve in Fig. 4.2 is the single exponential fitting result for surface hole relaxation at 287K for 60nm thick 212.4k i-PMMA on the silicon substrate. In all cases the data is well described by a single exponential function. If the Kohlrausch-Williams-Watts(KWW) equation ($\exp(-(t/\tau)^{\beta})$) is applied to fit the experimental data, values of the stretch exponent β between 0.8 and 1.0 could all be used to provide reasonable fits to the data. Therefore, all surface hole lifetimes in this study are obtained by the single exponential fitting. In Fig. 4.2, it is remarkable that even at 287 K, more than 30 K below the bulk T_g value, complete surface hole relaxation is observed in less than 200 minutes, which means that the i-PMMA film surface have much enhanced molecular mobility or is in the rubbery state, while the bulk material should be in the glassy state at the same temperature.

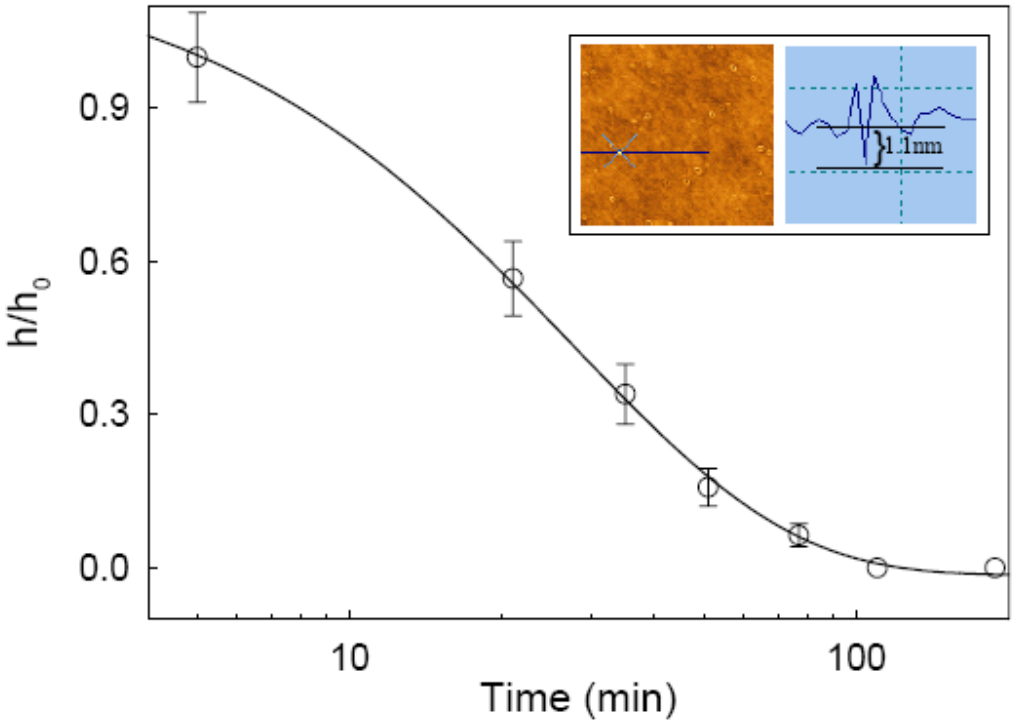

Fig. 4.2 Surface hole relaxation result at 287 K of 60 nm thick *i*-PMMA ($M_w = 212.4k$) film on Si; the solid curve is the single exponential fit. The inset shows some surface holes in the AFM image (left) and the line scan (right) for one surface hole (marked as a cross in the right image).

To study the temperature dependence of molecular dynamics of the first 1-3 nm of the near free surface region, we measured the nanometer surface hole relaxation at different temperatures ranging from 281 to 289K. The operation temperature range for the AFM is 278-313K[195]. The temperature range of 281-289K is the limited range available for the surface nano hole relaxation studies. To obtain the higher measurement temperature of 287-289K, we cool down the small room for at least two days to get the stable room temperature. That is, we use the whole AFM room as an isothermal oven. We use a plastic box to cover the AFM head and the sample during AFM imaging. A thermocouple is positioned close to the sample surface to monitor the temperature around the sample, which shows a temperature fluctuation of $\pm 0.3K$. To get the lower measurement temperature of 281-283K, extra ice in small bottles is put inside the AFM-head-covering box to maintain the measurement temperatures. To exclude the potential substrate effects on the near free surface dynamics, the samples used are thick (h>180nm) i-PMMA films on silicon.

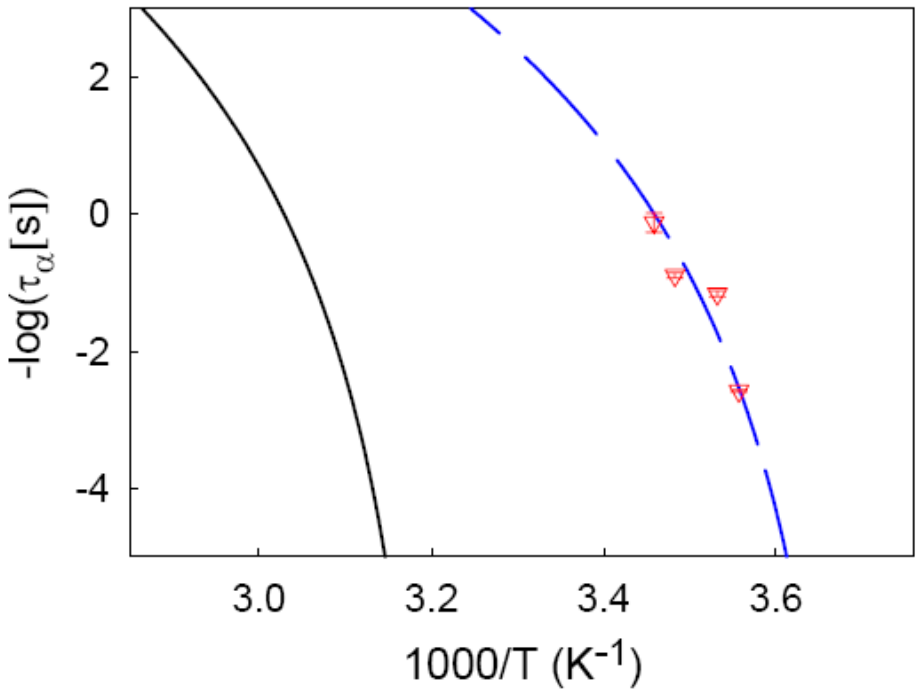

Fig. 4.3. Temperature dependence of the dynamical characteristic time for the first 2-3 nm of the 889k *i*-PMMA surface of films with thickness ≥ 180 nm. The solid curve is the relaxation curve for bulk *i*-PMMA [196] and the dashed blue curve is obtained with T_∞ shifted by 41 K from the bulk curve.

Fig. 4.3 shows the temperature dependence of the near free surface dynamics of thick i-PMMA films on silicon. The vertical axis is the negative logarithmic α relaxation characteristic times of polymers and the horizontal axis is for reduced temperatures. The solid curve is from Ref. [196] for bulk i-PMMA given by the equation

$$\log(\frac{\tau_\alpha}{100}) = -41.41 + \frac{55.17}{(T - T_\infty)^{0.1143}}, \tag{4.1}$$

where τ_α is the α relaxation time related to polymer chain segment motions, and T_∞ (311K) is the temperature at which the i-PMMA α relaxation time diverges. In Fig. 4.3 the downward triangle symbols are for our experimental characteristic times for the near free surface regions of i-PMMA films. To transfer from the measured surface nano hole lifetimes to the characteristic times, we use the relation in Ref. [90]

$$\tau_{\alpha} = \frac{\tau_{lifetime(measured)}}{1 + \frac{RG_0}{2\gamma}}, \tag{4.2}$$

where $\tau_{lifetime(measured)}$ is the experimentally measured surface nano hole lifetime, R is the initial radius of curvature of the surface holes, G_0 is the glassy modulus, and γ is the polymer surface tension. In Fig. 4.3 we see that a simple shift of 41K in T_{∞} results in the dash curve which is in good agreement with our data. A possible interpretation of this observation is that in this temperature range the 1-3 nanometer near free surface region of i-PMMA films is acting as if it has a T_g value that is about 41K less than that of the bulk i-PMMA, which may explain why in all the temperatures we tried the nanometer surface hole can relax completely because all these temperatures are around or above this "surface T_g". In ref [119], where the surface relaxation of common PMMA is studied and the similar temperature shift is found to be sufficient to provide agreement between surface relaxation data and those of bulk PMMA. The temperature shift in [119] is about 30K, which may be comparable with the 41K temperature shift in this work because the polymer used in [119] is PMMA with a bulk T_g of 389K and different polymer tacticity. What is more interesting is that in ref. [197] a second i-PMMA structural relaxation is found at a temperature of 40K below the bulk T_g. According to our result, it is very likely that what the authors observed in ref. [197] may be the surface structural relaxation in their case. The fact that similar values of surface T_g of i-PMMA are observed in both studies is very encouraging. However, this kind of data matching between polymer surface and bulk relaxation by a simple temperature shift is not true for polystyrene even using similar surface hole relaxation technique [90]. In [90] it seems polystyrene surface characteristic relaxation time data approaches bulk data continually from the low temperature side but with a very weak temperature dependence, and no apparent abrupt temperature shift is necessary when comparing surface and bulk properties. This suggests that while many (if not all) polymers exhibit enhanced surface dynamics, there remain significant material dependent features. In the cases of PMMA and PS, the physical properties of their specific side groups, e.g. the size and polarity of the side groups, are different. It is very likely that for the case of i-PMMA films there might be a unique surface structure feature which is different from that of the bulk part; while for the case of PS films the structural difference between the surface and

the bulk part may be not significant. Therefore, there is a unique surface T_g for i-PMMA films and a "jump" or "shift" between the relaxation dynamics of the surface and the bulk materials. In reference [198], some special i-PMMA molecular ordering is observed, which is another piece of evidence that i-PMMA is different from other non-polar polymers. Some future studies focusing on the potential structural differences between surfaces and the bulk part of i-PMMA films are necessary to test this prediction.

4.1.5 Surface hole relaxation as a function of film thicknesses, substrate materials and molecular weights

Based on the data of temperature dependence of i-PMMA surface relaxation measurements, we choose a temperature of 287K for detailed study of surface relaxation dependence on film thicknesses, substrate materials and molecular weights. Fig. 4.4 shows the combined results for these measurements. Every data point represents the surface hole lifetime at the specific measurement conditions, obtained by the single exponential fitting to the data set like that in Fig. 4.2. The upper solid curve in the main panel is a pure mathematic polynomial fitting to all data points for films on silicon substrates, which serve as the guide for eyes with no physical meaning. Similarly, the bottom solid curve serves as the guide for eye for the case of i-PMMA films on aluminum substrates. It can be seen that when the film is thicker than 180nm, the substrate effects are negligible for i-PMMA of the same molecular weight on different substrates (with native silicon oxide and aluminum oxide) , but for i-PMMA of different molecular weights the surface relaxation times are different. In Fig. 4.4 the surface hole lifetimes for i-PMMA with different M_w's are normalized using corresponding pure surface nano hole lifetimes of thick films as the reference hole lifetime. The value of 1 in the vertical axis of the main panel corresponds to about 14min for 212.4k, 36 min for 436k, and 53min for 889k i-PMMA films.

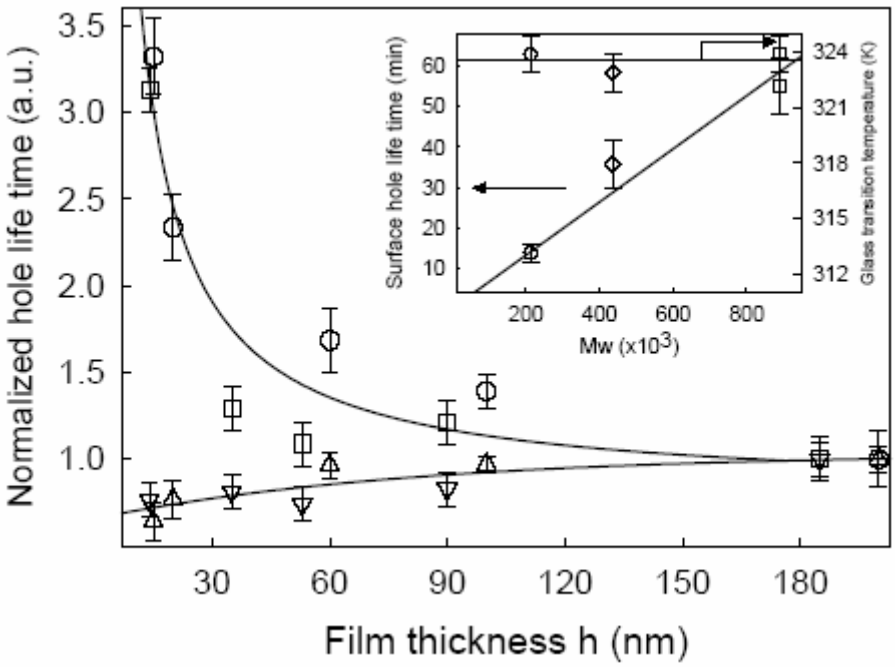

Fig. 4.4 Normalized surface hole lifetime versus thickness of *i*-PMMA films of different molecular weights on two kinds of substrates: 212.4k *i*-PMMA on Si (circle), 889k *i*-PMMA on Si (square), 212.4k *i*-PMMA on Al (upward triangle), 889k *i*-PMMA on Al (downward triangle); the solid curves serve as guides for the eye. The inset shows the surface nano hole lifetimes, and ellipsometrically measured T_g values of thick *i*-PMMA films (≥ 180 nm) on Si for three molecular weights: 212.4k (circle), 436k (diamond), and 889k (square).

In Fig. 4.4, we note that there is a clear difference for the i-PMMA surface nano hole relaxations on different substrates: For native silicon supported films, the surface relaxation times increase with deceasing film thickness; For native aluminum supported films, the surface hole relaxation times decrease with decreasing film thickness. Because there is a strong polymer/substrate interaction [13, 102] for the first case, where the hydrogen bond interaction dominates, the substrate dependence is very strong compared with the later case where the polymer/substrate interaction is weak[89]. Specifically, we note that complete relaxation of the surface is always observed at the measurement temperature (more than 30 K below bulk T_g), in particular even for films as thin as 10 nm on silicon substrates. Such films have been previously reported to exhibit overall T_g [65, 199] values greater than the bulk value which indicates slower overall dynamics. This disparity between surface

properties and whole film properties suggests highly heterogeneous dynamics in such systems. For the strong polymer/substrate interaction case, the near free surface dynamics are substantially affected (by 25%) when the film thickness is smaller than ~70nm.; while for the weak polymer/substrate interaction case, this length scale is ~20nm. In addition, we note the similarity between the substrate-dependent difference in surface relaxation time and measured T_g values for *i*-PMMA on the same substrate materials [65, 199]. Despite the similarity, there are significant quantitative differences. For example, for 20 nm films, the measured T_g value for *i*-PMMA on a Si substrate is 10–40 K greater than the bulk value, while the surface relaxation time increases by only a factor of 3, which is in contrast with a factor of ~3000 expected using the general WLF relation for a temperature variation of 10K around T_g. The dependence on substrate material of surface relaxation could be compared with differences observed in the conformational changes for PMMA at an Al interface [200], but in this case the free surface is 180 nm away from the solid interface. It is remarkable that this substrate dependence of surface relaxation times persists to a film thickness value of ~180 nm before the nano hole relaxation time is the same for films on different substrates. This observation means that the rheological properties of the first 1–3 nm of the *i*-PMMA surface are affected by the substrate even when the substrate is over 100 nm away from the free surface, and the bulk of the film is completely glassy. It is still an open question about how the interfacial effects propagate into or affect the whole polymer film dynamics. From the data in Fig. 4.4 it is clear that *the chain confinement effect plays no role in the mechanism of interfacial effects affecting whole film dynamics*, especially for the case of i-PMMA films on aluminum substrates where there no discernable difference for i-PMMA films of different molecular weights. The long range interfacial interactions in polymer systems are also noticed in [201, 202]. In [203], the AFM tip is used as an indenter to study the viscoelastic properties of a polymer material (styrene butadiene copolymer latex) and the effective probing area is the indenter covered region, which is much larger than the actual indentation depth. In the present study, when we do gold particle embedding at a temperature ~4K above the bulk T_g for ~10 minutes, the relatively big regions underneath the gold spheres are strained. These strained regions are frozen in after the gold sphere embedding procedure is finished and the samples are taken out of the oven to the room temperature. During nano surface hole relaxation measurements, it is possible that the free surface region is effectively connected to the polymer-substrate interfacial region by this extensive strained regions underneath the nano surface holes and the substrate effects play a role in the nano surface hole leveling process. This mechanism can be explained as two in-series connected Kelvin

viscoelastic models (shown in Fig. 4.5), one describes free-surface and embedding-induced strained region properties and the other describes the polymer-substrate interfacial region properties. For the case of i-PMMA films supported on silicon substrate, the polymer-substrate interactions are strong due to potential hydrogen bonds between i-PMMA and the silicon substrate, and accordingly the viscosity of the dashpot of the bottom Kelvin component in Fig. 4.5 can be large. For the case of i-PMMA supported on aluminum (with native oxidized layer) substrate, the polymer-substrate interactions are weak, and the corresponding viscosity for the bottom Kelvin component is small. Therefore, the nano surface hole relaxation times (as shown in fig. 4.4) have a substrate dependence.

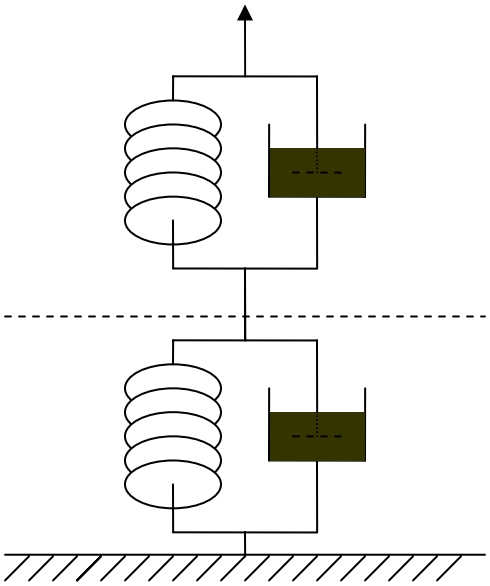

Fig. 4.5 Schematic representation of possible connection between free-surface&embedding-induced-strained region (top Kelvin component) and polymer-substrate interfacial region (bottom Kelvin component).

The inset of Fig. 4.4 shows the measured glass transition temperatures and surface hole relaxation times for thick i-PMMA films ($\geq 180nm$) of three molecular weights. We see that all T_g values are the same within the experiment uncertainty of $\pm 1K$. However, it is remarkable that the nanometer surface hole relaxation times at 287K have a linear molecular weight dependence within the measured M_w range. Therefore, the M_w dependence of near free surface region relaxation dynamics and the average whole film dynamics are very different. Since in all cases of this study the complete surface nano hole relaxation is observed, which means the near free surface regions for all our measurements

are in the melt state, it is reasonable to the first order approximation to treat the materials in this region as a viscous fluid. In this case, according to Eq. 4.2, the surface hole relaxation or leveling time

$$\tau = \tau_\alpha (1 + \frac{RG_0}{2\gamma}) \approx \frac{RG_0\tau_\alpha}{2\gamma} \approx \frac{R\eta}{\gamma}. \tag{4.3}$$

Considering the Rouse model for unentangled polymer chain melt, we obtain

$$\tau \approx \frac{R\eta}{\gamma} \propto N, \tag{4.4}$$

where N is the degree of polymerization. The molecular weight dependence of nanometer surface hole relaxation is in agreement with the relation in Eq. (4.4). It is very interesting to note that this observation of Rouse-like dynamics in the near free surface region of i-PMMA films is similar with that observed for high M_w PS confined to 2 nm confinements [204]. Even though the thick film surface relaxation times depend on the M_w of the *i*-PMMA, the limiting film thickness where this dependence vanishes does not appear to. Given the factor of 4 difference in the M_w values used, it is very unlikely that the dependence on substrate material is due to chain confinement over the whole film, which is also directly reflected by the normalized surface hole life times for i-PMMA films of different M_w's on two different substrates. Caution should be given that neither of us or ref. [204] claims that the near free surface region of PS films has such Rouse-like dynamics as well. In ref. [205], some M_w dependence of near free surface T_g values for PS mixture films is observed. In that case, the chain ends, especially from the low M_w component, can act as diluents. The M_w dependence of the surface relaxation dynamics of glassy *i*-PMMA is distinct from such conditions. Since only the near surface region of the polymer surface (of the order of a few nm) is able to relax at the measurement temperature, and the size of this region is much smaller than the molecular size, only a small fraction of the monomer units of any molecule should be in the mobile surface region (for ideal chains near an interface) [206]. It could be a specific property of *i*-PMMA, because of its molecular structure and possible short range ordering of the chains near the surface [198]. As

mentioned in the foregoing section, the comparison for the temperature dependence of near free surface relaxation dynamics between i-PMMA and PS [90] also indicate that the near free surface region of i-PMMA films has its own specific T_g, which may be related to the unique polymer chain structure as well. We observed, by a novel nano gold sphere embedding technique, the surface dynamics of glassy PS films do have no M_w dependence (see next chapter). Clearly, this is an observation of unique M_w dependence of the free surface region dynamics in i-PMMA films and the possible novel structural features will benefit substantially from more theoretical considerations.

4.1.6 Conclusions

We have used nanohole relaxation studies to probe the rheological properties of the near free surface region of *i*-PMMA with different film thicknesses, substrate materials, and M_w values. The results show an enhanced surface mobility compared to the bulk materials under all measurement conditions, but the actual relaxation time reveals a number of surprising features. The temperature dependence of the near free surface relaxation dynamics is distinct from that of PS films [90]. A surface T_g (~40K below bulk T_g) could be assigned to this region. The relaxation time of the first few nanometer of the surface appears to be affected by the substrate such that for films with a thickness of ~20 nm there is a factor of 3 difference in the relaxation time between films with the same thickness but different substrate. The substrate dependence of the surface relaxation time persists to a film thickness of ~200 nm. The surface relaxation time is observed to be dependent on the M_w value of i-PMMA. In the range 200k< M_w <800k, this M_w dependence appears to be linear, which means that the near free surface region of i-PMMA films can be treated as a Rouse-like viscous fluid. From the dependence of near free surface dynamics both on film thicknesses and on M_w data, the possible mechanism of the chain confinement effects contributing to the near free surface dynamics can be excluded. The unexpected M_w dependence together with the temperature dependence of the near free surface dynamics of i-PMMA films strongly indicate a unique structural difference between the free surface region and the bulk part— the first few nanometer free surface region may consists a substantial amount of near 2-dimensional chains, which may have some short range ordering due to the unique

property of i-PMMA chain molecules. However, such prediction warrants more experimental and theoretical studies.

4.2 Studies of near-free-surface dynamics of glassy polystyrene films

In Ref. [90], Fakhraai and Forrest found a weak temperature dependence of the nano surface hole relaxation in the near free surface region of glassy polystyrene films. Even at a temperature of ~94K below bulk PS T_g, the complete nano surface hole relaxation was observed still. The observation in Ref. [90] is rather surprising in that the weak temperature dependence of the nano surface hole relaxation is different from those of the bulk material α and β relaxation and in the measured deep glassy state the PS film surface seems having enhanced dynamics. To investigate if one can observe a complete glassy state for PS films, in this project we study the near free surface dynamics of thin PS films at a even lower temperature, ~128K below bulk PS T_g, using the same nano surface hole relaxation technique. The method to make nano surface holes in polymer films and ulta-low temperature treatment are described in detail in chapter 3.

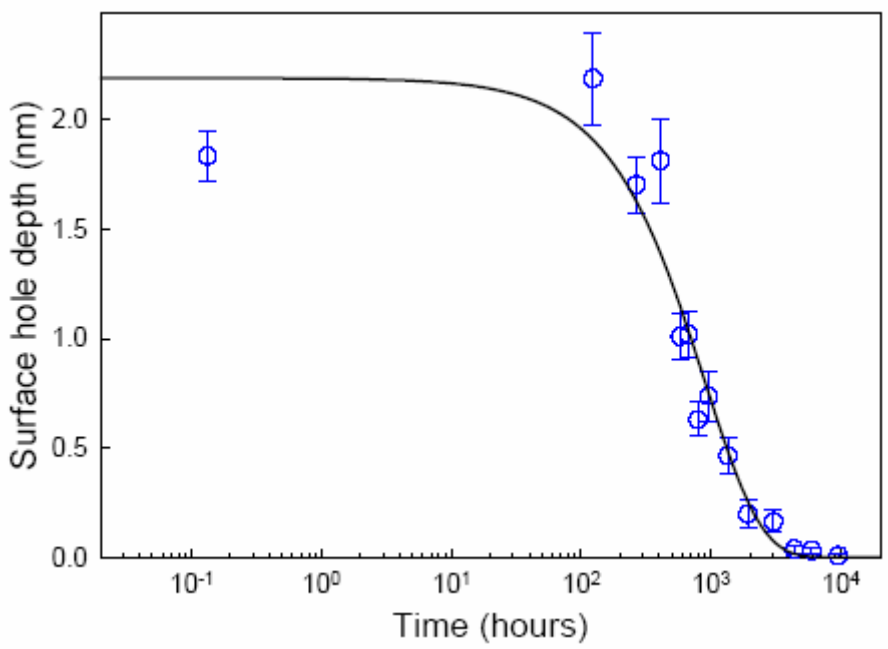

Fig. 4.6 Nano surface hole relaxation in the near free surface region of 100nm thick PS films at 243.15K.

Fig. 4.6 shows the results of the nano surface hole relaxation in the near free surface region of 100nm thick PS films at 243.15K. It can be seen that even at a temperature of ~128K below bulk PS T_g the nano surface hole can still completely relax. Considering that the nano surface hole leveling by AFM scanning is carried out at 287K, there might be some nano hole relaxation at this procedure. However, using the Boltzmann superposition principle and the fact that the total time of the sample at 287K is ~800 minutes, the hole leveling can estimated as ~0.06nm at 287K[90], which is negligible compared with the whole nano surface hole leveling. Therefore, the nano surface hole relaxation shows that even at such deep glassy state the PS films seems not completely glassy. In addition, we use a single exponential fitting (shown as bold curve in Fig. 4.6) to estimate the relaxation time of nano surface holes and transfer it to the characteristic chain segment relaxation time, which is shown as the blue downward triangle in Fig. 4.7.

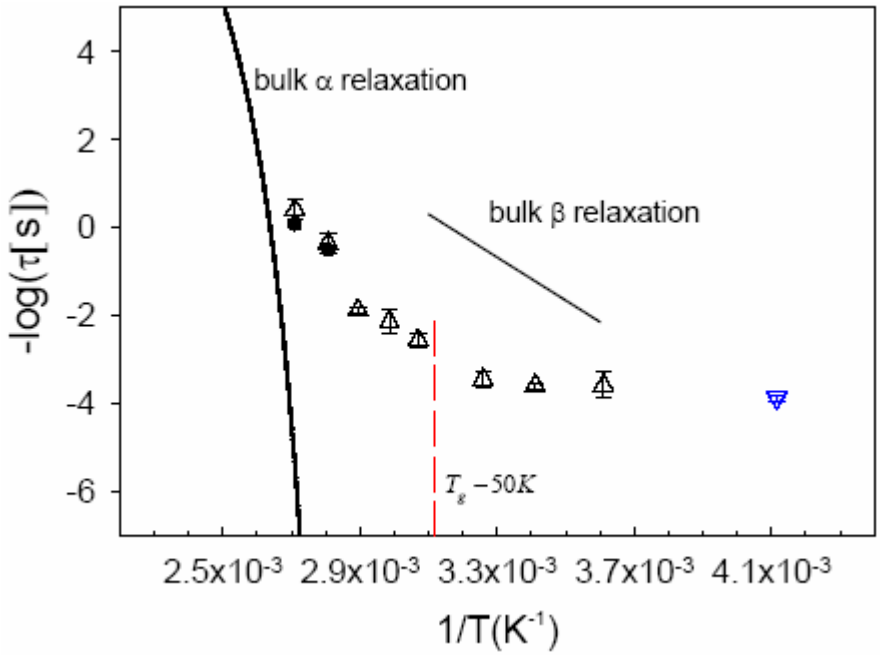

Fig. 4.7 Nano surface hole relaxation in the near free surface region of 100nm thick glassy PS films, compared with bulk material α and β relaxations. (Except the downward triangle data point, the other results from Ref. [90])

From Fig. 4.7, we note that the complete nano surface hole relaxations are observed in a wide experimental temperature range of ~126K. For data points above the temperature $\sim T_g - 50K$, the temperature dependence is weak compared with bulk material α (shown as bold curve in Fig. 4.7). Even remarkably is that when the temperature is below~ $T_g - 50K$, the temperature dependence is much weaker than that of the bulk β relaxation (shown as thin oblique line in Fig. 4.7), which is related to energy activation relaxation of small molecules— side groups in polymers. One possible cause for the nano surface hole relaxation and the corresponding much weaker temperature in deep glassy polymer films is some potential aging effects. After we embed gold spheres into PS films for ~4nm at a temperature of ~5K above T_g, we then take out such samples from the oven at the high embedding temperature to room temperature immediately. This quench procedure can induce aging effects in glassy polymer materials. However, from Fig. 4.7 we notice that when the measurement temperature is larger than ~ $T_g - 50K$ the nano surface holes may relax mainly driven by the Laplace effect which overwhelms the potential aging effects at such temperatures, which can be

drawn from the fact that within this temperature window the characteristic time obtained from both nano hole relaxation and the nano gold sphere embedding measurements (see next chapter) are in agreement very well— in the latter case there is no such quenching procedure as in the nano surface hole relaxation measurements. In addition, the Arrhenius molecular relaxation behavior may be explained using the basin-hopping mechanism— the glassy bulk material region underneath the near-free-surface region can form potential energy landscape and molecules or chain segments can hop or jump among local energy basins. In Fig. 4.7 we see that when the temperature is lower than $\sim T_g - 50K$ the temperature dependence is almost level off or disappear, which may be a temperature regime where the aging effect dominates. In [207], especially from b) of Fig. 2 therein, we can estimate such very weak temperature dependence of aging effect— although there is a temperature difference of 95K the two aging measurements have almost the same aging rate. In [208, 209, 210], the lack of temperature dependence of aging phenomena in glass forming materials are also observed.

Chapter 5
Nanometer gold sphere embedding studies of PS films

5.1 Introduction

The studies of thin polymer films have been more than one decade. The most noteworthy observation is the glass transition temperature T_g deviation from the bulk values [67, 73, 76, 86, 87, 88, 101]. There is continuously growing evidence showing that the interfacial effect plays the key role for the observed dynamical anomalies in thin polymer films [59, 60, 61, 62, 63, 67, 76, 77, 78, 79, 80, 81, 82, 83, 84, 85, 87, 88, 96, 100, 101]. Specifically, the polymer chain segment motions in the interfacial regions may be enhanced or inhibited compared with those in the bulk parts based on the nature of vacuum-/substrate-polymer interactions, which substantially contributes to the average measured dynamical quantities. Based on this picture, together with the consideration of the big dimension ratio in the surface normal and lateral directions of the thin film geometry, Forrest proposed a layered on-average dynamics heterogeneity model for thin polymer films [80], which can interpret most results of T_g measuring experiments. However, there are very few studies investigating how such on-average dynamics heterogeneity may vary at different conditions, or particularly, how the size of interfacial region might change with temperatures. This is important in that people do not know if or how this size of the interfacial region is related to the characteristic cooperative length scale mostly involved in

the glass transition [27, 28, 29, 30, 33, 34, 35, 36, 37]. In Ref. [66], Torkelson and co-workers found that the vacuum-polymer interfacial effects can propagate into thin polymer films as far as ~35 nm. In [162] by Teichroeb and Forrest, the surface mobile layer in glassy polystyrene films is experimentally observed to be on the order of 3-4nm thick. In [123], Herminghaus *et al.* observed a molten layer of thickness about 23nm at a temperature around T_g for 100nm polystyrene droplets and, in addition, the size of the molten layer increases with temperatures from below T_g. This temperature dependence of the liquid layer size is in contrast with that of the length scale of the cooperative regions of glass forming materials around the glass transition [28, 33, 34, 35, 36, 37]. The different experimentally measured liquid layer sizes and the different temperature dependence of characteristic length scales around T_g of glass forming materials raise new issues such as whether the measured liquid surface sizes by different techniques are comparable or what length scale is more related to the glass transition. More generally, how the dynamics in the near free surface region of thin polymer films deviate from those in the bulk parts is still elusive.

Since the free surface region— a specific local region of thin polymer films may be the major cause for many experimentally observed dynamics peculiarities, some efforts have been carried out to study properties in this region. In [90], Fakhraai and Forrest observed a rather weak temperature dependence of relaxation of nano surface holes in glassy thin polystyrene films. In [91], an unexpected molecular weight dependence of the near free surface dynamics is observed for thin i-PMMA films. Both findings indicate that the specific free surface region of glassy polymer films have a richer-than-imagine scenario. Although the nano surface hole relaxation technique is a novel method to study dynamical properties in the near free surface regions of thin polymer films, it is very hard to be used to investigate any potential dynamical depth dependence in this region. The fluorescence technique has been used for thin polystyrene film T_g distribution studies [66]. However, a dye doped or labeled trace layer is ~14 nm thick in this technique, which restricts any higher probe resolution better than 10nm if used to study the near free surface regions of thin polymer films. In this study, we use the nano gold sphere embedding technique, "a powerful tool to determine surface viscoelastic properties" [72], to comprehensively investigate rheology or dynamical properties of the near free surface region of thin polystyrene films. Some interesting findings have been observed.

5.2 Technique of nano gold sphere embedding for thin polymer film studies

Some novel techniques have been developed to directly measure the near free surface properties of thin polymer films. However, there are no consensus conclusions achieved yet. For example, some studies [93, 94, 211] using AFM techniques show either liquid-like or bulk-like free surface properties. Similarly, the polymer surface asperity relaxation studies [115,212] show opposite results about polymer film surface properties. There are some unclear issues in these techniques which are crucial to reach reliable conclusions, such as unknown contact areas and interactions between the probe tip and polymer materials, uncontrollable surface asperity sizes, and unsuitable probing forces and frequencies. Nano surface hole relaxation [90, 91] is a powerful technique for surface property studies of thin polymer films, but with some limitations as well— for example, it is hard to be used in terms of using ultra-sharp AFM tips and proper AFM scanning controlling, and it is hard to be used to study dynamical depth dependence studies in the near free surface region of thin polymer films. Compared with most techniques directly probing free surface property studies of thin polymer films, nano gold sphere embedding is a conceptly simple but powerful method for such studies [161, 162, 213]. One can use nano spherical gold spheres, ranging from 5nm to 60nm with narrow size distributions, to do isothermal embedding measurements in polymer films. The major point about this technique is that the sphere-polymer contact area can be well defined and the sphere embedding driving force (of order of nanonewtons) is much smaller than conventional solid contact probing techniques. Moreover, the experiments of nano sphere embedding in polymer films can be conducted in very wide time and temperature windows, which is necessary to capture some subtle features of dynamical properties of thin polymer films. Unfortunately, there have been some disputes about the interpretation of the embedding results [161, 213, 214, 215, 216].

The first qualitative nano gold embedding studies [162,217] revealed a liquid-like surface layer in thin glassy polymer films. Sharp, Teichroeb and Forrest [161] conducted, for the first time, the detailed quantitative analysis of the gold sphere embedding results and developed a viscoelastic contact mechanics model, referred to as STF model. In this model, when the nano gold sphere comes into contact with polymers in the melt state, the latter will wet the solid sphere and a meniscus contact

area is formed. The surface tension force of the outmost sphere-meniscus contact line is the major driving force for gold sphere embedding into the polymer film. See Fig. 5.1 for the schematic representation for this model.

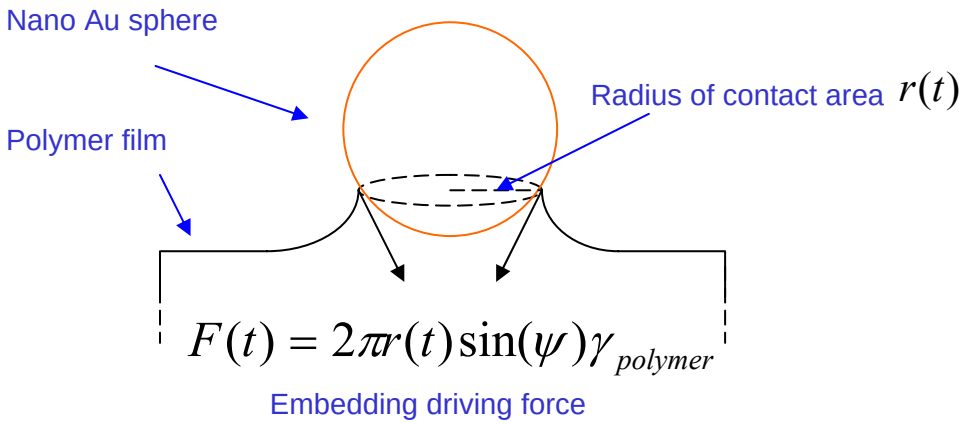

Fig. 5.1 The schematic representation for the STF model.

In the STF model, the embedding driving force is

$$F(t) = 2\pi r(t)\sin(\psi)\gamma_{polymer}, \tag{5.1}$$

where $r(t)$ is the radius of the contact area, ψ is the angle between $r(t)$ and the tangent of the contact line of polymers, and $\gamma_{polymer}$ is the surface tension of the polymer materials. By applying this driving force (~1 nano Newton) to the following equation, which is a previously developed theoretical framework for the embedding of spherical nano-indenters into the surface of a linear viscoelastic material, the nano sphere height $h(T,t)$ during embedding can be obtained

$$h(T,t) = 2R - \left[\frac{3(1-\upsilon)}{8\sqrt{R}}\int_0^t J(T,t-\xi)\frac{dF}{d\xi}d\xi\right]^{\frac{2}{3}}. \tag{5.2}$$

In Eq. (5.2), R is the radius of the nano spheres, υ is the Poisson's ratio and $J(T,t)$ is the creep compliance of the viscoelastic materials. When using Eq. (5.2) to do nano sphere embedding simulations, the temperature dependent creep compliance $J(T,t)$ is adjusted to let the simulated embedding data match the experimentally measured data and accordingly the rheology properties of the polymer film surface regions can be obtained. The major finding of the quantitative analysis of the experimentally measured gold sphere embedding results by means of the STF model is that a liquid-like surface layer with a lower bound of size ~3-4nm exists in thin glassy polymer films. In particular, the model simulated temperature, referred to as the rheological temperature T_{rheol} , is 374K, while the nano sphere embedding temperature $T_{\exp}$ is set at least 7K below the bulk PS T_g ~370K [161], which means that while the bulk part of the PS film is at the glassy state at 363K the near free surface region behaves as if it were in the melt sate at 374K.

Another nano sphere embedding model is developed by Hutcheson and McKenna [72, 214, 215], referred to as HM model. In this model, the very similar nano sphere height integration equation as Eq. 5.2 is used. However, there is a major difference for the embedding driving force functions between the STF and HM models. In the latter, the nano sphere embedding driving force is taken as the Au-PS work of adhesion force

$$F(t) = 2\pi r(t)(\gamma_{sphere} + \gamma_{polymer} - \gamma_{sphere-polymer}) . \tag{5.3}$$

In the case of nano gold sphere embedding in PS films, the embedding driving force in the HM model is ~25 times larger than that in the STF model, which results in a conclusion that the near free surface region of PS films is bulk-like since the HM model simulated temperature T_{rheol} is consistent with the experimental temperature $T_{\exp}$ in the glassy state.

The major controversial issues between the two models include: (1) The STF model can simulate the $T > T_g$ experimental embedding results very well— the simulated embedding temperature T_{rheol} matches the experimental temperature $T_{\exp}$, which the authors claimed is the minimum requirement for any embedding model [216]; for the $T < T_g$ case the simulated temperature T_{rheol} is ~7K larger

than the experimental temperature $T_{\exp}$, by which the existence of a liquid surface layer is claimed. As for the HM model, things are just the opposite: in the $T > T_g$ embedding case, T_{rheol} does not match $T_{\exp}$; in the $T < T_g$ embedding case, T_{rheol} and $T_{\exp}$ are in agreement with each other, by which the authors claimed that the properties of free surface region of PS films are bulk-like since both temperatures are the same and below bulk T_g. (2) Whether the small variations between the model simulation temperatures and experimental temperatures is crucial for the determination of the near free surface dynamical properties of thin polymer films. In Ref. [72], the authors claimed that "*the difference between T_{rheol} and $T_{\exp}$ from the HM analysis is not greater than approximately 7K*" and "… *not enough to explain the reduction of the T_g in polystyrene.*" However, in [216] the authors claimed that "*the temperature dependence of the properties of the near surface region is significantly different (and weaker) than that of bulk PS*" and the small amount of change of material properties in the surface regions "*could account for the magnitude of the T_g reductions that are observed in free standing PS films*."

From the above description we see that the differences between the two nano sphere embedding models origin from the different embedding driving forces. Although the magnitude difference of the embedding driving forces in the two models is less than 30 fold, the fundamental physical mechanism is very different. The most direct way to test these two models is to measure the real embedding force, for example, by somehow applying an upward force to the nano spheres to balance the downward embedding driving force. However this may be a terrible hard task in terms of both how to hold the nano spheres and applying a small force only around several nano Newtons.

One may ask since the fundamental model of nano sphere embedding is still unresolved what is the point to carry out more embedding measurements in this project? One direct answer is that it is possible to obtain near free surface properties of thin polymer films by *model independent data analysis*. Another reason is that as of today there is no comprehensive nano sphere embedding measurement in thin polymer films within wide time and temperature windows has been conducted. In this project, we conduct isothermal nano gold sphere embedding measurements in thin PS films with experiment temperatures ranging from 287K to 378K and long measurement times

$\sim 5 \times 10^4$ minutes. By analyzing the characteristic embedding times at different temperatures without considering any specific embedding driving force, we observe unexpected dynamical heterogeneity in the ~10nm near free surface regions of thin PS films and find that in glassy PS films there exists a liquid-like surface layer, whose dynamical properties have a weak temperature dependence. In addition, we find that the liquid surface size decreases with temperatures, which is in contrast with the temperature dependence of the characteristic length scales of glass transition related cooperative rearranging dynamics. Equally remarkable is that the nano gold sphere embedding in the ~5-8 nm near free surface regions is reversible. Moreover, the molecular characteristic times for the first ~5.5nm surface layer region obtained by the present model-free data analysis are indistinguishable from those obtained by the nano surface hole relaxation measurements[90] where the major driving force is the PS surface tension, which indirectly support the STF nano sphere embedding model.

5.3 General characterization of PS films

All polystyrene materials are bought from the Polymer Source Inc.: $M_w = 86.8k$, $r_{PDI} = 1.05$; $M_w = 220.9k$, $r_{PDI} = 1.03$; $M_w = 641.0k$, $r_{PDI} = 1.11$; $M_w = 1210.7k$, $r_{PDI} = 1.16$. Thin PS films are prepared by spin-coating polystyrene solutions in toluene onto small ($1 \times 1 cm^2$) pieces of silicon wafers (Silicon Quest International; single side polished; crystal orientation: <100>; front side surface roughness: 0.1-0.25nm) with native oxide layer intact. As mentioned in the technique section, the PS film thickness is a function of the spin-coating speed, solution concentration and polymer molecular weight. By adjusting such parameters, we make PS films of thickness of $100.0 \pm 2.8nm$ for all four M_w's. After spin-coating, the PS films are kept at room temperature for ~4 hours to let the solvent evaporate slowly and then put in the home-built oven at the preset temperature for annealing for more than 16 hours. The annealing process, carried out in a purge of dry nitrogen gas in the oven at a temperature of 399K(~28K above the bulk T_g), is necessary to remove residual solvent and stress resulting from the spin-coating procedure. After such treatments, the samples are ready for investigations.

The as-produced PS films are characterized using ellipsometry (Exacta 2000 self-nulling ellipsometer; Waterloo Digitlal Electronics) and atomic force microscopy (AFM, Veeco). The film

thickness is measured as $100.0 \pm 2.8nm$ using both techniques. The glass transition temperature T_g values are determined by the ellipsometry measurements using the same method for the i-PMMA work. Fig. 5.2 shows the typical ellipsometry measurement results for 100nm thick 641.0k PS films on silicon. The top graph is the raw results of the polarizer angle as a function of temperature. The bottom graph is the results of film thickness versus temperatures, which are transferred from the raw ellipsometry polarizer and analyzer angles using an optical model. In both graphs, the T_g values are defined as the intersection of the two lines fitted to the glassy and melt states respectively. We see that the T_g values obtained from the two data sets are very close. Fig. 5.3 shows the ellipsometry measurement results for 100nm thick PS films of four M_w's. The inset is the film thickness versus temperature data for different M_w's. In the main panel different M_w data are vertically shifted to match the $M_w =$ 1210.7k data. It is interesting to note that after shifting, the data for the four M_w's in the melt state overlap with each other well, which means that for the four PS films the thermal expansion coefficients are almost the same, ~0.02856 nm/K. However, in the glassy state the thermal coefficients for the three lower M_w's are close ~0.00991 nm/K and that for the 1210.7k PS film is slightly higher ~0.01092 nm/K. These thermal expansion coefficients are of the same order of magnitude with those in [57, 97], considering the volumetric thermal expansion coefficient $\alpha = -\rho^{-1}(d\rho / dT) \approx h^{-1}(dh / dT)$. The thermal coefficient difference between lower and higher M_w PS films of the same thickness can be explained in terms of the polymer chain confinement effect. We can get the radius of gyration R_g of the chain molecules without perturbations in good solvents according to the relation

$$R_g = \sqrt{\frac{Nb^2}{6}}, \tag{5.4}$$

where N is the degree of polymerization and b is the statistical Kuhn length(for PS $b = 0.67nm$ [218]). From table 1, the characteristic parameters for PS films, we see that for the case of 100nm thick 1210.7k PS films the chain molecules must be confined in the film surface normal direction compared with the free coiled molecular structure in good solvents. The stress due to the entropy penalty from the confinement effect can make some contributions to the thermal expansion

during the ellipsometry measurement. The chain confinement effect can not be completely removed even after the long-time high-temperature annealing treatment due to the intra- and inter-molecular interactions in the polymer films.

Table 1. Characteristic parameters for 100nm PS films

M_w ($\times 1000$)	T_g (K)	R_g (nm)	$100/R_g$
86.8	369.79	8.0586	12.4091
220.9	370.61	12.8557	7.7786
641.0	370.56	21.8992	4.5664
1210.7	370.77	30.0966	3.3226

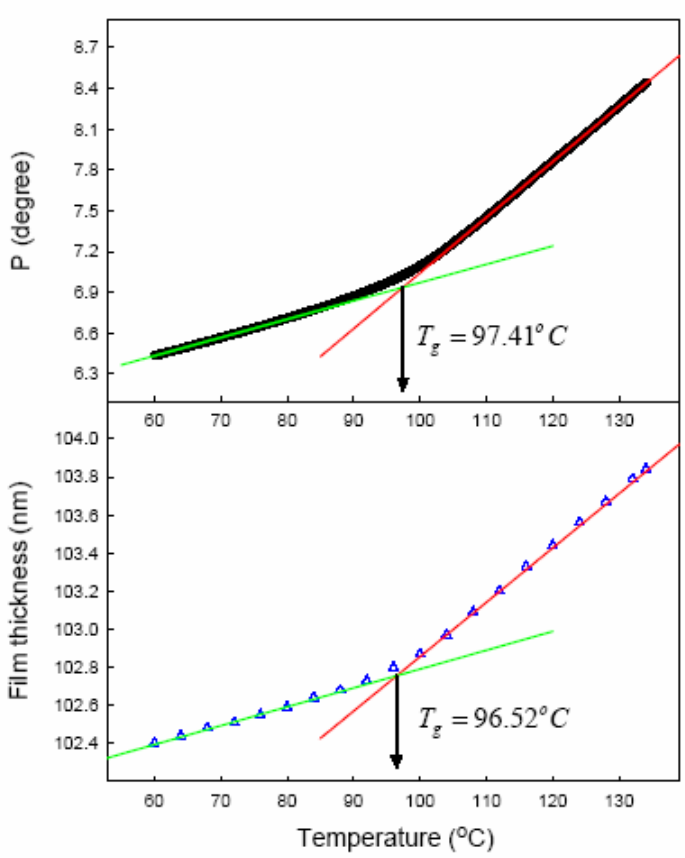

Fig. 5.2 Ellipsometry measurement results for 100nm thick 641k PS film on silicon: polarizer angle versus temperature (top); film thickness versus temperature. T_g values are defined as the intersection of the two lines fitted to the glassy and melt states respectively.

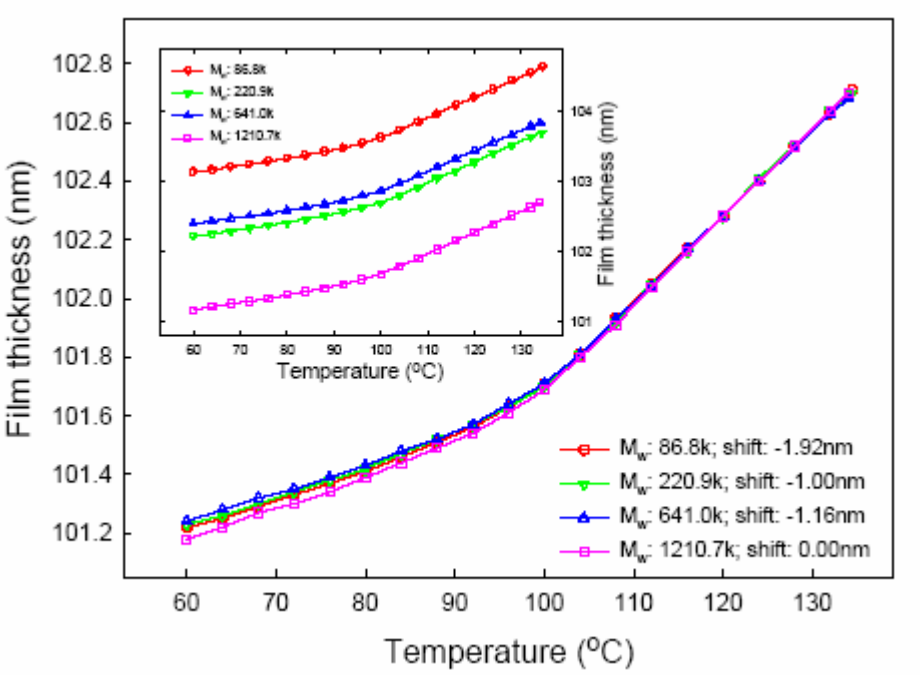

Fig. 5.3 Ellipsometry measurement results for 100nm thick PS films of four M_w's: results are vertically shifted to match the 1210.7k data (main panel); film thickness versus temperature data for different M_w's (inset).

5.4 Chain size dependence of dynamics in the near-free-surface region

In the i-PMMA work, we observed an unexpected chain size dependence for the dynamics of the first few nanometers of the near free surface regions of thick i-PMMA films in the glassy state (more than 30K below bulk T_g), using the nanometer surface hole relaxation technique[90, 91]. It is predicted that the surprising chain size dependence could result from the potential unique structure in the near free surface region where a substantial amount of two dimensional polymeric chain molecules exists and this unique structural property may be due to the specific molecular properties of i-PMMA. In this study, we investigate the chain size dependence of the near free surface dynamics of thin PS films. Since the PS films have no or very weak substrate dependence of dynamics [67], we study PS films of thickness 100nm in all cases. The method used is the relatively simple nanometer gold sphere

embedding technique, which we found is suitable for such study and has the similar results with those in [90] obtained by the nanometer surface hole relaxation technique [90]. This is a simple but powerful technique in that the established AFM technique can be used to probe the apparent gold sphere height variations during the isothermal embedding and the depth dependence of the few nanometers near free surface dynamics of thin polymer films can be studied as well. In addition, during the gold sphere embedding the systematic intrinsic driving force is around or less than one nano Newtons, which is the smallest known solid contact probe force in some AFM based studies[94, 211].The details of the technique of nano sphere embedding for studying polymer film surface properties are described in chapter 3.

Fig. 5.4 shows nano gold sphere isothermal embedding results for PS films of four M_w's. Every data point represents the average gold sphere height of more than 100 gold spheres in the AFM image. We note that the gold sphere embedding, shown as the continuous decrease in the apparent gold sphere height, proceeds with embedding times and after ~ 1000 minutes reaches an almost stable plateau for four different M_w PS films, beyond which the viscosity of the PS films at the measurement temperature is too high to allow any further embedding within the experimental measurement time. Considering that the experimental embedding temperature is ~16K below bulk PS T_g, if the near free surface regions of the thin PS films have the bulk properties then the whole film should be in the glassy state, in which no chain segmental motions are allowed for embedding more than 0.5nm[161,162]. If we use the VFT data of bulk PS to estimate the nano sphere embedding behavior, then it can be shown that at a temperature of ~4K below T_g there will be no embedding even after 4×10^4 minutes. Therefore, the observed ~5.5nm nano gold sphere embedding is the evidence that the near free surface region has enhanced chain segmental mobility compared with the glassy bulk part of thin PS films. In addition, this embedding depth provides the lower bound of the liquid surface size considering that the area underneath the gold spheres might have some different properties from those of the real uncovered free surface of thin polymer films. However, this liquid surface size of ~5.5nm is slightly bigger than that of 3-4nm in [161, 162]. We think the major cause for such difference may be that in this project the gold spheres are home made and slightly smaller than those commercial Colloidal gold spheres (Ted Pella) in [161, 162]. More remarkable in Fig. 5.4 is that the data points for four different M_w PS films overlap within the measurement error and can be fitted using a single

exponential function, which means that the characteristic embedding times for the four M_w PS films are of the same value. The characteristic embedding time reflects the dynamics of the probing area because how fast the gold spheres embed into the polymer films depends on the local molecular motions if the size of the gold spheres and the polymer surface tension are constant. Considering that the gold sphere embedding is conducted at a temperature of 16K below bulk T_g and only parts of the same PS molecules are in the mobile near free surface region, this lack of M_w dependence of the probed dynamics seems reasonable. However, this picture is in contrast with that of the i-PMMA work[91], where even at a temperature of more than 30K below bulk T_g, a linear M_w dependence of the dynamics of the near free surface region is observed. For the i-PMMA studies, it is predicted that the Rouse-like fluid dynamics in the near free surface region of thick i-PMMA films may be due to the existence of a substantial amount of 2-D chain molecules. In the present case of PS films, such picture seems different. In order to check if we can observe similar M_w dependence of the dynamics in PS films, we conducted gold sphere embeddings at higher temperatures.

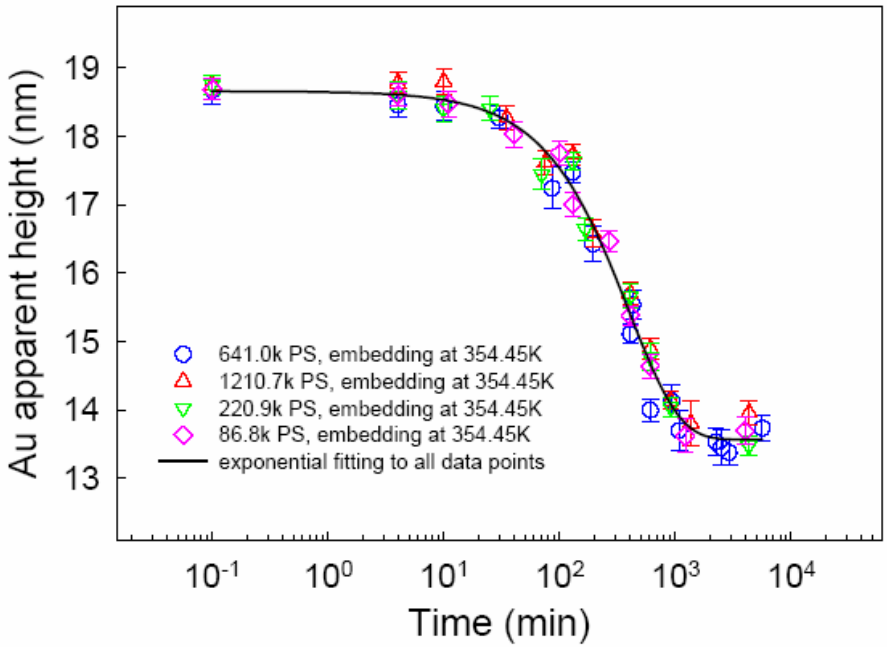

Fig. 5.4 Nano gold sphere isothermal embedding results for 100nm thick PS films of four M_w's at a temperature of ~16K below bulk T_g; the solid curve is the result of a single exponential fitting to all data points.

Fig. 5.5 shows nano gold sphere isothermal embedding results for 100nm thick PS films of three M_w's at a temperature around bulk T_g. Compared with the embedding results in Fig. 5.4, we note that the gold sphere embedding around bulk T_g can proceed beyond the first ~5.5 nm near free surface regions for all the three M_w PS films, which means the chain molecules in the region next to the near free surface region have some segmental mobilities allowing for further gold sphere embedding at the measurement temperature. We know that the glass forming process is not a sharp kinetics arresting transition [67, 121] and the molecular translational or rotational motions are not completely frozen out instantaneously around the temperature of bulk T_g, which may explain why the gold embedding can be carried out in deeper regions of PS films. Another remarkable feature in Fig. 5.5 is that the embedding data can not be fitted using a single exponential function— instead, a three-component exponential function has to be applied with different exponential indexes β as shown in Fig. 5.5 to obtain acceptable fitting. The characteristic gold sphere embedding times, obtained from the data fitting, for the first ~5.5 nm regions are plotted in Fig. 5.7, which will be analyzed in more detail later. In order to investigate the nano gold sphere embedding behavior in the melt state of thin PS films, another set of gold sphere embedding measurements at a temperature ~7K above bulk T_g are conducted, of which the results are shown in Fig. 5.6. We note that the gold sphere embedding propagates into the PS films for about 14nm and the data can be fitted using a stretched exponential function with the stretching exponent β being 0.8. We also note that even after a long time(~8000minutes) of embedding the gold spheres are not completely submerged into the PS films, which we think may be the final equilibrium state of embedding— when the contact angle between gold and polystyrene reaches the equilibrium angle $\sim 60^0$ [161] no big enough driving force for further embedding. For embedding results shown in Fig. 5.6, the average characteristic times for three M_w PS films are obtained using the relation [120]

$$\langle \tau \rangle = \int_0^\infty \exp(-\left(\frac{t}{\tau}\right)^\beta) dt \,. \tag{5.5}$$

The as-obtained results are plotted in Fig. 5.7 as well.

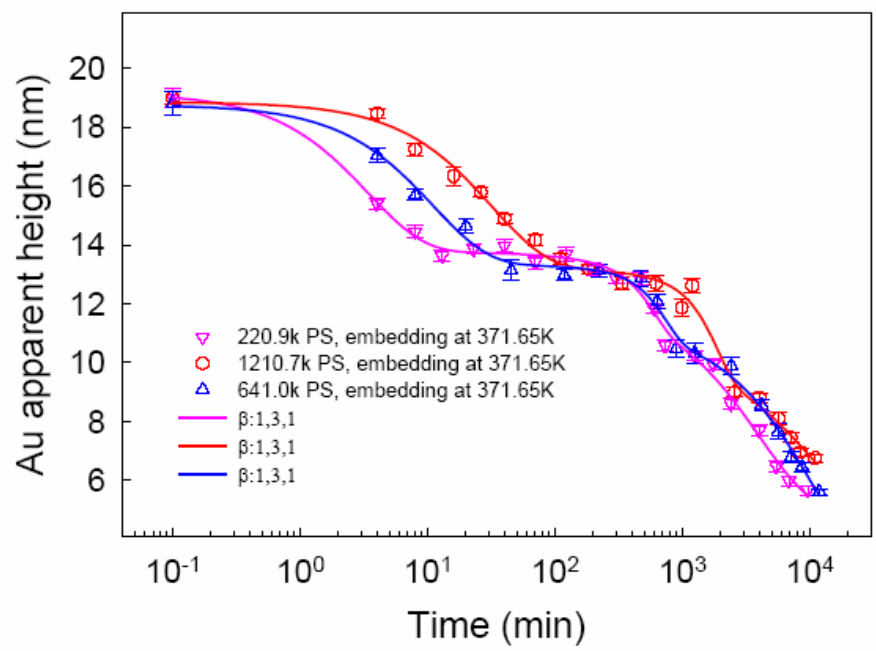

Fig. 5.5. Nano gold sphere isothermal embedding results for 100nm thick PS films of three M_w's at a temperature around bulk T_g; solid curves are results of three-component-exponential fittings.

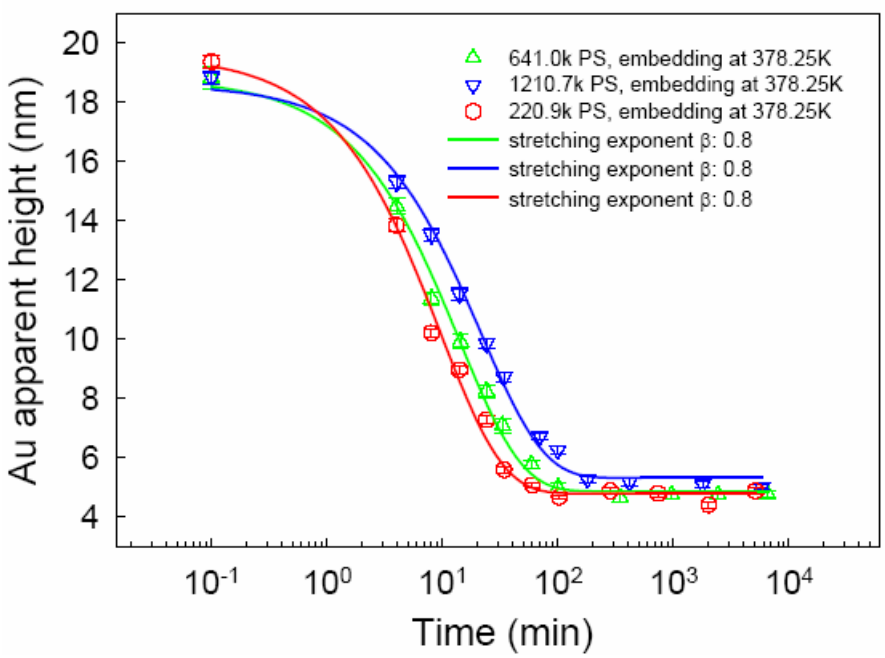

Fig. 5.6. Nano gold sphere isothermal embedding results for 100nm thick PS films of three M_w's at a temperature ~7K above bulk T_g; solid curves are results of stretched exponential fittings.

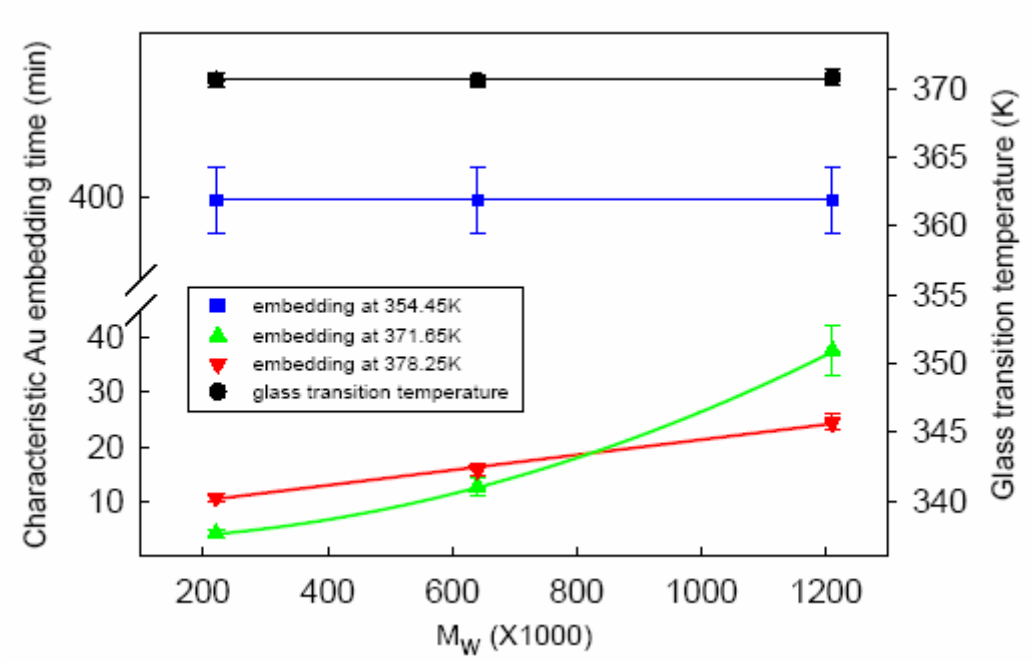

Fig. 5.7 Glass transition temperatures and characteristic gold sphere embedding times for 100nm thick PS films of three M_w's; the solid straight lines are results of linear fittings; the solid curve represents a quadratic fitting to the data of embedding at 371.65K.

In Fig. 5.7, we see that the characteristic times for gold sphere embedding at 378.25K increase with increasing M_w and can be fitted using a linear function, which means $\tau \propto \eta \propto N$ [1,91] and the polymer materials can be treated as a Rouse-like viscous fluid. This feature is similar with that of the i-PMMA work. However, the probing region in the present case is about 14nm and the polymer molecules involved in gold sphere embedding do not have to be 2-D objects. The characteristic times for embedding at 371.65K can be fitted using a quadratic function of $y_0 + ax^2$, which means at this temperature the characteristic embedding time $\tau \propto N^2$ and accordingly the dynamics in the mobile near free surface region are slower than the Rouse-like dynamics. This $\tau \propto N^2$ dependence is also different from that of simple polymer reptation model $\tau \propto \eta \propto N^3$ [1], which is the theoretical prediction for entangled polymer melts. It is rather surprising that the characteristic embedding time at 378.25K for the 220.9k PS films is larger than that at 371.65K, which means that the gold sphere embedding at the higher temperature is slower than at the lower temperature. This is physical unreasonable. One possible explanation for this is that the gold embedding at the higher temperature

involves more PS materials (~14nm deep) than those at the lower temperature embedding (~5.5nm deep) and maybe it is not suitable to compare them directly. Another possible explanation may be that the dynamics in PS films are highly heterogeneous and at the higher embedding temperature the dynamics in the ~8.5nm region underneath the free surface area are still slow and contribute more to the observed average characteristic embedding time, which accordingly is larger than that at the lower embedding temperature. In Fig. 5.7, we also note that the characteristic time of embedding at 378.25K for the 1210.7k PS films is smaller than that at the embedding temperature of 371.65K. In this case, considering the PS chain molecule sizes for different M_w's (see Table 1), the total film thickness is only $\sim 3.3R_g$ and the pronounced chain confinement effect[59,77,117, 219] may overwhelms the highly heterogeneous dynamics effect, which results in enhanced molecular motions and renders faster gold sphere embedding. For the cases of 86.8k and 641.0k PS films the film thickness is $\sim 12.4R_g$ and $\sim 4.6R_g$ respectively and the chain confinement effect is not very big. Consequently, the high dynamical heterogeneity effect plays the major role in determining the measured characteristic embedding times. By comparing the fitted curves, we notice that only when the PS molecular weight is around or higher than 800k can the high dynamical heterogeneity effect be balanced by the chain confinement effect. One more point we should stress about results in Fig. 5.7 is that at temperatures around bulk T_g we observe some M_w dependence of dynamics and possible highly dynamical heterogeneity in the near free surface regions of PS films, while in the $T < T_g$ embedding experiments for the same PS films such features are not observed, which is shown as the solid line fitted to the data of nano gold sphere embedding at 354.45K. The major reason for this is that the glass transition temperature experiments indirectly measure dynamics of the whole polymer systems and any features in smaller domains are averaged out. Since the embedding regions for measurements at temperatures of 371.65K and 354.45K are almost the same near free surface regions, we estimate the temperature dependence of dynamics in this region by comparing the characteristic embedding times. The average the characteristic embedding times at 354.45K is ~398minutes and that at 371.65K is ~16minutes, which indicates a ~26 fold difference. However, the 17.2K embedding temperature difference crossing T_g for bulk polymers indicates ~8 logarithmic decade's difference($\sim 2.5\times10^8$) in chain dynamics using conventional notions of the glass transition event [161]. Therefore, by comparing such big difference between dynamical properties in the near free surface regions of thin polymer films and the bulk materials, we can see that there is a very weak

temperature dependence of dynamical properties in the near free surface regions of thin polymer films, which is in consistent with the findings in Ref. [90]. In Fig. 5.7, we notice that even although we observe the aforementioned dynamical features in the near free surface regions of thin polymer films, such findings can not be observed by the glass transition temperature measurements— the measured T_g's are almost identical for PS films of three M_w's. This is understandable considering that the measured T_g exhibits the *average dynamical properties* and for these 100nm thick PS films the substantial dynamical contribution comes from the bulk parts.

In this study we use the nanometer gold sphere embedding technique to investigate dynamics of the near free surface region of PS films and found that the first several nm free surface region has enhanced molecular mobility at a temperature as low as 16K below bulk T_g. By the chain size dependence measurements some quadratic or linear M_w dependence of dynamics in the near free surface region at temperatures around or above bulk T_g is observed, while at temperatures lower than bulk T_g no M_w dependence is observed. These features are different from those for i-PMMA films, where even at a temperature of ~36K below the bulk T_g the near free surface region can be treated as a Rouse-like viscous fluid and the linear M_w dependence of dynamics is observed. This dynamical difference between i-PMMA and PS strongly indicates a potential big structural difference in the near free surface regions of thin polymer films. The comparison between characteristic times for nanometer gold embedding at the two temperatures around bulk T_g indicates highly dynamical heterogeneity in polystyrene films. In addition, the different temperature dependence of dynamical properties in the near free surface regions of thin polymer films and the bulk polymer materials is observed as well.

5.5 Depth dependence of dynamics in the near-free-surface region

Based on the measurement results of chain size dependence of dynamics of the near free surface region of PS films, we do further gold sphere embedding around and below bulk T_g for PS films of

M_w =641.0k. The reason of studying PS films of this M_w is that in such 100nm thick films, the chain confinement effect can be negligible and the gold sphere embedding is not so fast.

Nano gold sphere embedding at $T < T_g$

In [162], Teichroeb and Forrest experimentally observed a ~3-4nm liquid surface layer in glassy thin PS films using the nano gold embedding technique. However, the lowest experiment temperature they measured is only ~7K below bulk T_g and there is not any clue about at what temperature such liquid layer can not be experimentally observed. In other words, is it possible that a *complete glassy* state of thin polymer films can be experimentally measured? In such complete glassy state, one would expect that the polymer film will be in a dynamically homogeneous state in terms of the concept of average layered dynamics [80] in thin polymer films, and the viscosity of the complete glassy polymer films will be too high and no gold sphere embedding can be observed. To investigate such complete glassy state of polymer films has both fundamental and application significance. On the fundamental research level, people observe dynamical homogeneous state at high temperatures and dynamical heterogeneous state at temperatures around bulk T_g for glass forming materials. One question may be asked is the dynamical heterogeneous state always true at any temperature below T_g ? If not, what would that mean? On the technical application level, if under some circumstance the thin polymer films are in the complete glassy state, then such issue about adhesion, lubrication, or even optical properties of thin polymer films should be different from those at normal conditions. Therefore, in this project we take the advantage of the feasibility of experiment long time investigation of the nano gold sphere embedding technique and measure the near free surface dynamics of thin PS films in much deeper glassy states by means of this simple but powerful technique. In the “chapter 3” the thermal treatment methods for thin polymer films have been described in details. In this section, we focus on data analysis.

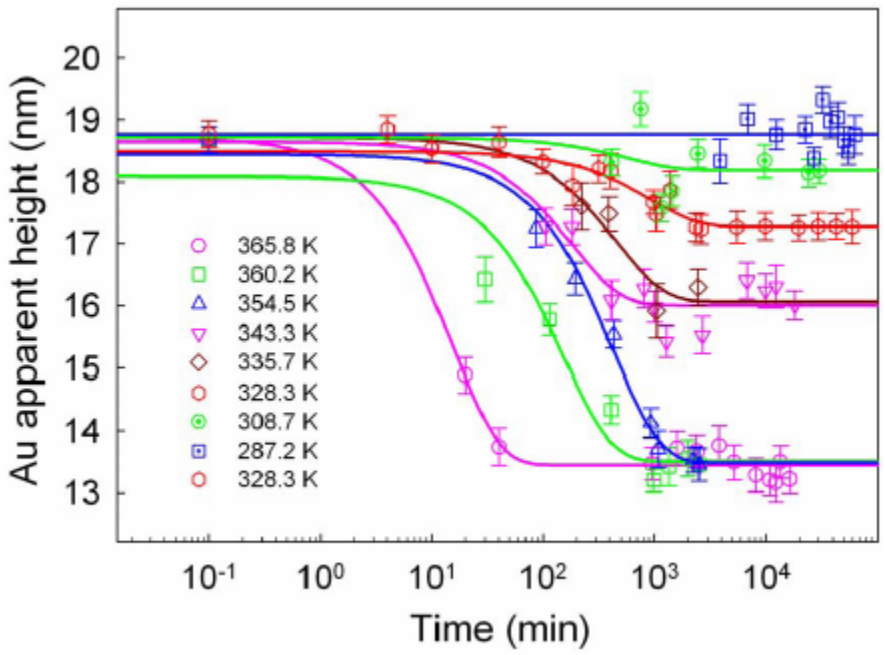

Fig. 5.8 Nano gold sphere embedding in glassy ($T < T_g$) 100nm 641k PS films on silicon.

Fig. 5.8 is the results of isothermal nano gold sphere embedding measurements in glassy PS films within a probe temperature window of ~78K wide and observing time window of $> 10^4$ minutes. All the data are fitted using a single exponential function. There are a number of interesting findings can be seen from these results.

Firstly, at the three highest temperatures, nano gold spheres embed in PS films ~5.5nm, which means within this temperature range a liquid layer ~5.5 nm exists in glassy PS films (bulk $T_g = 370.56K$). This size of the liquid layer in glassy PS films is slightly larger than that of 3-4nm in [162], which may be due to the different nano gold spheres used. We note that with decreasing temperatures the gold sphere embedding proceeds slower and slower, which is reasonable considering that the viscosity of polymer materials increases with decreasing temperatures.

Secondly, a very surprising feature is observed for embedding at temperatures ($308.7K < T < 343.3K$) in the middle of the whole experiment temperature window. We see that after the "initial stages" of embedding, which is still longer than 1000minutes, the nano gold sphere embeddings at these temperatures reach different plateaus in the measurement time window. This is

surprising in that for glass forming materials with homogeneous dynamics one would expect that the only change of embedding with decreasing temperatures would be the increasing viscosity and accordingly the increasing of characteristic dynamical times as expressed in VFT [39, 40] or WLF [10] relations for polymers. The different long time embedding plateaus in the near free surface region of glassy PS films means that the dynamics in this region are highly heterogeneous. This highly heterogeneous dynamical phenomena can only be observed within much different temperature regions— in a relatively narrow temperature window, for example in [162] and in the present work of $354.5K < T < 365.8K$ and $335.7K < T < 343.3K$, the dynamics may be treated as homogeneous.

Thirdly, the nano gold sphere embedding at the temperature of 287.2K indicates, within the measurement error range, there is no embedding observed. The situation is that *the polymer sample viscosity is too high or the measurement temperature is too cold and it is very hard for the nano gold spheres to go further into these complete glassy PS films.* Maybe this statement is too qualitative. If we refer to the STF model calculation [161], we see that for bulk polymer materials at a temperature ~7K below bulk T_g the model prediction of embedding would be ~0.5nm. In this work, for the near free surface region, the observed embedding depth at the temperature of ~62K below bulk T_g the embedding depth is ~0.5nm. If we assign a glass transition temperature to the near free surface region of PS films, based on the large experimentally observed T_g reduction of ~70K for free standing PS films[76, 77, 79], to be ~303K, then at a the temperature of ~15K below this "surface T_g" any embedding should be less than 0.5nm. Considering all of these, the complete glassy state probed by the nano gold sphere embedding is reasonable. As far as we know, this is the first time experimental observation of the complete glassy state with the smallest solid contact probe technique after the first observation [108] of T_g reduction phenomena in thin polymer films. Also, we want to stress that at some temperatures much lower than bulk T_g as in this work of 287.2K the dynamics in glassy polymer films may be homogeneous again.

Lastly, already described in chapter two and the references therein, there is a large body of studies in literature showing the existence of a liquid layer in glassy thin polymer films. In addition, two models predict that the size of the liquid layer increase with temperatures from below bulk T_g [108, 123]. However, there is only one study showing experimental evidence of the temperature dependence of

the liquid surface size in nanometer scales polymer systems [123], in which the samples are ~100nm polystyrene($M_w = 2k; T_g(bulk) \approx 338K$) droplets in water and the measured largest size of the liquid surface layer is ~23nm. Considering that the specific experimental conditions of this study is different from most thin polymer film studies, the unambiguous experimental evidence of the temperature dependence of the potential liquid surface size in thin polymer films is very important in that, for example, it can test the theoretical models. From the fittings of our nano gold sphere embedding data showing in Fig. 5.8, we can obtain the liquid surface size of glassy polystyrene films as a function of temperatures, which is shown in Fig. 5.9. We note that the liquid surface size increases with increasing temperatures from below bulk T_g, which is in agreement with the model predictions. In Fig. 5.9, the red solid curve is the data fitting to the model in [123]:

$$h = \frac{h_0 T}{T_g - T}, \tag{5.6}$$

where h_0 is material specific constant, which is proportional to surface or interfacial tension. The model fitted h_0 is 0.47nm in [123] and 0.82nm in [137, 220]. From the fitting in Fig. 5.9 of our results, we obtain a h_0 value of 0.76nm. The 0.47nm h_0 value results from the relatively low water-PS (low M_w) interfacial tension. In both cases of ours and that in [137, 220], considering that the samples are thin PS films and the polymer surface tension has a weak M_w dependence [221, 222], the model fitted h_0 values of 0.76nm and 0.82nm are in fair agreement. In Fig. 5.9, the green dash curve is the data fitting results using the model in [108]. This model has an empirical prediction of liquid surface size h as a function of T

$$h = A(1 - \frac{T}{T_g})^{\nu}, \tag{5.7}$$

where A and ν are material dependent model constants. In [108], the two model constants A and ν have fitted values for PS films of 3.2nm and -0.56 respectively. In our experimental results, the fitted values for A and ν are 3.0 and -0.44 respectively and the data fitting curve is shown in Fig. 5.9 as

the dash green curve. However, this fitting curve using the aforementioned model constants has to be downwardly shifted by 2.9nm to match our data, which means that the model prediction of the liquid surface size is larger than the experimental result. Actually, in [108] there is also a liquid surface size difference of ~5nm between the model prediction and the experimental result.

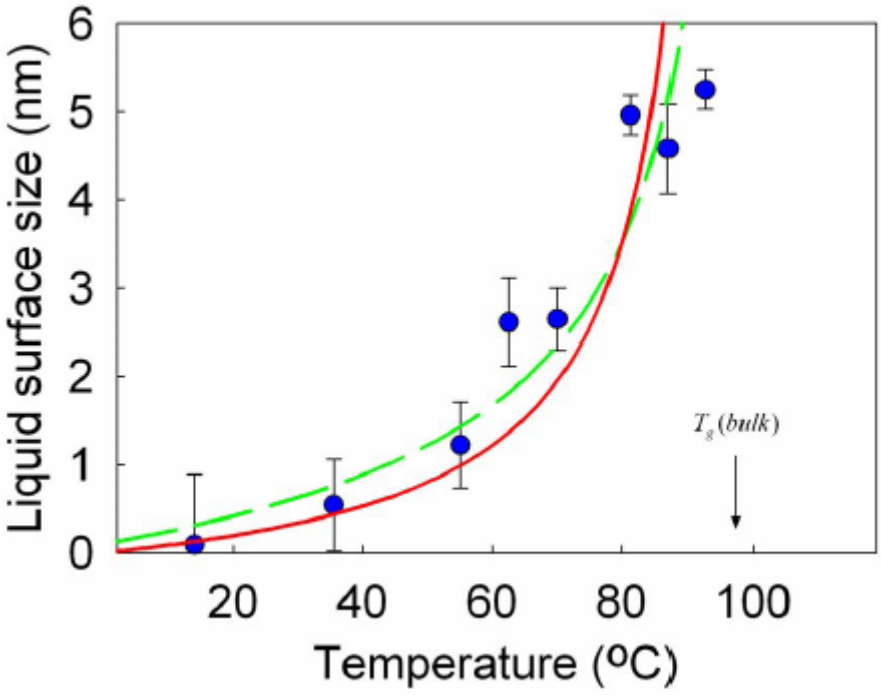

Fig. 5.9 Liquid surface size of glassy PS films as a function of temperature; the red solid curve and the green dash curve are the fittings to model in [123] and [108] respectively.

From our experimental observation of temperature dependence of the size of the liquid surface region of glassy thin polymer films, we see that the size of the near free surface region with enhanced dynamics increase with temperatures. This temperature dependence is in contrast with that of the characteristic length scale of cooperative rearranging regions (CRR) around bulk T_g for glass forming materials [27, 28,33, 34, 35,36, 37], which increases with decreasing temperatures. The latter shows that when the temperature of glass forming materials decreases in the temperature window of $T < T_g$, more and more molecules or larger and larger regions should move cooperatively to render motions in glassy materials. From the VFT relation for dynamics of polymers, for example, the one shown in the following Fig. 5.11, we see that the molecular motions slow down with decreasing

temperatures. Therefore, one should be noted that the temperature dependence of the characteristic length scale of cooperative rearranging regions in glass forming materials only stress the variation of domain sizes rather than the absolute variations of the molecular motions. That is to say, for example, at a certain low temperature the length scale of CRR's maybe large, but the specific molecular dynamics may not permit any large scale motions, e.g., any nano gold sphere embedding in our case. The reason that the length scale of CRR is heavily studied is that people pursue testing some glass transition theories [26] and investigating finite size effects in some glass forming materials. In our case of nano gold sphere embedding measurements, we would say that this technique is more sensitive to the absolute molecular motions. Therefore, at some higher temperatures but still lower than T_g the length scale of CRR's may be small but the molecular dynamics are fast enough for nano sphere embedding. Both characteristic length scales of CRR's and experimentally probing accessible dynamics are closely related to the glass transition phenomena. Due to the limited available measurement techniques, the latter is rarely studied.

Nano gold sphere embedding at $T \sim T_g$ and $T > T_g$

From the above $T < T_g$ nano gold sphere embedding measurements, we observe the existence of a liquid surface region in thin glassy PS films and the heterogeneous dynamics in this region with a spatial resolution high than sub-5nm. Because the glass transition is not a sharp transition, we do further nano gold sphere embedding measurements at temperature around and higher than bulk T_g to investigate more dynamical or structural properties of the near free surface regions of thin PS films. Again the similar nano gold spheres and thermal treatments are described in the technique chapter. Here we just focus on the experimental data and interesting observations.

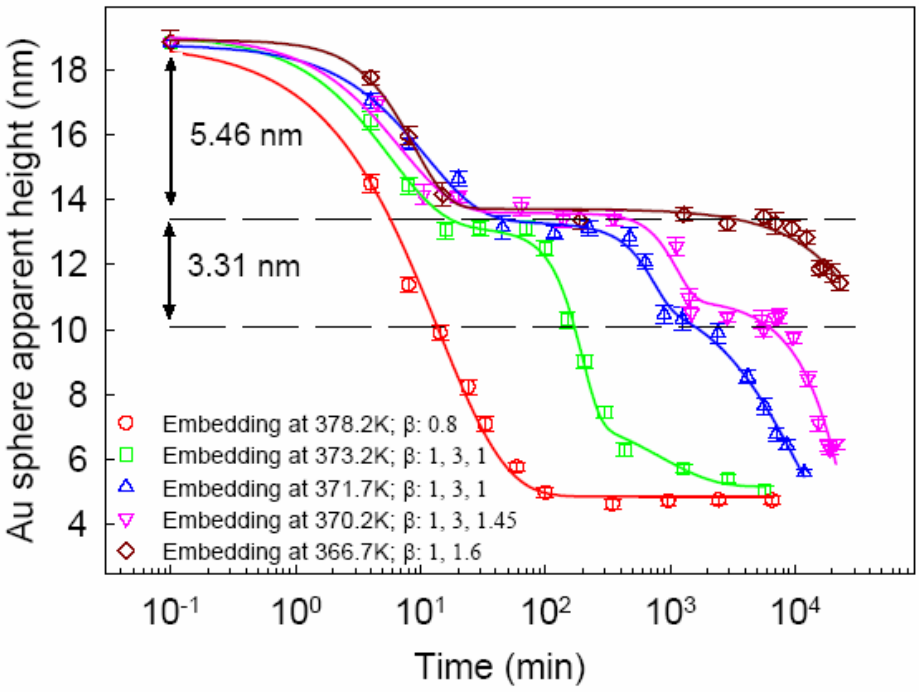

Fig. 5.10 Nano gold sphere embedding in 100nm 641k PS films on silicon at temperatures around and higher than bulk T_g (370.56K).

Fig. 5.10 shows the experimental results of nano gold sphere embedding in 100nm 641k PS films on silicon at temperatures around and higher than bulk T_g. Compared with the single decay behavior of nano gold sphere embedding at $T < T_g$ in the near free surface region of glassy PS films shown in Fig. 5.8, the major feature shown in Fig. 5.10 is that the nano gold embedding can proceed further or deeper at higher temperatures and multiple exponential fittings have been used to fit the data at $T > T_g$ temperatures (except at 378.2K), shown as the solid fitting curves for different embedding temperatures. First, let us take a look at the embedding data at 378.2K, which is ~7.6K above the bulk T_g. We see that at this embedding temperature the nano gold spheres can be embedding into the PS films for ~14nm, which is much larger than the estimated liquid surface size of ~5.5nm in glassy PS films. In addition, the corresponding data can be fitted using a stretched exponential function $y = y_0 + a\exp(-(bx)^{\beta})$ with exponent index $\beta = 0.8$. The stretched exponential relaxation dynamical behavior is usually related to cooperative rearranging motions in glass forming materials [56]. The data of nano gold sphere embedding at ~7.6K above bulk T_g means that the molecular

dynamics are still not complete homogeneous around bulk T_g. When embedding temperatures decrease further, we note a surprising multiple decay relaxation behavior from the nano gold sphere embedding data. In particular, the data in the first decay can be fitted by an exponential function with exponent index $\beta \sim 1$; for the second decay, the exponent index $\beta > 1$ which corresponding to a compressed exponential; for the third decay, the exponent index $\beta \sim 1$ again. The multiple step decay behavior in a narrow temperature window ~6.5K around T_g is unexpected, which is a manifestation of rich dynamical properties during the glass transition or colloidal gelation transition [11, 184, 248, 249, 250, 251, 252, 253]. In the near free surface region of thin polymer films the time-temperature superposition principle does not hold since both stretched and compressed exponential relaxations are observed. In addition to this surprising multiple-step decay behavior, the domain size for different decays are different: the size of the near free surface region corresponding to the first decay is ~5.46nm, which is in agreement with that observed from the $T < T_g$ embedding studies; for the second decay, the size of this region is ~3.31nm; for the third decay, due to the limitation of the nano gold size used no apparent domain size can be extracted from the data.

The observation of ~3.31nm sub-surface layer region with compressed exponential dynamics in thin PS films is very surprising. One possible explanation may be that during the nano gold particle embedding, due to the nature of long chain polymer molecules and possible inter- and intra-molecular entanglements, there might be some stress/strain built up in the adjacent underneath area of nano gold spheres. On the one hand, due to the reduced chain entanglement density in the near free surface region [223, 224, 225], the built up stress may come from deformations of a few polymer chain molecules. On the other hand, if we assume a stress-start-built-in deformation of ~5.5nm, then this length scale is ~25% of the free radius of gyration R_g of the PS molecules used in this study. In the case of the near free surface region of thin PS films, the actual deformation must be much larger that 25%. Therefore, the large deformation induced stress (entropy penalty stress) may be not negligible during nano gold sphere embedding at low temperatures around T_g. Because the embedding in this region is a long time process, such built-in stress may relax as well and the corresponding relaxation dynamics can be a described by a compressed exponential decay behavior as in the embedding results of this study. The compressed exponential decay with relatively large values of exponent index ~2.79-4 for super-cooled glass forming liquids has been observed in [226] as well. However, another

possible interpretation about the sub-surface layer relaxation may be that there might be some unique structural properties in this region [227, 228, 229]. At the present time, we could not provide any substantial evidence to distinguish such two mechanisms.

Now let us see if we can make a strong argument of the existence of any liquid surface layer in glassy thin PS films from the present nano gold sphere embedding studies. As already mentioned, there is no conclusive agreement of different nano sphere embedding models [161,162, 213,214,215, 216,230]. In particular, the conclusion about whether there is a liquid-like surface layer in thin glassy polymer films is different from the two models with much different embedding driving forces. In this nano gold sphere embedding studies, we do data analysis to the nano sphere embedding results *without considering any model-specific embedding driving forces*— we extract, from a pure mathematical perspective, characteristic relaxation times from the multiple exponential data fitting in Fig. 5.10. In Fig. 5.11, we compare our model-free fitted characteristic relaxation times with those in [90] and those for bulk PS materials. It can be seen that the characteristic relaxation times extracted for the third decays in Fig. 5.10 are in agreement with the α relaxation times of bulk PS. One should note that the black VFT curve for bulk PS is downwardly shifted by 2.6474(=log(444)) according to [90, 91]. Although we use the characteristic time transfer technique of [90], the match between the bulk α relaxation data and the present nano gold sphere embedding data should be model independent. It is noteworthy that the characteristic relaxation times from the second decays in Fig. 5.10 have different temperature dependence with those of the bulk and the nano surface relaxation data in [90]. In addition, although obtained by different techniques, the consistency of the nano gold sphere embedding data (downward triangles) and those of the nano surface hole relaxation (upward triangles) for the near free surface region of glassy of films is very encouraging. It is remarkable, from the results in Fig. 5.11, that the near free surface region dynamics are enhanced compared with those of bulk materials and the temperature dependence for the near free surface region of glassy PS films is much weaker than that of the bulk materials. It is very interesting that the relaxation times of the near free surface layer region, the sub-surface layer region and the bulk material region merge at a common point of $1/378.2K$ within the measurement error, *which quantitatively and qualitatively shows that when the sample temperature is higher than 378.2K the dynamics of the whole polymer film is homogeneous and when the sample temperature is lower than 378.2K the dynamics of the polymer film is heterogeneous in terms of the on-average layered dynamics distribution.*

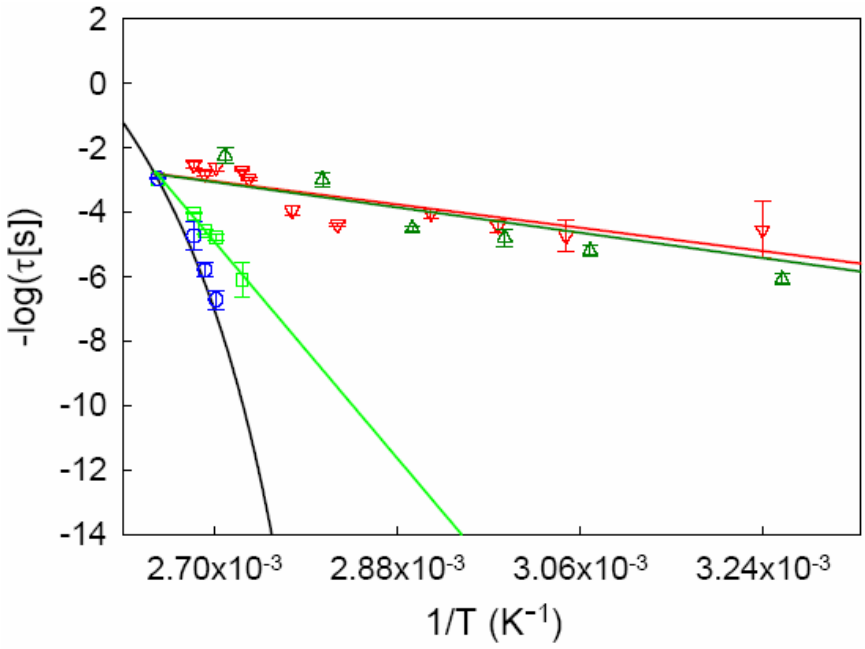

Fig. 5.11 Characteristic embedding times in the near free surface region of PS films as a function of inverse temperature, which are compared with the results in [90]: dark green upward triangles are for nano surface hole relaxation results; the black curve is for bulk PS α relaxation downwardly shifted by 2.6474; the three straight lines(from bottom to top) are linear fitting results for sub-layer nano sphere embedding relaxation(this work), nano surface hole relaxation([90]) and first layer nano sphere embedding relaxation(this work).

5.6 Elastic properties in the near-free-surface region

In the measurements of gold sphere embedding around bulk T_g, we observe that a function of compressed exponential is necessary to fit the embedding data for the region of ~3.3nm next to the near free surface region, which means there might be some elastic effects in this region. Therefore, we have to do more measurements to check if this elastic effect can be experimentally observed or not.

First, we re-measured some old gold sphere embedding samples which were kept at a temperature of 287.15K for more than 4 months. Table 2 show the comparison between average gold sphere heights measured before and after more than 4 months. For the two sets of samples, the gold spheres were

embedded into the first ~5.5nm near free surface region and into the deeper regions beyond the ~8.8nm regions at two different temperatures respectively. From the results in table 2 we see that the measured average gold sphere heights are almost identical within measurement errors before and after more than four months. Therefore, after stopping gold sphere embedding and the samples are frozen at a much lower temperature, no further embedding or reversible effect is observed in these two regions. This observation is in consistent with the findings of depth dependence studies of dynamics in the near free surface region of PS films, where no compressed exponential fitting is needed for these two regions— the first ~5.5nm near free surface region and the beyond ~8.8nm deep region.

Table 2. Comparison between average gold sphere heights measured before and after more than 4 months.

Gold sphere embedding T(K)	Au height(nm) (just after embedding)	Au height (nm) (>4 months later)
371.65	12.9814+/-0.1978	12.5769+/-0.2340
370.15	13.3867+/-0.2613	13.3894+/-0.1934
371.65	5.6068+/-0.1089	5.7665+/-0.1358
370.15	6.4881+/-0.1512	6.4445+/-0.1415

However, one more question should be asked: What happens during the immediate freezing of gold sphere embedding by taking out the sample from the high embedding temperature and then putting the sample at much lower measurement temperature of 278.15K for AFM imaging? Or is it possible that the already embedded gold spheres can be embedded further or bound back due to the different thermal expansion coefficients between gold and PS materials? To address such questions, we conducted real-time *in situ* gold sphere embedding measurements. In this case, we do gold sphere embedding by putting the PS sample (already covered with gold spheres) on a Linkam heating unit which is specially designed and mounted on the AFM imaging stage. Therefore, when gold sphere embedding proceeds the AFM imaging can be carried out at the same time. In addition, given that the ambient temperature in our AFM small room is 287.15K, the real temperature for the PS sample surface can not be the same as the setting temperature for the Linkam heating unit; accordingly, the later temperature is usually set higher than the expected PS sample surface temperature. First we set the controlling temperature for the Linkam heating unit as 350.15K, but we found there is too much

noise when doing AFM imaging. Then, we set the heating unit controlling temperature as 340.15K for the real-time *in situ* gold sphere embedding.

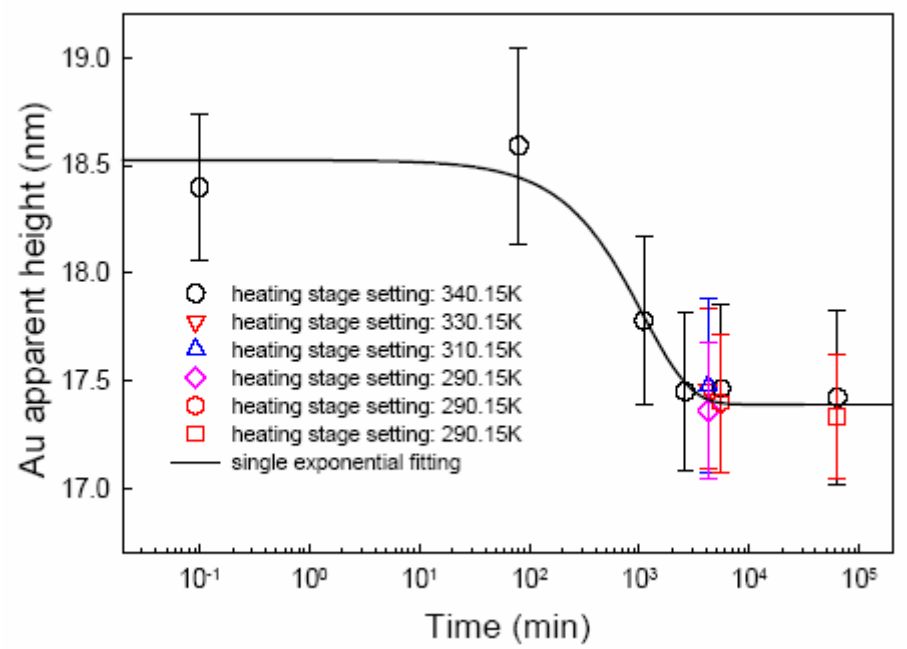

Fig. 5.12 Real-time *in situ* gold sphere embedding results; the solid curve is the result of a single exponential fitting.

The real-time in situ gold sphere embedding results are shown in Fig. 5.12. In the first ~2600 minutes of embedding, we do AFM imaging regularly. After then, to quantitatively check if there is any difference for the measured average gold sphere apparent heights due to the sudden temperature drop as we did for the other ex situ embedding measurements when we take out the PS samples from the high temperature oven to much lower room temperature for AFM imaging, we change the controlling temperature for the Linkam heating unit to lower temperatures, as shown in Fig. 5.12, and then do AFM imaging. We did this kind of AFM imaging at higher temperatures and then at lower temperatures at different embedding times. From the results in Fig. 5.12, we see that there is no difference, within the measurement error, for the measured average gold sphere heights due to sudden temperature drop for AFM imaging. One more thing we should mention is that by comparing the results in Fig. 5.12 with those in Fig. 5.8 we would say that the real PS sample surface temperature during the real time in situ gold sphere embedding measurements is around 328K while the

controlling temperature for Linkam heating unit is set as 340.15K and the ambient temperature in the AFM imaging room is 287.15K.

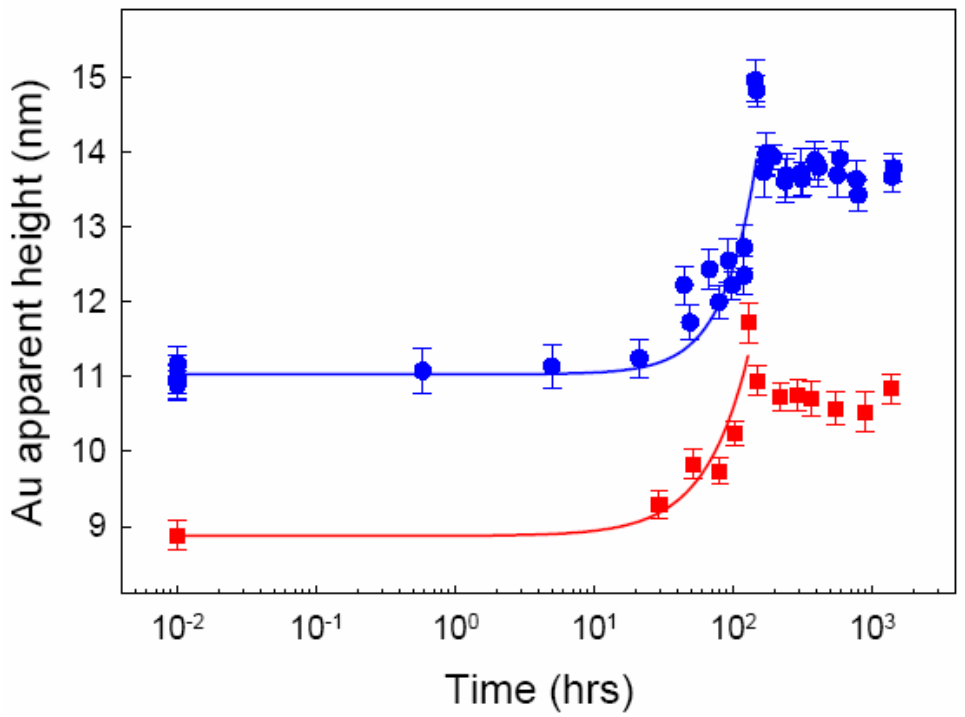

Fig. 5.13 Reversible gold sphere embedding in the region of ~5.5-~8.8nm from the vacuum/polymer interface of 100nm thick 641.0k PS films: every data point stands for the average gold apparent height of more than 100 gold spheres; 3 samples embedding at 370.15K (blue circles); one sample embedding at 371.65K (red squares); after embedding, the samples are kept at 287.15K for measurements.

Given that the compressed exponential, with exponent index β of value 3, is necessary to fit gold sphere embedding data for the region of ~5.5-~8.8nm from the vacuum/polymer interface, we conducted detailed measurements at two embedding temperatures(370.15K and 371.65K) to check if the embedding is reversible or not. To do this, first we embed the gold spheres into the 100nm thick 641.0k PS films to some depth around 10nm and then the samples are kept at 287.15K for AFM imaging to measure the average gold sphere heights at some time intervals. Fig. 5.13 shows the measurement results. Blue circles represent the results of three samples with an embedding temperature of 370.15K and red squares are results of one sample embedded at 371.65K. It is

remarkable that after being embedded at higher temperatures the gold spheres do bounce back at lower temperatures, and after overshooting are stabilized at a certain level. We need to stress that this surprising reversible elastic effects are observed for four samples and the overshooting effects are reproducible. In addition, after more than 1300 hours of measurements, the gold spheres seem being stabilized. In addition, more quantitative analysis reveals some new interesting features. In Fig. 5.13, the solid curves are compressed exponential fitting to the data before overshooting, with compressing exponent β of value of 1.8 (upper blue curve) and 1.4 (lower red curve) and characteristic bouncing time τ_b of value of 104.7075 hours (upper blue curve) and 87.1289 hours (lower red curve). These characteristic values are in contrast with the results of the embedding measurements (specifically showing in Fig. 5.10 as downward and upward triangles): compressing exponent $\beta = 3$ and characteristic embedding time $\tau = 16.8811$ hours and 10.9673 hours respectively. It is noteworthy that the lower temperature characteristic bouncing times increase with a factor of ~7 compared with the higher temperature embedding times in the cases studied with a temperature drop ~ 84K from bulk T_g. We can see that there is a very weak temperature dependence for dynamics in regions ~5.5-~8.8nm deep in thin PS films, which is in stark contrast with those in bulk polymer materials where the characteristic relaxation time diverges at a temperature ~50K below bulk T_g.

From the results of both measurements shown in Fig. 5.10 and Fig. 5.13, it is observed that there is an unexpected elastic effect in the region ~5.5-~8.8nm deep in thin PS films. However, from the results shown in Fig. 5.12 and Table 2, such elastic effect is not observed in the region of the first ~5.5nm and the region beyond ~8.8nm in thin PS films. As mentioned before, we are not sure if the compressed exponential relaxation or the elastic phenomena in this sub-surface layer comes from some potential intrinsic structural properties in this region or not.

5.7 Nano gold sphere size dependence of the embedding in PS films

In the aforementioned sections, we use nano gold spheres of size ~19nm for the embedding measurements. In [161], it is shown that the embedding driving force is ~1nN and when the nano gold

spheres are embedded in the PS film surfaces for more than 0.2nm the embedding stress is less than the polystyrene yield stress of 88.5 MPa measured at 298 K. Another method to check if there is any effect of nano gold spheres on the near free surface dynamical properties of thin polymer films is to use nano spheres of different sizes for embedding and compare the resulting observations. In this study, we tried more embedding measurements using three nano gold sphere sizes. The results are shown in Fig. 5.14. We notice that for the embedding measurements using the two smaller nano gold spheres of average size of ~16nm and 19nm, three-step decay behavior is observed, and for the ~30nm nano gold sphere embedding results two-step decay is observed within the measurement time window. For the first and second embedding decays in all three cases the data are exponentially fitted with exponent index $\beta = 1$ and 3 respectively (shown as the solid fitting curves in Fig. 5.14). The inset shows the corresponding characteristic relaxation times for the first two embedding relaxation decays. We note that the linear fitting can be applied to the characteristic relaxation times, which means that the embedding relaxation times linearly dependent on the nano gold sphere size. From [90, 91], we know that

$$\tau_{measure} = \tau_{\alpha}(1 + \frac{RG_0}{2\gamma}), \tag{5.8}$$

where $\tau_{measure}$ is the characteristic relaxation time for polymer surface features, τ_{α} is the chain segment alpha relaxation time, R is the radius of curvature of the polymer surface feature, G_0 is the polymer glassy modulus, and γ if the polymer surface tension. In Eq. 5.8 the characteristic relaxation time $\tau_{measure}$ is linearly dependent on the radius of curvature of the polymer surface features. If we use Eq. 5.8 to fit the data in the inset of Fig. 5.14, we can obtain the characteristic segmental relaxation times from the slops of the linear fitted lines to be 1.6s and 45.6s for the surface layer (corresponding to the first decay) and the sub-surface layer(corresponding to the second decay) respectively. If we assume the alpha relaxation time around bulk T_g to be 100s[4,55], then we can, by means of the WFL equation, estimate a temperature of ~6K above T_g at which the molecular relaxation time is around 1.6s. Therefore, we can say that while the bulk materials in the thin polymer films are in the glass transition zone the surface region behaves as if it is at a temperature of ~6K above T_g, and the dynamics is these two regions are heterogeneous. Another conclusion we can draw

from Fig. 5.14 is that the sizes for the surface layer and the sub-surface layer of thin PS films have no nano gold sphere size dependence, which means that the nano gold spheres used for the embedding measurements have no or negligible effect on the dynamical properties of the near free surface region of thin polymer films.

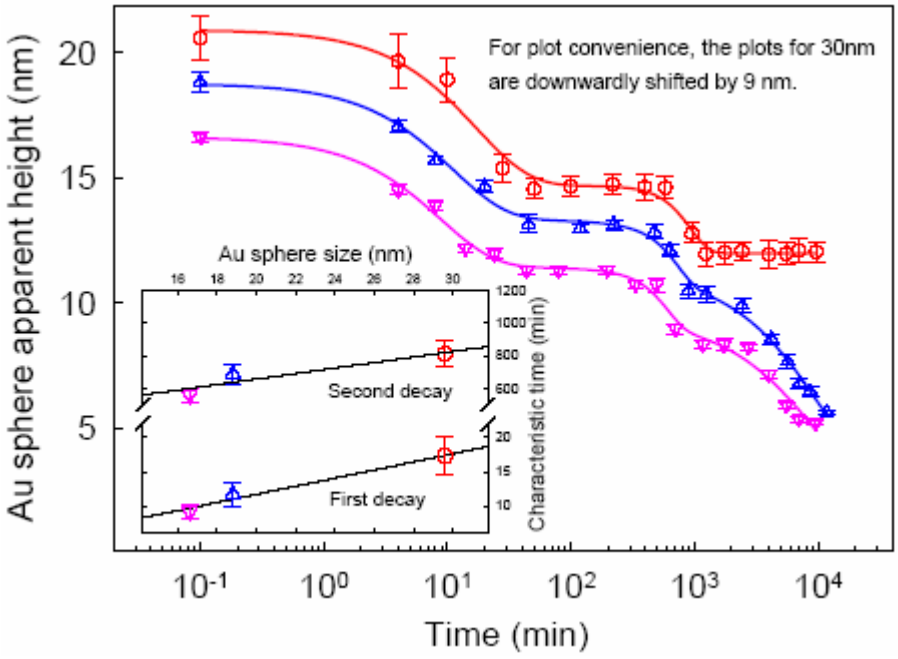

Fig. 5.14 Nano gold sphere size dependence of embedding at 371.7K; for plot convenience the data for the 30nm gold sphere embedding are downwardly shifted by 9nm; the solid curves are multiple exponential fitting to different data sets with exponent index $\beta = 1$ and 3 for the first and the second decay; the inset shows the characteristic relaxation times for the three cases of embedding measurements.

5.8 Conclusions

In this study, we probed the near free surface dynamical properties of thin polystyrene films with the nano gold sphere embedding technique. Within the wide time and temperature measurement windows some interesting observations are found by this simple but powerful technique, which has the smallest probing perturbations to polymer samples among solid-contact surface probing techniques. *For the*

first time, we quantitatively show the evolution of the thin polystyrene films from the melt state to the complete glassy state with the nanometer resolution. In the melt state, the thin polystyrene films are dynamically homogeneous; at temperatures around bulk glass transition temperature T_g on-average dynamical heterogeneity can be observed; at temperatures ~83K below bulk T_g the samples are observed to be on-average dynamical homogeneous again in the complete glassy state(please note this dynamical homogeneous is different from the microscopically dynamics heterogeneous). In particular, the following dynamical features of the near free surface region of polystyrene films are observed.

1. It is found that there is a liquid surface layer in glassy thin polystyrene films and the liquid surface size decreases with decreasing temperature, which is in agreement with some surface models. This finding may raise new questions in the glass studying academia: since the temperature dependence of liquid surface size is different from that of the CRR regions, what kind of characteristic length scale researchers should look for, or what kind of characteristic length scale is more related to the glass transition phenomena, for nanometer scale confined glass forming materials?

2. In this work, the depth dependence of dynamics or relaxation *with the nanometer resolution* is observed in glassy polystyrene films. In addition, the practical (with the smallest well known solid contacts) complete glassy state is first observed in this work: at temperatures below ~287K the PS films are too hard/glassy for nano Au particles to be embedded further into the samples.

3. The region of enhanced dynamics in thin polymer films is observed to be ~10nm (including the surface layer and the sub-surface layer), which is smaller than that of ~35nm observed using the fluorescence technique.

4. In the near free surface region of thin polymer films the time-temperature superposition principle does not hold since both stretched and compressed exponential relaxations are observed at temperatures around and below T_g. For the surface layer region, the exponent index β is ~1, for the sub-surface layer, β is ~3, and for the bulk material region β is 1 again

5. The dynamics gradient for the near free surfaced region (including the surface layer and the sub-surface layer region) is not smooth and the heterogeneous dynamics are observed, which is in contrast to the finding in [66], in which when polymer films are thinner than ~25nm the dynamics are homogeneous.

6. It is observed that the nano gold sphere embedding is reversible in the sub-surface layer region and irreversible in the surface layer region and the bulk material region. At present, there is no substantial evidence to distinguish whether this elastic effect in the sub-surface layer region is the consequence of the intrinsic structural property of glass forming materials or due to build- in stress during nano gold sphere embedding. No matter what type of mechanism contributes to this phenomena, the reversible effect in the near free surface region of polymer films has some potential applications in nanotechnology in the future.

7. The molecular weight dependence in the near free surface region of thin polystyrene films is different from that of the i-PMMA work in [91]— in the deep glassy state no molecular weight dependence is observed in the present study, which may indicate that there might be some potential structural difference in the near free surface regions of i-PMMA and PS films.

Chapter 6
Polarization noise measurements of thin polymer films

In chapter 3, we described the home-built low level noise measurement system. To test the performance of the noise detecting system, we did some measurements with different input signals/devices to check the corresponding measured results. In graph a) of Fig. 6.1, we see that when the Lock-in amplifier input (the first-stage signal amplifying unit) connectors are connected with a commercial resistor, in the corresponding power spectral density curve which is the average of 200 consecutive spectra, the $1/f$ noise can be seen when the frequency is lower than around 2-3 Hz, beyond which the white noise is observed, which is due to the thermal fluctuation of charge carriers in the resistor. The source noise in reference [231] is similar with that of our system. Two commercial capacitors were also tested by our noise measurement system; both of the corresponding spectral curves were typical for capacitors [232]. From the results of the test measurements, we also see that there are some interference peaks with frequency higher than 10 Hz although we have done something to screen the environmental electromagnetic fields such as the application of coaxial cables, vibration isolation bench units and metallic shielding boxes. It seems that more critical shielding factors should be considered, such as putting the whole measurement system in an electromagnetic field shielding room, if we conduct some studies with interesting dominant dynamics in a higher frequency range.

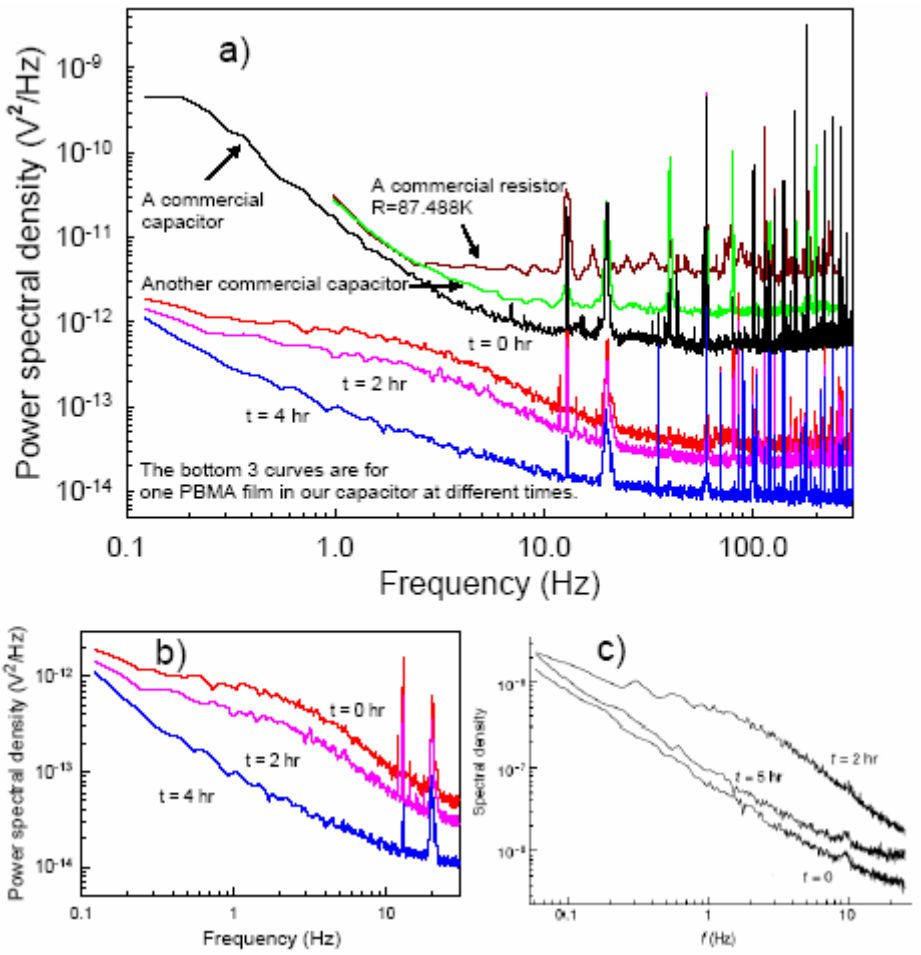

Fig. 6.1 Some preliminary measurement results of the home-built low level noise detecting system: a) is for different input signals; the comparison between our results (b) and results(c) in of Ref. [233].

Results for Poly(n-butyl methacrylate)(PBMA) films

The PBMA films are spin-coated onto one hand-polished round steel plate (see chapter 3) from the solution of Poly(n-butyl methacrylate) ($M_n = 173.9k$, $M_w = 182.6k$, $r_{PDI} = 1.05$; Polymer Source, Inc.) in toluene, which are then annealed at $55^o C$ for ~6 hours. The as-prepared PBMA film is ~40nm thick (determined by AFM) and its glass transition temperature T_g is $31.2^o C$ determined by Ellipsometry(Exacta 2000 self-nulling ellipsometer; Waterloo Digitlal Electronics).

In Fig. 6.1, graph b) shows the results of the power spectral density curves of the thin PBMA film measured by our low level noise measurement system. The polymer film is put in the steel-plate

based capacitor. The experiment is conducted at 293K and the data are collected at night till early morning. It is remarkable that our results are very similar with those of reference [233] (see the above graph c)). In [233], an AFM-tip based capacitor is used to measure the polarization noise of $\sim 1 \mu m$ thick poly-vinyl-acetate (PVAc) films and the characteristic spectral knee in graph c) is associated to heterogeneous molecular dynamics of PVAc near the glass transition. The results in graph b) are obtained using the "geometry 1 capacitor" (see the technique chapter 3) and the surface roughness of the capacitor electrode steel plate is ~50nm. Therefore, it is not suitable to be used for ultra-thin polymer film studies. We tried capacitors with ultra-flat electrodes for more studies.

Results for PVAc films

We use the silicon-wafer based capacitors to measure the polarization noise of Poly Vinyl Acetate (PVAc) films ($M_n = 145k$, $M_w = 217k$, $M_w / M_n = 1.5$; Polymer Source, Inc; $T_g \sim 302 - 308K$ [234, 235, 236]). As described in the technique chapter 3, the ultra-flat aluminum coating layer on the silicon wafers is 1.2nm in roughness and ~100nm in thickness (determined by AFM). To our knowledge, there are very few studies using ultra-flat parallel plate capacitors to investigate dynamical properties of thin polymer films [237]. Fig. 6.2 shows the power spectral density of consecutive 40 hours of one PVAc film. After spin-coating PVAc solution in toluene onto the silicon based capacitor electrodes, the as-produced films are annealed at $333K$ for ~16 hours. The details about the polarization noise measurements can be found in the technique chapter 3. From Fig. 6.2 we see that the power spectral density of the PVAc film fluctuates with time. Although these PSD curves mainly peaked and fluctuated around 5 ± 1Hz, the fluctuations occurred at the other frequencies as well. Therefore, we integrate the specific PSD curves and compare the integrated PSD shown in the inset. The similar analysis technique is used in [238]. It is interesting that the integrated PSD of the PVAc film fluctuates around a certain level. Equally remarkable is that after some time period there are relatively big jumps in the integrated PSD's. In [233], the probing area is of ~50nm scale and the characteristic spectral feature in the PSD curve can only be observed sporadically. According to [233], in the thermal polarization noise measurements, the thermal noises dominate in the low frequency regime, but at higher frequency the spectral feature like that in Fig. 6.1 (c) can be observed, which is related to cooperatively rearranging motions of molecules. In our measurements, the PVAc film is 14mm in diameter and ~50nm in thickness. Considering that the size of the cooperative rearranging regions in glassy polymers is 2-5nm around T_g and ~10nm at the

measurement temperature ~10K below bulk T_g [234], in our samples studied there must be a large number of such mobile regions which work as fluctuators. From Fig. 6.2 we see that the dominate molecular relaxation frequency is around 5 Hz. The relatively big jumps in the inset may indicate the merging of some slow CRR regions since the cooperative rearranging dynamics are both temporal and spatial evolving [233]. Fig. 6.3 shows the polarization noise measurement results for a thinner PVAc film (~30nm in thickness). It seems both the amplitude and the fluctuation of the polarization noise of the thinner film are larger than those of the thicker film. Quantitatively, from the insets of both figures we can get the average PSD integrated area and the corresponding standard deviation of $30.68\times10^{-12}V^2$ and $15.85\times10^{-12}V^2$ for the thicker PVAc film, and $142.47\times10^{-12}V^2$ and $72.68\times10^{-12}V^2$ for the thinner film respectively. This finding is interesting in that the thinner film seems have more thermal energy, but with almost the same dominate cooperative rearranging relaxation rate ~5Hz, which means that there are more mobile CRR's or fluctuators in the thinner film and no appreciable frequency shift can be experimentally measured. In [237, 239], no dependence of microscopic relaxation time on PVAc film thickness is observed either. Unfortunately, we could not get the structural α relaxation time corresponding to the measurement temperature in our present investigation from [237], in which we found that the relaxation times of the PVAc films as a function of temperatures (Fig. 5 of [237]) are obtained with a probing frequency of 120Hz indicated in Fig. 3 of [237]. To check the effects of the number of mobile CRR's or fluctuators on the measured PSD data, we measured the thermal fluctuation polarization noise of 100nm PVAc film without the free surface. We prepared this kind of sample in the following way: First, we prepare two samples on two silicon based capacitor electrodes using the same method of making the 50nm samples; such two samples are annealed at 333K for 3 hours and then are put together with PVAc films face to face to be annealed at 333K for 5.5 more hours. The measurement results for this kind of thick PVAc film without the free surface are shown in Fig. 6.4, from which we note that the dominate relaxation rate is still around 5 Hz. However, compared the data in Fig. 6.2, both the PSD peak amplitude and fluctuations of the data of the 100nm PVAc film are larger. From the inset, we see that the average and standard deviation of the integrated PSD are $161.86\times10^{-12}V^2$ and $63.07\times10^{-12}V^2$ respectively.

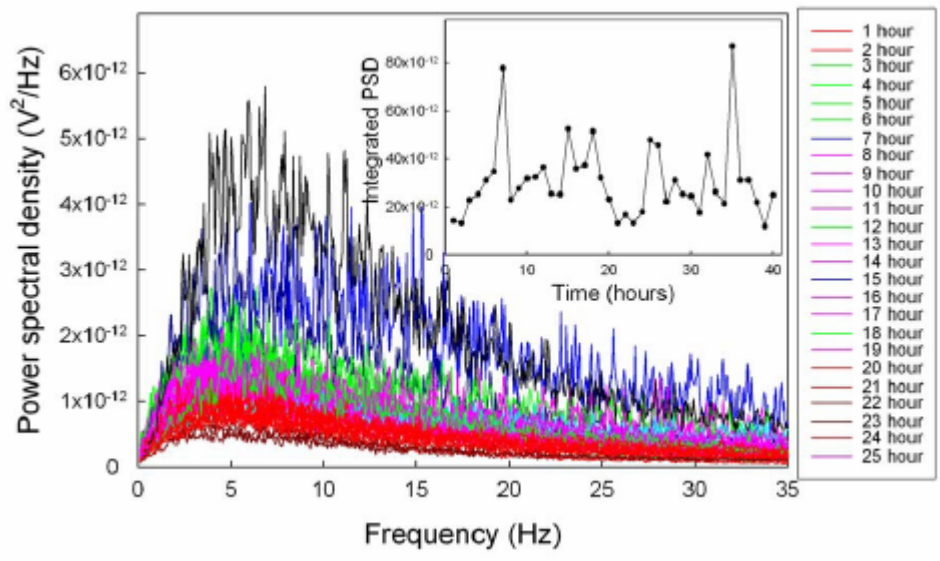

Fig. 6.2 Power spectral density of consecutive 40 hours of 50nm PVAc film; the legend only shows 25 cases due to the limitation of the SigmaPlot software; the inset shows integrated PSD data as a function of successive times.

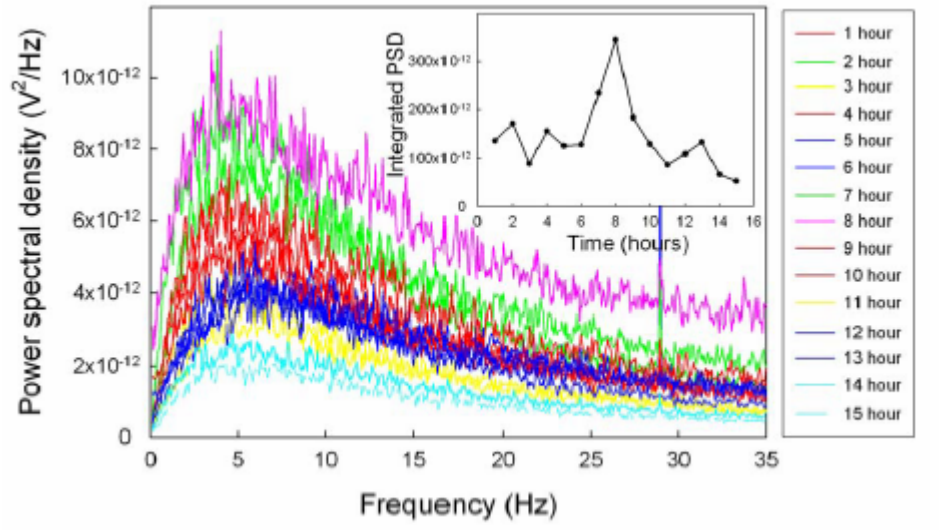

Fig. 6.3 Power spectral density of consecutive 15 hours of 30nm PVAc film; the inset shows integrated PSD data as a function of successive times.

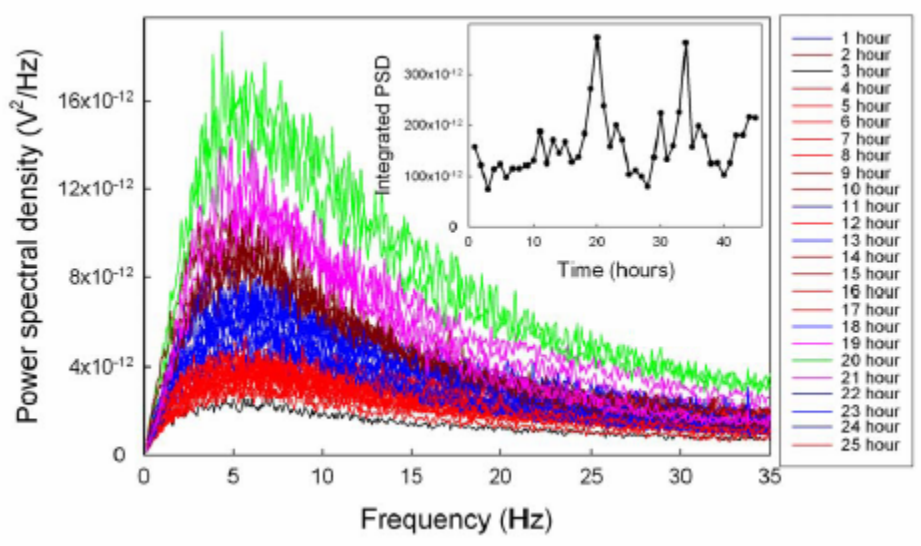

Fig. 6.4 Power spectral density of consecutive 45 hours of 100nm PVAc film without free surface; the legend only shows 25 cases due to the limitation of the SigmaPlot software; the inset shows integrated PSD data as a function of successive times.

By comparing the data in Fig. 6.2 and Fig. 6.4, we see that for thicker films both the average integrated PSD area (energy) and the standard deviation are larger than thinner films, which may indicates that in the thicker films there more fluctuating CRR's working as fluctuators. For very thin PVAc films with one free surface(data shown in Fig. 6.3), more CRR's or fluctuators are observed because the enhanced mobilities in the near free surface regions may produce more CRR's in the underneath bulk material part.

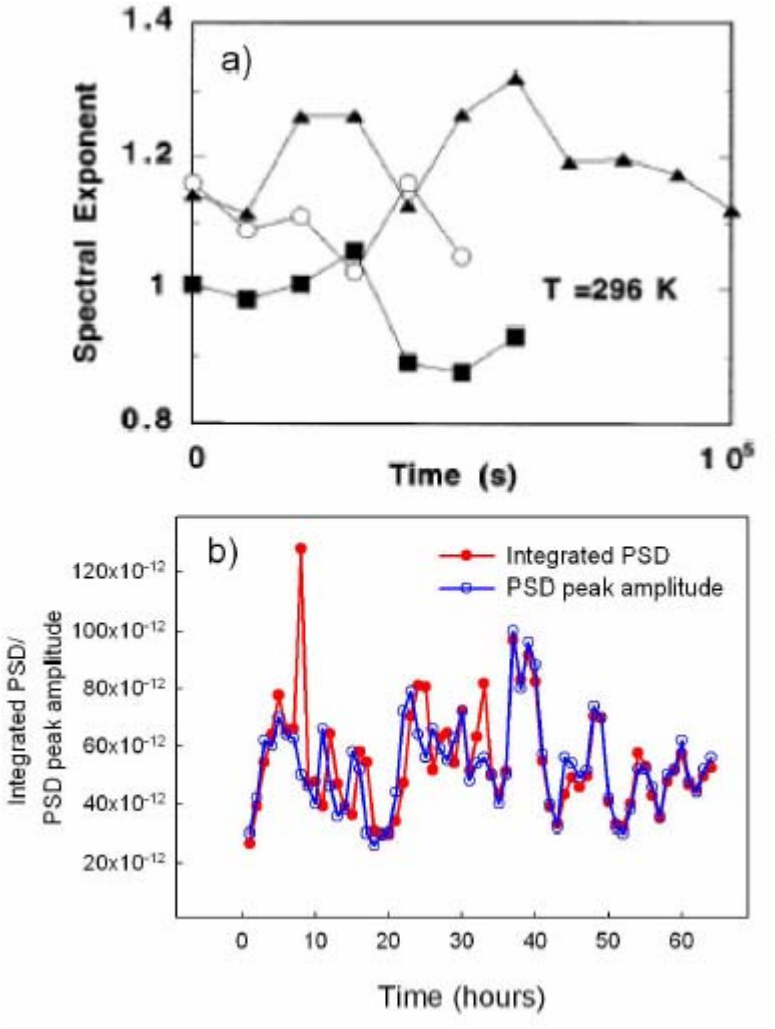

Fig. 6.5 Variations of PSD data in the present study and those in [234].

The relative big jumps in the integrated PSD data are interesting. If we focus only on the PSD peak amplitude in data analysis, it is hard to observe such features. Fig. 6.5 shows the comparison of variations of PSD data obtained from successive measurements for similar systems. The graph a) is the results of [234], in which an AFM tip based noncontact capacitance measurement technique is used to study heterogeneous dynamics in nanometer scaled PVAc films. We see from this graph that the thermal fluctuation noise exponent varies or evolves with successive measurement times but no systematic trend is observed. Graph b) of Fig. 6.5 shows our present results within the similar long time window of a time scale of more than 10^5 s. The hollow circles show the variation of the amplitude of the PSD peak, from which we see these PSD peaks fluctuate with time. The filled circles

show the integrated area underneath the successive PSD curves. Please note, the hollow circle data are multiplied by 40 in order to be compared with the filled circle data. It is remarkable that in the integrated PSD data there are some big jumps (also shown in Fig. 6.2, Fig. 6.3 and Fig. 6.4), which is in contrast to the non-feature thermal noise fluctuation PSD data in both the present study and that of [234]. The relatively big jumps in the integrated PSD data may indicate some potential merging event of some CRR regions in the samples studied.

In summary, we built a low level noise measurement system to measure the polarization noise in thin polymer films. We use the pre-amplifying stage of a lock-in amplifier, which has the very low voltage noise and very high input impedance, for the first stage amplifying unit, and use a precision low offset voltage operational amplifier for the second-stage voltage amplifying unit, which has a high amplifying gain, low offset voltage and ultra low input bias current. To study the thermal polarization noise of thin polymer films, we designed capacitor electrodes of ultra-flat electronically conductive metal coatings with the surface roughness ~1.2nm. To our knowledge, there are very few measurements have been conducted measuring noise or dielectric properties of ultra-thin polymer films sitting on ultra-flat electric-conductive capacitor electrodes [237]. Conventionally, in dielectric spectroscopic measurements the electrodes used are polished metal plates which have relatively high surface roughness.

We observe heterogeneous dynamics in thin glassy polymer films by means of the home-built low level noise measurement system. No discernable relaxation rate shift is observed with decreasing polymer film thickness down to around 30nm, which is consistent with the findings in [237, 239]. However, for thinner films we observe relatively higher thermal fluctuation energy which is suggested to result from the increasing number of cooperative rearranging regions in thinner polymer films. This mechanism provide a possible solution to the issue that in some dielectric spectroscopic measurements there might be no microscopic relaxation rate shifts for ultra-thin polymer films while in some macroscopic thermal or mechanical measurements the T_g deviation or dependence of film thickness can still be observed.

Since we have built a low-level noise measurement system, the next interesting work may be to study the temperature dependence of the polarization noise in ultra-thin polymers by means of this system. To do this, a big challenge will be to control the sample temperature without introducing electric or

vibration noise to the sample. It is hard to realize this because normal sample temperature controlling in labs are carried out by means of electronic resistors or flowing thermal baths, of which the electronic or vibration noises are not negligible especially for low level polarization noise measurements.

Chapter 7

Nano rheology measurements of thin polymer films

In the previous chapters, it is shown that there is much evidence indicating enhanced dynamics in the near free surface region of thin polymer films. However, this is not the only picture about thin polymer film studies. In [94], Ge *et al* measured the glass transition temperatures of the near free surface of thin polymer films by means of the shear modulation force microscopy technique and found no T_g deviation for the surface region compared with that of bulk polymers. Considering the high shear modulation frequency of 1400 Hz applied in [94], the findings may be questionable because some studies [24] shows that abnormal dynamics can not be observed with techniques of probing frequency higher than ~1Hz. Therefore, similar studies with much lower probing frequency may be helpful in resolving such controversy. In this project, we investigate the near free surface dynamics of polymer films using a novel nano rheology technique.

The schematic representation of the operation principle of the technique we used is shown in Fig. 7.1. When the AFM tip is in contact with the sample surface, a suitable lateral displacement is applied to the rear end of the AFM cantilever, which can twist without slide, and the relaxation of the local polymer sample surface area surrounding the tip can be studied by measuring the left-minus-right (L-R) signal of the quadrant photodiode detector (refer to Fig. 3.13 of Chapter 3 for the AFM optical detecting scheme). The major point of this technique is that a transient torsional force is applied to the local surface region of the polymer sample and the subsequent sample relaxation is measured within

the time domain, which is different from the dynamic AFM technique working with the torsional tip mode [94, 240, 241]. In addition, there is a compromise requirement for the cantilever spring constant in the dynamic AFM torsion mode techniques: on the one hand, to improve measurement sensitivity AFM cantilevers with low spring constant are more suitable; on the other hand, the lateral dithering cantilever/tips around the resonance frequency can produce too much noise if the cantilever spring constant is too low. In the technique of the present study, the AFM cantilever/tip with much lower spring constant can be used since no resonant cantilever/tip vibration is involved and accordingly the measurement sensitivity is very high.

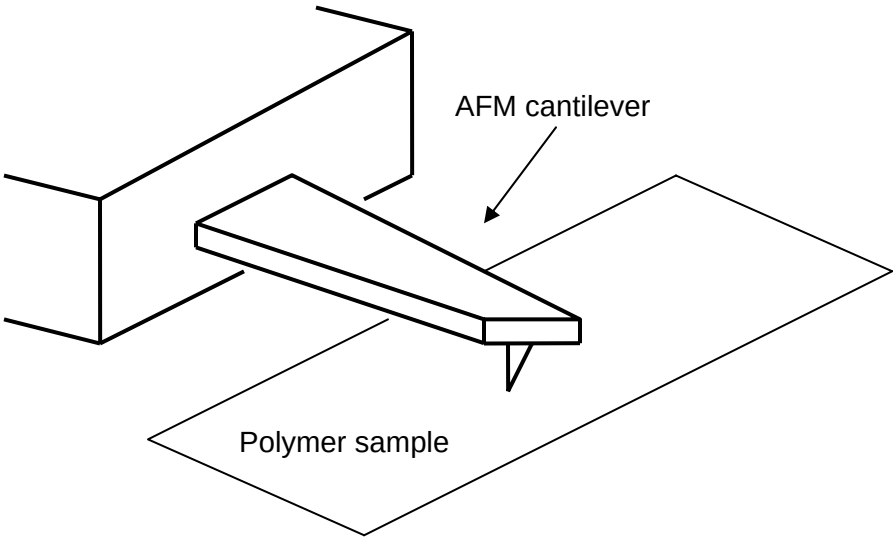

Fig. 7.1 Schematic representation of the operation principle of the nano rheology AFM technique.

The AFM tips used in this study are purchased from the Veeco company. The tip characteristics are: contact mode MPP-32100-50; cantilever thickness: 1.5-2.5 μm; cantilever length: 515-535 μm; cantilever width: 25-35 μm; resonance frequency: 11-14 kHz; spring constant: 0.1N/m; tip radius: 10nm; tip height: 15-20 μm. The procedure of the operation of the present nano rheology technique is as follows:

(1) The AFM works in the contact mode. After the AFM system is tuned in feedback, the tip is moved to position (X, Y) and stays at this position for 60 seconds to stabilize the AFM tip/cantilever.

(2) To etch the AFM tip into the sample surface following this procedure: the AFM feedback controlling system is turned off; the tip/cantilever is raised by 46nm above the sample surface and stabilized for 40 seconds; the tip/cantilever is lowered by 46nm and stabilized for 30 seconds (the tip just touches the sample at this point as normal contact mode operation); the tip/cantilever is lowered further by a distance less than 10nm and stabilized for 30 seconds.
(3) A lateral displacement ΔX is applied to the rear end of the AFM cantilever with a suitable moving rate, which results in twisting of the cantilever without sliding because the very end of the cantilever is fixed with the AFM tip being etched in the sample surface (see Fig. 7.1).

(4) The local sample surface region contacting with the AFM tip is deformed/strained on the nanometer scale due to the torsional force applied by the twisted cantilever. The corresponding retardation response in the local nano-strained sample region can be studied by measuring the time dependent variation of the L-R signal of the quadrant photodiode.

(5) After data recording, the AFM tip is retracted from the sample surface, the previous feedback system is restored, and the AFM tip is moved back to the original position.

(6) To do more measurements the above procedure is repeated but different areas are probed.
All the above steps are carried out by means of a controlling program written in the Microsoft Visual Basic language (see appendix for the program).

We tried different measurements on polyisoprene (PI) and PVAc films using the aforementioned nano rheology technique to obtain optimum measurement controlling parameters. All polymer films are prepared by spin-coating solutions in toluene onto silicon wafers and well annealed at a temperature of ~30K above bulk T_g for at least 8 hours. The film thickness is chosen to be larger than 100nm because if very thin polymer films are studied the potential AFM tip-substrate interactions may involve complex data interpretations.

Fig. 7.2 shows some typical relaxation results for PI and PVAc films. Considering the fact that the cantilever length is ~515-535 μm and the AFM tip height is ~15-20 μm and the cantilever spring constant is very low(0.1N/m), small lateral displacement ΔX at the rear end of the cantilever can

only produce weak variation in the AFM L-R signal, which can be seen in Fig. 7.2. In particular, for the case of PI samples the L-R signal variation is ~ 10% for the 5nm cantilever rear end displacement while that for the 100nm displacement is ~300%; for the case of PVAc film, the L-R signal variation is ~ 30% if the applied cantilever rear end displacement is 60nm. Original or final L-R signals before or after sample surface deformations vary from case to case because the laser alignment or the tip state after being etched in the sample surface may be different among different measurements. In the present work, dynamical properties of polymer film surfaces are obtained by studying the relative variation of L-R signals as a function of time and temperature. One should note that the present method to produce AFM tip/cantilever tosional motion is different from those methods applied in [94, 240, 241], where the oscillating driving electric signal is applied to the AFM piezo to let the AFM tip dither with the cantilever resonance frequency and no lateral cantilever displacement is involved. In the present nano rheology technique we take advantage of the low spring constant(0.1N/m) long AFM cantilever ($>515\mu m$) and tip ($>15\mu m$). If the cantilever rear end lateral displacement is 100nm, the deformation of the local sample surface area surrounding the AFM tip is less than a few nanometers because the long cantilever is both deflected along the X direction and twisted along the Y direction. Moreover, to avoid tip-sample slippage a tip moving rate of 100nm/s is applied for all measurements and no apparent sample surface scratch is found after nano rheology measurements.

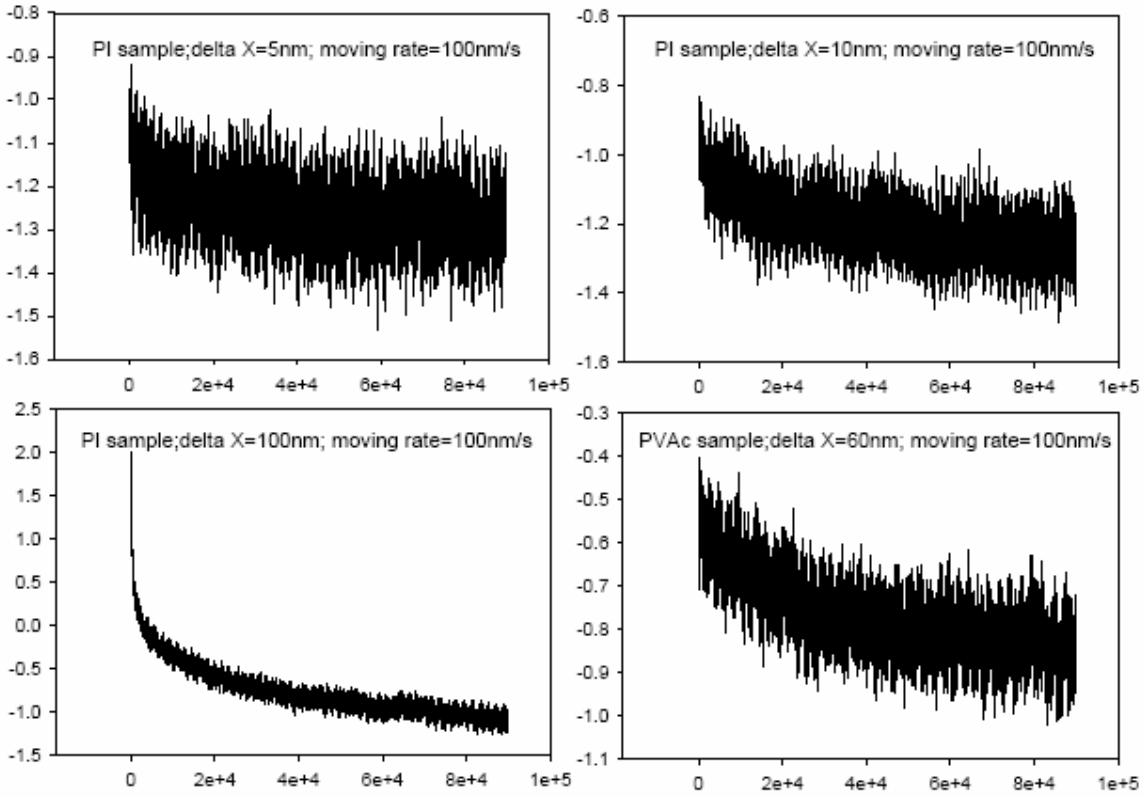

Fig. 7.2 Typical relaxation results for PI and PVAc films using different cantilever rear end displacements; the vertical axis is the AFM L-R signal in ADC units, and the horizontal axis is time in milliseconds.

To study the surface dynamics as a function of temperatures, we conducted measurements for PVAc films at different temperatures. The polymer samples are positioned on the AFM stage and the sample temperature is controlled by a Linkam hot stage (Linkam Scientific Instrument Ltd, UK; temperature controlling precision: $0.1^{\circ}C$), which is covered with a plastic box. In addition, we tried different vertical load forces applied to the AFM tip and almost no load dependence is observed within the load range tried. All data can be fitted with an exponential function $y_0 + a\exp(-bx)$; if the stretched exponential function $y_0 + a\exp[-(bx)^{\beta}]$ is used, the exponential index β within the range of 0.8-1 is suitable to do data fitting. Fig. 7.3 shows some typical data for PVAc surface relaxations at different temperatures using two vertical tip loads. It can be seen that the L-R signals for lower measurement temperatures exponentially decay slowly and those for higher measurement

temperatures decay faster, which reflects different microscopic chain segment motions at different temperatures. Every data set is obtained by probing different virgin areas of the sample surfaces.

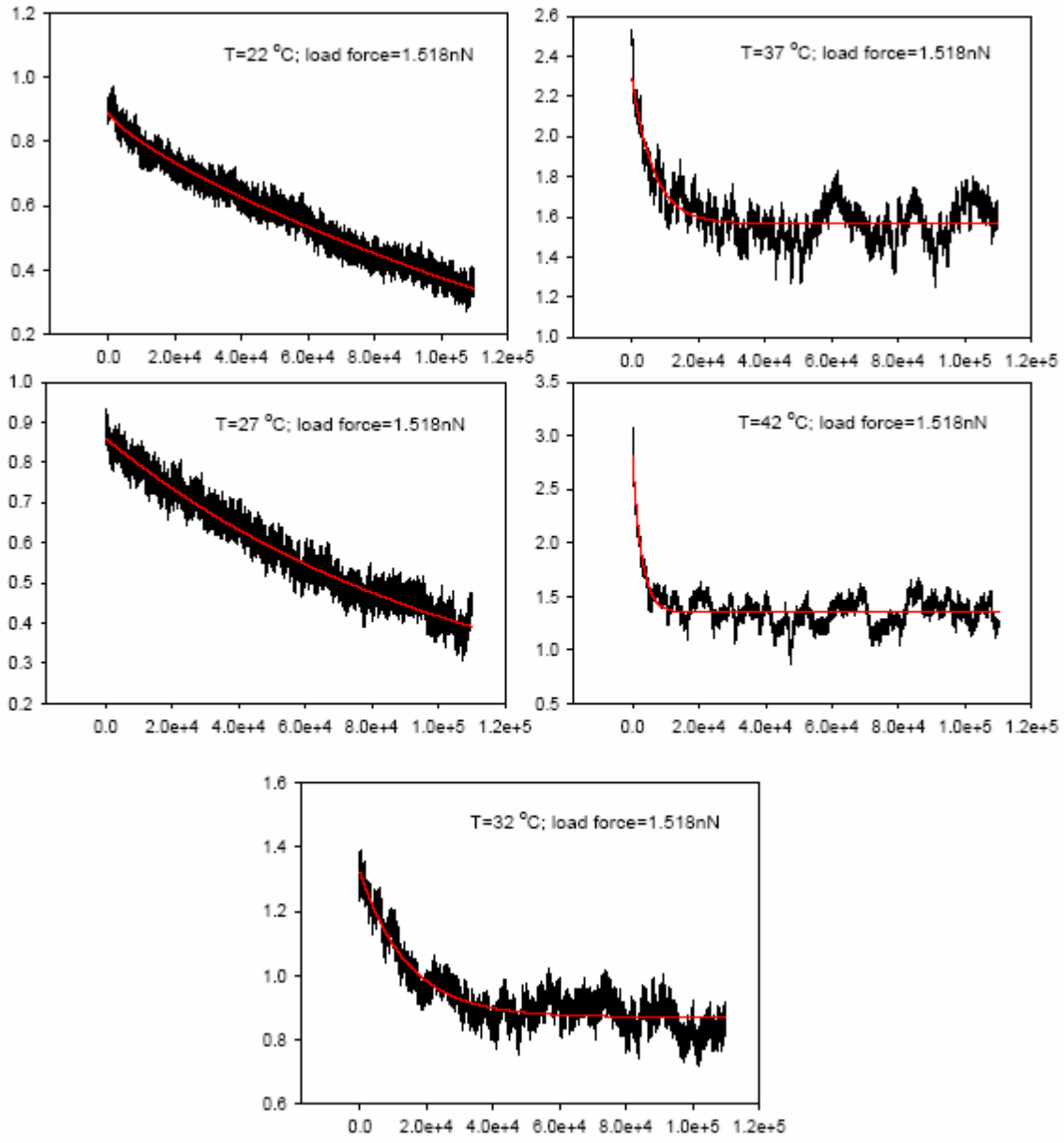

Fig. 7.3a Typical data for PVAc surface relaxations at different temperatures using vertical tip load=1.518nN: the vertical axis is the AFM L-R signal in ADC units, and the horizontal axis is time in milliseconds; the thin red curves are exponential fitting to the raw data.

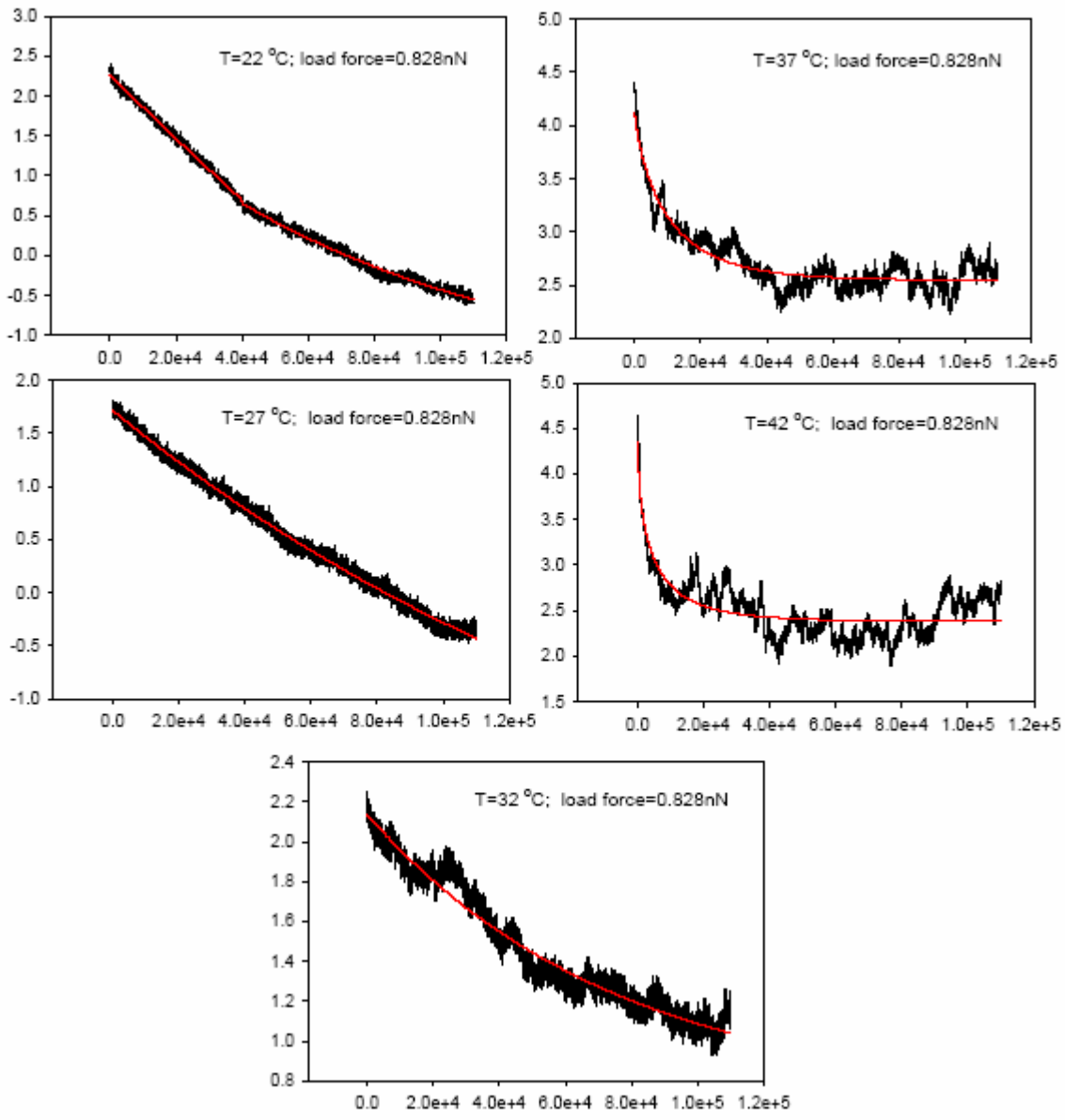

Fig. 7.3b Typical data for PVAc surface relaxations at different temperatures using vertical tip load=0.828nN: the vertical axis is the AFM L-R signal in ADC units, and the horizontal axis is time in milliseconds; the thin red curves are exponential fitting to the raw data.

From the data fittings for all measurements we obtain the characteristic relaxation times at different temperatures, which are shown in Fig. 7.4. The data points (circles) represent local surface characteristic relaxation times of PVAc films in the present study. Two vertical loading forces of

0.828nN and 1.518nN are applied to the AFM tips and the corresponding results of the local surface characteristic relaxation times are indistinguishable. In Fig. 7.4, the solid curve and filled circles are for data of bulk PVAc from [242], which are downwardly shifted by 1.1. The data in [242] is obtained by the dielectric spectroscopy technique while in the present study we use the mechanical retardation technique (on nanometer scale) to obtain the characteristic polymer surface relaxation times. Generally, there is a scaling factor for characteristic times obtained by different techniques [4,242]. Therefore, the shift to the data of [242] to be compared with the present results is reasonable, which can be proved by the fact that the data points (triangles in Fig. 7.4) from [243] are in agreement with the as-shifted "bulk" data from [242]. In [243] another novel nano rheology technique is used to measure properties of PVAc(of similar molecular weight with the present study) films and bulk like properties(triangles in Fig. 7.4) are observed for films of original thickness of 47nm. There are a few points one need to pay attention about the comparison between the results of this study and those of [243]: (1) In [243], as mentioned by the authors, the actually measured films have thickness of 27.5nm because the films are pre-strained by ~25% during the annealing treatment; (2) The force applied to the samples is estimated to be of the order of ~1000nN, which is much larger than the forces(several nN's) in the present study; (3) In [243], the measured properties are for the average dynamics of the whole sample films(actually free standing films). In free standing film studies [76, 78] by Forrest and co-workers, it is shown that there must be some regions with bulk properties in thin free standing films. In the present study, we measured the local near free surface properties of substrate supported films (more than 100nm thick).

It is noteworthy that at the temperature of ~9K above bulk T_g the present surface characteristic relaxation time is in agreement with that for bulk PVAc while the surface characteristic relaxation times below this temperature deviate from those for bulk materials and have a weak temperature dependence compared with the later case. The similar polymer surface dynamical feature has also been observed for PS films [90, 244, 245]. These studies show that at temperatures higher than bulk T_g the polymer surface dynamics are approximate to or identical with those of bulk materials, which also indicates homogeneous dynamics in thin polymer films. When temperatures are below bulk T_g the dynamics in thin polymer films are heterogeneous with the surface regions having enhanced molecular motions. The different temperature dependences of dynamics for the near free surface region and the bulk material region of polymer films suggest different mode of molecular motions.

However, different findings are observed for PMMA or i-PMMA films [91, 119], where the surface characteristic relaxation times have similar temperature dependence of bulk materials but with a more than 30K shift along the temperature axis and a local surface T_g may be assigned to the near free surface regions of polymer films. These observations indicate some polymer-specific properties in the near free surface region of thin polymer films.

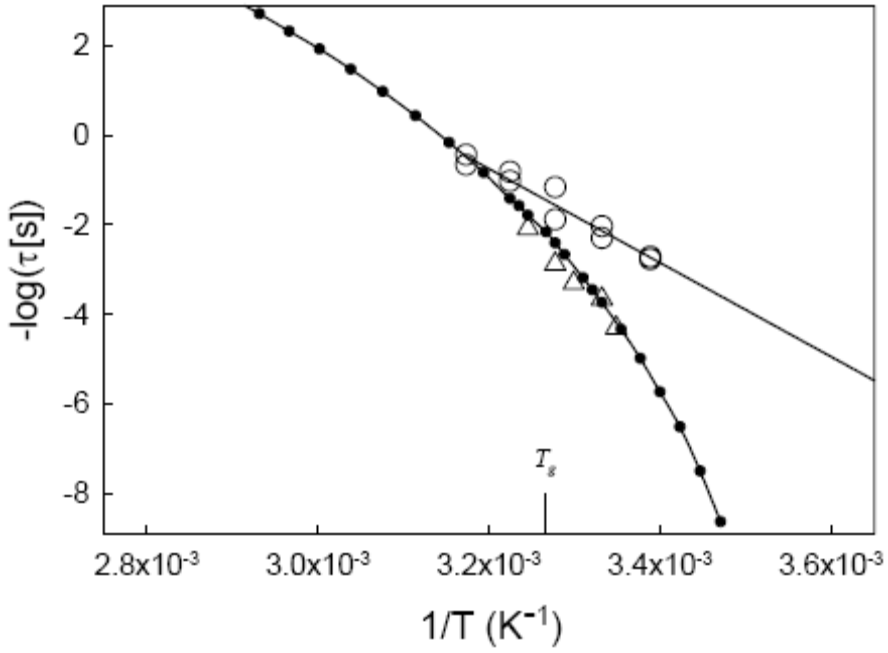

Fig. 7.4 Temperature dependence of characteristic relaxation times for PVAc: data points(circles; standard error being less than the symbol size) are results of the present study with two AFM tip loading forces(0.828nN and 1.518nN); the solid straight line is the linear fitting to the present data points(circles); the small filled circles and the corresponding solid curve are for data from [242], which is downwardly shifted by 1.1; the triangle data points are from[243].

In conclusion, in this study we developed a novel nano rheology AFM technique to study the near free surface dynamics of thin PVAc films. In contrast to most dynamic AFM technique working with the torsional tip mode, the present technique probes the transient retardation response of the local polymer surface region within the time domain. Enhanced dynamics and weak temperature dependence of the near free surface region of PVAc films are observed, which is observed for polystyrene films as well. Some potential molecular motion mode different from that in bulk

materials may be responsible for the observed weak temperature dependence of the near free surface dynamics of thin polymer films. As mentioned in chapter 5, this mechanism may be related to some potential energy landscape basin-hopping motions.

Chapter 8

Concluding remarks and future work

Concluding remarks for work in this study

In this study we focus on researching the near free surface dynamical properties of ultra-thin polymer films using some novel measurement techniques. The major motivation of this project results from the growing consensus that the interfacial properties of nanometer scale polymer systems may play a key role in determining the average dynamical properties of the whole system. In particular, many studies show that near free surface region, as a specific interface, has enhanced molecular mobilities, which is the dominant cause for experimentally observed glass transition temperature anomalies in many nanometer scale polymer systems. However, the study of properties of this specific near free surface region of thin polymer films is very rare due to the limited suitable experimental techniques. In the present studies, we developed some novel polymer surface property measurement techniques by which some interesting polymer thin film near free surface properties are observed.

In the first part of this study, we developed the nano surface hole relaxation technique to investigate the ~2-4 nm near free surface dynamics of i-PMMA films, which is a model system showing a strong substrate dependence. It is shown that the near free surface region of i-PMMA films has enhanced molecular mobilities and a local surface T_g (~40K below bulk T_g) could be assigned to this region. Although it is still not clear why the near free surface region has enhanced molecular mobilities, from the dependence of near free surface dynamics both on film thicknesses and on M_w data of this study, the possible mechanism of the chain confinement effects contributing to the near free surface

dynamics can be excluded. A surprising molecular weight dependence of the near free surface dynamics is observed, which may indicate a substantial amount of 2-D molecules in this region due to the specific properties of i-PMMA chain molecules. In addition, by studying the near free surface dynamics using different substrates, it is shown that substrate effects can propagate into i-PMMA films as far as ~180nm.

The second part of this study focuses on the near free surface dynamics of another polymer model system— polystyrene films, using the simple but powerful nano gold sphere embedding technique. Three sections of measurements are conducted in this work. The work of first section is intrigued by the aforementioned i-PMMA work. We study the chain size dependence of the near free surface dynamics of PS films using four different molecular weights and find that at temperatures above bulk T_g there exists a M_w dependence which can be explained using the Rouse dynamics for melt polymers. However, at a temperature of ~16K below bulk T_g all nano gold embedding data collapse together within the measurement error and no M_w dependence is discernable, which is in contrast to that for i-PMMA films where even at a temperature of ~36K below bulk T_g a M_w dependence of the near free surface dynamics is still observed. This finding indicates that the near free surface properties of thin polymer films are material specific. In the second section of this work, we study the nano gold sphere embedding behavior within a wide temperature and time window, and for the first time the depth dependence of the near free surface dynamics with the nanometer scale resolution is observed. By the embedding-model-free data analysis the results show that when the measurement temperature is above a temperature of ~378K for polystyrene films the whole film average dynamics are homogeneous; when the temperature is below this temperature the average dynamics for the PS films are heterogeneous, which is pronounced in the deep glassy state; when the measurement temperature is below around 287K no gold sphere embedding is observed and the PS films are in the complete practical glassy state— the whole film average dynamics are homogeneous again. It is found that for the first ~5.5nm surface region the dynamics are enhanced compared with those in the bulk material region and the liquid surface size decreases with decreasing temperatures; there exists an ~3.3nm sub-surface layer region where the gold sphere embedding data has to be fitted using the compressed exponential function, which indicates some elastic properties in this region; in regions beyond the first ~8.8nm of glassy PS films the dynamics are similar with those of bulk materials. Both the liquid surface size and the heterogeneous dynamics in the near free surface region are in contrast to some

other studies. The third section of this work focuses on the viscoelastic or elastic properties of near free surface region of glassy polystyrene films. It is shown that for the first ~5.5nm free surface layer the gold sphere embedding in not reversible. However, for the ~3.3nm sub-surface layer region the gold sphere embedding is reversible, for which there is no strong evidence to differentiate the two possible mechanisms: is this phenomenon due to any built-in stress during gold sphere embedding or any potential intrinsic structural properties in this region?

In the third part of this study we build a low level noise measurement system to study the thermal polarization noise in thin polymer films. The polymer films are sandwiched between two ultra-flat electrodes and pure thermal polarization noise can be collected and amplified by the noise measurement system. Because the vertical size of the polymer films is only several or tens of the size of the mobile cooperative rearranging regions of the glassy polymer system, the noise power spectral density of thin polymer films is found to fluctuate around a certain average level. For thinner polymer films, both the fluctuation and the integration (energy) of the power spectral density are found to be larger than those of the relatively thicker films, which we think is due to the increase of the number of the mobile cooperative rearranging regions in the former case. There is no dependence of the dominant PSD peak position on polymer film thickness is observed, which is in agreement with findings in some other dielectric spectroscopy studies. For the first time we observe that in the integrated power spectral density there are some relatively big jumps or fluctuations at some times of the successive measurements, which may indicate some energy exchange between different microscopic domains in glassy polymer systems. One more interesting work can be done using the low level noise measurement system: studying the temperature dependence of the polarization noise in ultra-thin polymers. However, it may be a big challenge because it is hard to control the sample temperature without introducing electric or vibration noise. Normally, sample temperature controlling in labs is carried out by means of electronic resistors or flowing thermal baths, of which the electronic or vibration noises are not negligible especially for low level polarization noise measurements.

In the fourth section of this study we developed a novel nano rheology AFM technique to study the near free surface dynamics of thin polymer films. Being different from common AFM techniques working with the dynamic torsional AFM tip mode, the technique in this study measures the transient retardation response of the polymer film surfaces to the step-like applied tip torsional force within the

time domain. Studies showed bulk like properties can be measured in thin polymer films if a high probing frequency is used. In this study, enhanced near free surface dynamics, with weak temperature dependence, are observed for PVAc films. Similar surface dynamical features are also observed in thin PS films. However, different findings are observed for PMMA or i-PMMA films. These observations indicate some polymer-specific properties in the near free surface region of thin polymer films.

Some future work

Specific near future work based on this study

(1) In the project of studying near free surface dynamics of thin i-PMMA films using the nano surface hole relaxation technique, the findings suggest specific structural properties in the near free surface region of i-PMMA films. It is worthwhile to conduct more studies to investigate any potential structural properties in this region. One possible method may be to effectively remove this unique free surface and to study the molecular weight dependence of the fresh "surface" region of as-prepared i-PMMA films. Another way may be to study the properties of the substrate-related "free surface", which can be obtained by dissolving the substrate of thin polymer films.

(2) In both projects of probing near surface dynamics of PS films using the nano gold sphere embedding technique and studying near free surface dynamics of PVAc films using the nano rheology AFM technique, enhanced surface dynamics with weak temperature dependence are observed. Further studies may focus on interpreting the elusive weak temperature dependence of near free surface dynamics, which will improve our understanding of how the near free surface dynamics affect the average whole polymer film dynamics as observed in many T_g measurement studies.

(3) The sub-surface layer dynamics observed in the nano gold sphere embedding studies is very interesting. More work should be carried out to make clear whether the observed sub-surface layer relaxation is due to the built-in stress during the nano gold sphere embedding process or results from some intrinsic local polymer structural properties. One possible theoretical

candidate for such considerations may be the surface capillary wave theory. Some works have shown that the thermal capillary wave play a role in determining surface properties of nano polymer film systems [123,246, 247].

(4) From the project of measuring thermal polarization noise in thin polymer films, the results indicate both temporally and spatially evolving cooperative rearranging dynamics in thin polymer films. Due to the hardness of proper temperature control without introducing electric or vibration noise to the samples, we did not study the temperature dependence of such thermal polarization noise in thin polymer films at that time. It is worthwhile to carry out such studies in the near future.

(5) We observe heterogeneous dynamics in glassy polymer films with the nanometer resolution, which is in contrast to the sole T_g distribution studies [66]. It will be rewarding to conduct more T_g or direct dynamics distribution studies in thin polymer films although it is a very hard task for such projects due to limited available experimental techniques.

(6) In the PS film nano surface hole relaxation studies, surface relaxation is observed even at a temperature of ~130K below bulk T_g. Some aging effect studies using this technique may answer such question as how much the potential aging effect may contribute to the observed weak temperature dependence of polymer surface dynamics.

General future work

There is still a long way to go to improve our understanding of dynamical properties in nano confined polymer systems. By and large, this research area is more experimental observation motivated than theoretical predictions warranted. The major reason for this is that the nano world is whole new to researchers. More experimental and theoretical research efforts in studies of nano-scale confined polymer systems are always necessary.

From the perspective of broad condensed matter physics studies, it is interesting to note that some areas such as polymer systems, colloidal systems, granular systems, and even electronic systems are

all related to one open and deepest question of *the glass transition*. Recall the equation of $dU = TdS - PdV + \mu dN$, we note that, more or less, most research effects focused (or are focusing) on the consideration of the energy of the glass forming systems, e.g. Adam-Gibbs theory frame considering configuration entropy of cooperative rearranging regions, the free volume theory considering the specific volume of the glass forming systems. As of today, no theory has been developed by considering the possible chemical potential or molecule exchange in glass formers. In addition, we may ask one question: which factor substantially contributes to some physical properties of glass forming materials, microscopic structures or molecular motions (tremendous efforts focused on the later)? The answer to such fundamental questions may eventually help us resolving the notorious puzzle of the glass transition.

Bibliography

[1] M. Rubinstein and R. Colby, "*Polymer Physics*", Oxford University Press, 2003.

[2] D. I. Bower, "*An Introduction to Polymer Physics*", Cambridge University Press, 2002.

[3] http://www.cheme.washington.edu/images/cent/pmma_orig.gif

[4] G. Strobl, "*The Physics of Polymers*", Springer-Verlag Berlin Heidelberg, 1997.

[5] M. Doi and S. F. Edwards, *"Theory of Polymer Dynamics"*, Clarendon Press, 1986.

[6] G. Strobl, "*Condensed Matter Physics*", Springer-Verlag Berlin Heidelberg, 2004.

[7] J. D. Ferry, "*Viscoelastic Properties of Polymers*", John Wiley & Sons, 1980.

[8] J. Furukawa, "*Physical Chemistry of Polymer Rheology*", Kodansha Ltd., 2003.

[9] N. G. McCrum, B. E. Read and G. Williams, "*Anelastic and Dielectric Effects in Polymeric Solids*", John Wiley & Sons Ltd., 1967.

[10] M. Takahashi, M. C. Shen, R. B. Taylor and A. V. Tobolsky, *"Master curve of some amorphous polymers"*, J. Appl. Polymer Sci. 8, 1549(1964).

[11] P. N. Segrè, V. Prasad, A. B. Schofield, and D. A. Weitz, *"Glasslike Kinetic Arrest at the Colloidal-Gelation Transition"*, Phys. Rev. Lett. 86, 6042-6045(2001).

[12] M. Bernabei, A. J. Moreno, and J. Colmener, *"Dynamic Arrest in Polymer Melts: Competition between Packing and Intramolecular Barriers",* Phys. Rev. Lett. 101, 255701-1-4(2008).

[13] L. Hartmann, W. Gorbatschow, J. Hauwede and F. Kremer, *"Molecular dynamics in thin films of isotactic poly(methyl methacrylate)"*, Eur. Phys. J. E. 8, 145-154(2002).

[14] S. Ge, Y. Pu, W. Zhang, M. Rafailovich, and J. Sokolov, *"Shear Modulation Force Microscopy Study of Near Surface Glass Transition Temperatures"*, Phys. Rev. Lett. 85, 2340-2343(2000).

[15] P. Bernazzani, S. L. Simon, D. J. Plazek and K. L. Ngai, *"Effects of entanglement concentration on Tg and local segmental motions"*, Eur. Phys. J. E. 8, 201-207(2002).

[16] M. D. Ediger, C. A. Angell, Sidney R. Nagel, *"Supercooled Liquids and Glasses"*, J. Phys. Chem. 100, 13200(1996).

[17] W.Kauzmann, *"The nature of the glassy state and the behavior of liquids at low temperatures"*, Chem. Rev .43, 219–256(1948); Robin J.Speedy, *"Kauzmann's paradox and the glass transition"*, Biophysical Chemistry 105, 411–420(2003).

[18] P. G. Debenedetti & F. H. Stillinger, *"Supercooled liquids and the glass transition"*, Nature 410, 259-267(2001).

[19] C. A. Angell,K. L. Ngai, G. B. McKenna, P. F. McMillan, S. W. Martin, *"Relaxation in glassforming liquids and amorphous solids"*, J. Appl. Phys.88, 3113-3157(2000).

[20] D. W. Choi, *"Through the glass lightly"*, Science 267,1615(1995).

[21] Gregory B. McKenna, *"Glass dynamics: Diverging views on glass transition",* Nature Physics 4, 673-673(2008).

[22] Tina Hecksher, Albena I. Nielsen, Niels Boye Olsen, Jeppe C. Dyre, *"Little evidence for dynamic divergences in ultraviscous molecular liquids"*, Nature Physics 4, 737-741(2008).

[23] J. H. Gibbs and E. A. DlMarzio, *"Nature of the glass transition and the glassy state",* J. Chem. Phys. 28, 373-383(1958).

[24] Z. Fakhraai, J. A. Forrest, *"Probing slow dynamics in supported thin polymer films",* Phys. Rev. Lett.95, 025701-1-4 (2005).

[25] Nano gold sphere embedding(chapter 5) and nano rheology AFM(chapter 7) studies in the present work.

[26] G. Adam and J.H. Gibbs, *"On the temperature ependence of cooperative relaxation properties in glass-forming liquids"*, J. Chem. Phys. **43**, 139-146(1965).

[27] M. Arndt, R. Stannarius, H. Groothues, E. Hempel, and F. Kremer, *"Length Scale of Cooperativity in the Dynamic Glass Transition"*, Phys. Rev. Lett. 79, 2077-2080(1997).

[28] E. R. Weeks, J. C. Crocker, A. C. Levitt, A. Schofield, D. A. Weitz, *"Three-Dimensional Direct Imaging of Structural Relaxation Near the Colloidal Glass Transition",* Science 287, 627(2000).

[29] C. Donati, S. C. Glotzer, P. H. Poole, W. Kob, and S. J. Plimpton, *"Spatial correlations of mobility and immobility in a glass-forming Lennard-Jones liquid"*, Phys. Rev. E. 60, 3107-3119(1999).

[30] E. Vidal Russell and N. E. Israeloff, *"Direct observation of molecular cooperativity near the glass transition"*, Nature 408, 695-698(2000).

[31] Ludovic Berthier, *"Time and length scales in supercooled liquids",* Phys. Rev. E 69, 020201-1-4(2004).

[32] E. Hempel, G. hempel, A. Hensel, C. Schick, and E. Donth, *"Characterisrtc length of dynamics glass transition near Tg for a wide assortment of glass-forming substances",* J. Phys. Chem. B 104, 2460-2466(2000).

[33] H. C. Andersen, *"Molecular dynamics studies of heterogeneous dynamics and dynamic crossover in supercooled atomic liquids"*, PNAS 102, 6686–6691(2005).

[34] L. Berthier, G. Biroli, J.-P. Bouchaud, L. Cipelletti, D. El Masri, D. L'Hoˆte, F. Ladieu, M. Pierno, *"Direct Experimental Evidence of a Growing Length Scale Accompanying the Glass Transition"*, Science 310, 1797-1800(2005).

[35] W. Kob, C. Donati, S. J. Plimpton, P. H. Poole, and S. C. Glotzer, *"Dynamical Heterogeneities in a Supercooled Lennard-Jones Liquid"*, Phys. Rev. Lett. 79, 2827-2830(1997).

[36] C. Donati, J. F. Douglas, W. Kob, S. J. Plimpton, P. H. Poole, and S. C. Glotzer, *"Stringlike Cooperative Motion in a Supercooled Liquid"*, Phys. Rev. Lett. 80, 2338-2341(1998).

[37] C. Donati, S. C. Glotzer, and P. H. Poole, *"Growing Spatial Correlations of Particle Displacements in a Simulated Liquid on Cooling toward the Glass Transition",* Phys. Rev. Lett. 82, 5064-5068(1999).

[38] studies in chapter 6 of the present thesis.

[39] C. M. Roland, *"Characteristic relaxation times and their invariance to thermodynamics conditions"*, Soft Matter 4, 2316-2322(2008).

[40] K. L. Ngai1 and K. Y. Tsang, *"Similarity of relaxation in supercooled liquids and interacting arrays of oscillators"*, Phys. Rev. E 60, 4511-4517(1999).

[41] P. A. O'Connell, and G. B. McKenna, *"Arrhenius-type temperature dependence of the segmental relaxation below* T_g *",* J. Chem. Phys. 110, 11054-11060(1999).

[42] M. Antonietti, D. Ehlich, H. Sillescu and M. Wesselmann, *"Applications of "forced rayleigh scattering" and "photon correlation spectroscopy" for the examination of transport properties in polymer melts"*, Progr Colloid & Polymer Sci80: 83-92(1989)].

[43] A. Dhinojwala, G. K. Wong, J. M. Torkelson, *"Rotational reorientation dynamics of disperse red 1 in polystyrene: CE-r elaxation dynamics probed by second harmonic generation and djelectric relaxation"*, J. Chem. Phys. 100, 6046 (1994).

[44] N. G. McCrum, B. E. Read and G. Williams, *Anelastic and Dielectric Effects in Polymeric* Solids, John Wiley & Sons Ltd (1967).

[45] A. K. Doolittle, *"Studies in Newtonian flow. II the dependence of the viscosity of liquids on free-space",* J. Appl. Phys. 22, 1471-1475(1951).

[46] M. L. Ferrer, C. Lawrence, B. G. Demirjian, and D. Kivelson, C. Alba-Simionesco, G. Tarjus, *"Supercooled liquids and the glass transition: Temperature as the control variable",* J. Chem. Phys. 109, 8010-8015(1998).

[47] Z. Fakhraai, *"Dynamics of polymer thin films and surfaces",* PhD thesis, University of Waterloo (2007).

[48] R. A. Riggleman, H. Lee, M. D. Ediger, and J. J. de Pablo, *"Free volume and finite-size effects in a polymer glass under stress",* Phys. Rev. Lett.99, 215501-1-4(2007).

[49] P. Scheidler, W. Kob, and K. Binder, *"The relaxation dynamics of a supercooled liquid confined by rough walls",* J. Phys. Chem. B 108, 6673-6686(2004).

[50] A. K. Doolittle, *"Studies in Newtonian flow. II. The dependence of the viscosity of liquids on free-space"*, J. Appl. Phys.22, 1471-1475(1951).

[51] A. S. Keys, A. R. Abate, S. C. Glotzer and D. J. Durian, *"Measurement of growing dynamical length scales and prediction of the jamming transition in a granular material",* Nature Physics 3, 260-264(2007).

[52] Götze W and Sjögren L, "*The glass-transition singularity"*, Z. Phys. B - Condensed Matter 65, 415-427 (1987).

[53] W Gotze, *"The mode-coupling theory of liquid-to-glass transitions",* J. Phys.: Condens. Matter 2, SA201-SA205 (1990).

[54] David R Reichman1 and Patrick Charbonneau, *"Mode-coupling theory",* J. Stat. Mech. (2005) P05013, doi: 10.1088/1742-5468/2005/05/P05013.

[55] E. Donth, "*The glass transition relaxation dynamics in liquids and disordered materials"*, Springer (2001)

[56] M. D. Ediger, *"Spatially heterogeneous dynamics in supercooled liquids",* Annu. Rev. Phys. Chem. 51, 99–128(2000).

[57] G. Beaucage, R. Composto, and R. S. Stein, *"Ellipsometric Study of the Glass Transition and Thermal Expansion Coefficients of Thin Polymer Films",* J. Poly. Sci.: Part B: Polymer Physics, Vol. 31, 319-326(1993).

[58] J. L. Keddie, R. A. L. Jones and R. A. Cory, *"Size-Dependent Depression of the Glass Transition Temperature in Polymer Films"*, Europhys Lett. 27, 59-64(1994).

[59] Joseph Q. Pham and Peter F. Green, *"The glass transition of thin film polymer/polymer blends: Interfacial interactions and confinement",* J. Chem. Phys. 116, 5801-5806(2002).

[60] Joseph Q. Pham and Peter F. Green, *"Effective Tg of Confined Polymer-Polymer Mixtures. Influence of Molecular Size",* Macromolecules 36, 1665-1669(2003).

[61] K. Fukao and Y. Miyamoto, *"Glass transitions and dynamics in thin polymer films: Dielectric relaxation of thin films of polystyrene"*, Phys. Rev. E 61, 1743-1754(2000).

[62] L. Hartmann, W. Gorbatschow, J. Hauwede, and F. Kremer, *"Molecular dynamics in thin films of isotactic poly(methyl methacrylate)"*, Eur. Phys. J. E 8, 145–154 (2002).

[63] Yves Grohens, Maurice Brogly, Clorinthe Labbe, Marie-Odile David, and Jacques Schultz, *"Glass Transition of Stereoregular Poly(methyl methacrylate) at Interfaces",* Langmuir14,2929-2932(1998).

[64] P. Carriere, Y. Grohens, J. Spevacek, and J. Schultz, *"Stereospecificity in the Adsorption of Tactic PMMA on Silica",* Langmui, 16, 5051-5053(2000).

[65] Y. Grohens, L. Hamon, G. Reiter, A. Soldera, and Y. Holl, *"Some relevant parameters affecting the glass transition of supported ultra-thin polymer films"*, Eur. Phys. J. E 8, 217–224 (2002).

[66] C. J. Ellison, J. M. Torkelson, *"The distribution of glass-transition temperatures in nanoscopically confined glass formers"*, Nature Materials 2, 695-700(2003).

[67] J. A. Forrest, K. Dalnoki-Veress, *"The glass transition in thin polymer films"*, Advances in Colloid and Interface Science 94, 167-196(2001).

[68] S. F. Edwards, *"The glass transition in polymers",* Polymer 35, 3827-3830(1994).

[69] S. F. Edwards and K. E. Evans, *"Dynamics of Highly Entangled Rod-like Molecules"*, J. Chem. Soc., Faraday Trans.2, 78, 113-121(1982).

[70] C. B. Roth, K. L. McNerny, W. F. Jager, and J. M. Torkelson, *"Eliminating the enhanced mobility at the free surface of polystyrene: fluorescence studies of the glass transition temperature in thin bilayer films of immiscible polymers",* Macromolecules 40*,* 2568-2574(2007).

[72] S.A. Hutcheson and G.B. McKenna, *"Comment on "The properties of free polymer surfaces and their influence on the glass transition temperature of thin polystyrene films" by J.S. Sharp, J.H. Teichroeb and J.A. Forrest",* Eur. Phys. J. E 22, 281–286 (2007).

[73] J.A. Forrest and R.A.L. Jones, "*The Glass Transition and Relaxation of Polymer Films and Surfaces",* Polymer Surfaces Interfaces and Thin Films, edited by A. Karim and S. Kumar, World Scientific, Singapore (2000)

[74] G. B. DeMaggio, W. E. Frieze, D. W. Gidley, M. Zhu, H. A. Hristov, A. F. Yee, "*Interface and Surface Effects on the Glass Transition in Thin Polystyrene Films"*, Phys. Rev. Lett. 78, 1524-1527(1997).

[75] W. E. Wallace, J. H. van Zanten, and W. L. Wu, *"Influence of an impenetrable interface on a polymer glass-transition temperature"*, Phys. Rev. E 52, R3329 - 3332 (1995).

[76] K. Dalnoki-Veress, J.A. Forrest, C. Murray, C. Gigault, J.R. Dutcher, *"Molecular weight dependence of reductions in the glass transition temperature of thin freely standing polymer films"*, Phys. Rev. E 63, 031801-1-10(2001).

[77] J.A. Forrest, K. Dalnoki-Veress, J.R. Dutcher, *"Interface and chain confinement effects on the glass transition temperature of thin polymer films",* Phys. Rev. E 56, 5705-5716(1997).

[78] J. Mattsson, J.A. Forrest, L. B¨orgesson, *"Quantifying glass transition behavior in ultrathin free-standing polymer films"*, Phys. Rev. E 62, 5187-5200(2000).

[79] J. A. Forrest, K. Dalnoki-Veress, J. R. Stevens, and J. R. Dutcher, *"Effect of Free Surfaces on the Glass Transition Temperature of Thin Polymer Films"*, Phys. Rev. Lett. 77, 2002-2005(1996).

[80] J. A. Forrest, J. Mattsson, *"Reductions of the glass transition temperature in thin polymer films: Probing the length scale of cooperative dynamics"*, Phys. Rev. E 61, R53-56(2000).

[81] K.L. Ngai, A.K. Rizos, D.J. Plazek, *"Reduction of the glass temperature of thin freely standing polymer films caused by the decrease of the coupling parameter in the coupling model",*
Journal of Non-Crystalline Solids 235-237, 435-443(1998).

[82] K. Tanaka, A. Takahara, T. Kaijiyama, *"Effect of Polydispersity on Surface Molecular Motion of Polystyrene Films"*, Macromolecules 30, 6626-6632(1997).

[83] A. M. Mayes, *"Glass transition of amorphous polymer surfaces*", Macromolecules 27, 3114-3115(1994).

[84] P. Cifra, E. Nies, F. E. Karasz, *"Free surface profile and surface tension in a polymer melt: a Monte Carlo study",* Macromolecules 27, 1166-1171(1994).

[85] K. Tanaka, A. Taura, S. -R. Ge, A. Takahara, T. Kajiyama, *"Molecular weight dependence of surface dynamic viscoelastic properties for the monodisperse polystyrene film",* Macromolecules 29, 3040-3042(1996).

[86] Fengchao Xie, H. F. Zhang, Fuk Kay Lee, Binyang Du, and Ophelia K. C. Tsui, Y. Yokoe, K. Tanaka, A. Takahara, and T. Kajiyama, Tianbai He, *"Effect of Low Surface Energy Chain Ends on the Glass Transition Temperature of Polymer Thin Films",* Macromolecules35, 1491-1492(2002).

[87] J.S. Sharp, J.H. Teichroeb, and J.A. Forrest, *"The properties of free polymer surfaces and their influence on the glass transition temperature of thin polystyrene films",* Eur. Phys. J. E 15, 473-487 (2004).

[88] J. S. Sharp, J. A. Forrest, *"Free Surfaces Cause Reductions in the GlassTransition Temperature of Thin Polystyrene Films",* Phys. Rev. Lett. 91, 235701-1-4 (2003).

[89]Koji Fukao, Shinobu Uno, Yoshihisa Miyamoto, Akitaka Hoshino, and Hideki Miyaji, *"Dynamics of α and β processes in thin polymer films: Poly(vinyl acetate) and poly(methyl methacrylate)"*, Phys. Rev. E64, 051807-1-11(2001).

[90] Z. Fakhraai and J. A. Forrest, *"Measuring the Surface Dynamics of Glassy Polymers", Science* 319, 600-604(2008).

[91] D. Qi, Z. Fakhraai, and J. A. Forrest, *"Substrate and Chain Size Dependence of Near Surface Dynamics of Glassy Polymers"*, Phys. Rev. Lett. 101, 096101-1-4(2008).

[92] Ophelia K. C. Tsui and H. F. Zhang, *"Effects of Chain Ends and Chain Entanglement on the Glass Transition Temperature of Polymer Thin Films",* Macromolecules34, 9139-9142(2001).

[93] X. P. Wang, O. K. C. Tsui, and Xudong Xiao, *"Dynamic Study of Polymer Films by Friction Force Microscopy with Continuously Varying Load",* Langmuir 18, 7066-7072(2002).

[94] S. Ge, Y. Pu, W. Zhang, M. Rafailovich, and J. Sokolov, C. Buenviaje, R. Buckmaster, and R. M. Overney, *"Shear Modulation Force Microscopy Study of Near Surface Glass Transition Temperatures"*, Phys. Rev. Lett. 85, 2340-2343(2000).

[95] J. Erichsen, T. Shiferaw, V. Zaporojtchenko, F. Faupel, *"Surface glass transition in bimodal polystyrene mixtures",* Eur. Phys. J. E 24 243-246(2007).

[96] David S. Fryer, Richard D. Peters, Eui Jun Kim, Jeanne E. Tomaszewski, Juan J. de Pablo, and Paul F. Nealey, Chris C. White and Wen-li Wu, *"Dependence of the Glass Transition Temperature of Polymer Films on Interfacial Energy and Thickness",* Macromolecules 34, 5627-5634(2001).

[97] O. K. C. Tsui and T. P. Russell, C. J. Hawker, *"Effect of Interfacial Interactions on the Glass Transition of Polymer Thin Films"*, Macromolecules 34, 5535-5539(2001).

[98] P. Bernazzania and R.F. Sanchez, *"Effect of substrate interactions on the melting behavior of thin polyethylene films",* Eur. Phys. J. E 26, 427–434 (2008).

[99] David S. Fryer, Paul F. Nealey, and Juan J. de Pablo*, "Thermal Probe Measurements of the Glass Transition Temperature for Ultrathin Polymer Films as a Function of Thickness",* Macromolecules 33, 6439-6447(2000).

[100] J. H. van Zanten, W. E. Wallace, W.-li. Wu, *"Effect of strongly favorable substrate interactions on the thermal properties of ultrathin polymer films"*, Phys. Rev. E 53, R2053-2056(1996).

[101] J.A Torres, P. F. Nealey, and J. J. de Pablo, *"Molecular Simulation of Ultrathin Polymeric Films near the Glass Transition"*, Phys. Rev. Lett.85, 3221-3224(2000).

[102] R. D. Priestley, L. J. Broadbelt, and J. M. Torkelson, *"Physical aging of ultrathin polymer films above and below the bulk glass transition temperatures: effects of attractive vs neutral polymer-substrate interactions measured by fluorescence"*, Macromolecules 38, 654-657(2005).

[103] P.G. de Gennes, *"Glass transitions in thin polymer films",* Eur. Phys. J. E 2, 201–205 (2000).

[104] John D. McCoy, John G. Curro, *"Conjectures on the glass transition of polymers in confined geometries"*, J. Chem. Phys. 116, 9154-9157(2002).

[105]Y. Grohens, L. Hamon, G. Reiter, A. Soldera, and Y. Holl, *"Some relevant parameters affecting the glass transition of supported ultra-thin polymer films"*, Eur. Phys. J. E 8, 217-224 (2002).

[106] J. S. Sharp and J. A. Forrest, *"Dielectric and ellipsometric studies of the dynamics in thin films of isotactic poly(methylmethacrylate) with one free surface"*, Phys. Rev. E 67, 031805-1-9(2003).

[107] J. L. Keddie, R. A. L. Jones, R. A. Cory, *"Interface and surface effects on the glass-transition temperature in thin polymer films"*, Faraday Discussion 98, 219-230(1994).

[108] J.L. Keddie, R.A.L. Jones, and R.A. Cory, *"Size-Dependent Depression of the Glass Transition Temperature in Polymer Films",* Europhys. Lett. 27, 59-64 (1994).

[109] D. Long and F. Lequeux, *"Heterogeneous dynamics at the glass transition in van der Waals liquids, in the bulk and in thin films",* Eur. Phys. J. E 4, 371–387 (2001).

[110] S. Merabia, P. Sotta, and D. Long, *"Heterogeneous nature of the dynamics and glass transition in thin polymer films"*, Eur. Phys. J. E 15, 189-210 (2004).

[111] E. R. Weeks, J. C. Crocker, A. C. Levitt, A. Schofield, and D. A. Weitz, *"Three-Dimensional Direct Imaging of Structural Relaxation Near the Colloidal Glass Transition"*, Science 287, 627-631 (2000).

[112] Sharon C. Glotzer, *"Spatially heterogeneous dynamics in liquids: insights from simulation",* J. Non-Crys. Solids 274, 342-355(2000).

[113] P.G. de Gennes, *"Glass transitions in thin polymer films",* Eur. Phys. J. E 2, 201–205 (2000).

[114] Hiroshi Morita, Keiji Tanaka, Tisato Kajiyama, Toshio Nishi and Masao Doi, *"Study of the Glass Transition Temperature of Polymer Surface by Coarse-Grained Molecular Dynamics Simulation",* Macromolecules 39, 6233-6237(2006)

[115] Tobias Kerle, Zhiqun Lin, Ho-Cheol Kim, and Thomas P. Russell, *"Mobility of Polymers at the Air/Polymer Interface"*, *Macromolecules*, *34,* 3484-3492(2001).

[116] Kyusoon Shin, Sergei Obukhov, Jiun-Tai Chen, June Huh, Yoontae Hwang, Soonchun Mok, Priyanka Dobriyal, Pappannan Thiyagarajan, Thomas P. Russell, *"Enhanced mobility of confined polymers"*, Nature Material6, 961-965(2007).

[117] E. Manias, H. Chen, R. Krishnamoorti, J. Genzer, E. J. Kramer, and E. P. Giannelis, *"Intercalation Kinetics of Long Polymers in 2 nm Confinements",* Macromolecules, 33, 7955-7966(2000).

[118] Kenji Yoshimoto, Tushar S. Jain, Paul F. Nealey, and Juan J. de Pablo, *"Local dynamic mechanical properties in model free-standing polymer thin films"*, J. Chem. Phys. 122, 144712-1-6(2005).

[119] R. M. Papaléo, R. Leal, W. H. Carreira, and L. G. Barbosa, I. Bello and A. Bulla, *"Relaxation times of nanoscale deformations on the surface of a polymer thin film near and below the glass transition",* Phys. Rev. B 74, 094203-1-5(2006)

[120] Ali Dhinojwala, George K. Wong and John M. Torkelson, *"Rotational reorientation dynamics of disperse red 1 in polystyrene: α -relaxation dynamics probed by second harmonic generation and dielectric relaxation",* J. Chem. Phys. 100 (8), 6046-6054(1994).

[121] S. Kawana, R. A. L. Jones, *"Character of the glass transition in thin supported polymer films"*, Phys. Rev. E. 63, 021501-1-6(2001).

[122] Work in the present chapter 5, to be published.

[123] S. Herminghaus, R. Seemann, and K. Landfester, *"Polymer Surface Melting Mediated by Capillary Waves"*, Phys. Rev. Lett.93, 017801-1-4(2004).

[124] Song-Ho Chong, and Walter Kob, *"Coupling and Decoupling between Translational and Rotational Dynamics in a Supercooled Molecular Liquid",* Phys. Rev. Lett. 102, 025702-1-4(2009).

[125] Marco Bernabei, Angel J. Moreno, and Juan Colmenero, *"Dynamic Arrest in Polymer Melts: Competition between Packing and Intramolecular Barriers",* Phys. Rev. Lett. 101, 255701-1-4 (2008).

[126] Pinaki Chaudhuri, Srikanth Sastry, and Walter Kob, *"Tracking Heterogeneous Dynamics During the _ Relaxation of a Simple Glass Former",* Phys. Rev. Lett., 190601-1-4 (2008).

[127] Claudio Donati, Jack F. Douglas, Walter Kob, Steven J. Plimpton, Peter H. Poole, and Sharon C. Glotzer, *"Stringlike Cooperative Motion in a Supercooled Liquid",* Phys. Rev. Lett. 80, 2338-2341(1998).

[128] S. Peter, H. Meyer, J. Baschnagel and R. Seemann, *"slow dynamics and glass transition in simulated free-standing polymer films: a possible relation between global and local glass transition temperatures"*, J. Phys.: Condens. Matter 19, 205119-1-11(2007)].

[129] P. Scheidler, W. Kob and K. Binder, *"Cooperative motion and growing length scales in supercooled confined liquids"*, Europhys. Lett. 59, 701–707 (2002).

[130] S. K. Kumar, M. Vacatello, and D. Y. Yoon, *"Off-lattice Monte Varlo simulations of polymer melts confined between two plates",* J. Chem. Phys.89, 5206-5215(1988).

[131] I. A. Bitsanis, G. ten Brinke, *"A lattice monte Carlo study of long chain conformations at solid-polymer melt interfaces",* J. Chem. Phys.99, 3100-3111(1993).

[132] I. Bitsanis and G. Hadziioannou, *"Molecular dynamics simulations of the structure and dynamics of confined polymer melts"*, J. Chem. Phys.92, 3827-3847(1990).

[133] J. A. Torres, P. F. Nealey, and J. J. de Pablo, *"Molecular simulation of ultrathin polymeric films near the glass transition",* Phys. Rev. Lett. 85, 3221-3224(2000).

[134] F. Varnik, J. Baschnagel, and K. Binder, *"Reduction of the glass transition temperature in polymer films: A molecular-dynamics study",* Phys. Rev. E65, 021507-1-13(2002).

[135] S. Kamath, R. H. Colby, and S. K. Kumar, J. Baschnagel, *"Thermodynamics signature of the onset of caged dynamics in glass-forming liquids"*, J. Chem. Phys. 116, 865-868(2002).

[136] K. Vollmayr-Lee, W. Kob, K. Binder, A. Zippelius, *"Dynamical heterogeneities below the glass transition"*, J. Chem. Phys. 116, 5158-5166(2002).

[137] S. Herminghaus, K. Jacobs, and R. Seemann, *"The glass transition of thin polymer films: some questions, and a possible answer",* Eur. Phys. J. E 5, 531-538(2001).

[138] W. B. Lacy, J. M. Williams, L. A. Wenzler, T. P. Beebe, and J. M. Harris, *"Characterization of SiO2-Overcoated Silver-Island Films as Substrates for Surface-Enhanced Raman Scattering"*, Anal. Chem. 68 (6), 1003-1011(1996); L. A. Wenzler, G. L. Moyes, L. G. Olson, J. M. Harris, and T. P. Beebe, *"Single-Molecule Bond-Rupture Force Analysis of Interactions between AFM Tips and Substrates Modified with organosilanes",* Anal. Chem.69, 2855-2861(1997); Note: $R_a \approx 0.15nm$, AFM scanning area: $500 \times 500nm^2$; our result: $R_a = 0.6493nm$, AFM scanning area: $5000 \times 5000nm^2$.

[139] K. Norrman, A. Ghanbari-Siahkali and N. B. Larsen, *"Studies of spin-coated polymer films"*, Annu. Rep. Prog. Chem., Sect. C 101, 174–201(2005).

[140] D. B. Hall, P. Underhill, and J. M. Torkelson, *"Spin Coating of Thin and Ultrathin Polymer Films"*, Polym. Eng. Sci. 38, 2039-2045(1998).

[141] C. J. Lawrence, *"The mechanics of spin coating of polymer films",* Phys. Fluids 31, 2786-2795(1988).

[142] L. L. Spangler, J. M. Torkelson and J. S. Royal, *"Influence of Solvent and Molecular Weight on Thickness and Surface Topography of Spin-Coated Polymer Films",* Polym. Eng. Sci. 30, 644-653(1990).

[143] B. T. CHEN, *"Investigation of the Solvent-Evaporation Effect on Spin Coating of Thin Films"*, Polym. Eng. Sci. 23, 399-403(1983).

[144] K. Fukao and Y. Miyamoto, *"Glass transition temperature and dynamics of α -process in thin polymer films"*, Europhys. Lett.46, 649-654 (1999).

[145] S. Kim, C. B. Roth, J. M. Torkelson, *"Effect of Nanoscale Confinement on the Glass Transition Temperature of Free-Standing Polymer Films: Novel,Self-Referencing Fluorescence Method",* J. Polym. Sci.: Part B: Polym. Phys. 46, 2754–2764 (2008).

[146] P. A. O'Connell and G. B. McKenna, *"Rheological Measurements of the Thermoviscoelastic Response of Ultrathin Polymer Films",* Science 307, 1760-1763 (2005).

[147] A. Gitsas, and G. Floudas, *"Pressure Dependence of the Glass Transition in Atactic and Isotactic Polypropylene",* Macromolecules 41, 9423-9429 (2008).

[148] J. S. Sharp, J. A. Forrest, *"Free Surfaces Cause Reductions in the GlassTransition Temperature of Thin Polystyrene Films",* Phys. Rev. Lett. 91 235701-1-4(2003).

[149] E R. Weeks, J. C. Crocker, A. C. Levitt, A. SchoÞeld, D. A. Weitz, *"Three-Dimensional Direct Imaging of Structural Relaxation Near the Colloidal Glass Transition",* Science 287, 627-631(2000).

[150] A. Kasper, E. Bartsch, and H. Sillescu, *"Self-Diffusion in Concentrated Colloid Suspensions Studied by Digital Video Microscopy of Core−Shell Tracer Particles"*, Langmuir 14, 5004-5010(1998).

[151] K. A. Cavicchi, K. J. Berthiaume, T. P. Russell, *"Solvent annealing thin films of poly(isoprene-b-lactide)",* Polymer 46, 11635–11639(2005).

[152] K. C. Grabar, R. G. Freeman, M. B. Hommer, and M. J. Natan, *"Preparation and Characterization of Au Colloid Monolayers",* Anal. Chem. 67, 735-743(1995).

[153] G. Tsutsui, S. Huang, H. Sakaue, S. Shingubara and T. Takahagi, *"Well-size-controlled Colloidal Gold Nanoparticles Dispersed in Organic Solvents",* Jpn. J. Appl. Phys. 40, 346–349(2001).

[154] http://mrsec.wisc.edu/Edetc/nanolab/gold/index.html and references therein.

[155] A. Pal, *"Preparation of ultrafine colloidal gold particles using a bioactive molecule"*, J. Nanoparticle Research 6, 27–34(2004).

[156] R. G. DiScipio, *"Preparation of Colloidal Gold Particles of Various Sizes Using Sodium Borohydride and Sodium Cyanoborohydride",* ANALYTICAL BIOCHEMISTRY 236, 168–170 (1996).

[157] A. K. Boal, F. Ilhan, J. E. DeRouchey, T. Thurn-Albrecht, T. P. Russell & V. M. Rotello, *"Self-assembly of nanoparticles into structured spherical and network aggregates",* Nature 404, 746-748(2000).

[158] A. D. McFarland, C. L. Haynes, C. A. Mirkin, R. P. Van Duyne, and Hilary A. Godwin, *"Color My Nanoworld",* J. Chem. Educ. 81, 544A-544B (2004).

[159]Gerald Steiner, Cordelia Zimmerer, and Reiner Salzer, *"Characterization of Metal-Supported Poly(methyl methacrylate) Microstructures by FTIR Imaging Spectroscopy",* Langmuir 22, 4125-4130(2006).

[160]Young-Soo Seo, Eusung Kim, Soo Yong Kwon, Huaiyu Jing, Kwanwoo Shin, *"AFM study of phase-separated morphology in immiscible blend thin films",* Ultramicroscopy 108, 1186–1190(2008).

[161] J.S. Sharp, J.H. Teichroeb, and J.A. Forrest, *"The properties of free polymer surfaces and their influence on the glass transition temperature of thin polystyrene films",* Eur. Phys. J. E 15, 473-487 (2004).

[162] J. H. Teichroeb and J. A. Forrest, *"Direct Imaging of Nanoparticle Embedding to ProbeViscoelasticity of Polymer Surfaces",* Phys. Rev. Lett. 91, 016104-1-4(2003).

[163] F. Faupel, R. Willecke, A. Thran, *"Diffusion of metals in polymers",* Mater. Sci. Eng. Rep. R22, 1-55(1998).

[164] H. Baumgartner, V. Fuenzalida, and I. Eisele, "*Ozone cleaning of the Si-SiO2 system"*, Appl. Physics. A 43, 223-226(1987).

[165] M. Tabe, *"UV ozone cleaning of silicon substrates in silicon molecular beam epitaxy"*, Appl. Phys. Lett. 45, 1073-1075(1984).

[166] J. R. Vig, *"UV/ozone cleaning of surfaces",* J. Vac. Sci. Technol. A 3, 1027-1034(1985).

[167] J. E. Curran, J. S. Page and U. Pick, *"The Influence of some evaporation parameters on the structure and properties of thin aluminum films",* Thin Solid Films, 97, 259-276(1982).

[168] N. E. Israeloff and Xiangzhou Wang, *"High-sensitivity dielectric polarization noise measurements"*, Rev. Sci. Instrum. 68(3), 1543-1546(1997).

[169] Manual of "Model 7280 wide bandwidth DSP lock-in amplifier", PerkinElmer Corporation(2000).

[170] http://www.chembio.uoguelph.ca/educmat/chm729/afm/details.htm

[171] http://www.siliconfareast.com/afm.htm

[172] http://en.wikipedia.org/wiki/Atomic_force_microscope

[173] http://www.polymer-physics.uwaterloo.ca/equipment/afm.htm

[174] http://www.nanosensors.com/PPP-NCH.htm

[175] http://www.mechmat.caltech.edu/~kaushik/park/1-2-1.htm

[176] A. Yurtsever, A. M. Gigler and R. W. Stark, *"Frequency modulation torsional resonance mode AFM on chlorite (001)"*, J. Phys.: Conference Series 100, 052033-1-4(2008).

[177] M. Reinstadtler, U. Rabe, V. Scherer, U. Hartmann, A. Goldade, B. Bhushan, W. Arnold, "*On the nanoscale measurement of friction using atomic-force microscope cantilever torsional resonances",* Appl. Phys. Lett.82, 2604-2606(2003).

[178] Y. Roiter and S. Minko, *"AFM Single Molecule Experiments at the Solid−Liquid Interface: In Situ Conformation of Adsorbed Flexible Polyelectrolyte Chains"*, JACS 127, 15688-15689(2005).

[179] http://en.wikipedia.org/wiki/Ellipsometry

[180] D. J. De Smet, *"A child's garden of ellipsometry",* 2001(unpublished).

[181] www.polymer-physics.uwaterloo.ca/equipment/afm.htm.

[182] Manual of EXACTA 2000 ellipsometer, Waterloo Digitlal Electronics(1999).

[183] http://ece-www.colorado.edu/~bart/book/ellipsom.htm

[184] S.V. Ahir and E. M. Terentjev, *"Fast Relaxation of Carbon Nanotubes in Polymer Composite Actuators"*, Phys. Rev. Lett. 96, 133902-1-4(2006).

[185] J.A. Forrest*, "A decade of dynamics in thin films of polystyrene: Where are we now?"*, Eur. Phys. J. E 8, 261–266 (2002).

[186] M. Alcoutlabi and G. B McKenna*, "Effects of confinement on material behaviour at the nanometre size scale"*, J. Phys.: Condens. Matter 17, R461–R524(2005).

[187] J. A. Forrest, K. Dalnoki-Veress, *"The glass transition in thin polymer films"*, Advances in Colloid and Interface Science 94, 167-196(2001).

[188] P. Gasemjit and D. Johannsmann, *"Thickness of the Soft Layer on Glassy Polystyrene Surfaces"*, J. Polym. Sci., Part B: Polym. Phys. 44, 3031-3036(2006).

[189] V. M. Rudoy, O. V. Dement'eva, I. V. Yaminskii, V. M. Sukhov, M. E. Kartseva, and V. A. Ogarev, *"Metal Nanoparticles on Polymer Surfaces: 1. A New Method of Determining Glass Transition Temperature of the Surface Layer",* Colloid Journal 64, 743-754(2002).

[190] J. H. Teichroeb and J. A. Forrest, *"Direct Imaging of Nanoparticle Embedding to ProbeViscoelasticity of Polymer Surfaces",* Phys. Rev. Lett. 91, 016104-1-4(2003).

[191] J.S. Sharp, J.A. Forrest, Z. Fakhraai, M. Khomenk, J.H. Teichroeb, and K. Dalnoki-Veress, *"Reply to comment on "The properties of free polymer surfaces and their effect upon the glass transition temperature of thin polystyrene films" by S.A. Hutcheson and G.B. McKenna",* Eur. Phys. J. E 22, 287–291 (2007).

[193] S. Peter, H. Meyer, J. Baschnagel and R. Seemann, *"Slow dynamics and glass transition in simulated free-standing polymer films: a possible relation between global and local glass transition temperatures"*, J. Phys.: Condens. Matter 19, 205119 (2007).

[194] Jones, R. A. L., *Commentary to "Glass transitions in thin polymer films",* Eur.Phys. J. E **2,** 205 (2000).

[195] Explorer AFM instrument operation manual, ThermoMicroscopes Corporation 1996-2000.

[196] D. J. Plazek, J. Polym. Sci., Polym. Phys. Ed. **20**, 729-742(1982).

[197] Qifeng Li, Rui Hua, Ignatius J. Cheah, and Keng C. Chou, *"Surface Structure Relaxation of Poly(methyl methacrylate)"*, J. Phys. Chem. B, 112, 694-697(2008).

[198] Y. Grohens, M. Brogly, C. Labbe and J. Schultz*, "Interfacial conformation energies of stereoregular poly(methyl methacrylate) by infra-red reflection absorption spectroscopy"*, Polymer 38, 5913-5920(1997).

[199] J. S. Sharp and J. A. Forrest, *"Dielectric and ellipsometric studies of the dynamics in thin films of isotactic polyÑmethylmethacrylateÖ with one free surface"*, Phys. Rev. E 67, 031805-1-9(2003); Data Sheet from Polymer Source, Inc.

[200] K. Konstadinidis, B. Thakkar, A. Chakraborty, L. W. Potts, R. Tannenbaum, M. Tirrell, and J. F. Evans, *"Segment level chemistry and chain conformation in the reactive adsorption of poly(methyl methacrylate) on aluminum oxide surfaces",* Langmuir 8, 1307-1317(1992).

[201] R. D. Priestley, C. J. Ellison, L. J. Broadbelt, J. M. Torkelson, *"Structural Relaxation of Polymer Glasses at Surfaces, Interfaces, and In Between",* Science 309, 456-459(2005).

[202] J. Berriot, H. Montes, F. Lequeux, D. Long and P. Sotta, *"Gradient of glass transition temperature in filled elastomers"*, Europhys. Lett. 64, 50-56 (2003).

[203] C. Basire and C. Frétigny, C.R. Acad. Sci. Paris, Ser. 2b 325, 211-220(1997).

[204] E. Manias, H. Chen, R. Krishnamoorti, J. Genzer, E. J. Kramer, and E. P. Giannelis, *"Intercalation Kinetics of Long Polymers in 2 nm Confinements",* Macromolecules *33,* 7955-7966(2000).

[205] J. Erichsen, T. Shiferaw, V. Zaporojtchenko, and F. Faupel, *"Surface glass transition in bimodal polystyrene mixtures"*, Eur. Phys. J. E 24, 243–246 (2007).

[206] I. A. Bitsanis and G. ten Brinke, *"A lattice Monte Carlo study of long chain conformations at solid-polymer melt interfaces",* J. Chem. Phys. 99, 3100-3111(1993).

[207] R. D. Priestley, L. J. Broadbelt, and J. M. Torkelson, *"Physical aging of ultrathin polymer films above and below the bulk glass transition temperatures: effects of attractive vs neutral polymer-substrate interactions measured by fluorescence"*, Macromolecules 38, 654-657(2005).

[208] A. Vaknin, Z. Ovadyahu, M. Pollak, *"Aging Effects in an Anderson Insulator",* Phys. Rev. Lett.84, 3402-3405(2000).

[209] E. Abd El-Wahabb, M.M. El-Samanoudy, M. Fadel, *"Effect of thickness and heat treatment on the electrical and optical properties of (Ge2S3)1(Sb2Se3)1 thin films"*, Applied Surface Science 174, 106-117(2001).

[210] A. Giridhar, P.S.L. Narasimham and S. Mahadevan, *"Electrical properties of Ge-Sb-Se glasses"*, J. Non-Crystal. Solids 37, 165-179(1980).

[211] J. A. Hammerschmidt, and W. L. Gladfelter, G. Haugstad, *"Probing Polymer Viscoelastic Relaxations with Temperature-Controlled Friction Force Microscopy",* Macromolecules, *32,* 3360-3367(1999).

[212] M. Hamdorf, D. Johannsmann, *"Surface-rheological measurements on glass forming polymers based on the surface tension driven decay of imprinted corrugation gratings"*, J. Chem. Phys. 112, 4262-4270(2000).

[213] J. G Diaz Ochoa, K. Binder and W. Paul, *"Molecular dynamics simulations of the embedding of a nano-particle into a polymer film",* J. Phys.: Condens. Matter 18, 2777–2787(2006).

[214] S. A. Hutcheson and G. B. McKenna, *"Erratum: Nanosphere Embedding into Polymer Surfaces: AViscoelastic Contact Mechanics Analysis [Phys. Rev. Lett. 94, 076103 (2005)]"*, Phys. Rev. Lett. 94, 189902-1(2005).

[215] S. A. Hutcheson and G. B. McKenna, *"Nanosphere Embedding into Polymer Surfaces: A Viscoelastic Contact Mechanics Analysis",* Phys. Rev. Lett. 94, 076103-1-4(2005).

[216] J.S. Sharp, J.A. Forrest, Z. Fakhraai, M. Khomenk, J.H. Teichroeb, and K. Dalnoki-Veress, *"Reply to comment on "The properties of free polymer surfaces and their effect upon the glass transition temperature of thin polystyrene films" by S.A. Hutcheson and G.B. McKenna",* Eur. Phys. J. E 22, 287–291 (2007).

[217] V. M. Rudoy, O. V. Dement'eva, I. V. Yaminskii, V. M. Sukhov, M. E. Kartseva, and V. A. Ogarev, *"Metal Nanoparticles on Polymer Surfaces: 1. A New Method of Determining Glass Transition Temperature of the Surface Layer",* Colloid Journal 64, 743-754(2002).

[218] R. Ivanova, R. Staneva, S. Geppert, B. Heck, B. Walter, W. Gronski, B. Stuhn, *"Interplay between domain microstructure and nematic order in liquid crystalline/isotropic block copolymers",* Colloid Polym. Sci. 282: 810–824(2004).

[219] M. K. Mukhopadhyay, X. Jiao, L. B. Lurio, Z. Jiang, J. Stark, M. Sprung, S. Narayanan, A. R. Sandy, and S. K. Sinha, *"Thickness Induced Structural Changes in Polystyrene Films",* Phys. Rev. Lett.101, 115501-1-4(2008).

[220] S. Herminghaus*, "Polymer thin films and surfaces: Possible effects of capillary waves"*, Eur. Phys. J. E 8, 237-243 (2002).

[221] J. C Moreira, N. R. Demarquette, *"Influence of Temperature, Molecular Weight, and Molecular Weight Dispersity on the Surface Tension of PS, PP, and PE. I. Experimental"*, J. Appl. Polym. Sci. 82, 1907–1920 (2001).

[222] J. Brandrup, E. H. Immergut and E. A. Grulke, *"Polymer Handbook-Fourth Edition"*, John Wiley & Sons, Inc(1999).

[223] H. R. Brown and T. P. Russell, *"Entanglements at Polymer Surfaces and Interfaces"*, Macromolecules *29,* 798-800(1996).

[224] L. Si, M. V. Massa, K. Dalnoki-Veress, H. R. Brown, and R. A. L. Jones, *"Chain Entanglement in Thin Freestanding Polymer Films",* Phys. Rev. Lett. 94, 127-801(2005).

[225] H. Meyer, T. Kreer, A. Cavallo, J. P. Wittmer, and J. Baschnagel, *"On the dynamics and disentangelemnt in thin and two-dimensional polymer films",* Eur. Phys. J. Special Topics 141, 167-172(2007).

[226] G. Biroli, J.-P. Bouchqud, A. Cavagna, T. S. Grigera and P. Verrocchio, *"Thermodynamic signature of growing amorphous order in glass-forming liquids",* Nature Physics 4, 771-775(2008).

[227] C. Fradin, A. Braslau, D. Luzet, D. Smilgies, M. Alba, N. Boudet, K. Mecke & J. Daillant, *"Reduction in the surface energy of liquid interfaces at short length scales ",* Nature 403, 871-874(2000).

[228] F. P. Buff, R. A. Lovett & F. H. Stillinger, *"Interfacial density profile for fluids in the critical region"*, Phys. Rev. Lett. 15, 621-623 (1965).

[229] M. P. Gelfand & M. E. Fisher, *"Finite-size effects in fluid interfaces",* Physica A 166, 1-74 (1990).

[230] S. Streit, C. Gutt, V. Chamard, A. Robert, M. Sprung, H. Sternemann, and M. Tolan, *"Two-Dimensional Dynamics of Metal Nanoparticles on the Surface of Thin Polymer Films Studied with Coherent X Rays",* Phys. Rev. Lett.98, 047801-1-4(2007).

[231] M. Akiba, *"1/f dielectric polarization noise in silicon p-n junctions",* Appl. Phys. Lett. 71(22), 3236-3238(1997).

[232] K. P. O'Brien, M. B. Weissman, D. Sheehy, D. D. Viehland, *"Small-scale polarization noise in a relaxor ferroelectric"*, Phys. Rev. B 56, R11365-11368(1997).

[233] E. Vidal Russell and N. E. Israeloff, *"Direct observation of molecular cooperativity near the glass transition*", Nature 408, 695-698(2000).

[234] E. Vidal Russell, N. E. Israeloff, L. E. Walther, and H. Alvarez Gomariz, *"Nanometer Scale Dielectric Fluctuations at the Glass Transition"*, Phys. Rev. Lett. 81, 1461-1464(1998).

[235] L. E. Walther, N. E. Israeloff, E. Vidal Russell, and H. Alvarez Gomariz, *"Mesoscopic-scale dielectric relaxation at the glass transition",* Phys. Rev. B 57, R15 112-15 115(1998).

[236] R. Richert, *"Scaling vs. Vogel—Fulcher-type structural relaxation in deeply supercooled materials",* Physica A 287, 26-36(2000).

[237] A. Serghei, H. Huth, C. Schick, and F. Kremer, *"Glassy Dynamics in Thin Polymer Layers Having a Free Upper Interface"*, Macromolecules 41, 3636-3639(2008).

[238] C. J. Ellison, M. K. Mundra, and J. M. Torkelson, *"Impacts of Polystyrene Molecular Weight and Modification to the Repeat Unit Structure on the Glass Transition−Nanoconfinement Effect and the Cooperativity Length Scale",* Macromolecules 38, 1767-1778(2005).

[239] A. Serghei, L. Hartmann, F. Kremer, *"Molecular dynamics in thin films of isotactic poly(methylmethacrylate) – revisited",* Journal of Non-Crystalline Solids 353, 4330–4333(2007).

[240] G. Meyer and N. M. Amer, *"Simultaneous measurement of lateral and normal forces with an optical-beam-deflection atomic force microscope",* Appl. Phys. Lett57, 2089-2091(1990).

[241] S. Kawai, S. Kitamura, D. Kobayashi, H. Kawakatsu, *"Dynamic lateral force microscopy with true atomic resolution",* Appl. Phys. Lett87, 173015-1-3(2005).

[242] R. Richert, *"Scaling vs. Vogel-Fulcher-type structural relaxation in deeply supercooled materials",* Physica A 287, 26-36(2000).

[243] P. A. O'Connell, G. B. McKenna, *"Rheological measurements of the thermoviscoelastic response of ultrathin polymer films",* Science307, 1760-1763(2005).

[244] K. Tanaka, A. Takahara, and T. Kajiyama, *" Rheological Analysis of Surface Relaxation Process of Monodisperse Polystyrene Films",* Macromolecules33, 7588-7593(2000).

[245] D. Qi, J. A. Forrest, *"Nano gold sphere embedding studies of near surface dynamics of polystyrene films",* to be published.

[246] O. K. C. Tsui, Y. J. Wang, F. K. Lee, C.-H. Lam, and Z. Yang, *"Equilibrium Pathway of Spin-Coated Polymer Films"*, Macromolecules41, 1465-1468(2008).

[247] E. M. Blokhuis, J. Kuipers, and R. Vink, *"Description of the fluctuating colloid-polymer interface"*, Phys. Rev. Lett.101, 086101(2008).

[248] L. Cipelletti, S. Manley, R. C. Ball, and D. A. Weitz, *"Universal Aging Features in the Restructuring of Fractal Colloidal Gels "*, Phys. Rev. Lett. 84, 2275-2278(2000).

[249] L. Cipelletti, L. Ramos, S. Manley, E. Pitard, D. A. Weitz, E. E. Pashkovski and M. Johansson, *"Universal non-diffusive slow dynamics in aging soft matter",* Faraday Discuss.123, 237–251(2003).

[250] H. K. Nakamura, M. Sasai, M. Takano, *"Scrutinizing the squeezed exponential kinetics observed in the folding simulation of an off-lattice Go-like protein model",* Chem. Phys. 307, 259–267(2004).

[251] U. Raviv, J. Klein, and T.A. Witten*, "The polymer mat: Arrested rebound of a compressed polymer layer"*, Eur. Phys. J. E 9, 405–412 (2002).

[252] M. Bellour, A. Knaebel, J. L. Harden, F. Lequeux, and J.-P. Munch, *"Aging processes and scale dependence in soft glassy colloidal suspensions",* PHYSICAL REVIEW E 67, 031405-1-8(2003).

[253] R. Bandyopadhyay, D. Liang, H. Yardimci, D. A. Sessoms, M. A. Borthwick, S.G. J. Mochrie, J. L. Harden, and R. L. Leheny, *"Evolution of Particle-Scale Dynamics in an Aging Clay Suspension",* Phys. Rev. Lett. 93, 228302-1-4(2004).

Appendices

Appendix A: list of symbols and acronyms

Symbols

a_T	shift factor
b	Kuhn length
C	carbon
C	specific heat capacity
C_n	Flory's characteristic ratio
D	diffusion coefficient
D_R	diffusion coefficient of the Rouse chain
E	tensile modulus
F	free energy of polymer chains
F	intermediate scattering factor/function
φ	torsion angle
$G(t)$	shear modulus at time t
H	hydrogen
J	creep compliance
K	Kelvin (temperature unit)
k_B	Boltzmann constant
ς_R	total friction coefficient of a Rouse chain
ς_0	friction coefficient of one Rouse bead
$\xi(T)$	characteristic length scale related to CRR
M_0	molar mass of polymer chemical repeat unit
Mn	number average molecular weight
Mw	weight average molecular weight

N	degree of polymerization
N_A	Avogadro's number
Ω	number of long chain conformation states
P	pressure
$p(m)$	distribution function of polymer chains with molecular weight m .
ρ	density
r_{PDI}	polydispersity index
$\vec{R}_n$	end-to-end vector of polymer chain
$\left\langle R^2 \right\rangle$	mean-square end-to-end distance of polymer chain
R_g	radius of gyration
S	long chain molecule conformational entropy
$\tau_\alpha(T)$	alpha mode relaxation time at temperature T
T	absolute temperature
T_c	critical temperature in the mode coupling theory
T_g	glass transition temperature
T_k	Kauzmann temperature
T_m	melting temperature
T_V	Vogel temperature
γ	surface tension
υ	Poisson's ratio
τ_R	Rouse time(1^{st} Rouse mode)
τ_P	p^{th} mode Rouse time
U	potential energy
η	viscosity
τ_{rep}	reptation time of a polymeric chain molecule
σ	stress
ε	strain

$v_f(T)$	free volume at temperature T
v_o	molecular occupied volume
μ	chemical potential
V	volume

Acronyms

ADC	analog-to-digital converter
AFM	Atomic Force Microscopy
CRR	cooperative rearranging region
FF	Fox-Flory relation
KWW	Kohlrausch-Williams-Watts equation
LJ	Lennard-Jones potential
L-R	left-minus-right
MCT	mode coupling theory
MSD	mean square displacement
OTS	octadecyltrichlorosilane
PBMA	poly (butyl methacrylate)
PI	polyisoprene
PS	polystyrene
PSD	power spectral density
PMMA	poly (methyl methacrylate)
PVAc	poly (vinyl acetate)
SA	self-assemble
TEM	Transmission Electron Microscopy
VFT	Vogel-Fulcher-Tammann law
WLF	Williams-Landel-Ferry law

Appendix B: program code for doing nano rheology measurements on polymer surfaces

```
'The following program is for doing nano rheology measurements on polymer surfaces
'AFM lateral cantilever displacement is 100nm, moving rate is 100nm/s
'AFM tip etch depth is set by fQdepth; 0.01V corresponds 2.3nm
'Refer to the thesis(Chapter 7) for specific procedures

Dim fData(6000) As Double, fOldZvoltage1 As Double, fQQZvoltage As Double
Dim fDataaa(6000) As Double, fQdepth As Double
Dim Qa As Long, Qb As Long, Qc As Long, QDelayT As Long
Dim fQZminVolt As Double, fQZmaxVolt As Double, fXx As Double, fYy As Double
Dim iNn As Integer, iQi As Integer, iQQQ As Double
Dim fQQGetFeedbackADC As Double
Dim fQQMinFeedback As Double, fQQMaxFeedback As Double
Dim fQQUpdateFeedback As Double

Dim fOldZvoltage As Double, fOldSetPoint As Double
Dim fZnewSetVolt As Double, fTimeinterval As Double
Dim fPold As Double, fIold As Double, fDold As Double, fQMoverate As Double

Private Sub cmdDrawLine_Click()

   Timer1.Enabled = False
   'Delay (2000)

   QDelayT = 20
   fQdepth = 0.02
   iNn = 1
   fQMoverate = 100.0
```

```
fXx = 100
fYy = 100

'iQQQ = QDelayT * 5000

For i = 0 To 6000
  fData(i) = 0
  Next

For i = 0 To 6000
  fDataaa(i) = 0
  Next

'Declaring the variables
Dim fPold As Double, fIold As Double, fDold As Double
Dim iMoveXY As Integer, iQTipMove As Integer

Dim iGotFeedback As Integer
Dim fZdistAt As Double, fZcurrentVolt As Double
Dim fZnewSetVolt As Double

Qa = iGetADCMux(0)
Qb = iGetADCMux(1)
Qc = iGetADCMux(2)
Text6.Text = Format(Qa, "###0.00")
Text7.Text = Format(Qb, "###0.00")
Text8.Text = Format(Qc, "###0.00")

Call vsetADCMux(2, 1)
Delay (5000)
iMoveXY = 0
```

```
    'Get Old Paramaters
    Call vGetSetPoint(fOldSetPoint)
    Call vGetPID(fPold, fIold, fDold)
    Call vGetZvoltage(fOldZvoltage)
    Call vGetPresentZvoltage(fOldZvoltage1)

    'Text2.Text = Format(fPold, "###0.00")
    'Text3.Text = Format(fIold, "###0.00")
    'Text4.Text = Format(fDold, "###0.00")
    Text5.Text = Format(fOldZvoltage1, "###0.00")



For h = 1 To iNn
' Check to See if the system is in feedback, if not, put the system in Feedback

    Call vReadFeedback(fQQGetFeedbackADC)
    'fQQGetFeedbackADC = iReadADC(0)
    Call vGetFeedbackRange(fQQMinFeedback, fQQMaxFeedback)
    fQQUpdateFeedback = (fQQGetFeedbackADC * ((fQQMaxFeedback - fQQMinFeedback) /
65535)) + fQQMinFeedback
    Text2.Text = Format(fQQUpdateFeedback, "###0.0000")

    iGotFeedback = bInFeedback()
    If iGotFeedback = 0 Then
        Msg1 = "The system is not in Feedback." + Chr(10)
        Msg2 = Msg1 & "Please, put the system in feedback." + Chr(10) + Chr(10)
        Msg3 = Msg2 & "This Screen will Exit to the Example 6 Screen," + Chr(10)
        Msg4 = Msg3 & "to allow you to put the system in Feedback."
        MsgBox Msg4, 48, "Feedback Error"
        frmDrawLine.Visible = False
        Exit Sub
    End If
```

```
'Move to the Start Position
'Timer1.Enabled = False
iMoveXY = 0
'Delay (1000)


iMoveXY = bMoveToXY(fXx, fYy, 100, XYMOVE_DIST + XYMOVE_RATE)
Do While iMoveXY = 0
   Text1.Text = "the tip is moving"
Loop


'to get the tip stable (especially the L-R tip motion)
Delay (60000)

iMoveXY = 0

'Move with Etch Z Piezo Activated
If DragProbe(1).Value = True Then

    'Timer1.Enabled = False
    iMoveXY = 0

Call vReadFeedback(fQQGetFeedbackADC)
'fQQGetFeedbackADC = iReadADC(0)
'Call vGetFeedbackRange(fQQMinFeedback, fQQMaxFeedback)
fQQUpdateFeedback = (fQQGetFeedbackADC * ((fQQMaxFeedback - fQQMinFeedback) /
65535)) + fQQMinFeedback
Text3.Text = Format(fQQUpdateFeedback, "###0.0000")

Call vGetPresentZvoltage(fOldZvoltage1)
```

```
Text4.Text = Format(fOldZvoltage1, "###0.00")


'Set the PID's to 0, to turn off Feedback
Call vSetPID(0, 0, 0)
Call vHoldFeedback
iVal = iReadMirrorPort(39)

'Call vSetSetPoint(1)
Call vSetZvoltage(fOldZvoltage1 - 0.2)
Delay (40000)
Call vSetZvoltage(fOldZvoltage1)
Delay (30000)
Call vSetZvoltage(fOldZvoltage1 + fQdepth)
Delay (30000)

For i = 0 To 500
  fData(i) = iReadADC(2)
  Delay (QDelayT)
  Next

'move the cantilever
iMoveXY = bMoveToXY(fXx + 100, fYy, 100, XYMOVE_DIST + XYMOVE_RATE)

Do While iMoveXY = 0
 Text1.Text = "the tip is moving"
Loop

For i = 500 To 6000
'For i = 0 To 6000
  fData(i) = iReadADC(2)
  Delay (QDelayT)
```

```
  Next

For i = 0 To 6000
fData(i) = (fData(i) * 20 / 65535) - 10
Next

For i = 0 To 6000
   fDataaa(i) = fDataaa(i) + fData(i)
   Next

Call vDrawGraph

'Restore the original values to the PID's, the Set Point, and the Z Piezo Voltage

Call vGetPresentZvoltage(fOldZvoltage1)
fOldZvoltage1 = fOldZvoltage1 - fQdepth
Text6.Text = Format(fOldZvoltage1, "###0.00")

If (fOldZvoltage1 - 1) > 0 Then
        Call vSetZvoltage(fOldZvoltage1 - 1)
   Else
   Call vSetZvoltage(fOldZvoltage1)
   End If

Call vRestoreFeedback
Call vSetPID(fPold, fIold, fDold)
Call vSetSetPoint(fOldSetPoint)

Delay (30000)

Call vGetPresentZvoltage(fZcurrentVolt)
fZdistAt = ConvZvoltToDist(fZcurrentVolt)
```

```
        ZcurrentAt.Text = Format(fZdistAt, "###0.00")

        End If

        'fXx = fXx + 2
        'fYy = fYy + 100
Next h

        'in the end to return to origin

        iMoveXY = 0
        iMoveXY = bMoveToXY(0, 0, 50, XYMOVE_DIST + XYMOVE_RATE)

        Do While iMoveXY = 0
          Text1.Text = "the tip is moving"
        Loop

        iMoveXY = 0
        'Timer1.Enabled = True

        For i = 0 To 6000
           fDataaa(i) = fDataaa(i) / iNn
           fData(i) = fDataaa(i)
           Next

        Call vDrawGraph

  Open "c:\qi\lmry.txt" For Output As #1

        For i = 0 To 6000
           Write #1, fData(i)
           Next
```

```
        Close #1

      Open "c:\qi\lmrx.txt" For Output As #2

      For i = 0 To 6000
        Write #2, i * QDelayT
        Next
        Close #2

   cmdDrawLine.Caption = "OK!"
   Beep
   Beep
   cmdDrawLine.Caption = "Draw Line"
   Text7.Text = Format(999999999, "###0.00")
End Sub

Private Sub cmdExit_Click()

   Call vTipDisengage(0)
   frmDrawLine.Visible = False
   Timer1.Enabled = False
End Sub

Private Function ConvZdistToVolt(ByVal fZdist As Double) As Double
   'Get Z Range
   Dim fZgotRange As Double
   Call vGetZrange(fZgotRange)
   'Get Z Voltage Min / Max
   Dim fZminVolt As Double, fZmaxVolt As Double
   Call vGetZvoltageRange(fZminVolt, fZmaxVolt)

   fQZminVolt = fZminVolt
```

```
    fQZmaxVolt = fZmaxVolt
    Text9.Text = Format(fQZminVolt, "###0.00")
    Text10.Text = Format(fQZmaxVolt, "###0.00")

    ConvZdistToVolt = fZdist * ((fZmaxVolt - fZminVolt) / (fZgotRange * 1000))
End Function

Private Function ConvZvoltToDist(ByVal fZvolt As Double) As Double
    'Get Z Range
    Dim fZgotRange As Double
    Call vGetZrange(fZgotRange)
    'Get Z Voltage Min / Max
    Dim fZminVolt As Double, fZmaxVolt As Double
    Call vGetZvoltageRange(fZminVolt, fZmaxVolt)

    ConvZvoltToDist = 1000 * fZvolt * (fZgotRange / (fZmaxVolt - fZminVolt))
End Function

Private Sub Form_Activate()
    Timer1.Enabled = False
End Sub

Private Sub Form_Load()
    'Initially Set the Etch Surface Choice to "No"
    DragProbe(0).Value = True
    Call DragProbe_Click(0)
    'These are the initial values for the Start and Stop positions in the Draw Line Frame
    StartX.Text = Format(0#, "##0.00")
    StartY.Text = Format(0#, "##0.00")
    StopX.Text = Format(0#, "##0.00")
    StopY.Text = Format(0#, "##0.00")
    MoveRate.Text = Format(0#, "##0.00")
```

```
    'Get the Current Z Range
    Dim fZrange As Double
    Call vGetZrange(fZrange)
    ZRange.Text = Format(fZrange * 1000, "###0.00")
    'Get the Current Z Voltage and Change to Current Distance
    Call vGetPresentZvoltage(fQQZvoltage)
    Dim fCurrentZDist As Double
    fCurrentZDist = ConvZvoltToDist(fQQZvoltage)
    ZcurrentAt.Text = Format(fCurrentZDist, "###0.00")
    'Set Z Piezo Control Your Setting to 0 initially
    ZyourSet.Text = Format(fCurrentZDist, "###0.00")
    'Set the Current Set Point
    Call vGetSetPoint(fOldSetPoint)
    SetPointCurrentAt.Text = Format(fOldSetPoint, "###0.00")
    'Set Set Point Your Setting to 0 initially
    SetPointEtch.Text = Format(fOldSetPoint, "###0.00")
    Timer1.Enabled = False

End Sub

Private Sub Form_Unload(Cancel As Integer)
    Unload frmDrawLine
    Timer1.Enabled = False
End Sub

Private Sub MoveRate_KeyPress(KeyAscii As Integer)
    If (KeyAscii = 13) Then
        MoveRate.Text = Format(Val(MoveRate.Text), "###0.00")
    End If
End Sub

Private Sub vOutofScanRange()
```

```
    MsgBox "You have entered a value that is larger than the Scan Range"
End Sub

Private Sub Timer1_Timer()
  'Dim tempz As Double, Qtempz As Double
  'Call vGetPresentZvoltage(tempz)
  'f = ConvZvoltToDist(tempz)
  'ZcurrentAt.Text = Format(f, "###0.000")
  'Text1.Text = Format(tempz, "###0.00")
  'Call vGetSetPoint(Qtempz)
  'SetPointCurrentAt.Text = Format(Qtempz, "###0.00")
  'SetPointCurrentAt.Refresh

  'fData(iQi) = iReadADC(2)
  If iQi < 4999 Then
  fData(iQi) = iReadADCfromInterrupt(2)
  iQi = iQi + 1
  DoEvents
  Else
  iQi = 5555
  End If
  'Delay (QDelayT)

End Sub

Private Sub ZcurrentAt_KeyPress(KeyAscii As Integer)
    Beep
End Sub

Private Sub Zrange_KeyPress(KeyAscii As Integer)
    Beep
End Sub
```

```
Private Sub ZyourSet_KeyPress(KeyAscii As Integer)

   If (KeyAscii = 13) Then
      Dim fZnewSet As Double
      KeyAscii = 0
      fZnewSet = Val(ZyourSet.Text)
      If (fZnewSet > Val(ZRange.Text)) Or (fZnewSet < 0) Then
         MsgBox "You entered in a value that will be out of Range"
         Exit Sub
      Else
         fZnewSetVolt = ConvZdistToVolt(fZnewSet)
         Text1.Text = Format(fZnewSetVolt, "###0.00")
         ZyourSet.Text = Format(fZnewSet, "###0.00")
      End If
   End If
End Sub

Private Sub vDrawGraph()
   LineScan.NumPoints = 5999
   LineScan.AutoInc = 0

   For j = 0 To 5998

      LineScan.ThisPoint = j + 1
      LineScan.GraphData = fData(j)
      LineScan.XPosData = (QDelayT) * j
   Next
   LineScan.DrawMode = 2
   LineScan.DrawMode = 4
End Sub
```

Appendix C: journal papers published and to be published

1. D. Qi, Z. Fakhraai, and J. A. Forrest, *"Substrate and Chain Size Dependence of Near Surface Dynamics of Glassy Polymers"*, Phys. Rev. Lett. 101, 096101-1-4(2008).[based on work of project 1]

2. D. Qi, J. A. Forrest, *"Molecular weight dependence of near-free-surface dynamics of glassy polystyrene films"*, to be published. [based on work of project 2]

3. D. Qi, J. A. Forrest*, "Nanometer scale depth dependence of near-free-surface dynamics of glassy polymer films",* to be published. [based on work of project 2]

4. D. Qi, J. A. Forrest, *"Evidence of cooperative rearranging dynamics in glassy polymer films: a low level thermal polarization noise study",* to be published. [based on work of project 3]

5. D. Qi, J. A. Forrest, *"Stress relaxation in the near-free-surface region of glassy polymer films: nano surface rheology AFM measurement in time domain"*, to be published. [based on work of project 4]